Silica-bound supramolecular chromatographic stationary phases and their applications

Subba Reddy Mekapothula

A thesis submitted in partial fulfilment of the requirements of Nottingham Trent University for the degree of Doctor of Philosophy

November 2022

Dedication

I dedicate this thesis to all my teachers and parents who shaped me with the unconditional support, knowledge, and wisdom they provided throughout my life. This work would be impossible without them, and I am always thankful that their help has allowed me to achieve what I always dreamed of.

Acknowledgments

First, I would like to thank my director of studies Dr. Gareth Cave who has supported me in all aspects of completing the Ph.D. project. I am always grateful for his constructive guidance, perceptions, patience, and constant support during my Ph.D. studies. He has had an incredible and productive influence on my research work. He has excellent motivational power that can motivate anyone to reach their goals. His constant availability and great support have helped me overcome tough decisions that impact my Ph.D. studies much more easily. I am always thankful to him for enabling me to stand beside Chemistry Nobel Laureates Sir Fraser Stoddart and Sir David McMillan. I will also never forget the fun we all had with “20 mins burn” chilli sauce.

Secondly, my great appreciations go to Prof. John Wallis, my second supervisor, for his continuous support and inspiring words to help me achieve my Ph.D. He has been extraordinarily encouraging and kindly provided constructive suggestions and feedback at every stage of my work. His perceptions and recommendations impacted this thesis's and my chemistry skills, making me a better researcher. Dr. David Boocock, my third supervisor, has supported me and provided extensive mass spectrometric peptide analysis training. I thank Dr. Matthew Addicoat for performing on computational modelling and host-guest binding energy calculations of xylene isomers and its impurities with pillar[5]arene cavity, as described in Section 2.8.1. Also thank him for his continuous support and feedback on research work, which stood as another backbone to my Ph.D. work.

Special thanks to Dr. Dinga for performing in-silico host-guest binding energy calculations for synthetic peptides and fullerenes with pillar[5]arene and calix[4]arene cavity, as described in Sections 2.8.2, 2.8.3 and 2.8.4 respectively. He also provided endless support in compiling my research publications. I would also like to thank Dr. Christopher Garner, who has made my Ph.D. experience much more rewarding. A special thanks to Prof. Nagaraj Gowda for introducing me to flavor pharmaceutical analysis and his passion for analytical chemistry.

A special thanks to my friend Mike/Michael Korn for his generous support and for teaching me valuable life lessons. God bless you, Mike! He is the man who scared me with his driving skills at midnight. A special thanks to Eve Tallulah for looking after me when I need help during my Ph.D.

Many thanks to the incredible technical team in the Analytical Lab, Nigel Mould, Dave Edward, Diego, Ryan Lakey, Barbara Stevenson, Kelly and Chris Parker. My eternal thanks to all my research colleagues, Dr. Elvina, Dr, Claire, Dr Bilal, Felicity, Jack, Laura,

Anitha, Lenu, Soojin, Eden, Hasnain, Jim and Satinder, who of whom continuously believed in me and made my Ph.D. life so memorable. Finally, special thanks to all Master and project students I have met at the CELS, RFB, and ISTech labs, especially Ella and Aida (“the Brummie”). A special thanks to Vicky at KFC gastronomy restaurants for supporting me at my part-time job during my Ph.D. Special thanks to my buddies Anil and Ram for their never-ending support since I met them during my bachelor’s studies.

I have no words to express the support I had from my father Venkataswara reddy. I cannot convey my gratitude to my caring brothers Mani, his wife, Venkat, my sister Mahalakshmi, and her husband, Ravi, for providing incredible family support. Special thanks to my nephews Venkat and Harsha for making me happy with their innocence and fun. Furthermore, I have no words to express my gratefulness to Mrs. Katie Cave mam for her selfless care and love, which will be unforgettable in my life forever.

Finally, I thank my lovely girl Manisha Reddy for her encouragement and continuous support being a Ph.D. student.

Table of Contents

List of Figures

List of Tables

List of Abbreviations

- SFE: Supercritical fluid extraction
- CP: Critical point
- HPLC: High pressure liquid chromatography
- UPLC: Ultra pressure liquid chromatography
- LC: Liquid chromatography
- HILIC: Hydrophilic interaction LC
- FE-SEM: Field emission scanning electron microscopy
- SEM: Scanning electron microscopy
- TGA: Thermogravimetric analysis
- RPLC: Reverse phase liquid chromatography
- Si-C: Silica-Carbon
- Si-N: Silica-Nitrogen
- RP-HPLC: Reverse phase high pressure liquid chromatography
- GC: Gas chromatography
- IC: Ion chromatography
- CSP: Chiral stationary phase
- CEC: Capillary electrochromatography
- CE: Capillary electrophoresis
- EtP5: Perethylated pillar[5]are
- EtP6: Perethylated pillar[6]arene
- DMP[5]A: Dimethoxy pillar[5]arene
- TLC: Thin layer chromatography
- NMR: Nuclear magnetic resonance
- LC-MS: Liquid chromatography-Mass spectrometry
- qTOF: Quadrupole time of flight
- ES+: Electrospray Positive mode
- RT: Room temperature
- THF: Tetrahydrofuran
- TEA: Triethylamine
- ΔGBE: Gibbs free binding energies
- DFTB: Density functional tight binding
- UFF: Universal force field
- ADF: Amsterdam Density Functional

- GBSA: Generalized Born solvation model with Solvent Accessible Surface Area
- MOFs: Metal-organic frameworks
- TF: Tailing factor
- Rs: Peak resolution
- PES: Polyethersulfone

List of Publications

Journal articles from PhD work

- **S. Mekapothula**, A. D. D. Wonanke, M. A. Addicoat, D. J. Boocock, J. D. Wallis, and G. W. V. Cave, *International Journal of Molecular Sciences*, 2021, **22**, 5726. (Impact factor- 6.208). https://www.mdpi.com/1422-0067/22/11/5726/htm

  Title: Silica bound co-pillar[4+1]arene as a novel supramolecular stationary phase.

- **S. Mekapothula**, A. D. Wonanke, M. A. Addicoat, J. D. Wallis, D. J. Boocock and G. W. V. Cave, New Journal of Chemistry, 2020, 45, 141-46. (Impact factor- 3.288). https://pubs.rsc.org/en/content/articlehtml/2021/nj/d0nj03555f

  Title: A supramolecular cavitand for selective chromatographic separation of peptides using LC-MS/MS: a combined in silico and experimental approach.

- **S. Mekapothula**, M. A. Addicoat, D. J. Boocock, J. D. Wallis, P. J. Cragg and G. W. V. Cave, Chemical Communications, 2020, 56, 1792-1794. (Impact factor- 6.14). https://pubs.rsc.org/en/content/articlelanding/2020/cc/c9cc09656f

  Title: Supramolecular chromatographic separation of C_{60} and C_{70} Fullerenes: flash column chromatography vs. high pressure liquid chromatography.

Journal articles from collaborative work

- A. Alkhtib, D. Scholey, N. Carter, G. W. V. Cave, B. I. Hanafy, S. R. J. Kempster, **S. Mekapothula**, E. T. Roxborough and E. J. Burton, *Animals*, 2020, **10**, 1482. (Impact factor- 3.14). https://www.mdpi.com/2076-2615/10/9/1482

  Title: Bioavailability of Methionine-Coated Zinc Nanoparticles as a Dietary Supplement Leads to Improved Performance and Bone Strength in Broiler Chicken Production.

Resulting presentations

2022:

- Early Career Researcher MASC Meeting 2022, 28th July 2022, Loughborough, UK (**poster presentation**)
- Chirality 2022, 33rd International Symposium on Chirality, 17-20 July 2022, Chicago, USA (**poster presentation**)
- Calix2022 symposium, 16th International Conference on calixarenes, 10th-14th July 2022, New Orleans, USA (**oral and poster presentation**)

2021:

- Virtual JPAG pharmaceutical analysis research awards 2021 (**oral presentation**)
- Virtual RSC-Macrocyclic and Supramolecular Chemistry Early Career Virtual Symposium 2021 (RSC-vMASC-2021) (**oral presentation**)

2020:

- One day Chemical Biology and Biological Chemistry Group Annual Post-Graduate Symposium, May 2020, The Library Suite, RSC, Burlington House, London (**poster presentation**)

2019:

- The national RSC-Daltons meeting at the University of York, United Kingdom (**poster presentation**)
- RSC-Macromolecular and Supramolecular Conference (RSC-MASC2019), the University of Kent, United Kingdom (**poster presentation**)
- School of Science and Technology Annual Research Conference, 16-17 May 2019, Nottingham, UK (**poster presentation**)

Abstract

A novel co-pillar[4+1]arene incorporating bromo-octyl substituents has been synthesized for the first time using microwave irradiation in high yield (88%) in under four minutes. The yield of the new synthetic green methodology was validated while the traditional condensation method was repeated, which resulted in 26%. Subsequently, the co-pillar[4+1]arene was covalently bound to the surface of chromatographic silica particles. The resulting new stationary phase has been successfully validated to separate xylene isomers and their impurities, such as toluene and ethylbenzene, *via* flash column liquid chromatographic technique. Subsequently, the *in-silico* binding energy calculations *via* the Density Functional Tight Binding (DFTB) method implemented in DFTB+ version 1.3, were perfectly correlated with the observed experimental separation results.

The effective separation of a mixed peptide sample has been achieved *via* a computational strategy towards the bespoke design of a new silica bound supramolecular host capable of selectively interacting with different peptides *via* their morphology and amino acid functionalities. The experimental and in silico chromatographic behaviour of a sample of mixed peptides on a new co-pillar[4+1]arene bound silica HPLC stationary phase column was compared with RP-C18 and unfunctionalized silica (normal phase) column *via* liquid chromatography coupled with mass spectrometry (LC-MS/MS) and demonstrates superior separation selectivity and sensitivity for the mixed peptide solution being investigated.

A silica-bound C-butylpyrogallol[4]arene chromatographic stationary phase was prepared and characterised by thermogravimetric analysis, scanning electron microscopy, NMR and mass spectrometry. The chromatographic performance was investigated by using C_{60} and C_{70} fullerenes in reverse phase mode *via* flash column and high-pressure liquid chromatography (HPLC). The new stationary phase was observed to demonstrate size-selective molecular recognition as postulated from our in-silico studies. The silica-bound C-butylpyrogallol[4]arene flash and HPLC stationary phases were able to separate a C_{60}- and C_{70}-fullerene mixture more effectively than an RP-C_{18} stationary phase. The presence of toluene in the mobile phase plays a significant role in achieving symmetrical peaks in flash column chromatography.

1 Chapter 1: Introduction

1.1 Introduction to separation science

Separation is defined as a scientific process that permits a mixture or solution of chemical substances to separate individual products. With few exceptions, mixtures are energetically a more favourable environment due to the entropic driving forces, as such mixtures are more common than isolated substances. Almost all applied chemistry is essential for the isolation and separation of the mixture of components. Separations can be generally simple such as the distillation of water, or more complex such as separating uranium isotopes for nuclear power plants. Separation processes are ubiquitous across all fields, from wastewater treatment to the purification of drugs. These processes can be very costly, as in the case of biopharmaceutical purification.[1]

Separation science has emerged as an essential branch of science in the first half of the 20th century due to the accelerated industrialization in pharmaceutical research and development, food processing, biotechnology, development in petrochemical industries, and the advent of associated environmental contaminations.[1,2] Due to the demands as mentioned above, separation science has become an indispensable area in many sectors: for example, the separation of crude oils to lubricants, fuels, and other raw materials in the petroleum industry; separation and isolation of natural and synthetic drugs to meet analytical standards in the pharmaceutical sector while the mining industry separates and purifies metals.[1]

These demanding necessities have pushed separation science to expand from its modest to develop new methods generally focusing on qualitative and semi-quantitative analysis, utilizing complex instrumental developments to deliver a high level of sophistication, sensitivity, and automation.[2,3]

In general, separation is defined as the inert chemical reaction or physical process in which specific active ingredients are isolated from a mixture.[3] Separations are classified into three major categories based on the physical or chemical phenomena; equilibria separations, rate separations, and particle separations, as shown in Figure 1.1.

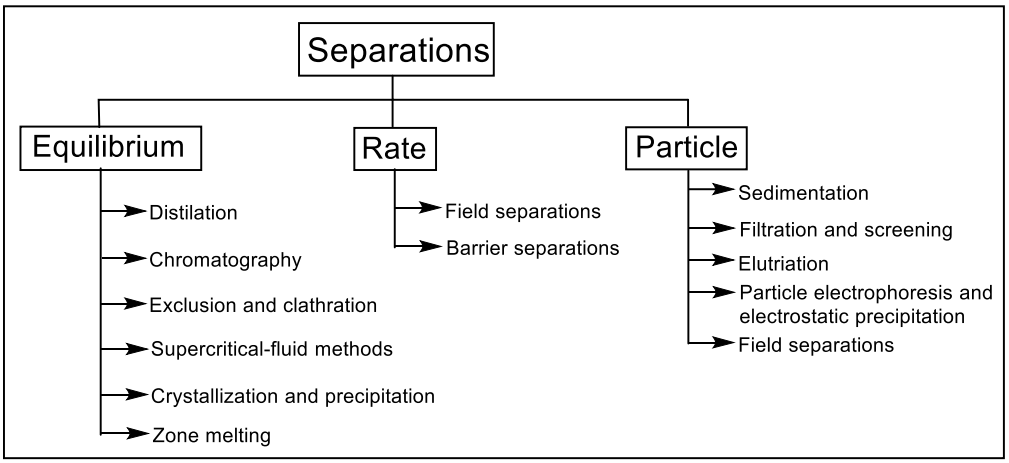

Figure 1.1. Schematic representation of the common separation techniques.

The separations based on equilibrium occur due to the analyte distribution among two phases where two systems are miscible. As the analyte tends to pass between two solvent systems, the concentration of the analyte is constant in the solvent phase system. This condition is called equilibrium, and describes by a distribution coefficient (K).[4]

$$K = \frac{concentration\ of\ analyte\ in\ organic}{concentration\ of\ analyte\ in\ aqueous} \qquad [1]$$

Separation evolves when the distribution coefficient for the analytes differ from each other. Henceforth, the separation is proportional to the distribution coefficients ratio and expressed as the separation factor (α), as shown in equation 3.[3]

$$\alpha = \frac{k2}{k1} \qquad [2]$$

$k1$ and $k2$ are the distribution coefficients of the two analytes.

Distribution constants help determine the analyte concentration in the solution after extraction. The analyte concentration remained in an aqueous solution followed by i times of extractions using an organic solvent ($[A]_i$), represented in the following equation 3.

$$[A]i = \left(\frac{V_{aq}}{V_{org}K+V_{aq}}\right) i[A]0 \qquad [3]$$

$[A]_i$ represents the analyte concentration in aqueous solutions after extraction of V_{aq} mL of the solution. $[A]_0$ is the initial concentration of an analyte.

For example, when the distribution constant of Iodine between organic solvent and water is 85. The I_2 concentration remained in the aqueous system, followed by extracting of 50 mL of 1.00 $*10^{-3}$ M I_2, having a quantity of the organic solvent is 50 mL and two 25 mL portions.

$[I_2]_1 = (50/50*85*50)^1 * 1.00*10^{-3} = 1.16 *10^{-5}$ M

$[I_2]_2 = (50/25*85*50)^2 * 1.00*10^{-3} = 5.28 *10^{-7}$ M

Hence, the distribution constant significantly determines the concentration of analytes after the extraction process.

1.1.1 Distillation

Distillation or rectification is one of the most extensively used separation techniques in the chemical, petrochemical, pharmaceutical, and food industries to fractionate liquid mixtures into their pure chemical constituents. The important principles behind this technique are generating a two-phase system: second, mass transfer through the two coexistent phases, and finally, separation of two phases.[5]

Today, distillation has been developed widely in its fundamentals (thermodynamics, vapour liquid equilibrium), process design, and distillation equipment such as packed columns. Even though the distillation methods have occupied the top rank in many industries, the drawbacks of this highly dominant technique are that it needs high energy, there is a risk of thermal degradation of the components, and the difficulty separating compounds with closely boiling points.[5]

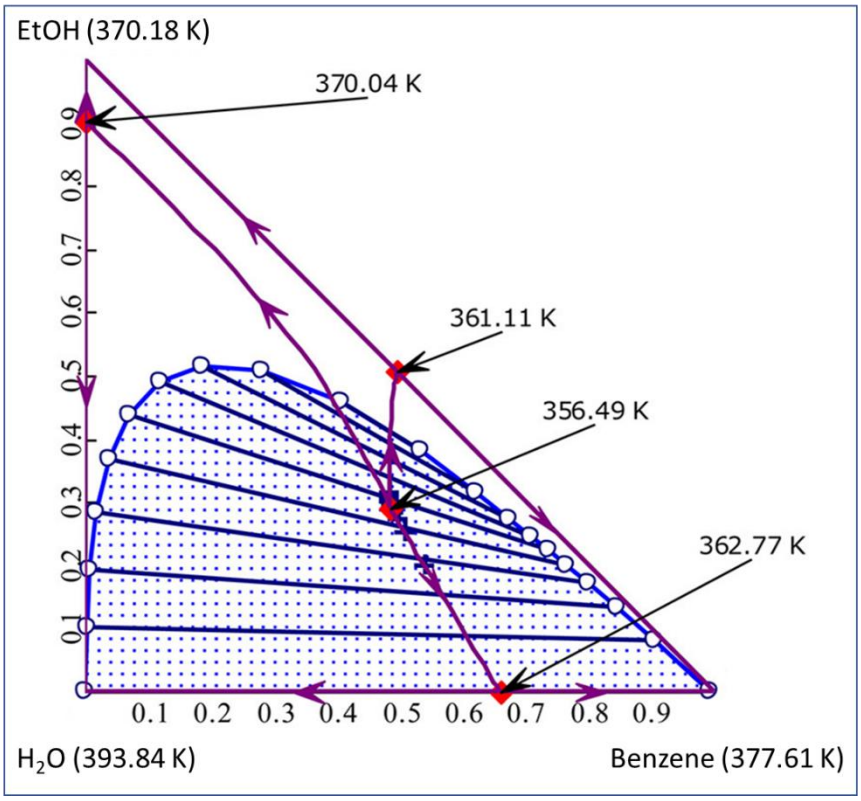

Figure 1.2 Ternary azeotrope diagram at 2 atm.[6]

A typical historical example of dehydrating the ethanol and water mixtures using an azeotropic entrainer. A ternary azeotrope is formed when benzene/isooctane/cyclohexane is added to the water/ethanol azeotrope binary, as shown in Figure 1.2. When this mixture is boiled further, the azeotrope vaporizes, leaving residue that contains ethanol entirely. This azeotropic entrainer help achieve ethanol with concentrations of water less than 50 ppm without distilling absolute ethanol beforehand. The solvent mixture could then be utilized directly as a carburant without any modification to car engines.[6]

1.1.2 Supercritical-fluid methods

In solid-liquid separation techniques, supercritical fluid extraction is considered green due to its lower energy requirements, little or no organic solvent system, and the lack of pre-treatments required, unlike in distillation. In supercritical fluid extraction (SFE), the supercritical fluid consisting solvating properties, which play an essential role in separating large complex mixtures into individual components, which can be developed by utilizing temperature and pressure beyond the compound's critical point.[7,8] The critical temperature is the highest when gas converts to a liquid by increasing pressure. The critical pressure is the most elevated pressure where a liquid converts to gas. These specific properties characterize the critical point (CP), as shown in Figure 1.3. Beyond the critical point, the region is a supercritical fluid. The compound is in a noncondensing single-phase fluid and exhibits some of the physicochemical properties of gases or liquids.[9,10] Supercritical fluid extraction is controlled by tunable intrinsic parameters like temperature, pressure and extrinsic characteristics such as sample matrix and interaction with target analytes. The main disadvantage of SFE is the high investment cost.[9]

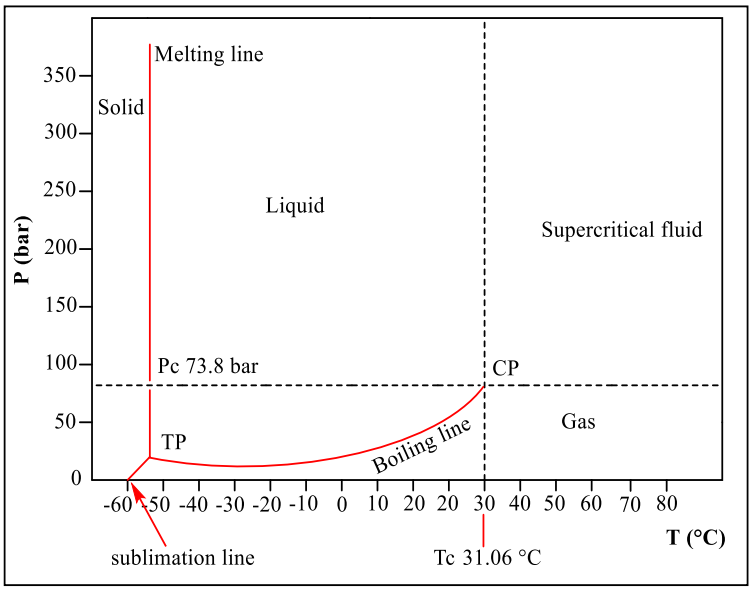

Figure 1.3. Pressure–temperature phase diagram of carbon dioxide.[10]

1.1.3 Crystallization and Precipitation

Crystallization has been an extensively used separation and purification technique to generate a wide variety of solid materials of regular lattice structure *via* phase change of a supersaturated solution. The non-equilibrium supersaturated condition arises by solvent evaporation, the addition of other solvents or solutes, variations in temperature or pressure, oxidation-reduction reactions, and any combinations of these. Precipitation is an irreversible process to obtain amorphous crystalline solid products by dropping from the liquid phase, which is achieved through an irreversible reaction between two reactants or from a solution containing the solvent and an anti-solvent.[11]

In both crystallization and precipitation processes, the lead process is initiated with supersaturation of the solution, followed by nucleation and subsequent growth of crystals. The solid crystals are collected by filtration or centrifugation. The precipitation process starts at high supersaturation, leading to rapid nucleation and crystal growth. Whereas crystallization can be a slow process.[12]

In the modern pharmaceutical and chemical industry processes, over 70% of products are particulate crystalline materials, such as active raw materials, intermediates, pharmaceutical products, fine chemicals, biochemicals, and food additives. Thus, crystallization is the most common separation process after distillation.[12]

In the pharmaceutical industry, recrystallization processes are carried out as batch processes either as a cooling, antisolvent or reactive recrystallization. Even though the batch process is systematic, with well-established methodologies to expand this crystallization process, the batch crystallization is still significantly struggling with batch-to-batch variabilities, which subsequently develop significant downstream processing issues for the isolated materials.[159] Continuous processing delivers increased reproducibility or to control of the physical parameters of the crystalline materials. Once a steady state is achieved, all the materials crystalize under ideal conditions to control or tune characteristic key features such as polymorphic form and distribution of crystal size. These features of continuous processing minimize the downstream operational difficulties in generating particles with uniformity for the development of solid drug dosage forms.[13]

For example, glucaric acid and mono-potassium glucarate crystals are produced *via* antisolvent crystallization and an azeotropic drying process. HCl is added to antisolvent crystallization 1 for pH control, while acetone was utilized for mono potassium glucarate in antisolvent crystallization 1. The isopropanol for glucaric acid in antisolvent crystallization 2 processes, as shown in Figure 1.4.[13]

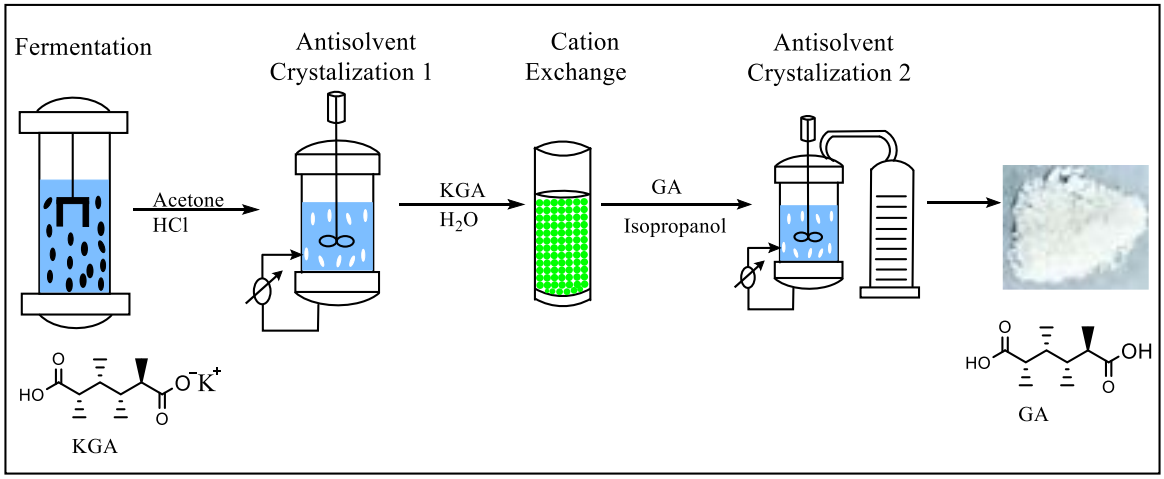

Figure 1.4 Process flow production of glucaric acid via antisolvent crystallization and azeotropic drying.[13]

1.1.4 Size Exclusion

The principle behind the separation by exclusion and clathration is variations in the size of the molecule. In the exclusion separation method, molecular sieves show a significant role in separating the analytes based on the size of the sieves; larger particles elute first, followed by smaller ones.[15] An example of this technique, is size exclusion chromatography, which involves larger molecules being separated *via* their size. The SEC process is independent of the solvent system utilized and how the macromolecule synthesized. The larger molecule sizes cannot enter the pores of stationary phase particles, while smaller sizes penetrate the pores of the stationary phase and subsequent retention in the column, as shown in Figure 1.5.[14]

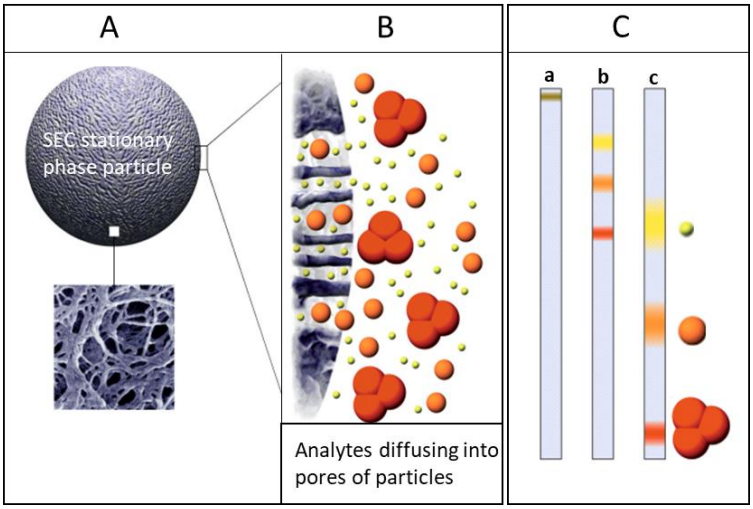

Figure 1.5 A) Enlarged electron microscopic image of SEC gel material, B) Sample molecules diffusing through pores, and C) Separation process of large molecular weight molecules. (Reprinted with permission from Cytiva).[14]

In 1959, Porath and Flodin reported first commercial SEC column consisted of hydrophilic chains cross-linked polydextran gels separating macromolecules under a polar aqueous system, as shown in following Figure 1.6.[15]

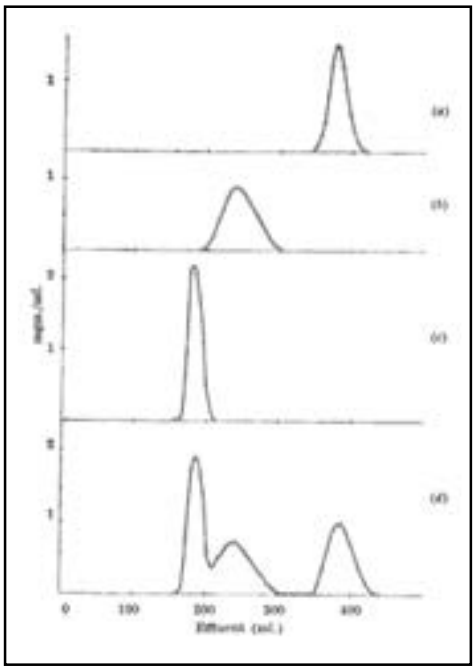

Figure 1.6 The diagrams illustrate 'molecular sieving'. Aqueous solutions (1%) of a) glucose, b) dextran M_n 1000, c) dextran M_n 20,000 and d) a mixture of glucose and dextran solutions filtered through a dextran gel column (4.0 x 36.5 cm).[15] (Reprinted with permission from Nature)

In 1964, Moore reported the utilization of cross-linked polystyrene as an SEC stationary phase under organic solvent systems.[16] Subsequently, various stationary phases have been reported based on silica and polymer for separating several polar solvents. For example, the Phenogel™ size exclusion column from Phenomenex is composed of highly cross-linked polystyrene-divinylbenzene. Several commercial columns available such as Waters® Styragel®, Agilent® PLgel™, Shodex® GPC KF-800 series, PSS SDV®, and Tosoh Bioscience® TSKgel®H-type columns to achieve high resolution and fast separation can be achieved as these the columns are available in various particle sizes and temperature stable up to 140°C.[17]

The modern SEC focus on a wide range of analytical applications, from the determination of purity and quality control to the study relationship of structure-property, which further determines the mass, composition, branching, or end groups. SEC has become a powerful analytical characterization technique for assessing various properties of synthetic and natural macromolecules due to its broad applicability and ease of automatization.[18]

1.1.5 Zone melting

John Desmond Bernal fist reported zone melting, William G. Pfann extended this work further to prepare high-purity materials, including semiconductors, to manufacture transistors. Zone melting is a separation technique to purify a substance *via* melting a short region/zone. Subsequently, the molten zone travels along a long ingot or a solid charge of the material. The molten zone melts the impurities from the solid. It leaves solidified pure material behind while impurities pass *via* the ingot, as the impurities are more soluble at the melting state than in the solid state.[19]

Zone melting has played significant roles in the purification of compounds for crystal growth (zone refining), to produce crystals with uniform composition (zone levelling), and growing crystals devoid of containers (float zone method).[19]

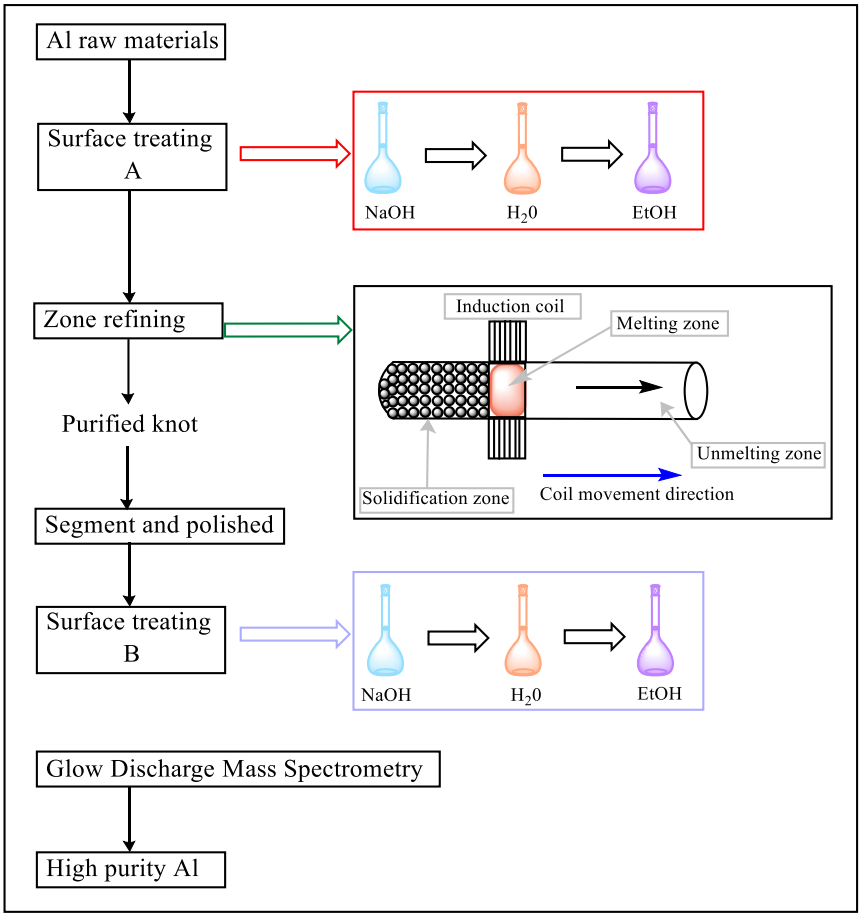

Figure 1.7 The schematic representation of the high-purity Aluminium preparation by zone melting.

In the early 1950's, zone melting/refining has widely industrialized to deliver high purity, such as aluminium, selenium, germanium, tellurium, cadmium, and silicon *via* a unidirectional solidification/segregation separation mechanism. The separation of aluminium to achieve high purity *via* zone melting initiates with surface treating raw

materials using NaOH, Water, and alcohols, as shown in Figure 1.7. The impure Al crystal is kept in the zone melting oven under inert gas. Subsequently, the heating coil at a specified speed starts to move when the Al raw material initiates to melt. When the molten zone reaches the end of the Al sample, both the moving and heating devices will be closed. Subsequently, the coil retained back to its initial position. Both the moving and heating melting zone process repeats at a pre-determined time. The sample will be cooled to room temperature after purification for further purification analysis *via* glow discharge mass spectrometric analysis.[20,21]

Zone melting utilizes the solubility differences in melt and crystal to separate the unwanted elements from the target metals. The equilibrium distribution coefficient (K_0) is measured by the concentration ratio of impurities between the solid (C_S) and liquid (C_L). The K_0 is a constant parameter when the temperature variations among the liquidus and solidus. When the K_o is smaller, the maximum separation efficiency is achieved as the impurities consist of tremendous solubility variations in the equilibrium state. For example, the K_0 values for Si, Fe, Cu, and other impurities are less than one. The law of distribution is depicted in Figure 1.8 (a) zone melting able to demonstrate the separation of impurities from the Al Figure 1.8 (b) shows that separating impurities in the separation process offers a high purity Al achieved. However, it is crucial to note that the purification process is ineffective when K_0 is higher than one. This is due to the traveling of impurities back in the direction of the melting zone.[20,21]

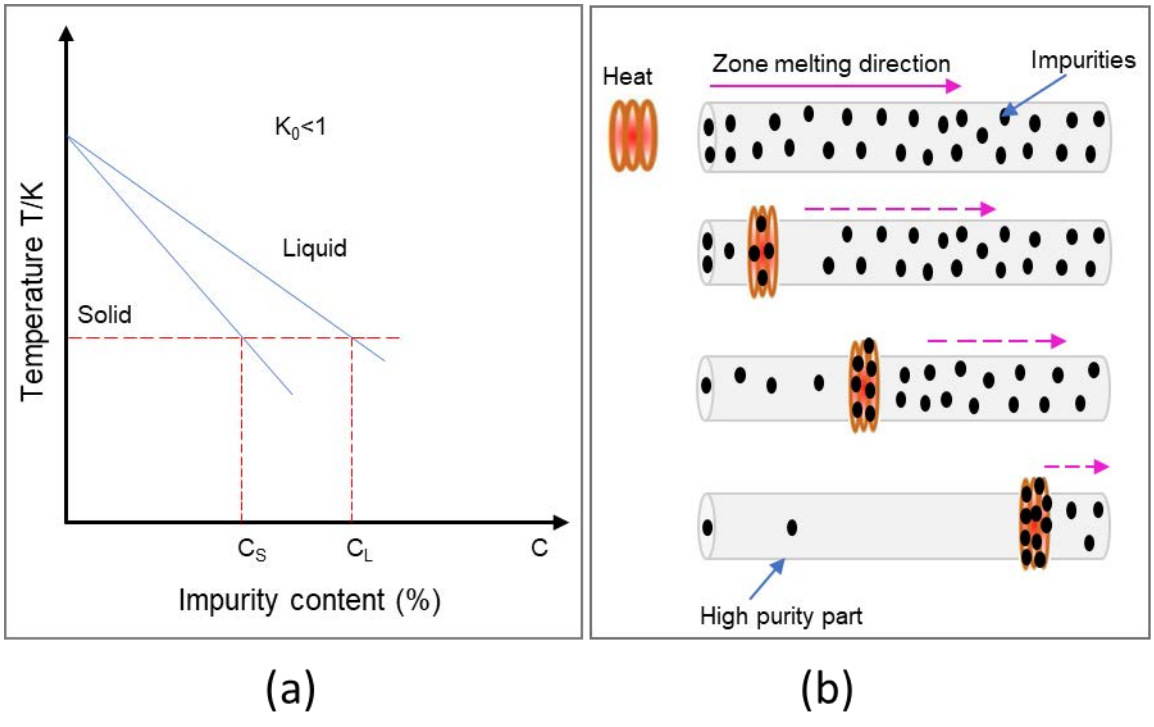

Figure 1.8 Demonstration of separation of impurities from Al.

Zone melting is a costly method to receive pure single crystals with a purity of $1:10^9$. Zone melting methods have a significant role in producing single crystal silicon for solar cells. Zone melting is essential in removing impurities from semiconductors such as Ge, Ga, and Si. In addition, Zone melting has the disadvantage of being a relatively slow and expensive process.[21]

1.1.6 Chromatography

Chromatography is the predominant separation technique that offers unparalleled separation power to separate large complex molecules more than any other type of separation technique. The chromatography contributes a variety of benefits to the chemical and biological sciences such as biochemistry,[22] pharmaceutical science,[23] clinical pharmacology,[24] therapeutics, and toxicology.[25]

The IUPAC defines chromatography as:

"*…a physical method of separation in which the components to be separated are distributed between two phases, one of which is stationary (stationary phase) while the other (mobile phase) moves in a defined direction*."[26]

The stationary phase retains strong interacting molecular species while eluting the molecular species with more affinity towards the mobile phase. Subsequently, strong interacting molecular species elute by varying the polarity of the mobile phase.[27]

Chromatography has been considered a method for separating, identifying, measuring, and elucidating the structure of both small and complex molecules. Still, with the required theoretical base for modern chromatography, it became a branch of science. The detailed history, separation mechanism, instrumental developments and column chemistry advancements will be explained later.[28]

1.2 History of chromatography

Chromatography could be considered the "science of sciences" in the past century due to its revolutionarily impact on research techniques and enhancing the potential fields of natural sciences. Even after a century, chromatography continues to be an enormously rich research area, with numerous scientists working to refine it. Yet, some of the latest discoveries often face resistance from the scientific community, usually when the new ideas rebut generally accepted concepts developed by "incontestable" authorities.

In the 20th century, chromatography was evaluated with the earlier inventions by the Russian botanist Mikhail Semenovich Tswett. His early inventions describe the separation

of various plant pigments such as chlorophyll, carotenoids, and xanthophylls *via* a packed calcium carbonate in the column as a stationary phase using petrol ether: ethanol as an eluent solution. In the 1906, Tswett published two fundamental research works in the *Berichte der Deutschen Botanischen Gesellschaft*, where he focused the investigations on chlorophyll, while the second one aimed to describe the characteristics features of chromatography, including the selection of adsorbent material, how to select the appropriate solvent system and correct column dimensions.[29,30]

Tswett's early-stage chromatography work was not exempt from criticism. The research work was under the embryo stage until taken up by Leroy Sheldon Palmer. He relied on and focused on the adsorptive chromatography principle invented by Tswett. Subsequently, in 1910, he demonstrated the separation of carotenoids from butter fat *via* sucrose as adsorptive material and an alternative to calcium carbonate. In 1922, Palmer's research was recognized worldwide after the detailed description of chromatography and its application in his book "Carotenoids and Related Pigments: The Chromolipids". This book further has become a monograph series from the American Chemical Society. Henceforth, Palmer's research innovations have bridged the early 1960s chromatography research work and the rise of chromatography innovations from R. Kuhn, E. Lederer, and P. Karrer in the 1930's.[31]

Adsorption chromatography principles were a predominant chromatography technique between 1903-1930. In 1941, the breakthrough in chromatography emerged from the Archer J.E. Martin and Richard L.M. Synge at Cambridge University. They introduced partition chromatography to separate the acetylamino acids *via a* water-embedded silica column using chloroform as a mobile phase and plate theory to explain the principles of chromatography. This subsequently resulted in the development of a new "partition chromatography" principle based on a stationary liquid immobilized on the surface of inert silica. This leads to the partition of analytes between the liquid bed and mobile phase system. Their subsequent chromatography research work on the separation of amino acids and peptides revolutionized biochemical studies, and subsequently, they both shared the Nobel Prize in Chemistry in 1952.[32] Furthermore, the partition chromatography sub-branched to various chromatographic techniques, including paper chromatography, thin-layer chromatography, gas-liquid partition chromatography, and high-performance liquid chromatography.[32] In the late 1950s, an amino acid analyzer employing ion-exchange chromatography was introduced as an essential precursor to high-pressure liquid chromatography (HPLC).[33] Subsequently, Moore invented gel-permeation chromatography and commercialized by the Water Associates (now Waters Corporation).[34]

In the late 1960's, liquid chromatography progressed to "High-Performance" *via* small particle-packed columns requiring high-pressure pumps. Horvath, Kirkland and Huber introduced the first generation of high-performance liquid chromatography. Waters Associates and DuPont introduced the commercial HPLC systems. The first HPLC book was published in 1971 by J.H. Kirkland.[35]

These fundamental and instrumental research advances of HPLC and the commercial progress of detectors and reliable injectors helped explosive growth of HPLC which became a sensitive and quantitative technique. In the late 1980's, the availability and accuracy of HPLC made it essential not only in pharmaceuticals but also in other diverse industries.

Today, HPLC has undergone a revolutionary transformation to modern ultra-performance liquid chromatography (UPLC) to achieve higher speed and increased peak capacity and sensitivity by reducing particle size and column dimensions. The primary drivers behind UPLC are the rapid evolution of column packing materials and the commercial availability of mass spectrometric detectors.[36] Acquity UPLC™ system from Waters, Sciex NanoLC 400 and 1290 Infinity II from Agilent are leading UPLC systems in the current chromatography market.

1.3 Fundamentals of liquid chromatography

In Liquid Chromatography (LC), analyte retention occurs due to various molecular interactions of analytes with the stationary phase packed in the column. In addition, analyte retention also depends on the active diffusion of the analyte between the surface of the stationary phase and mobile phase at the stage of secondary equilibrium.[37] In general, LC theory is further classified into two major areas, such kinetic and thermodynamic properties. The kinetic system represents the determination of band broadening and peak width. The thermodynamic system underpins the retention of the analyte and controls the position of the peak in the chromatogram.

The demonstration of the efficient separation in LC is directly proportional to the instrument's optimization parameters, size, the shape of the stationary phase particle, and dimensions of the column. Also, the analyte's separation selectivity or retention behaviour majorly occurs due to the intermolecular interactions, mobile phase composition, nature of the eluent, and temperature conditions. In LC, the separation is performed under a sufficient number of theoretical plates to achieve separation efficiency. This is usually achieved due to the proper selection of separation mode, consideration of stationary phase chemistry, and the mobile phase conditions in the separation process.[37,38]

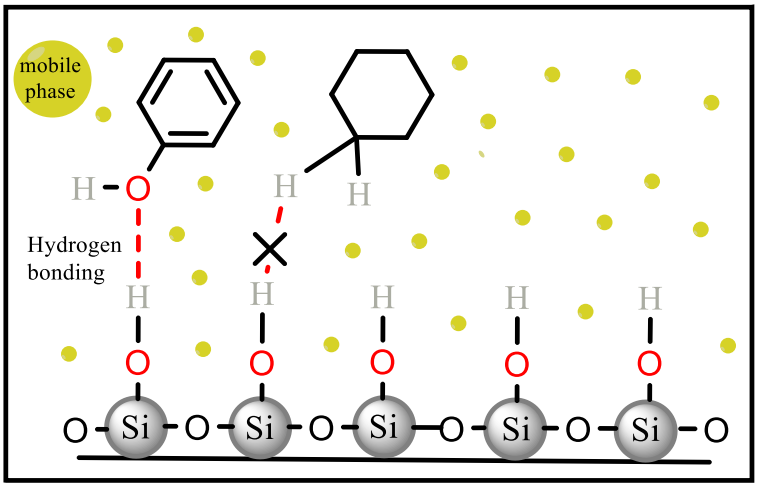

Figure 1.9 Graphical representation of analyte interaction with the normal phase silica column.

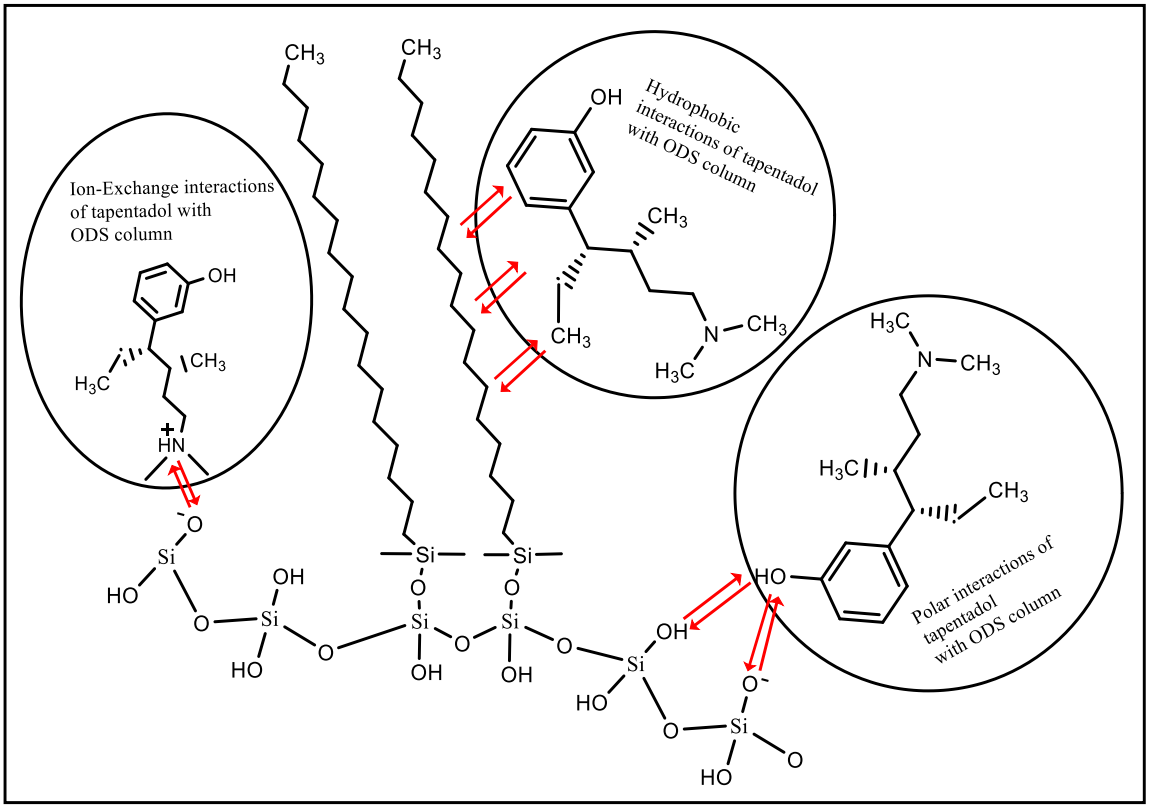

Figure 1.10 Cumulative separation interactions involved in the separation of tapentadol on Octadecylsilyl silica gel (ODS).

In an adsorption chromatography system, the stationary phase is generally an inert adsorptive solid consisting of a porous or ion-exchange resin or a gel. The mobile phase usually elutes through the stationary phase. The analytes are non-covalently bound to the surface of the stationary phase *via* hydrophobic, hydrophilic, lipophilic and dipole-dipole interactions. Several analytes demonstrated various affinities towards the stationary phase due to the chemical interactions that occur between the analyte and stationary phase materials under the normal phase and reverse phase mode of LC, as shown in Figures 1.9

and 1.10. Generally, the analyte with a strong interaction with the stationary phase is retained in the column for a long time than the analyte with less interaction with the stationary phase. This leads to the successful separation of analytes from the mixture of two or more analytes.[39(p.3)]

Based on the separation retention mechanism and the instrument, the classification of chromatography described in Table 1.1.

Table 1.1. General classification chromatography.

Chromatography	
Based on Instrument	*Based on the Retention Mechanism*
❖ Column chromatography ❖ column adsorption ❖ column partition ❖ Paper chromatography Ascending Descending Circular Two-dimensional chromatography ❖ Thin layer chromatography Normal TLC Two dimensional High performance TLC ❖ Gas chromatography Gas-liquid chromatography Gas-solid chromatography ❖ High pressure liquid chromatography Normal phase Reverse phase ❖ Supercritical fluid chromatography ❖ Electrophoretic chromatography	❖ Adsorption Gas-solid chromatography Thin layer chromatography Column chromatography HPLC ❖ Partition Paper chromatography Ion exchange chromatography Size exclusion chromatography ❖ Miscellaneous Ion pair chromatography Chiral chromatography Affinity chromatography

1.4 Column efficiency *via T*heoretical Plate Number

1.4.1 Plate theory

The theoretical plate number (N) is the fundamental foundation of chromatographic theory. This is an important parameter to measure the column efficiency in chromatography

A. J. P. Martin and R. L. M. Synge developed the theory of chromatography based on the theoretical plate concept.[40]

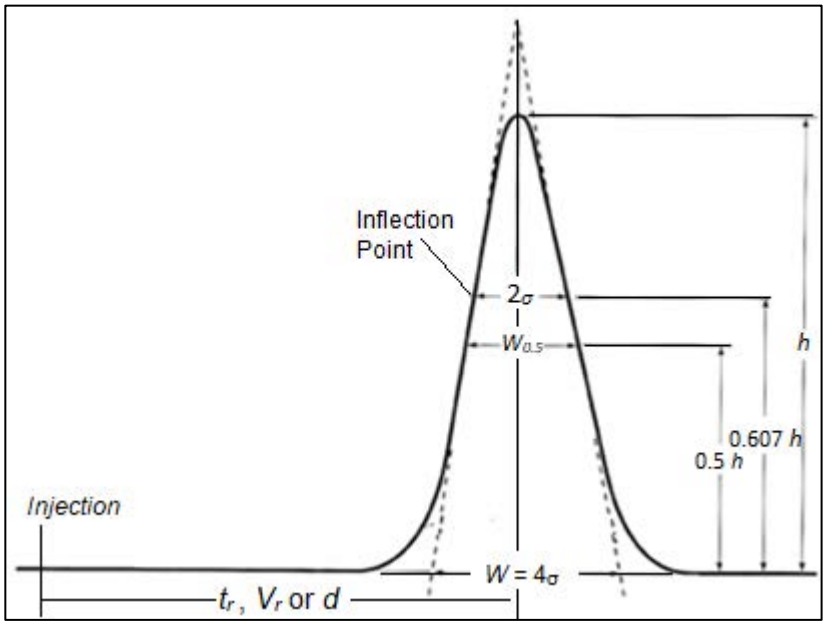

Figure 1.11 Gaussian chromatographic peak.[40]

As shown in Figure 1.11, a Gaussian distribution curve is utilized to demonstrate the solute concentration, which is a function of retention time t.

Where,

t_r = peak maxima

σ= standard deviation

$x = t\text{-}t_r$

$$C = (1/\sqrt{2\pi})e - 1/2(x^2/\sigma^2 \qquad [4]$$

Based on the above equation, the following equation can be derivatized.

$$N = 2\pi \left(h^2 l^2 / A^2\right) \qquad [5]$$

Where,

L= distance between the point of injection to the peak maximum

h= peak height

A= peak area

Subsequently, equation 5 is transformed into a traditional plate number, as shown in equation 6. Martin and Synge described it as a ratio of retention squared to peak variance by.[40]

$$N = 16\frac{(t_r)^2}{(W_t)^2} \qquad [6]$$

Where,

I = retention time (tr) and area and height are converted to peak width in the units of time.

This iconic equation allows the study of the column efficiency to compare among the columns and is an essential key to optimizing the experimental parameters, including composition of mobile phase, stationary phase composition, gradient profile, column temperature, injection volume and amount, flow rate, columns dimensions, length and configuration, particle size, shape, and pore size.[40-42]

The relationship between the theoretical plate number (*N*), column length (*L*), and height equivalent of the theoretical plate (*H*), is represented in equation 7 to measure the column efficiency.[40-42]

$$N = \frac{L}{H} \qquad [7]$$

During the stepwise transfer of solutes between the plates, the separation of solute molecules occurs with an affinity toward stationary and mobile phases. The efficiency column improves when the theoretical plate number increases, subsequently increasing the number of equilibrations.[42]

1.4.2 Rate Theory

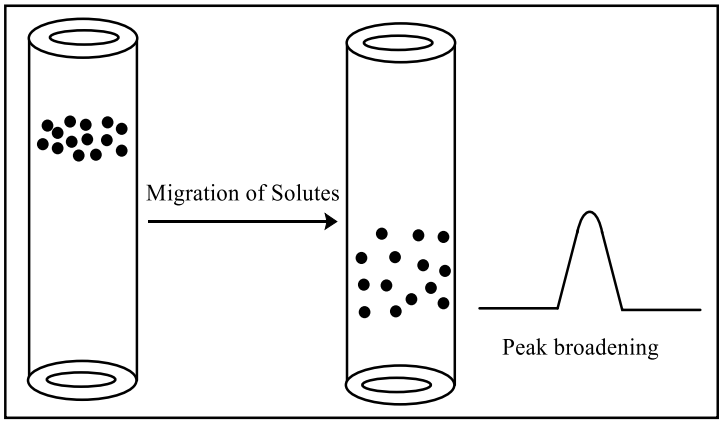

Figure 1.12 Migration of solutes in the column leading to peak broadening.

As shown in Figure 1.12, bandwidth increases when the solute molecules move further down in the column. Bandwidth is directly proportional to retention time and inversely proportional to the mobile phase's velocity. Van Deemter's equation can explain brand broadening. The van Deemter equation is an experimental formula to illustrate the correlation between plate height (H) and linear flow velocity, as shown in equation 8.[40-43]

$$H = A + \frac{B}{\mu} + C_{\mu} \qquad [8]$$

Where *H*= height equivalent to theoretical plates
A= Eddy diffusion
B= Longitudinal diffusion
C= Mass transfer (Cs and Cm)
μ= Average linear velocity of mobile phase

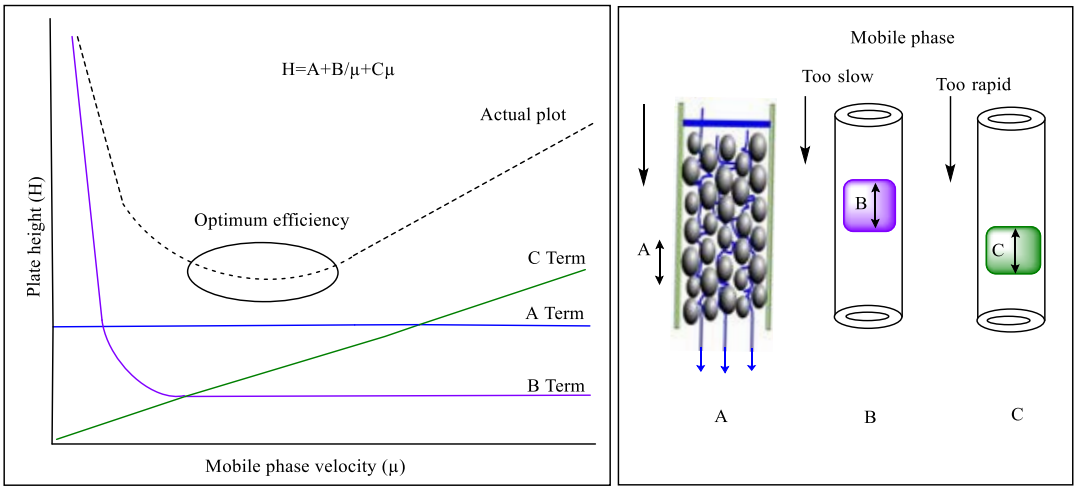

Figure 1.13 the van Deemter equation represents the relationship between the mobile phase velocity and column efficiency.

The van Deemter equation is controlled by three cumulative factors: eddy diffusion; longitudinal diffusion; and mass transfer. These three factors play essential elements that contribute to the band broadening, as shown in Figure 1.13. Optimum mobile phase velocity is required to achieve minimum plate height, subsequently increasing the plate number to increase the equilibration rate to achieve separation and column efficiency.[40-44]

1.4.2.1 Eddy diffusion

Eddy diffusion originates from the turbulence in the solute flow path around the packing particles, which is also independent of flow rate.

$$A = \lambda d_p \qquad [9]$$

Where,
D_p= diameter of the particle
λ= function of packing uniformity and geometry of column.

When a column is not packed with uniformly sized silica particles, solute flow leading to unequal path lengths in the column. Subsequently, some solute molecules of the same species travel a short path and elute from the column, while others travel a long path to elute from the column. This leads to peak broadening. To minimize the eddy diffusion, the average diameter of packing particle in the column must be small and packed uniformly. As

the particle size decreases, the efficiency of the column increases, as shown in Figure 1.14. Also, the back-pressure increases as particle size decrease.[40-44]

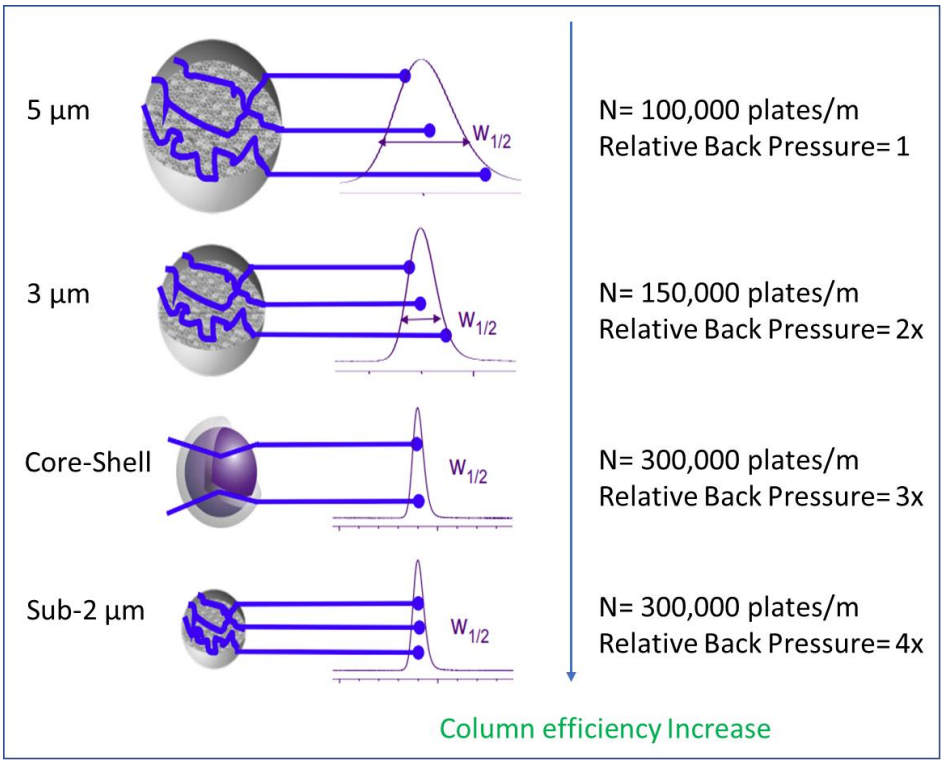

Figure 1.14 Effect of particle size on band broadening.[44]

1.4.2.2 Longitudinal or axial diffusion

As the band of solute molecules travels in the mobile phase, solute molecules tend to diffuse in all directions, mainly in less concentrated regions.

$$B = 2_{\gamma} D_m \qquad [10]$$

Where,

γ=obstruction factor depends on column packing

D_m= solute diffusion coefficient in the mobile phase

When the mobile phase's velocity is slow, the high diffusion rates of solute in the mobile phase led to the solute molecules dispersing in all directions. Subsequently, solute molecules elute from the column slowly, leading to band broadening, as shown in Figure 1.15. Henceforth, the mobile phase flow velocity should be optimal to minimize the longitudinal diffusion.[40-44]

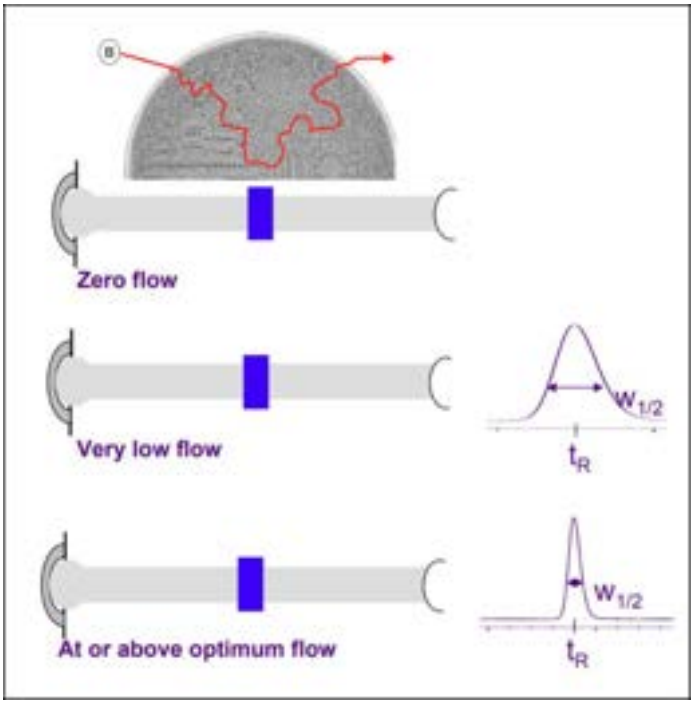

Figure 1.15 Effect of mobile phase's flow velocity on band broadening.[44]

Efficiency is also a function of the mobile phase flow rate. Moreover, all stationary phase particles have an optimal flow rate, a function of particle size. The narrow the particle size, the higher the optimal flow rate, as shown in Figure 1.16.[44]

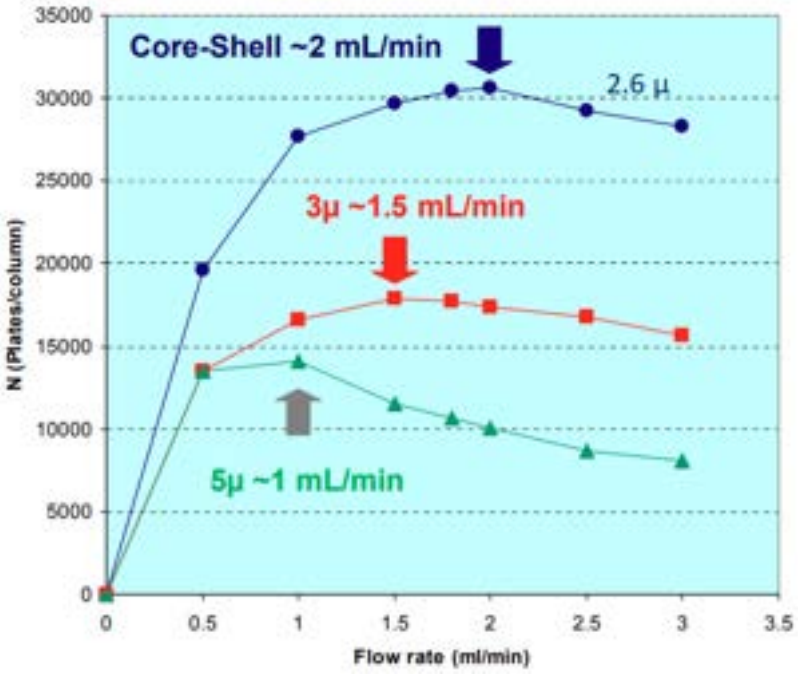

*Figure 1.16 Optimal flow velocity for different sized particles to determine column efficiency. (column dimensions 100*4.6 mm).*[44]

1.4.2.3 Mass transfer (Cs and Cm)

Mass transfer is a transfer of analyte or its mass between the stationary and mobile phases. Term Cs results from resistance to mass transfer in the packing material interface, as shown in equation 11. Cs is directly proportional to stationary phase thickness and inversely proportional to the solute diffusion coefficient in the stationary phase. The resistance to mass transfer means the solute molecules slowly enter the stationary phase and exit from it.[40-42]

$$H\ (mass\ transfer) = C_{ux} = (C_s + C_m)U_x \qquad [11]$$

The term Cm illustrates mass transfer between adjacent streamlines of the mobile phase.

When solute molecules enter larger and smaller stationary phase particles, the moment of solute is, which means resistance mass transfer is high in the larger particle compared to a smaller particle with a low resistance to mass transfer. Therefore, the solute molecule from smaller stationary phase particle elutes first, while solute from larger particles elutes slowly. If a mobile phase velocity is higher, the mass transfer will be less; subsequently, the solute band will be broader.[40-44]

In conclusion, band broadening is the cumulative effect of eddy diffusion, longitudinal diffusion, and mass transfer. To achieve a high column efficiency, one needs to have smaller uniform packing materials with optical linear flow velocity to achieve a higher plate number and increase separation.[40-44]

1.5 Development of LC

Liquid column chromatography has adopted many revolutionary advances *via* the development of instruments, design of columns and creation of new column packing materials to improve peak capacity, faster analysis times, and resolution since the first experiments with chlorophyll. This was achieved by developing principal components of LC such as pumps, injectors, detectors, recorders and data processing software.[45]

1.5.1 Instrumental and silica particle size developments

LC pumps have been improved to deliver a uniform pulse-free flow of mobile phases to the column under high pressures *via* various types of pumps, *i.e.* constant pressure, constant flow, syringe, single-piston reciprocating, dual-piston in-parallel, dual-piston in-series, high pressure mixing and low-pressure mixing pumps. Mobile phase

developments included novel solvents, gradient elution, blending of solvents to adjust the mobile phase strength, buffers and additives, and temperature control.[46]

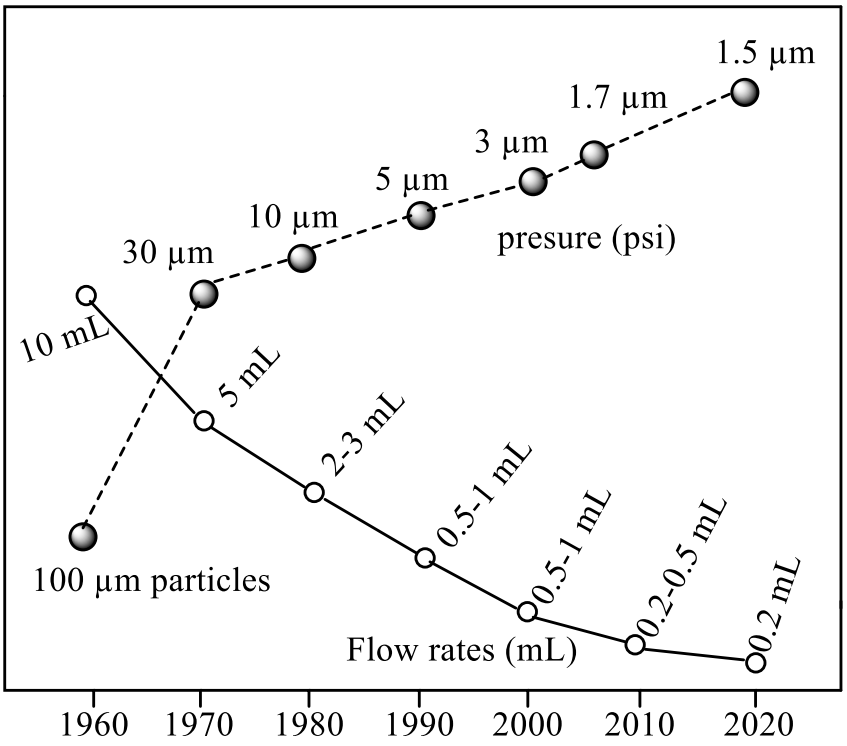

Figure 1.17. Graphical representation of a comparison of particle size v/s run times.

The particle size of the porous stationary phase has decreased to 1.5 µm from the initial 10 µm which was widely used in 1970's HPLC, as shown in Figure 1.17. The particle size reduction corresponds to the improvements in pumping, decreases in extra-column volume and rapid data acquisition.[47] As the size of the particle decreases, plate height decreases, which subsequently increases efficiency. With the development of the particle size of less than 2 µm in the packed columns, the pressure delivery had to be significantly enhanced, and the extra-column volumes decreased. This led to the introduction of ultra high-pressure liquid chromatography and the new generation of instruments able to utilize porous sub-2 µm stationary phases, which can hold pressures of up to 6000 psi.[48,49]

Column length has been reduced to increase the speed of HPLC analysis while reducing the run time. When the column length decreases, the number of theoretical plates will be reduced, and therefore the resolution of LC will decrease. Henceforth, the particle size has to be reduced to increase the column efficiency and resolution. Modern LC systems have revolutionized solvent management systems to deliver accurate and precise flow rates and gradients from 50 uL/min to several mL/min, using a wide range of chromatographic columns of various diameters and lengths.

1.5.2 Silica packing material developments

The column packing stationary phase revolutions involved new adsorbents[50,51], bonded phases,[52,53] pellicular particles,[54] pore-size control,[55] spherical particles,[56] type B silica (consists large pores and have a high capacity at high humidity),[57] chiral stationary phases,[58] end-capping,[59] polar end-capping,[60] embedded polar groups, hybrid silica,[61] and polymeric bonding.[62]

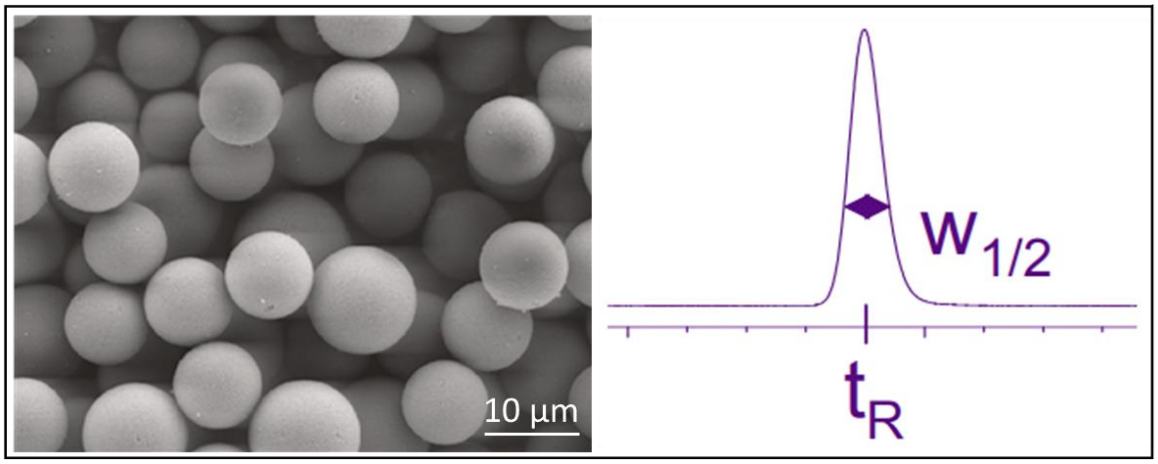

Figure 1.18. Field emission scanning electron microscopy (FE-SEM) image of Kromasil 3.5 um silica particles (100 Å) and demonstration of low peak broadening.[65]

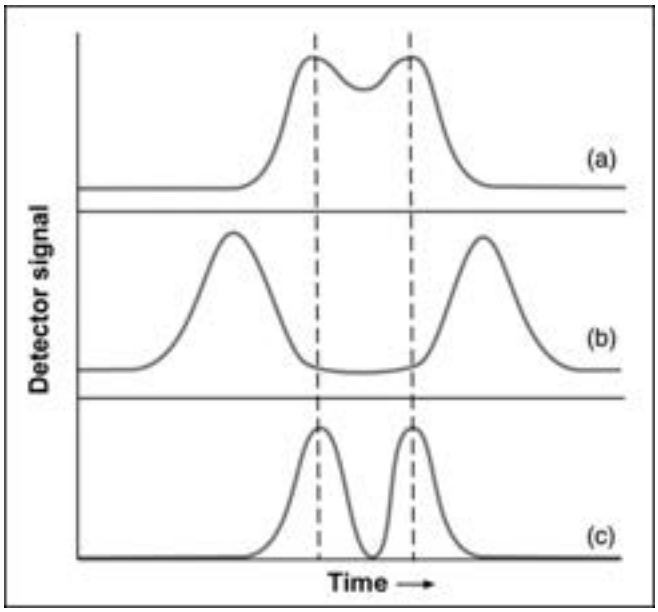

Figure 1.19Illustration of chromatograms with low efficiency (a), increased selectivity (b), and increased efficiency (c).[67]

In LC, silica is one of the most used inorganic packing materials, ahead of polymeric and hybrid materials.[63] Silica is the ideal support compared to other inorganic materials such hydroxyapatite, graphite, and metal oxides due to its good mechanical strength,

controllable pore structure and surface area and high chemical, and thermal stability.[64] In modern LC, 90% of packing materials are porous and comprise uniform spherical silica particles, as shown in Figure 1.18. The uniformity is essential to achieving low column pressure and peak broadening, as shown in Figures 1.18 and 1.19.[65] Due to uniform silica particles packed in the column; the optimal flow rate can be achieved, which in turn increases column efficiency, as shown in Figure 1.19

Core-shell silica particles were developed and introduced by Horvath and Kirkland in the late 1960s,[122] to overcome the limitations of porous silica particles *via* layer-by-layer self-assembly to assemble the durable, homogenous porous shell on the surface of spherical colloidal particles, as shown in Figure 1.20.[66,68].

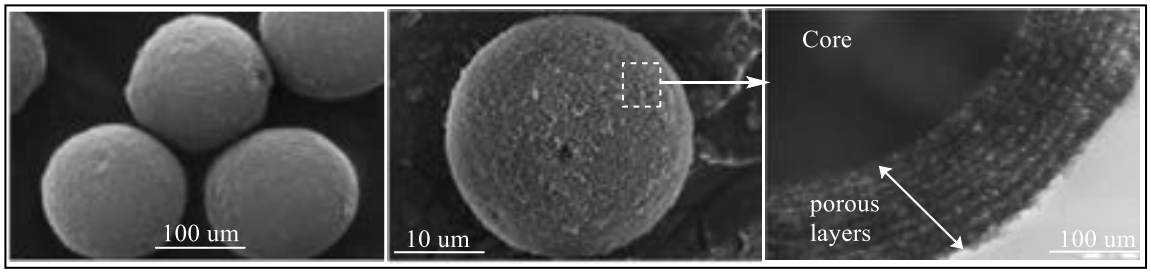

Figure 1.20 Core-shell Kinetex silica particles (1.7 µm).[69]

This particle morphology delivers exceptionally high efficiencies by reducing the band broadening compared to porous silica particles, as shown in Figure 1.21. Owing to the existence of the non-porous solid cores, the reduced diffusion path inside particles develops to lower mass transfer resistance and reduce the column height equivalent to a theoretical plate (HETP) in the core-shell particle packed column. Also, the larger particle size (core + shell) generates a relatively low operating backpressure, leading to fast separations at a higher flow speed. Subsequently, it results in a quicker separation with a narrower peak shape, as shown in Figure 21. These advantages make core-shell silica particles an excellent alternative to comparable porous particles.[70]

The first commercial column with 1.3 µm core-shell silica particles was developed where non-porous cores have 0.9 µm, and porous shell contains 0.2 µm in thickness. The average pore size is 100 Å. In general, core-shell silica particle-packed stationary columns are commercially available in the range of 1.3–5 µm and along with shell thicknesses of 0.15–1.0 µm.[70,71]

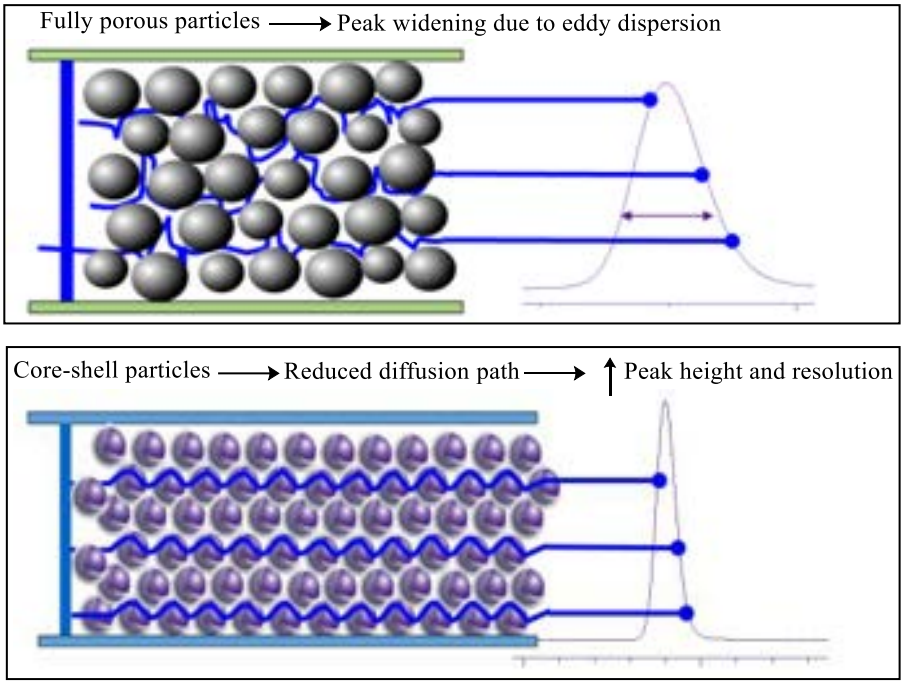

Figure 1.21 Demonstration of peak broadening between fully porous and core-shell silica particles. (Reprinted with permission from Phenomenex).[71]

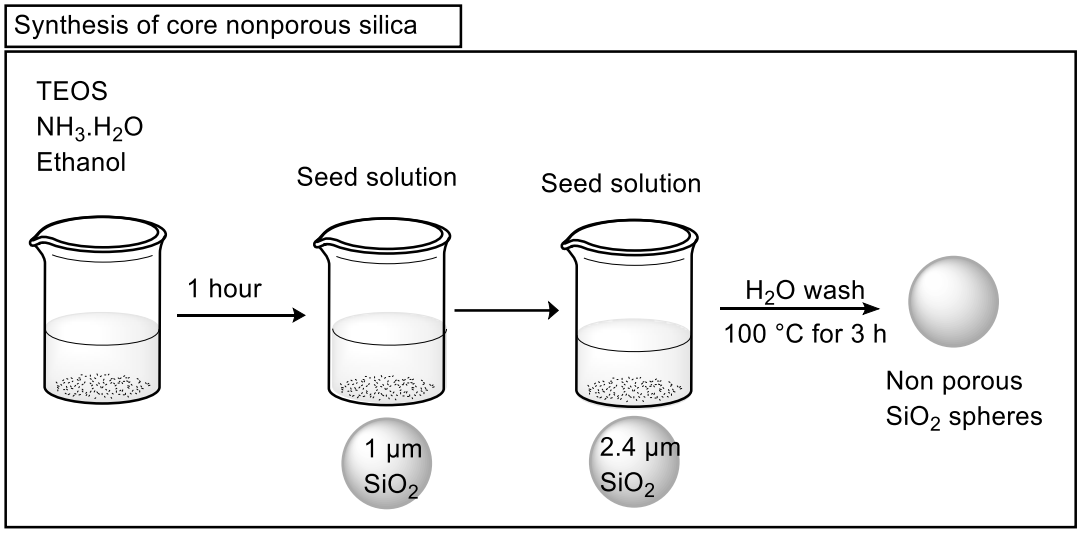

Figure 1.22. Synthesis of nonporous silica for core-shell silica.

Traditionally, the well-known Stober reactions synthesized the solid core silica in core-shell silica particles, followed by the treatment of surfactant and organic expander to form a shell around the core silica, as shown in Figure 1.22. The core-shell silica particles were prepared initially with solid silica cores coated with a porous shell *via* a multi-step layer-by-layer growth process. This process will be repeated more than 50 times to achieve the required thickness. Later, the particles will be calcinated to remove surfactant for stationary phase materials. Finally, the core-shell silica particles will be derivatized with C_{18} before packing into the columns, as shown in Figure 1.23.[70]

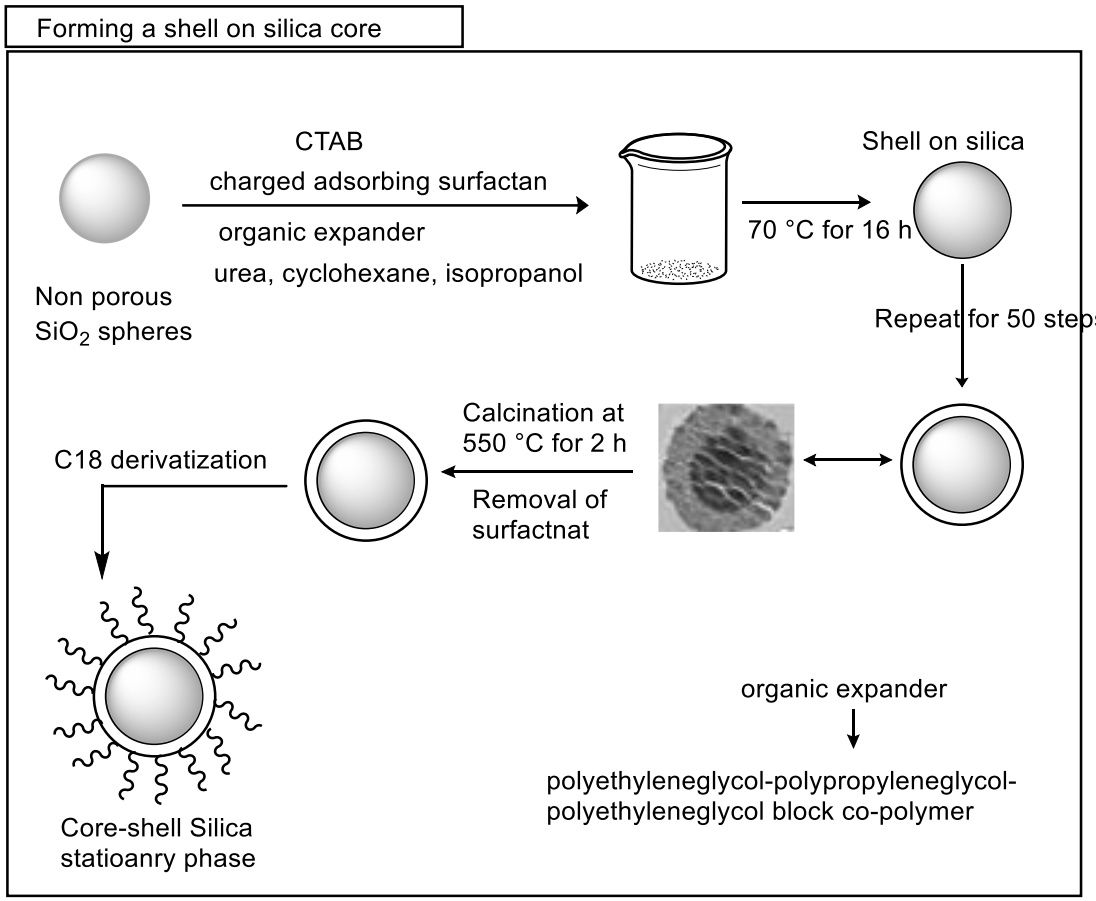

Figure 1.23 Synthesis of a shell coating on the silica core for core-shell silica stationary phase.

There are several commercially available core-shell silica phases with different chemistries from different chromatographic column manufacturers, such as Kinetex from Phenomenex, meteoric core C_{18} from YMC, superficially porous particle silica from Restek, Infinity Lab Poroshell 120 from Agilent and many more.[72]

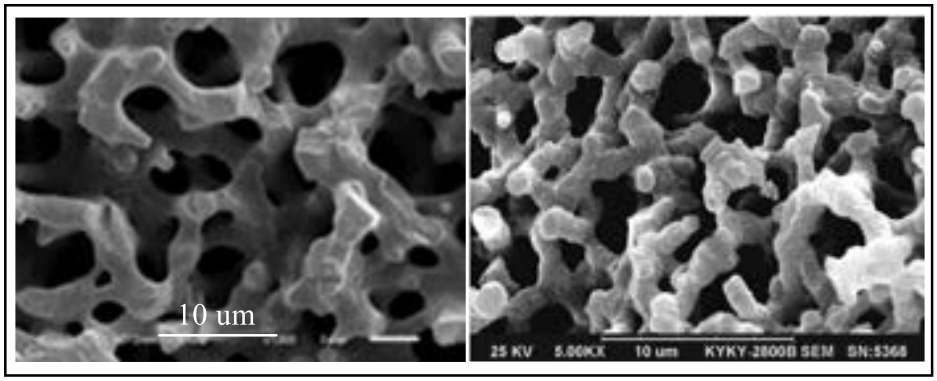

Figure 1.24. SEM images of silica monolithic materials.[76]

Monolithic silica materials have become very popular recently due to improved external porosity and permeability compared to packed silica bed columns, as shown in Figure 1.24.[73] These monolithic are generally synthesized by *in-situ* polymerization of the

monomer in solution and characterized by distinct pore size. The micron scale diffusion pores provide high loading capacity *via* increased surface area.[74,75] These columns play an essential role in high-throughput analysis and direct injection of viscous biological samples.[73]

1.6 Silica bonded stationary phases

The development of bonded stationary phases with different groups in reverse-phase (RP) chromatography is an ongoing research area for enhanced separation selectivity. The development of novel silica-bonded stationary phases contains seemingly unending potential for innovation due to the varieties of novel cavitands with different functionalities, which are traditionally chemically bonded, immobilized, or sorbed onto chromatographic silica. These can be designed selectively to separate compounds that are difficult to separate by commercially available RP stationary phases.[77]

Organic groups can be chemically bonded to the silica by three methods. The first one involves with etherification of silica with alcohols to produce silicate, as shown in Figure 1.25. Silicate phases have low hydrolytic stability, limiting their utility in reversed-phase LC with polar mobile phases. As a result, the use of silicates for LC separations has quickly become antiquated.[78]

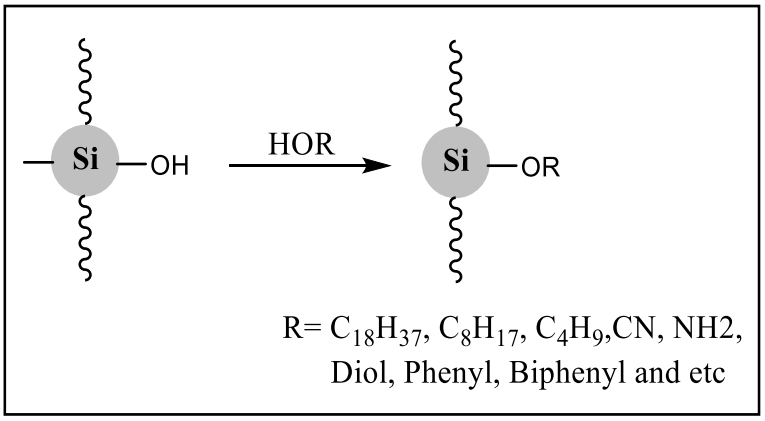

Figure 1.25. Etherification of silica with alcohols.

Silica-Carbon (Si-C) and Silica-Nitrogen (Si-N) linked materials were prepared by initial chlorination of silica's silanol groups followed by reaction with either a Grignard reagent, to synthesize Si-C bonds or with an amine to synthesize Si-N bonds as shown in Figure 1.26. However, these column packing materials suffer from low surface-bonded cavitands and undesired residues from Grignard reagents. Furthermore, Si-N to pH 4-8 when aqueous solutions are used as mobile phases.[79,80]

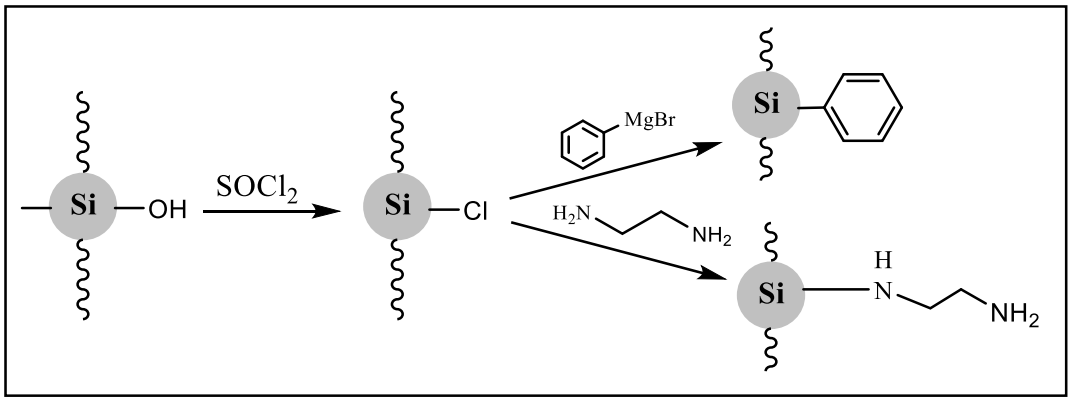

Figure 1.26 Si-C and Si-N bonded column packing materials.

The most commonly available silica column packing columns contain siloxane bonded phases (Si-O-Si-C) prepared *via* reacting organosilane reagents with silanol groups of a silica support, as shown in Figure 1.27. This produces stationary phase packing materials which are hydrolytically stable and have high column efficiency due to rapid mass transfer. Most of the commercially available stationary phases are prepared by this method.[81]

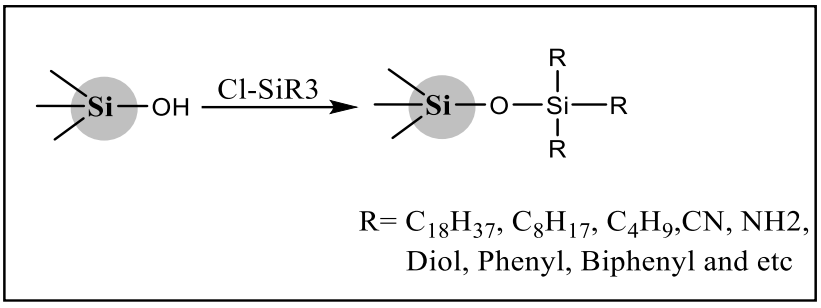

Figure 1.27 Siloxane column packing materials.

This led to chemically bonded stationary phases containing long-chain alkylsilane reagents bound covalently to the silica surface. These stationary phases subsequently increased the hydrolytic stability of the stationary phase and increased the column efficiency due to their mass transfer effects. These revolutionary innovations have become one of the significant factors in the development of LC. RP-C_{18} is the most traditional and popular reverse-phase stationary phase, widely used in LC separations of large numbers of compounds. The numerous commercial RP-C_{18} columns are generally prepared by siloxane chemistry and typically differ in their hydrophobic, ionic and polar properties.[77]

According to the United States Pharmacopeia, several column packing materials have been listed based on the chemical selectors functionalized covalently on the surface of chromatographic silica, as shown in Table 1.2. Several liquid chromatographic ligands and their bonding to the silica surface are commercially available with different brand names from several manufacturers, such as Phenomenex, Restek Corp., Waters, Agilent,

Supelco, Thermo Fisher, Merck KgaA, YMC Co., Ltd., Interchim-Advion, Akzo Nobel Separations, Chiral Technologies, Inc., Diazem, Metrohm-Peak, Inc., Hichrom and several vendors.

Table1.1.2. United States Pharmacopeia "l" column listing for ultra-pressure liquid chromatography

USP “L” column listing	Specifications	Particle size range	Particle shape
L1	Octadecyl silane (ODS or C_{18}) chemically functionalized to porous or non-porous silica	1.5-10 µm	Spherical
L2	Octadecyl silane (ODS or C_{18}) chemically functionalized to silica gel with controlled surface porosity, which bonded to the solid spherical core	30-50 µm	Irregular
L3	Porous chromatographic silica particles	1.5-10 µm	Spherical
L4	Silica particles with controlled porosity bound to the solid spherical core	30-50 µm	Irregular
L5	Alumina with controlled porosity bound to the solid spherical core	30-50 µm	Irregular
L6	Strong cation exchanger packing with sulfonated fluorocarbon polymer bound to a solid spherical core	30-50 µm	Irregular
L7	Octyl silane (C_8) bound to porous silica particles	1.5-10 µm	Spherical
L8	Monomolecular layer of aminopropyl silane bound to totally porous silica gel	1.5-10 µm	Spherical/irregular
L9	Strong acidic cation-exchange chemically boned to totally porous silica gel	3-10 µm	Spherical/irregular
L10	Nitrile groups chemically bonded to porous silica particles	1.5-10 µm	Spherical/irregular
L11	Phenyl groups chemically bonded to porous silica particles	1.5-10 µm	Spherical/irregular

L12	Anion exchanger packing synthesized by chemical bonding of quaternary amine to silica spherical core	30-50 µm	Irregular
L13	Trimethyl silane (C1) bound to porous silica particles	3-10 µm	Spherical
L14	Silica gel chemically bonded with strong basic quaternary ammonium anion exchanger (SAX) coating	5-10 µm	Spherical
L15	Hexylsilane (C_6) bound to porous silica particles	3-10 µm	Spherical
L16	Dimethylsilane (C2) bound to porous silica particles	5-10 µm	Spherical
L17	Strong cation exchange resin having sulfonated, cross-linked styrene-divinylbenzene copolymer in the hydrogen form	7-10 µm	Spherical
L18	Amino (NH_2) and Cyano (CN) groups bound to porous silica particles	3-10 µm	Spherical
L19	Strong cation exchange resin having sulfonated, cross-linked styrene-divinylbenzene copolymer in the calcium form	7 and 9 µm	Spherical
L20	Dihydroxypropane groups chemically bound to porous silica particles	3-10 µm	Irregular
L21	A rigid spherical styrene-divinylbenzene copolymer	5-10 µm	Spherical
L22	A cation-exchange resin with porous polystyrene consists of sulfonic acid groups	6,7 and 8 µm	Spherical
L23	Anion-exchange resin with porous polymethacrylate/polyacrylate gel with quaternary ammonium groups	2.5-10 µm	Spherical
L24	A semi-rigid hydrophilic gel having vinyl polymers with several hydroxyl groups on the surface of the matrix	32-64 µm	

L25	A polymethacrylate resin base, cross-linked with polyhydroxylated ether whose surface contained residual carboxyl functional groups	10 µm	Spherical
L26	Butylsilane (C_4) bound to porous silica particles	3-10 µm	Spherical
L27	Porous silica particles	30-50 µm	Irregular
L28	A multifunctional silica gel (100A°) bonded with an anionic exchanger-amine functionality along with conventional C_8 functionality	3-10 µm	Spherical
L29	Gamma alumina-based polybutadiene spherical particles, consists low carbon content	5 µm	Spherical
L30	Ethylsilane (C_2) bound to porous silica particles	3-10 µm	Spherical
L31	A hydroxide selective, strong anion-exchange resin-quaternary amine bound on latex particles connected to a core of macro-porous particles which contains ethylvinylbenzene crosslinked with 55% divinylbenzene	8.5 µm	
L32	A chiral ligand exchange packing with L-proline copper complex chemically bound to the silica particles	5-10 µm	Irregular
L33	pH stable Silica packing material has the capacity to separate proteins with 4,000-500,000 Da.	1.7 µm	Spherical
L34	Strong cation exchange resin having sulfonated, cross-linked styrene-divinylbenzene copolymer in the lead form		Spherical
L35	Zirconium-stabilized silica particles with a hydrophilic (diol-type) molecular monolayer bonded phase.	Spherical	

L36	A 3,5-dinitrobenzoyl derivative of L-phenylglycine chemically bonded to aminopropyl silica	5 µm	Spherical
L37	Polymethacrylate gel has the capacity to separate proteins by 2,000-40,000 Da		Spherical
L38	Methacrylate-based size-exclusion packing for water soluble analytes		Spherical
L39	A hydrophillic-polyhydroxymethacrylate gel consists of the totally porous spherical resin		Spherical
L40	Cellulose tris-3,5-dimethylphenylcarbamate coated porous silica particles	5-20 µm	Spherical
L41	α_1-acid glycoprotein immobilized on spherical silica particles	5 µm	Spherical
L42	Octylsilane (C_8) and octadecylsilane (C_{18}) groups chemically bonded to porous silica particles	5 µm	Spherical
L43	Pentafluorophenyl groups chemically bonded to silica particles *via* a propyl spacer	1.5-10 µm	Spherical
L44	A multifunctional silica gel (60A◦) bonded with a cationic exchanger-sulfonic acid functionality along with conventional C_8 functionality		
L45	ß-cyclodextrin, R, S-hydroxypropyl ether derivative bonded to porous silica particles	5-10 µm	Spherical
L46	Polystyrene or divinylbenzene substrate agglomerated with quaternary amine functionalized latex beads	9-10 µm	
L55	A strong cation exchange resin with porous silica coated contains a polybutadiene-maleic acid copolymer	5 µm	

L59	A silica or hybrid packing with a hydrophilic coating packing for the SEC separations of proteins with a range of 5 to 7,000 Da	1.5-10 µm	Spherical

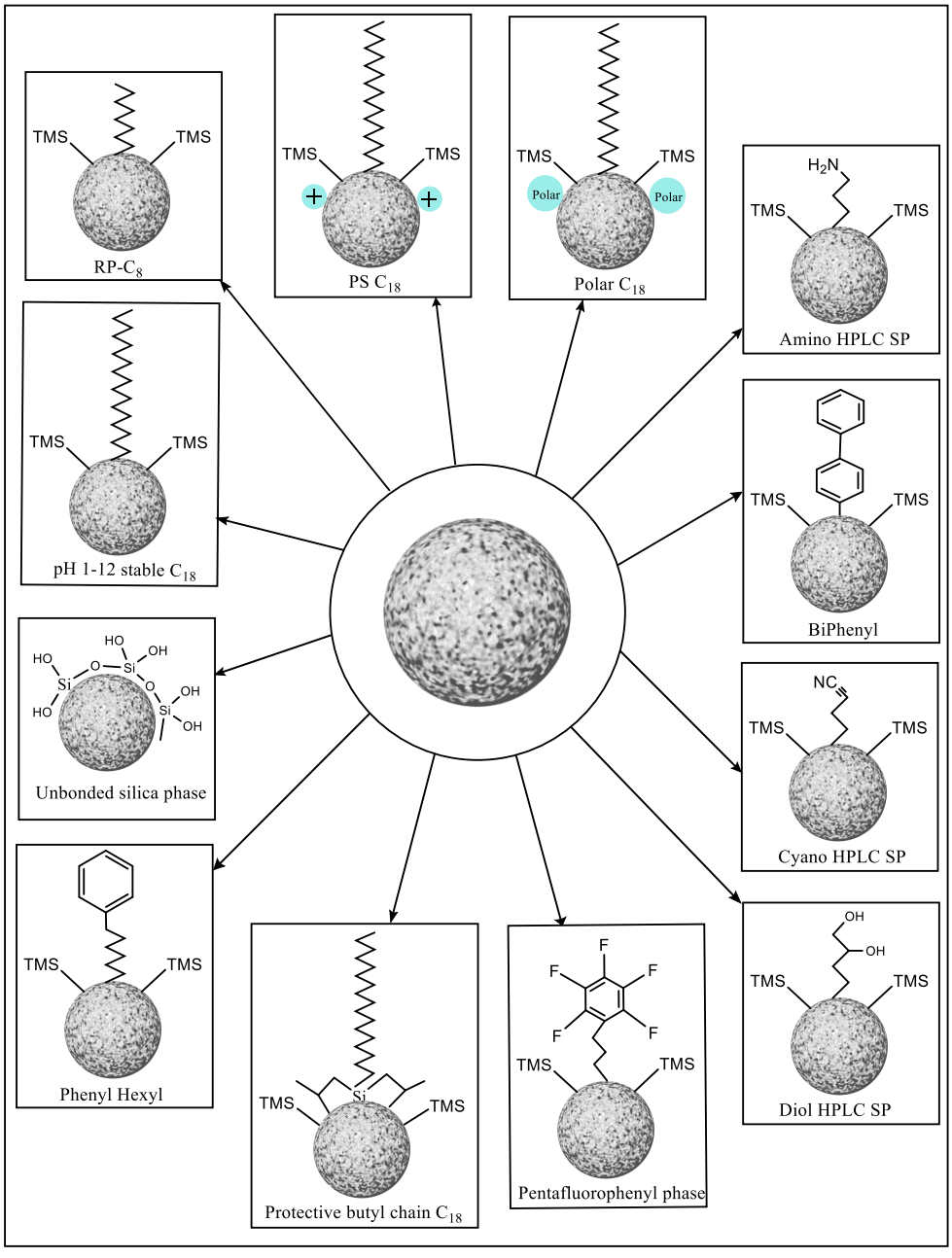

Figure 1.28 Commercially available reverse-phase chromatographic stationary phases.

Reverse phase liquid chromatography (RPLC) is the most frequently used High-Pressure Liquid Chromatography (HPLC) mode for separating nonpolar, weakly polar and polar

analytes. However, separating highly polar compounds on RPLC columns is far from easy; this can be overcome by employing hydrophilic interaction LC (HILIC) columns. Mixed-mode columns containing RPLC/HILIC, are typically employed to separate various aqueous-based analytes under the same column conditions, such as nonpolar, weakly, moderately, and highly polar. Mixed-mode stationary phases offer extended separation selectivity, separation efficiency, and loading capacity than traditional single-mode stationary phases. A few commercially available silica-bound reverse-phase liquid chromatographic stationary phases have been depicted in Figure 1.28.

The development of novel chromatographic bonded stationary phases, featuring multiple modes of interactions, including utilizing macrocyclic functionalized stationary phases, has attracted attention as a new generation of separation tools. The tunability of these new stationary phases goes beyond polarity to incorporate host-guest supramolecular interactions.

1.7 Introduction to supramolecular chemistry

Molecular chemistry was established as a successful procedure to synthesize and develop several molecules *via* covalent bonding. Similarly, supramolecular chemistry centered on the construction of chemical host-guest complex systems *via the* utilization of non-covalent interactions, such as dipole-ionic, van der Waals, hydrogen bonding, cation-π, and other interactions.[82] Subsequently, supramolecular chemistry has extended its applications to various chemical fields due to its ability to construct advanced molecules to interact with guest molecules to achieve host-guest interactions, as shown in Figure 1.29. Supramolecular chemistry revolutionized from its originating host-guest recognition to open up into self-assembly and self-organization of macrocycles at the nanometre scale.[83]

In 1987, Jean-Marie Lehn (Nobel Laureate) defined supramolecular chemistry as: "*Beyond molecular chemistry, supramolecular chemistry aims at constructing highly complex, functional chemical systems from components held together by intermolecular forces*".[82]

Complementary interactions are required to form a supramolecule. The interactions are incorporated by selective manipulation of the molecule at the molecular level. Subsequently, its effects are reflected in the molecular shape. Moreover, the supramolecule's shape also plays a crucial role in supramolecular interactions. Henceforth, the significant supramolecular intermolecular interactions, such as ion-dipole, dipole-dipole, and hydrogen-bonding, are directionally dependent. Furthermore, the stability of

supramolecules is controlled by forces, such as van der Waals and hydrophobic forces, and depends on the proximity of groups specifically interacting.[84]

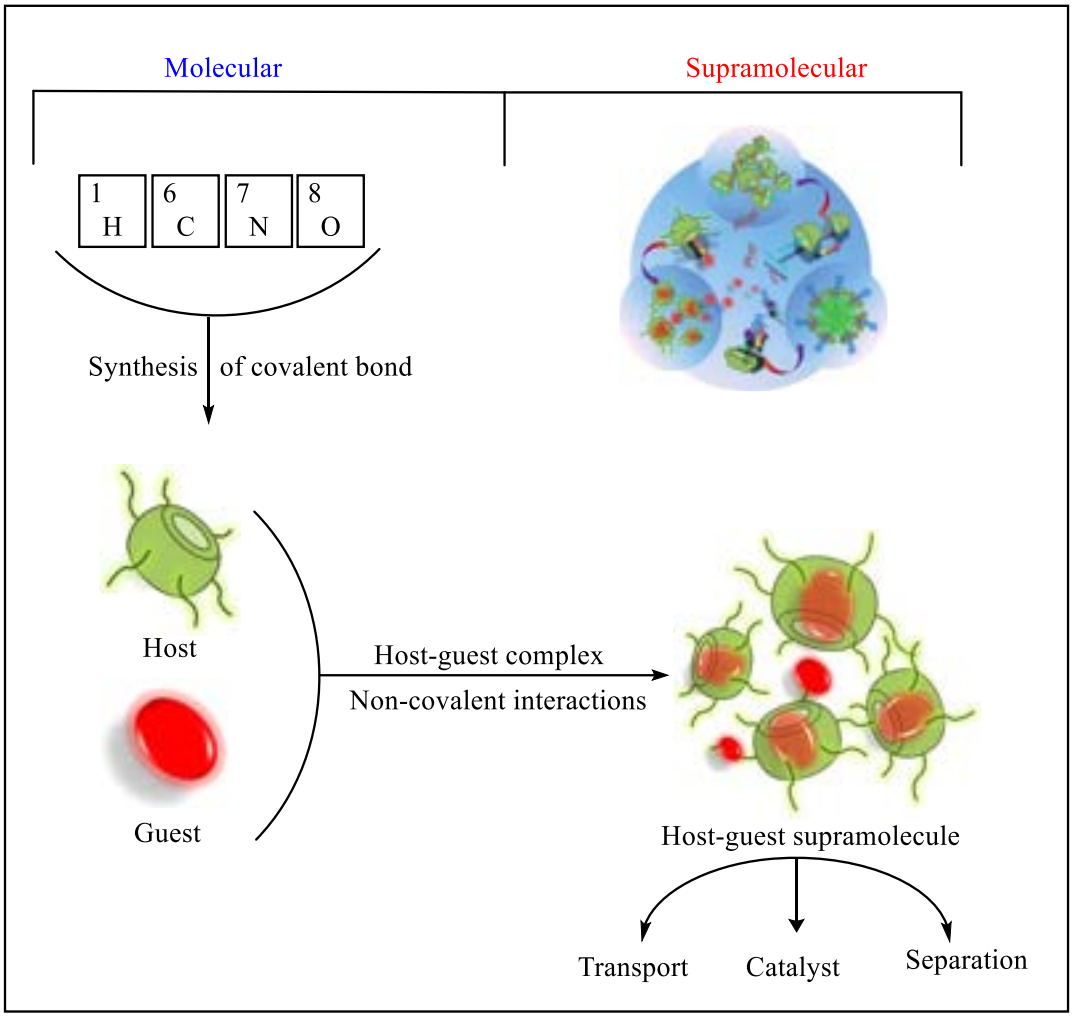

Figure 1.29 Schematic representation of the concept of molecular, supramolecular, and supramolecule assemblies.[84] (Reprinted with permission from the American Chemical Society).

Fischer and Koshland identified enzymes as a well-known complementarity in nature. Donald James Cram (Nobel Laureate) described:

"*…their non-biological equivalents as the 'host', an ion or organic molecule with convergent binding sites, in whose binding site the complex was assembled, and the 'guest' as the ion or molecule, with divergent binding sites, bound by the host*." [85]

The binding site are where the host and guest molecules interact due to their complementary sizes, geometries or general chemical natures.

1.7.1 Supramolecular interactions

The main aim of supramolecular chemists is to regulate and control the way of intermolecular bonds, which Lehn explained as constructing supramolecular cavitands with unique structures and functionalities for specific applications. Supramolecular host-guest complexes are held together *via* non-covalent interactions. The term 'non-covalent' includes an extensive range of attractive and repulsive effects. Non-covalent bonds have inter- and intra-molecular, dipole and ionic, cation-π, hydrogen bonds, hydrophobic, and van der Waals interactions. Covalent single-bond energy values range from 150 kJ mol^{-1} to 450 kJ mol^{-1} and are significantly greater than weaker non-covalent energies ranging between 2 kJ mol^{-1} and 300 kJ mol^{-1} for interionic interactions. These non-covalent interactions in a concerted approach can form a stable supramolecular complex.[86]

1.7.1.1 Dipole and ionic interactions

Dipole and ionic interactions are further classified into ion–ion, ion-dipole, and dipole-dipole interactions based on the coulombic attraction between opposite charges, as shown in Figure 1.30, resulting from the attraction of cation with an anion.[85,86]

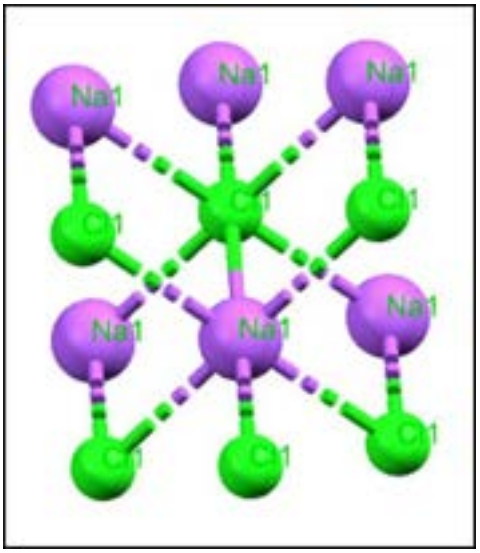

Figure 1.30 Representation of ion-ion interactions in sodium chloride crystal lattice

A partial translation of electron density occurs when two different electronegative atoms are bound together in heteroatomic covalent bonds, leading to the development of polarity among two atoms to form a dipole.

As shown in Figure 1.31a, dipoles have the ability to form coordinate bonds with ions, and this has become the fundamental basis of various inorganic complexes. In dipole-dipole interactions, dipoles interact with adjacent dipoles either perpendicularly or in parallel, as shown in Figures 1.31b and 1.31c.[86]

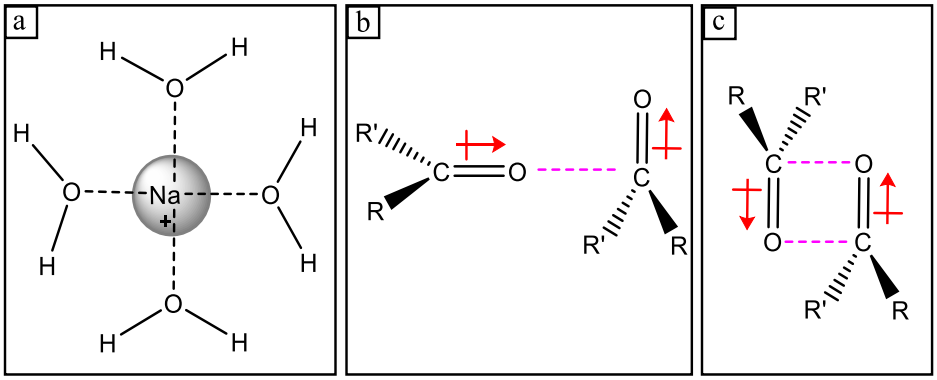

Figure 1.31 Ion-dipole coordinate bond between sodium and water (a), perpendicular dipole-dipole (b), and parallel dipole-dipole interactions between two carbonyls.[86]

1.7.1.2 Inter- and intra-molecular interactions

The construction and regulation of intermolecular bonds are essential to produce supramolecular cavitands for novel functional materials across a wide range of applications. Lehn described that intermolecular bonds could lead to various types at a molecular level during the construction of various supramolecular cavitands. The type of interactions in these describes the supramolecular structures and the novel functions of several supramolecule complexes.[85]

1.7.1.3 Hydrogen-bonds

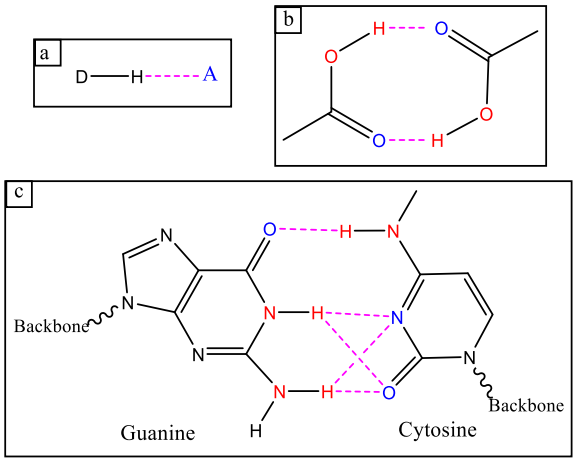

Figure 1.32 Examples of hydrogen bonding between a donor and an acceptor (a), two carboxylic groups, and (c) guanine and cytosine.[86]

Hydrogen bonding is one of the essential bonding among other non-covalent interactions. Hydrogen bonding plays a significant role in the recognition and stability of DNA while developing a double helix between two guanine and cytosine complementary oligonucleotides. One hydrogen attached to a strong electronegative donor (D) oxygen or nitrogen atom bonds to a different electronegative acceptor (A) atom. This is usually represented as D-H...A, as shown in Figure 1.32a.[85,86] For example, Cave *et al*.

demonstrated host-guest interactions of pyridine with pyrogallol[4]arene through hydrogen-bonding interaction, while two pyrogallol[4]arene derivative capsules were held together *via* hydrogen bonding, as shown in Figures 1.33 and 1.34.[87,88]

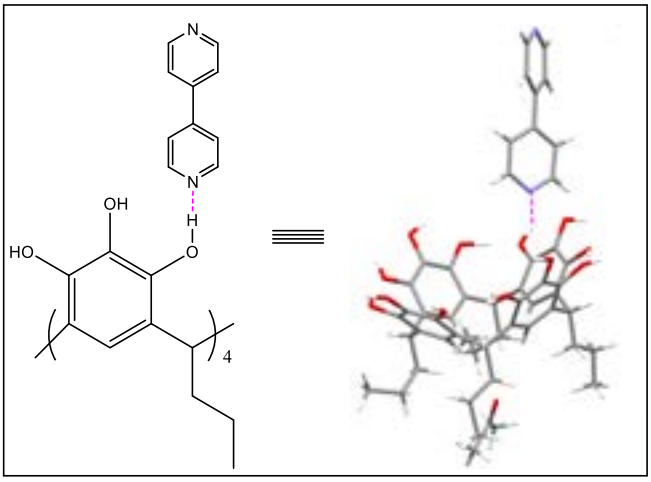

Figure 1.33 Hydrogen bonding interaction between the upper rim of pyrogallol[4]arene derivative and the lower pyridine.[133]

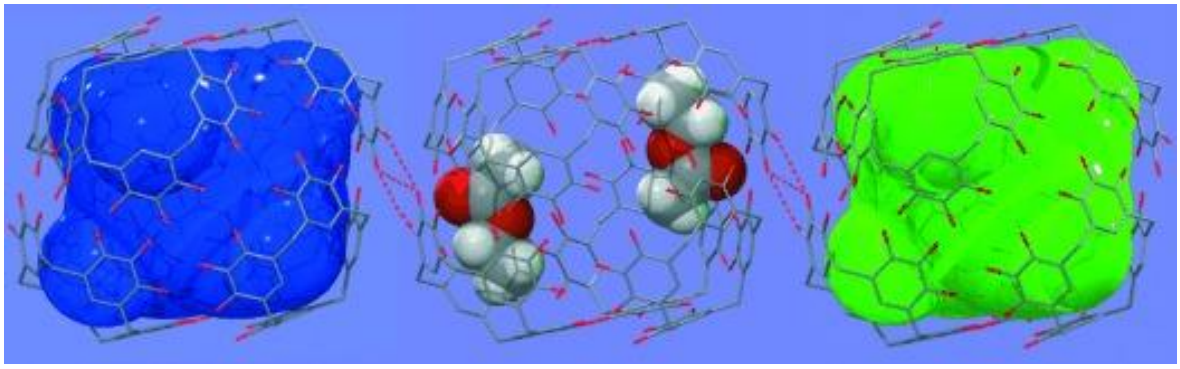

Figure 1.34 Hydrogen-bonding interactions between two nanocapsules of pyrogallol[4]arene derivative.[132]

1.7.1.4 Cation-π interactions

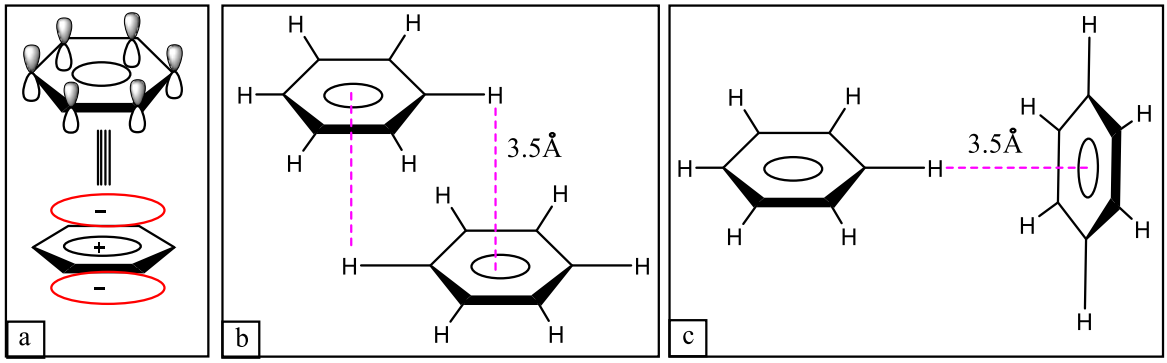

Figure 1.35 π system in aromatic benzene (a), face-to-face π-π interaction, and (c) edge-to-edge interaction.[86]

There is no permanent dipole moment for the electron-rich π system in the aromatic compounds. However, they carry a partial negative charge top and bottom of the aromatic

ring's plane, as shown in Figure 1.35a. Subsequently, it facilitates the system's interaction with ions. Figures 1.35b and c demonstrate the π-π interaction face-to-face and edge-to-face interaction. Cation-π is commonly useful in DNA stacking.[89] For example, cation– π interactions of Cs^+ and Cl^- with *C*-alkylpyrogallol[4]arene and neutral calix[4]resorcinarenes dimer are shown in Figure 1.36.

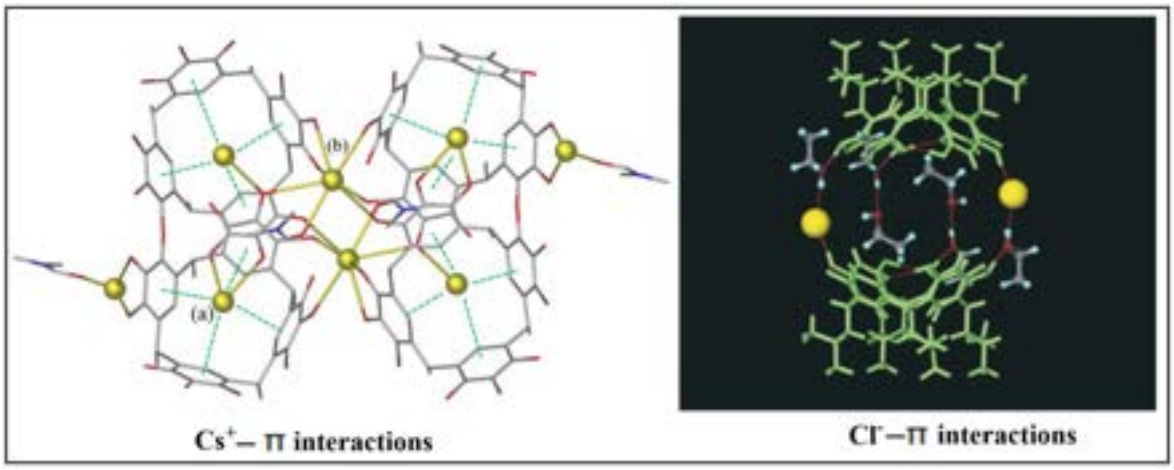

Figure 1.36 Cation– π interactions of Cs^+ and Cl^- with C-Alkylpyrogallol[4]arene and neutral calix[4]resorcinarenes dimer. The $Cs^+$and Cl^- counterions are shown in yellow colour .[90,91]

1.7.1.5 Van der Waals interactions

Van der Waals interactions occur due to a polarisation of the electron cloud arising from the close proximity of an adjacent nucleus, leading to a weaker attraction force. Traditionally, these interactions offer attractive interaction for polarisable soft species with interaction energy proportional to the surface area of contact, as shown in Figure 1.37. Due to their non-directional and unspecific, they have a restricted range in the construction of supramolecular cavitands for selective host-guest complexation.[86,92]

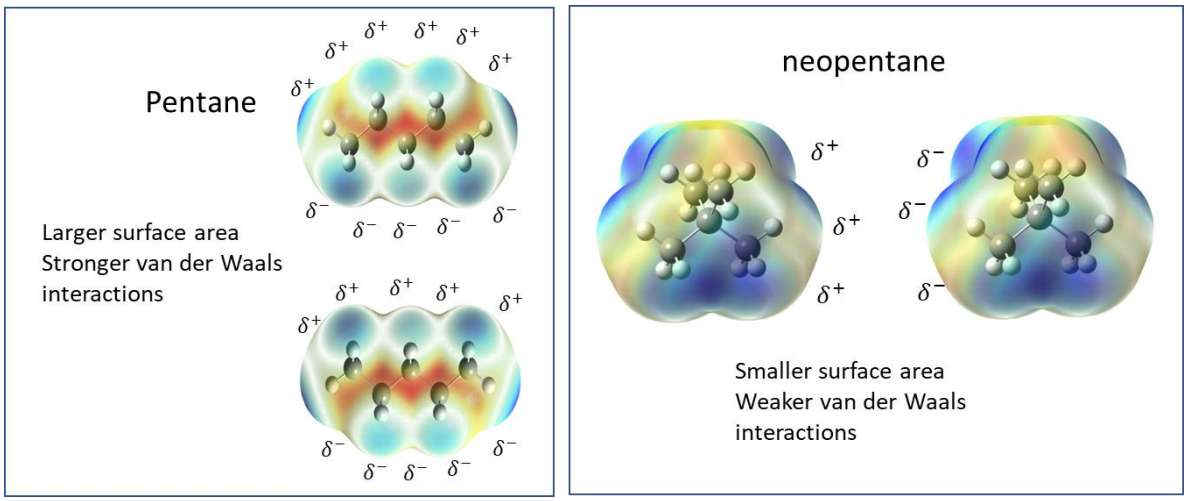

Figure 1.37 van der Waals interactions of pentane and neopentane.

However, van der Waals interactions are essential in supramolecular chemistry in forming inclusion compounds, where the organic molecules are loosely incorporated in the crystal lattices or molecular cavities. For example, the inclusion of toluene in the *p*-tert-butylcalix[4]arene cavity is shown in Figure 1.38.[93]

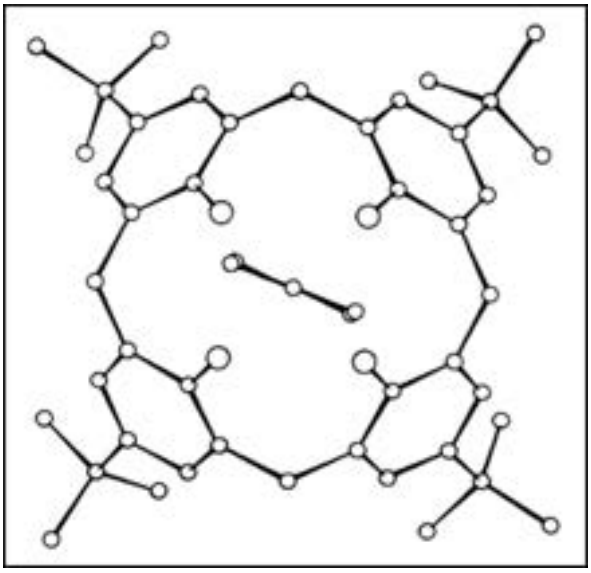

Figure 1.38 van der Waals interactions of toluene with p-tert-butylcalix[4]arene cavity.[93]

1.7.1.6 The hydrophobic effect and Solvation effect

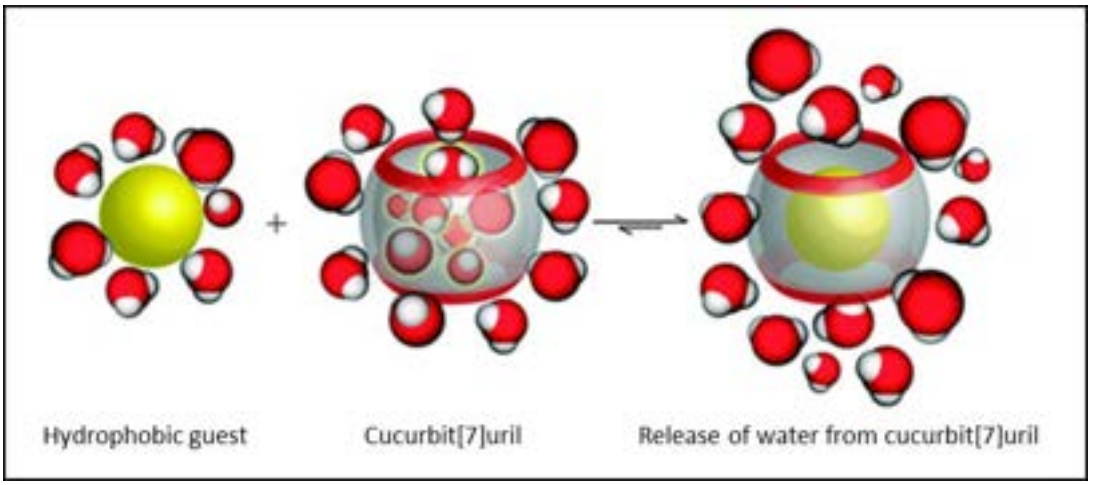

Figure 1.39 Schematic representation of release of water molecules from CB7 after binding hydrophobic guest molecules.[94] (Reprinted with permission from the Royal Society of Chemistry)

The solvation effect occurs because of the interaction of polar solvents with molecules using electrostatic interactions. This solvation effect plays a crucial role in chemical binding and self-assembly recognition. Due to these features, solvents can be carefully incorporated into the supramolecular cavitands. This could also be termed a hydrophobic effect if water is employed in the system, as shown in Figure 1.39. For example, the hydrated guest molecule is incorporated into the host with solvated properties.

Subsequently, the host-guest complex will be formed. This significantly releases nonpolar entities from an aqueous solution.[85,86]

1.8 Macrocyclic bound silica stationary phases

Due to the limitations associated with the use of silica-bound chromatographic stationary phases, such as single mode of interactions, the importance of the development of novel stationary phases for RP-HPLC focus on three primary aspects: (i) stationary phases with long-term stability to pH and temperature; (ii) novel ligands with multiple interaction sites to improve the selectivity of the stationary phase, specifically for isomeric analytes, and (iii) the development of novel synthetic protocols for efficient functionalization of the surface of chromatographic silica.[95]

Supramolecular host-guest recognition is closely associated with selective separation in liquid chromatography (LC) by creating a host with multiple recognition sites for the guest analytes to improve separation selectivity.[96] Over the last decade, a wide of supramolecular cavitands with selective functionalities have been explored as desirable hosts to study the chromatographic separation selectivity for small molecular analytes. Due to these specific characteristic features, developing supramolecular chromatographic stationary phases for multiple mode of interactions *via* host-guest interactions has become one of the active research areas in separation science.[97]

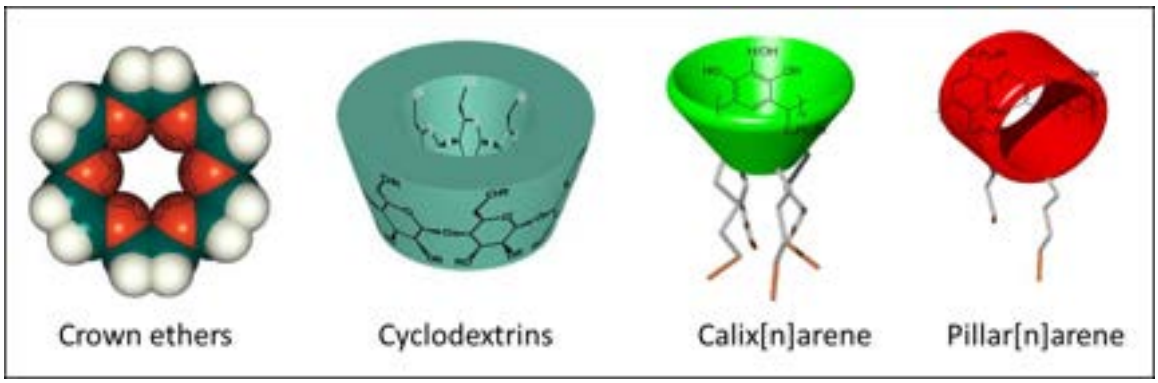

Figure 1.40 Graphical representation of supramolecular macrocycles.[98-99] (Reprinted from permission of the American Chemical Society).

As shown in Figure 1.40, organic supramolecular macrocycles have attracted researchers' attention to develop new stationary phases, particularly crown ethers,[98] cyclodextrins,[99] calix[n]arenes,[100] and pillar[n]arenes.[101] These supramolecular cavitands bound to stationary phases exhibit superior column efficiency and selectivity to various analytes compared to RP-C_x (x= 18, 8, 4) columns. The involvement of multiple recognition motif interactions between aromatic rings, polar groups and heteroatoms of supramolecular cavitand and guest analytes, facilitate host-guest interactions, *i.e.* π-π, hydrogen bonding,

dipole-induced dipole, and some specific interactions due to the supramolecular structure and confirmational rigidity.[102]

The design and synthesis of new functional supramolecular host cavitands and their subsequent applications in chromatography have demonstrated efficient separation efficiency and selectivity over a range of analytes and this subsequently advanced the supramolecular chemistry and chromatography science.

1.8.1 Crown ethers

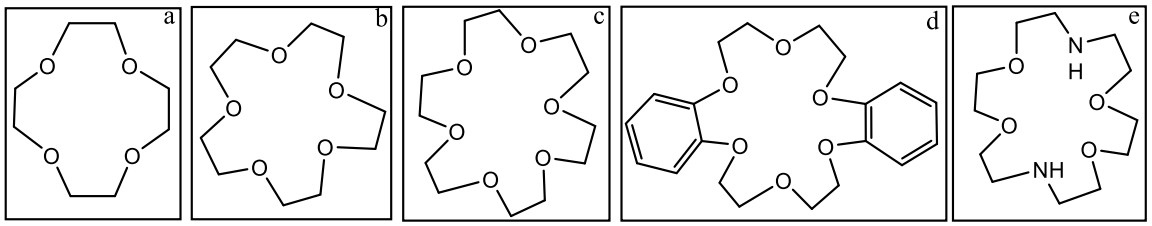

Figure 1.41. Common crown ethers: 12-crown-4 (a), 15-crown-5 (b), complexation of 18-crown-6 with potassium(c), dibenzo-18-crown-6 (d) and aza-crown ether (e).

As shown in Figure 1.41, crown ethers have been widely used since their discovery to extract various metal ionic species due to their ability to form host-guest complexes with metal ions, as shown in Figure 1.42.[103] The size of crown ethers cavity plays a vital in the selective host-guest complexation. Crown ethers of various sizes enable various specific interactions with metal ions. In the crown ether, the host-guest interaction occurs due to the ion-dipole interactions between the cation and the oxygen in the cyclic polyether.[104] As shown in Figure 1.43, crown ether and their derivatives can form host-guest complexes with several guest naphthalene diimide-based guest molecules.

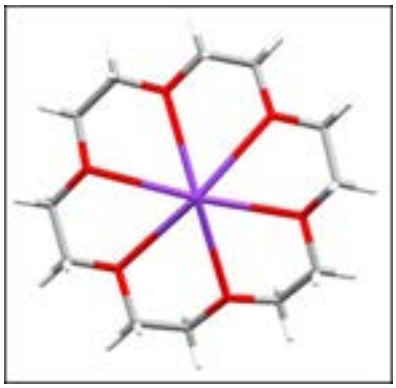

Figure 1.42 Complexation of Potassium with Crown ether.

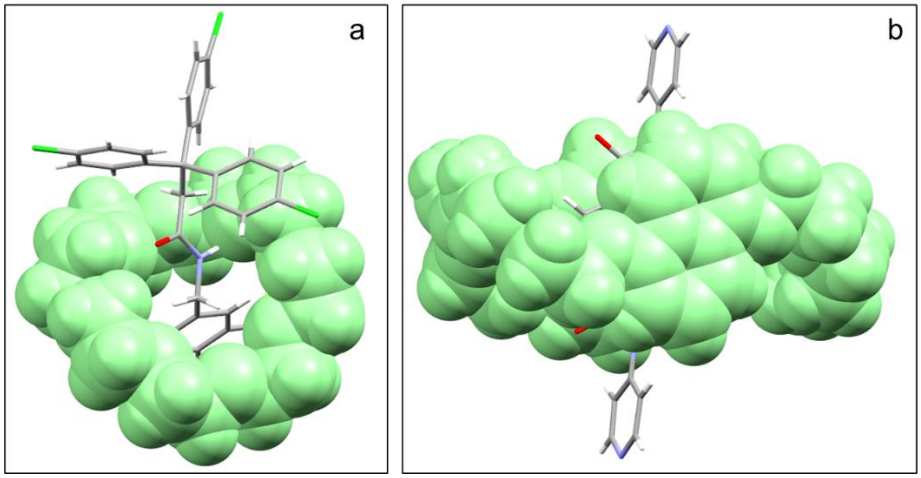

Figure 1.43 Host-guest complexation of crown ether–amide-axle rotaxanes (a) and crown ether derivative with naphthalene diimide-based guest (b).[104]

The crown ethers were extensively used as chromatographic stationary phases *via* polymerization and immobilization of crown ethers on the surface of solid chemically inert substances. Polymeric crown ethers have high chemical resistance, temperature, and radiolysis characteristics. Crown ethers bonded stationary phases are used as packing material in capillary gas chromatography, due to their high coating efficiency and distinctive separation selectivity for polar analytes having similar boiling points. In addition, chromatographic techniques with chiral stationary phases *via* a chiral crown ether selector bound to silica have been used for chiral separation.[105]

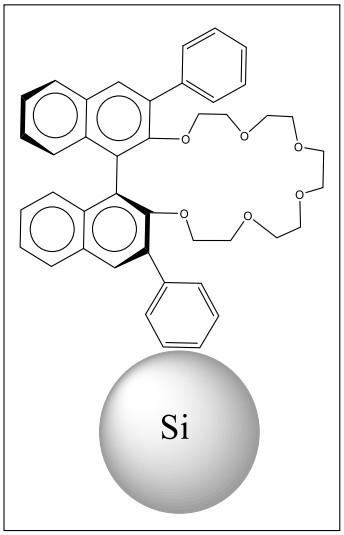

Figure 1.44. Coated chiral crown ether-based Crownpak CR(+) on silica.[106]

In the 1970's, Sogah and Cram developed the first chiral stationary phase particles (CSPs) based on crown ethers.[107] However, due to their low chromatographic performance, the CSPs have not attracted commercial availability. Subsequently, In 1987 Shinbo and co-workers developed the first commercial CSPs based on crown ether by coating the crown

ether on ODS silica support to resolve chiral primary amines and amino acids. This chiral CSP was commercially available as CROWNPAK CR, as shown in Figure 1.44.[108.]

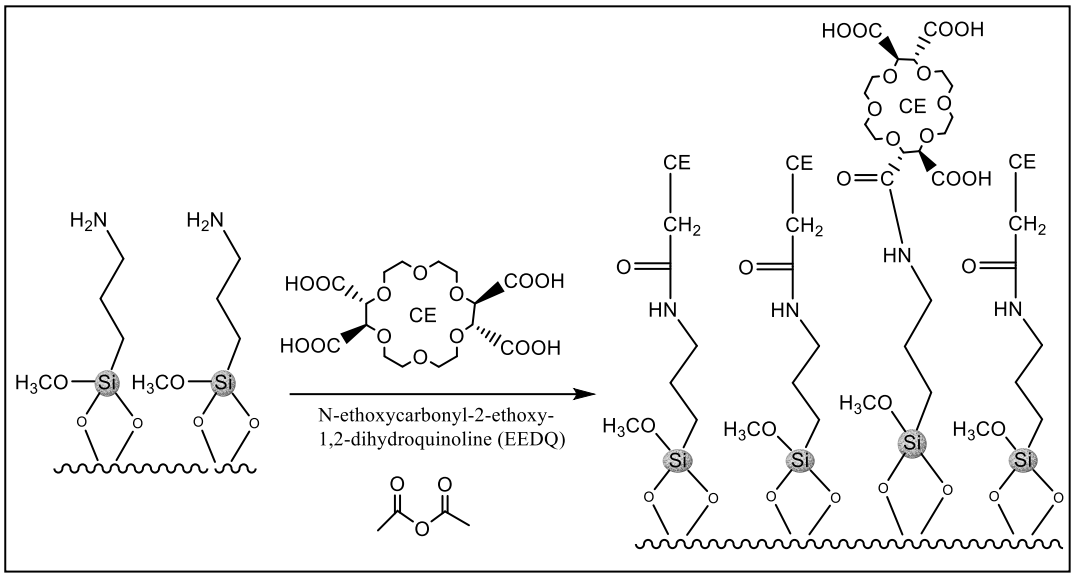

Figure 1.45 Synthesis of the chiral stationary phase using (+)-18-crown-6-2,3,11,12-tetracarboxylic acid via *amide bond linkage.*[123]

However, at the time the mobile phase solvent systems were limited due to the dynamic coating process.[109] Subsequently, several researchers reported a wide variety of crown ether and its derivatives chemically immobilized on a chromatographic silica support. Machida and co-workers reported CSPs utilizing a chiral selector, (+)-18-crown-6-2,3,11,12-tetracarboxylic acid, and subsequently attached to chromatographic silica gel *via* an amide linkage, as shown in Figure 1.45.[110] Hyun and co-workers reported a silica-bound CSPs *via* a modified bonding process.[111] Subsequently, Bradshow developed CSPs utilizing metacyclophane framework comprising a pyridine moiety.[112]

Several crown ether selector-bound stationary phases[113-118] have been designed to functionalize on the surface of chromatographic silica, as shown in Figure 1.46, for a wide range of various racemic mixtures resolution of chiral amino compounds such as amines, amino alcohols, and amino acids *via* HPLC,[119] gas chromatography (GC),[120] ion chromatography (IC),[121] and capillary electrochromatography (IEC).[122]

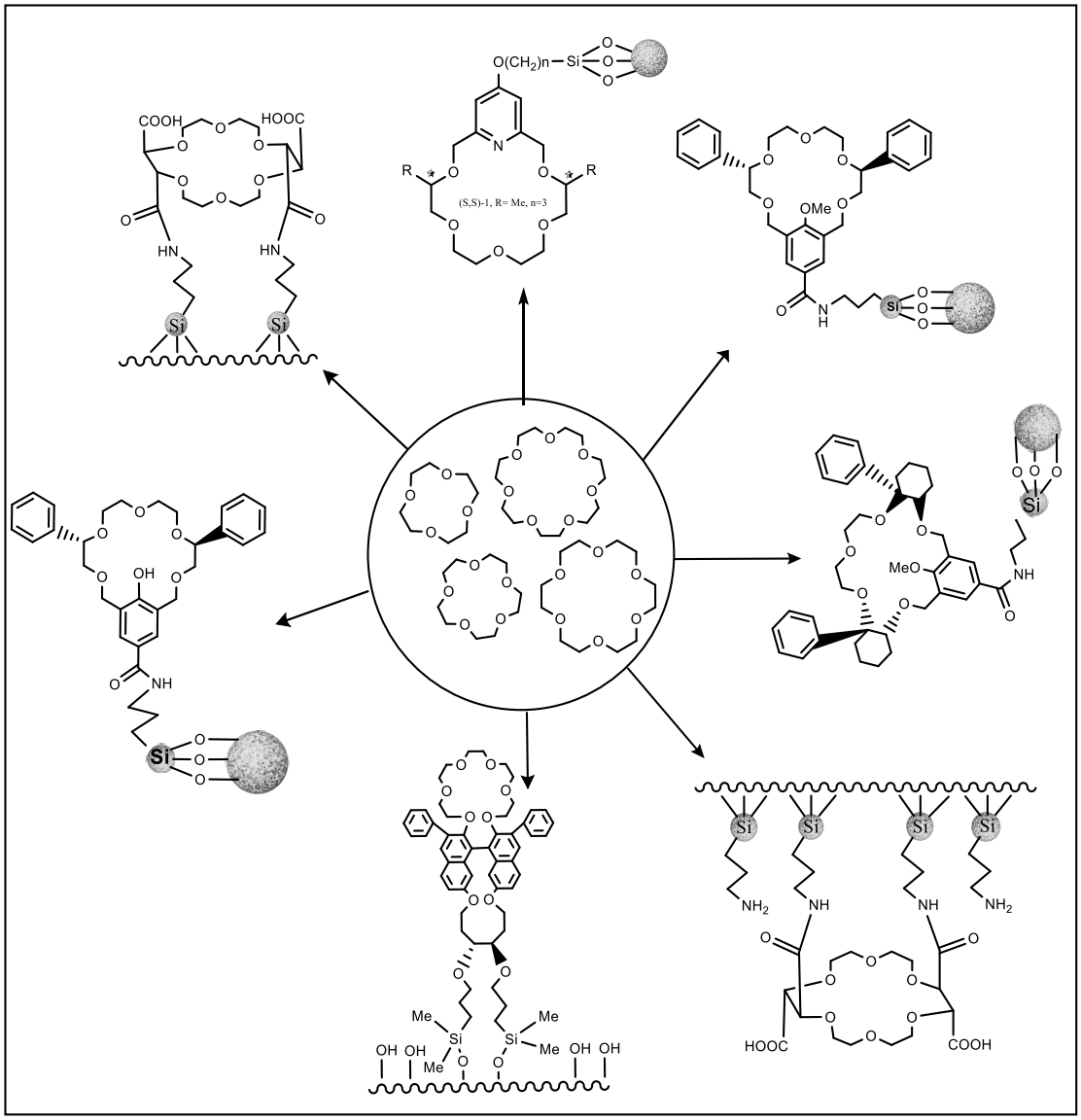

Figure 1.46 Examples of crown ether derivatives bonded covalently to chromatographic silica.

1.8.2 Cyclodextrins

Enzyme-modified starch derivatives, toroidal-shaped cyclodextrins are naturally occurring cyclic oligosaccharides that consist of *D*-glucopyranose units (usually 6, 7 and 8) bridged by α-1,4-glycosidic linkages as shown in Figure 1.47. The three significant CDs are *α*-CD, *β*-CD, and *γ*-CD containing the six, seven, and eight glucose units, respectively.[124]

Cyclodextrin's inner cavity is hydrophobic due to the glycosidic oxygen bridges and hydrogen atoms. The outer cavity is hydrophilic due to hydroxyl groups with all three classes of cyclodextrins being water-soluble. These characteristics allow cyclodextrins to accumulate hydrophobic substances in the cavity *via* non-covalent reversible inclusion complexes, as shown in Figure 1.48.

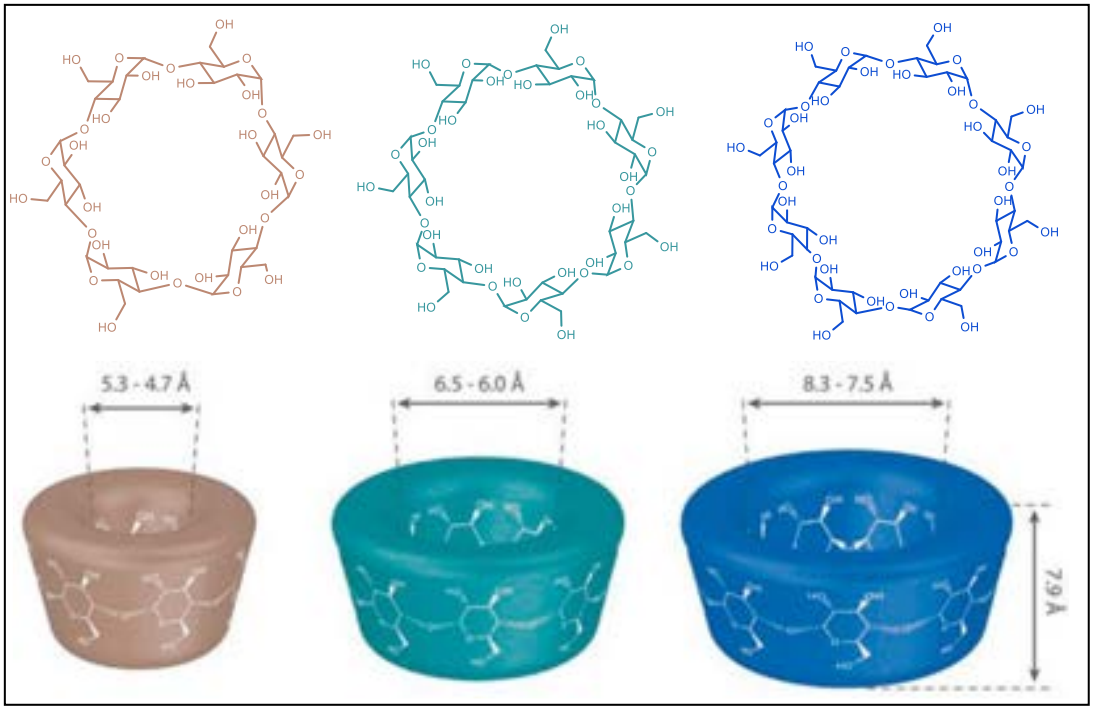

Figure 1.47. The structures of -α, β, and γ-cyclodextrins.[124]

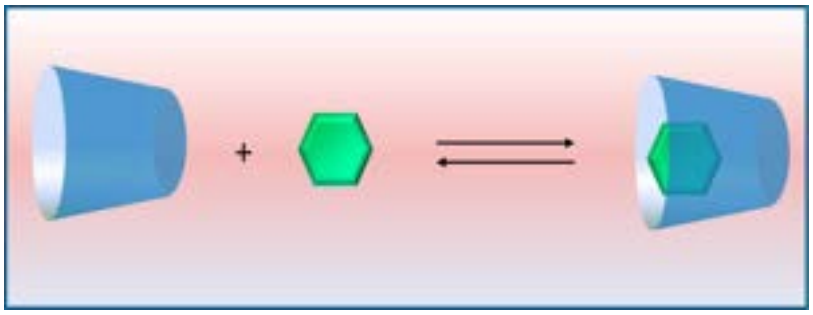

Figure 1.48 Graphical representation of Cyclodextrin host-guest complexation with the guest molecule. [124] *(Reprinted with permission from the American Chemical Society)*

Cyclodextrins are very widely used in applied analytical chemistry due to their host-guest complex formation or supramolecular recognition process. Due to these host-guest complexation abilities of cyclodextrins, as shown in Figure 1.49, their subsequent utilization for a wide range of analytical applications has become a significant research area. Currently, cyclodextrins are functional materials for host-guest molecular recognition analytical methods, including separation science, spectroscopic techniques, electroanalyses, single-molecule sensing, and clinical diagnostics. These distinctive structural features allow cyclodextrins to make inclusion complexes with chiral and achiral molecules.[125]

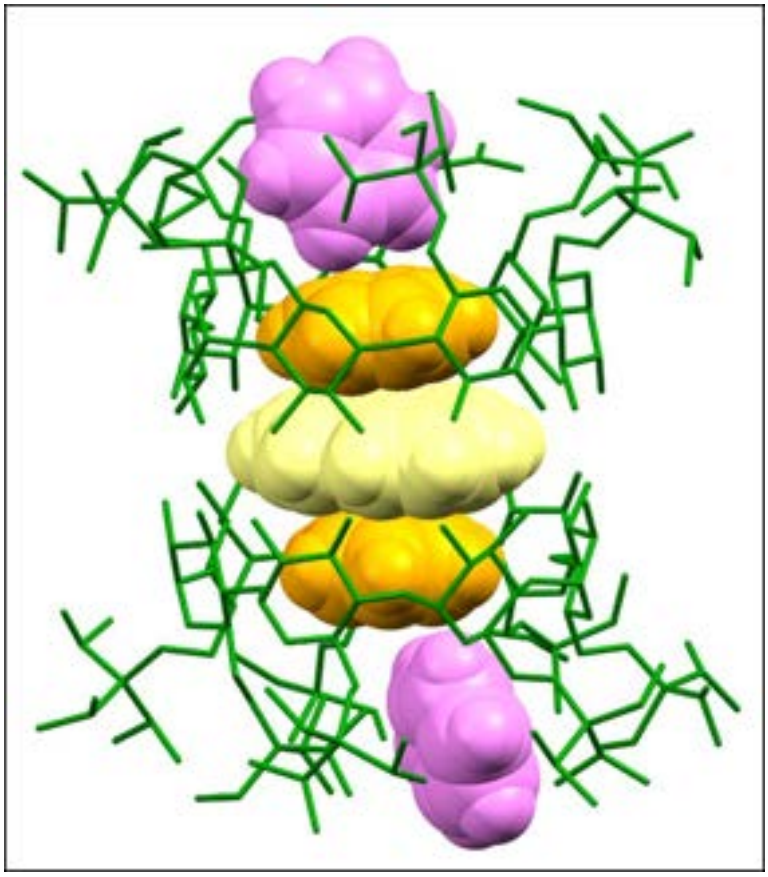

Figure 1.49 Inclusion complex of heptakis(6-O-triisopropylsilyl)-β-cyclodextrin (TIPS-β-CD) with pyrine in benzene and cyclohexane.[126]

Cyclodextrins have been extensively utilized in different separation techniques, such as chromatographic methods, electrophoresis, isotachophoresis, isoelectric focusing, microdialysis, separation on hollow fibers, foam flotation enrichment, solid- and liquid-phase extractions, separation through liquid and composite membranes, applications in molecularly imprinted polymers, etc.[127] Undoubtedly, one of the significant useful analytical applications of CDs are their use in the enantiomeric separation.[127]

Several factors influence the effectiveness of cyclodextrin chiral recognition, such as the chemical moiety at the inner and outer cavities of cyclodextrins. In cyclodextrin-dependent chiral separations, the host-guest complexations are not only a driving force. This was observed and reported as the cumulative effect of several reversible non-covalent interactions.[128] Armstrong described the enantio-recognizing properties of CDs mainly due to the highly ordered, stereochemically D-glucose units forming the macrocycle. It is also explored that the chiral glucose units in chair confirmation, the clockwise-directed secondary hydroxyl groups, and the anticlockwise-directed primary hydroxyl groups play a significant role in the enantiomeric recognition with guest molecules.[129] Armstrong also proposed two primary enantioselective retention mechanisms. In the normal phase eluent mode, the separation of the chiral analyte occurs due to the cumulative effect of hydrogen

bonding and dipolar interactions. In reverse-phase elution mode, the separation of analytes occurs due to hydrophobic interactions. He also reported that hydrogen bonding and steric interaction at the mouth of cyclodextrins significantly impact chiral recognition.[129]

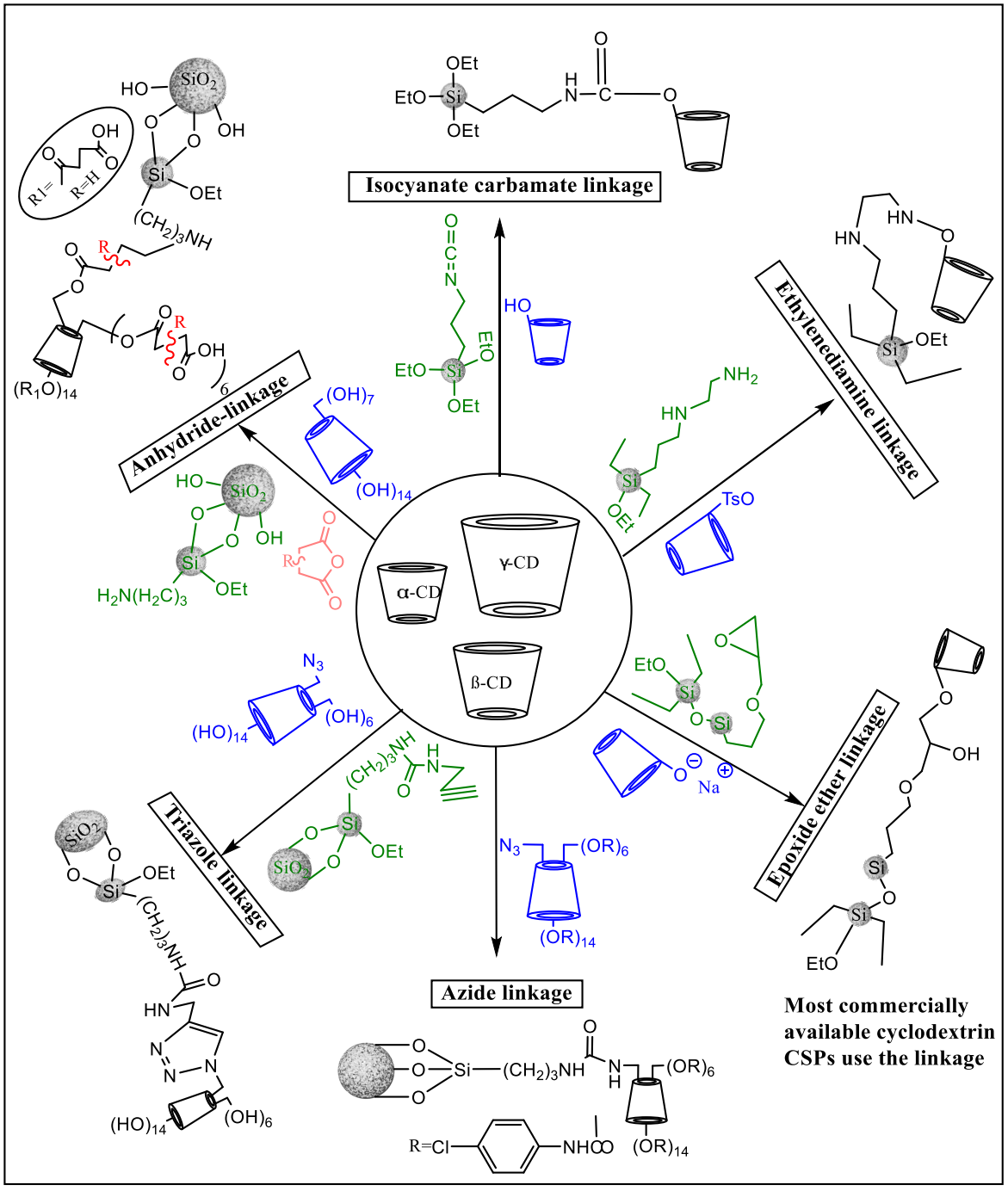

Figure 1.50 Chemical bonding of cyclodextrins to chromatographic silica.

Several novel cyclodextrin derivatives with selective functional groups have been used widely to study host-guest interactions as chiral stationary phase (CSP) selectors or as mobile phase additives in the chiral resolution of racemic mixtures in pharmaceutical,

agrochemical, and food industries using HPLC, supercritical fluid chromatography (SFC), gas chromatography (GC), capillary electrochromatography (CEC) and capillary electrophoresis (CE).[130] As shown in Figure 1.50, several cyclodextrin chiral stationary phases have been synthesized by supporting cyclodextrin ligands on the surface of chromatographic silica *via a* physical coating,[131] or a chemical loading based on ether,[132] urea,[133] amino,[134] triazole,[135] anhydride,[136] and other linkages.[137]

Several groups have successfully utilized to bound cyclodextrin cavitands to chromatographic silica particles. Initially, Amine linkages were employed for the first bound cyclodextrins to silica gel. However, the amine linkages proved to be deficient. Subsequently, the epoxide linkage was the first successful linkage. This epoxide linkage offers a free of nitrogen atoms and fewer hydrogen bonding groups. The epoxide linkage has been used to bound the cyclodextrins to chromatographic silica for the most commercially available chiral stationary phases. There are several factors play an essential role in the cyclodextrin-bound silica stationary phases, such as the particle size of silica, the linkage between the cyclodextrins and silica, the availability of free silanol groups, chemical moieties of functionalized cyclodextrins. Several commercially available cyclodextrin-derivatized stationary chromatographic phases are available, including Cyclobond, ChiraDex, Nucleodex for selective enantio-recognitions.[122]

The monosubstituted CDs, pure CD derivatives bearing various substituents, are widely used cyclodextrins in preparing stationary phases. The cyclodextrin chiral stationary phases are typically native cyclodextrin CSPs, derivatized cyclodextrin CSPs and aromatic derivatized cyclodextrin CSP. The majority of native cyclodextrin CSPs are effective with polar organic eluents. The difference in the retention, selectivity and resolution within native CSPs are due to differences in the size of the α, β, and γ-cyclodextrins and analytes interactions with the hydroxyl groups which inhabit different spaces and geometries on the cyclodextrin. Native cyclodextrin CSPs have shown significant enantiomeric resolution of many compounds such as optical, geometrical , and structural isomers, as shown in Figure 1.51, including metallocene enantiomers, underivatized amino acids, glycyl di- and tri-peptides, racemic beta-adrenergic blocking agents, enantiomers of dinitrophenyl amino acids, enantiomeric and diastereomeric terpenic alcohols and many more.[138]

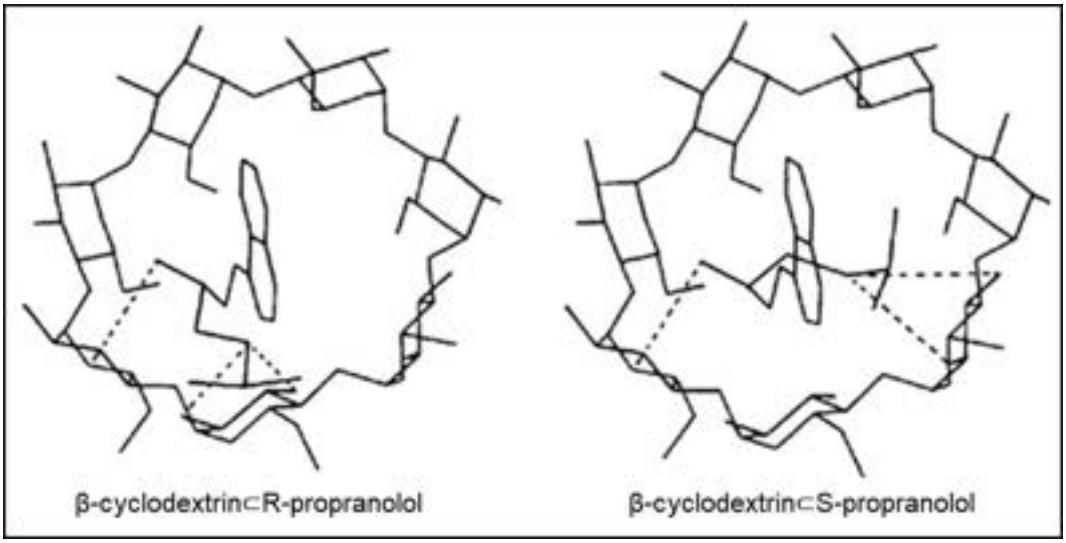

Figure 1.51 Inclusion of complex β-cyclodextrin with R-propranolol (a) and S-propranolol (b).[139]

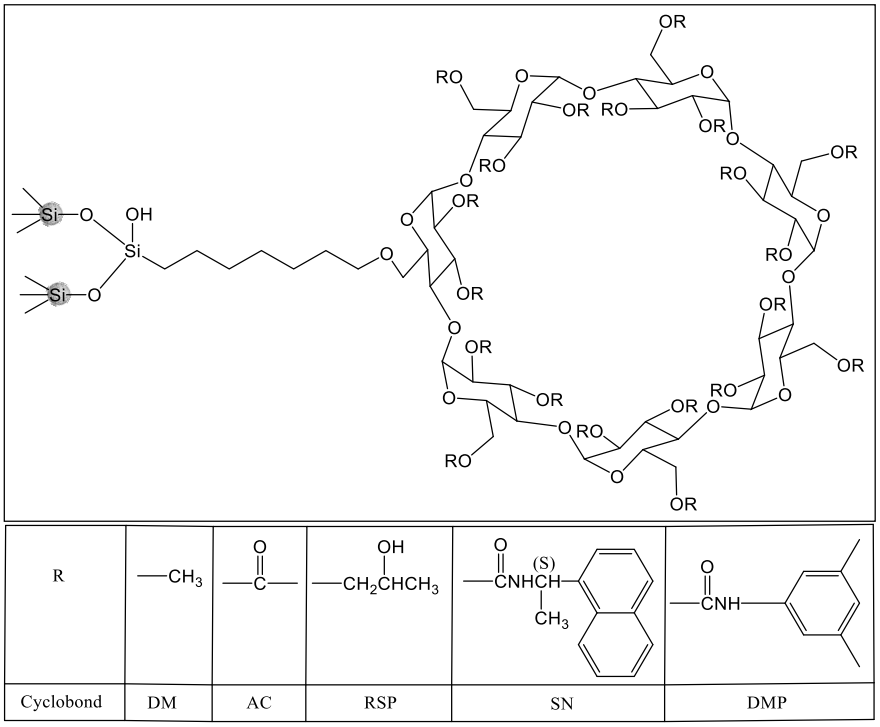

Figure 1.52 General structures of Cyclobond silica stationary phases.[140]

Derivatized cyclodextrin CSPs, as shown in Figure 1.52 such as 2,3-dimethylated-β-cyclodextrin (Cyclobond I DM) and acetylated β-cyclodextrin (Cyclobond I AC) are less effective as chiral selectors. Still, they have enantioselectivity for particular groups of molecules that are poorly resolved on native cyclodextrin chiral stationary phases. However, hydroxypropyl derivatized β-cyclodextrin (Cyclobond I RSP) and the naphthyl-ethylcarbamolyated-β-cyclodextrin (Cyclobond I-RN and SN) CSPs are more effective in reverse phase mode. Among all derivatized cyclodextrin CSPs, hydroxypropyl derivatized β-cyclodextrin (Cyclobond I RSP) is the most broadly applicable stationary phase. Chiral

hydroxypropyl moieties derivatize the seven hydroxyl groups. Subsequently, this allows each group as an extra stereogenic centre in the derivatized cyclodextrin molecule.[138.140]

Aromatic derivatized cyclodextrin CSPs are more effective in normal phase mode, and these contain an aromatic group linked to the secondary hydroxyls of the CDs cavity *via* a carbamate linkage. The commercially available stationary phases of this type are dimethylphenylcarbamate-β-cyclodextrin and naphthylethylcarbamate-β-cyclodextrin.[138]

1.8.3 Calix[n]arenes

Calix[n]arenes are considers to be a third-generation supramolecular cavitand host after cyclodextrins and crown ethers. They consist of phenolic rings linked *via* methylene spacers in meta positions to each other, as shown in Figure 1.53. Due to the ease of chemical functionalization of the lower and upper rim, and the cavity size, various methods for the functionalization of calixarenes have been developed, and subsequently, several calixarene derivatives have been reported to study the supramolecular host-guest interactions, as shown in Figure 1.54.[141]

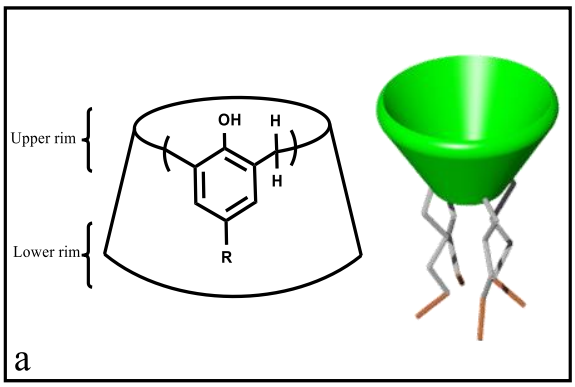

Figure 1.53. Calixarene monomer structure and graphical representation of calixarene cavity with pendant chains.

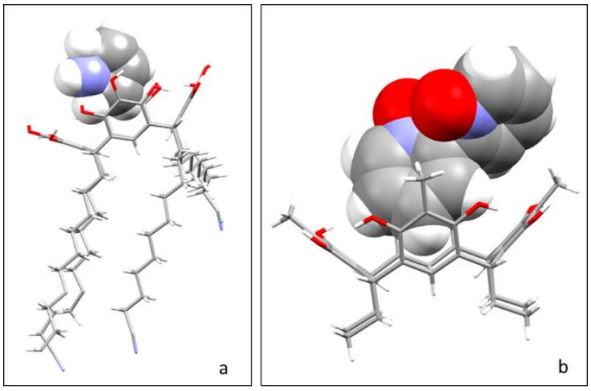

Figure 1.54 Host-guest complexation of pyridinium with cyano-footed pyrogallol[4]arene (a) and C-Ethyl-2-methylresorcinarene and aromatic N,N'-Dioxides.[142]

The calix[4]arene macrocycle has four characteristic conformations. The first cone confirmation holds all aryl groups in *syn* position. The partial cone confirmation contains one aryl position in *anti-syn* to the other three aryl positions. The 1,2-alternative confirmation has adjacent pairs of aryl groups in *anti-syn* and *syn* positions. The last 1,3-alternative consists of *syn* to *anti-syn* aryl groups, as shown in Figure 1.55.[143]

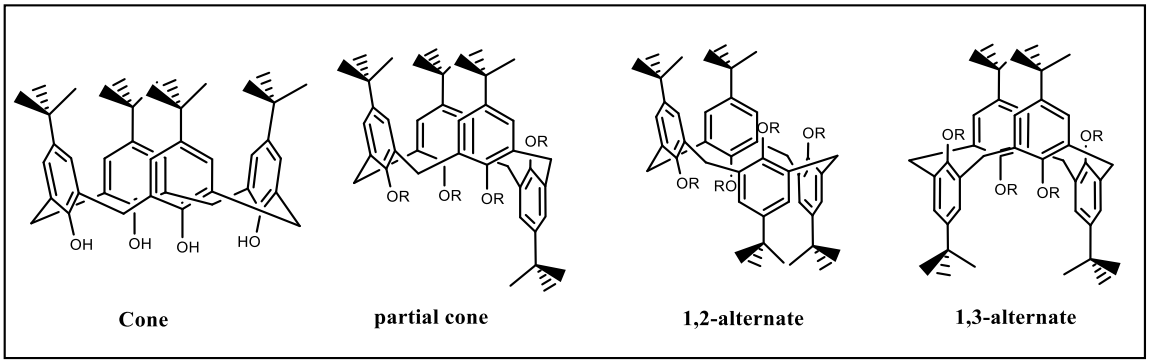

Figure 1.55. Different conformers of calixarenes.

Calixarenes have excellent reversible complexation ability with ions and neutral molecules. The confirmation of calixarene functional moieties, the number, and the nature of additional groups play an essential role in ion-binding properties.[91] Donald Cram (Nobel Laureate in Supramolecular Chemistry-1987) described the host-guest relationship as:

"…involves a complementary stereo electronic arrangement of binding sites in host and guest molecules. Complexes are comprised of two or more molecules, or ions held altogether in distinctive structural relationships by electrostatic forces other than those of full covalent bonds".[144,145]

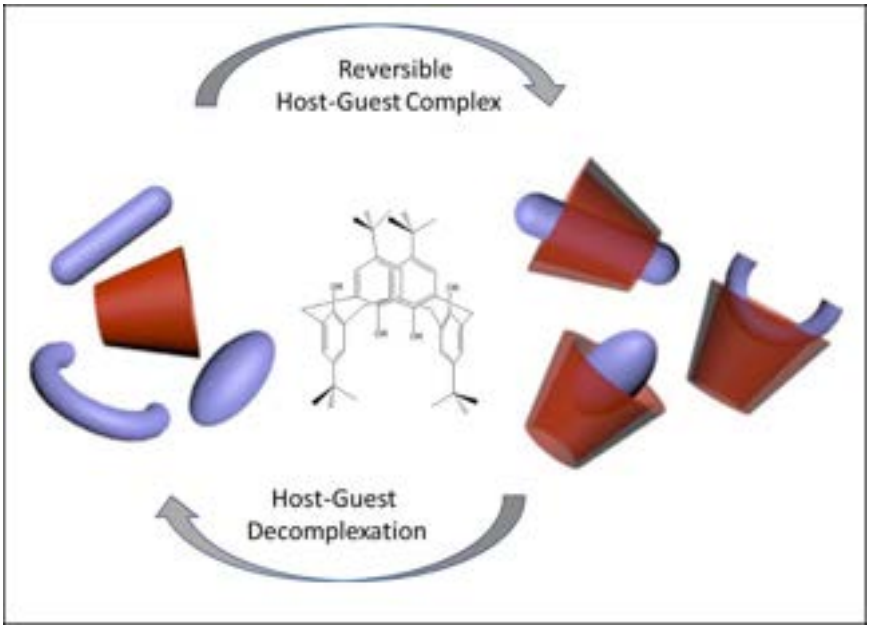

Figure 1.56. Calixarene reversible host-guest complexation with guest molecules and decomplexation of host-guest system.[147](Reprinted with permission from Elsevier).

Due to these characteristic host-guest complexation features, calixarenes are widely employed in purification, chromatography, catalysis, enzyme mimics, ion-selective electrodes, phase transfer, transport across membranes, ion channels, and self-assembling monolayers.[146]

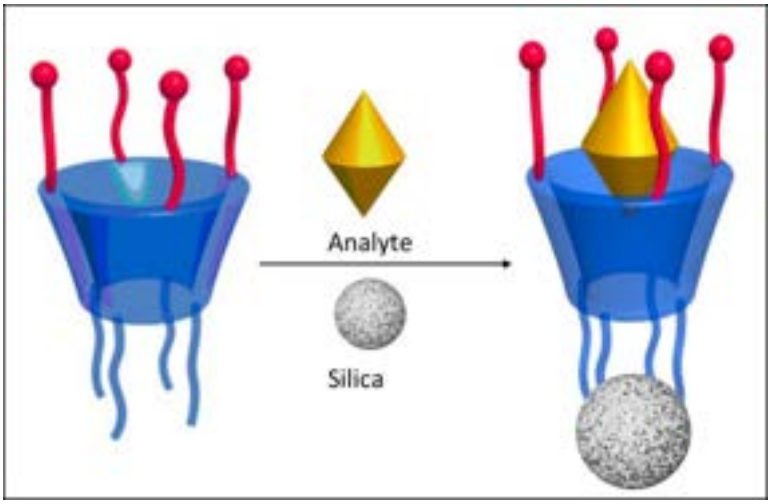

Figure 1.57 Graphical representation of host-guest interactions on surface of silica-bound calix[n]arene statioanry phase.[147] (Reprinted with permission from American Chemical Society)

Calixarenes have attracted many researchers' attention as sorbent or stationary phase in sorption and chromatography due to their reversible complexation abilities. Several functionalized calixarene derivatives in the cone confirmation have been extensively studied as selectors in LC, as shown in Figure 1.56 and 57.[147] Calixarene derivatives have been obtained by (a) modifications of calixarene conformations, (b) the chemistry of functional groups, (c) functional substituents of the upper and lower rims of calixarenes, (d) the ring size of calixarene, and (e) the type of spacer to bond the calixarenes on the surface of silica gel.[147]

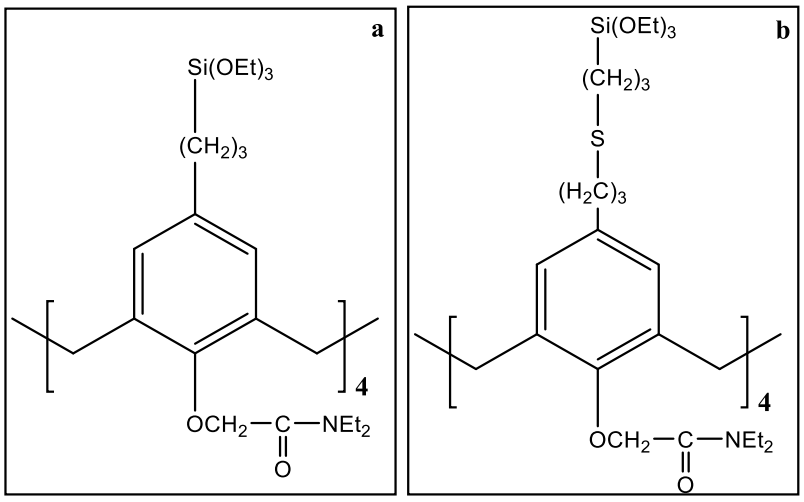

Figure 1.58. Triethoxysilyl derivatives of (a) tetraethyl p*-n-propylcalix[4]arene tetraacetate and (b)* p*-di-n-propylsulphidecalix[4]arene tetraacetyldiethylamide.[147]*

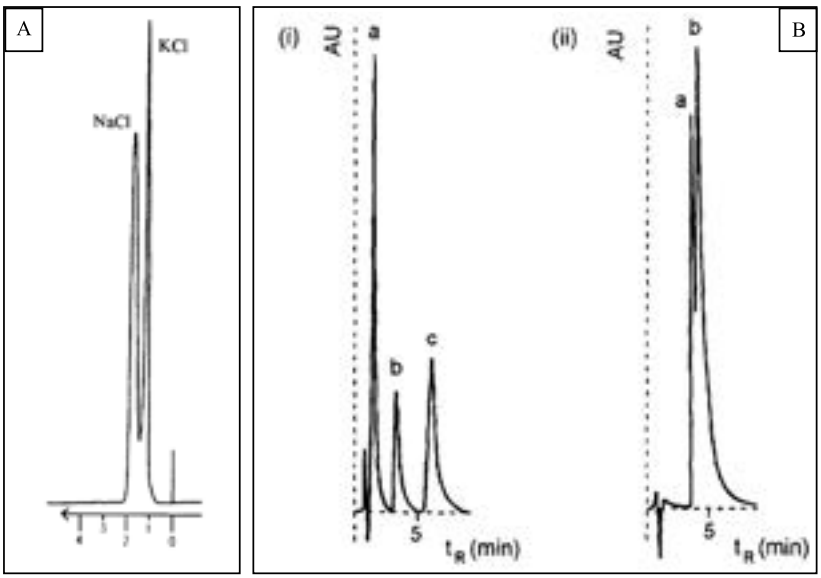

Figure 1.59. Chromatographic separation of (A) NaCl and KC1 on a silicabonded calix[4]arene tetraamide column (5 mM) mobile phase: H_2O; flow-rate:1.0 ml min^{-1}; Detector:conductivity detection. (B) the hydrochloride salts of:(i) (a) L-aspartyl-L-phenylalanine methyl ester, (b) β-alanine ethyl ester and (c) L-tryptophan methyl ester. (ii) (a) L-Phenylalanine ethyl ester and (b) L-phenylalanine methyl ester. (Mobile phase:20% ACN-H_2O; flowrate:1 ml min^{-1}.[147] (Reprinted with permission from Elsevier).

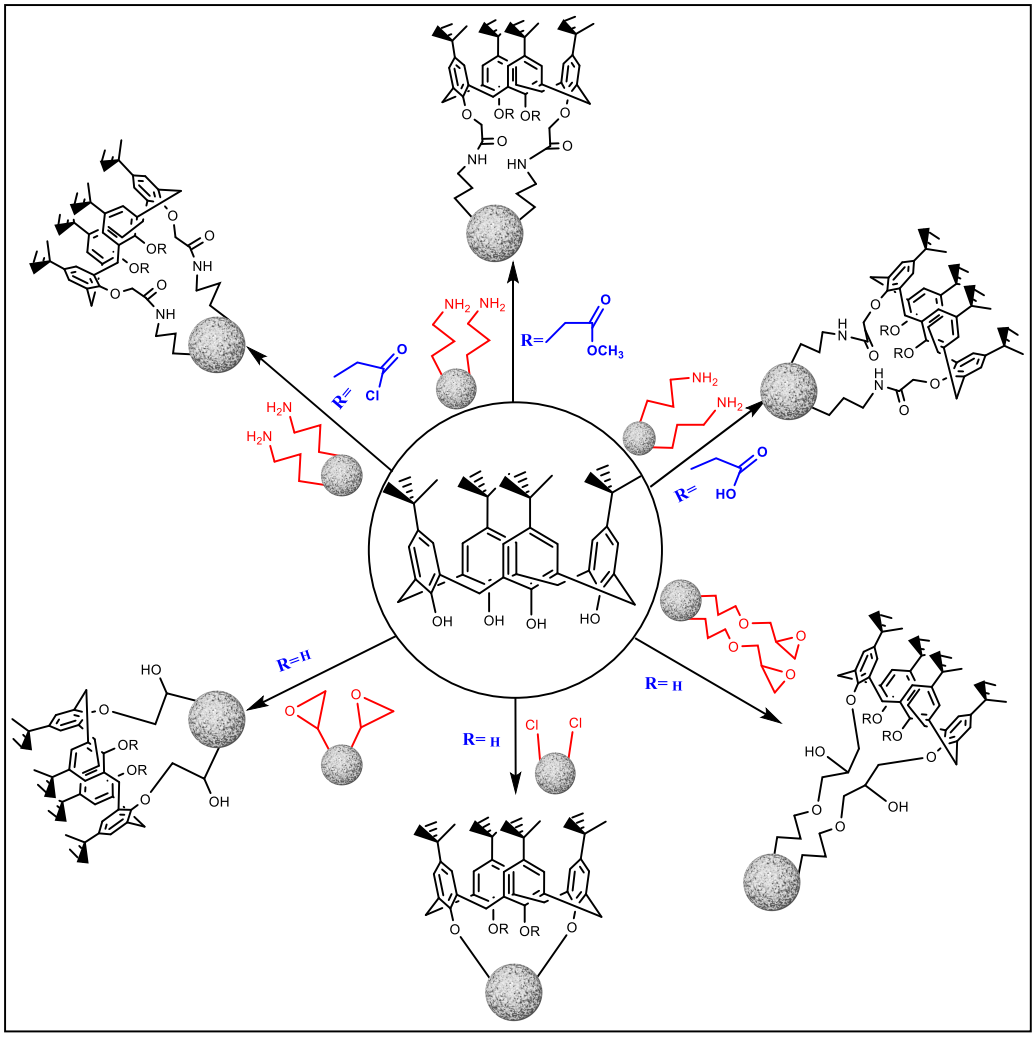

Figure 1.60. Commonly used methods of calixarene immobilization on a silica support.

J.D. Glennon *et.al* reported first silica bound calix[4]arene tetradiethylamide phase chromatographic statioanry phase to evalaute the chromatographic retention of alkali and alkaline earth metal ions, such as Na^+ and K^+, as shown in Figure 1.58, while using water as the mobile phase *via* detection by conductivity. Subsequently, A series of amino acid ester hydrochlorides were separated on the new calix[4]arene bound statioanry based on hydrophobicity while using aqeous mobile phase, as shown in Figure 1.59. He reported that chromatographic retention of these anlytes is dependant on the concentration of organic modifier in the mobile phase.

Subsequently, immobilization of calixarene ligands onto a silica support is critical to obtaining a hydrolytic allyl stable stationary phase. The overall success of the immobilization process is dependent on the chemical nature of the support material and calixarene ligand, the spacer arm length, and the method of immobilization.[148] The immobilization of calixarene ligands onto silica support is conducted by either activating the surface of the solid support to react with the calixarene ligand or by ligand activation using chemical means to react with the solid support. Amide, ether, thioether, amine, and imine linkages are generally applied to immobilize the calixarene cavitands on the surface of silica gel, as shown in Figure 1.60. The spacer arm's length and chemistry significantly influence the immobilization yield and chromatographic performance of the stationary phase, as shown in Figure 1.60.

Various solid supports, such as silica, polymers, and magnetic nanoparticles, have been used to immobilize the ligands. Particle-based silica support materials are used extensively in the immobilization process rather than monolithic silica supports.[149] Moreover, calixarene functionalized silica monolithic, as shown in Figure 1.61, would need to be explored in the separation of high molecular weight species such as proteins as monolithic has several advantages such as ease of *in situ* preparation, increased column permeability, effective to minimize the sample matrix effect, and possibly enhanced resolution with fast analysis.[150]

A wide range of calixa[n]arenes and its derivatives have been extensively explored as chromatographic stationary phases to separate positional and geometrical isomers,[151] aromatic positional isomers,[152] polyaromatic hydrocarbons (PAHs),[153] amino acids and nucleosides,[154] quinolones and sulphonamides,[155] water-soluble vitamins,[156] barbituric acids, benzoxepin and thioxanthene derivatives.[157]

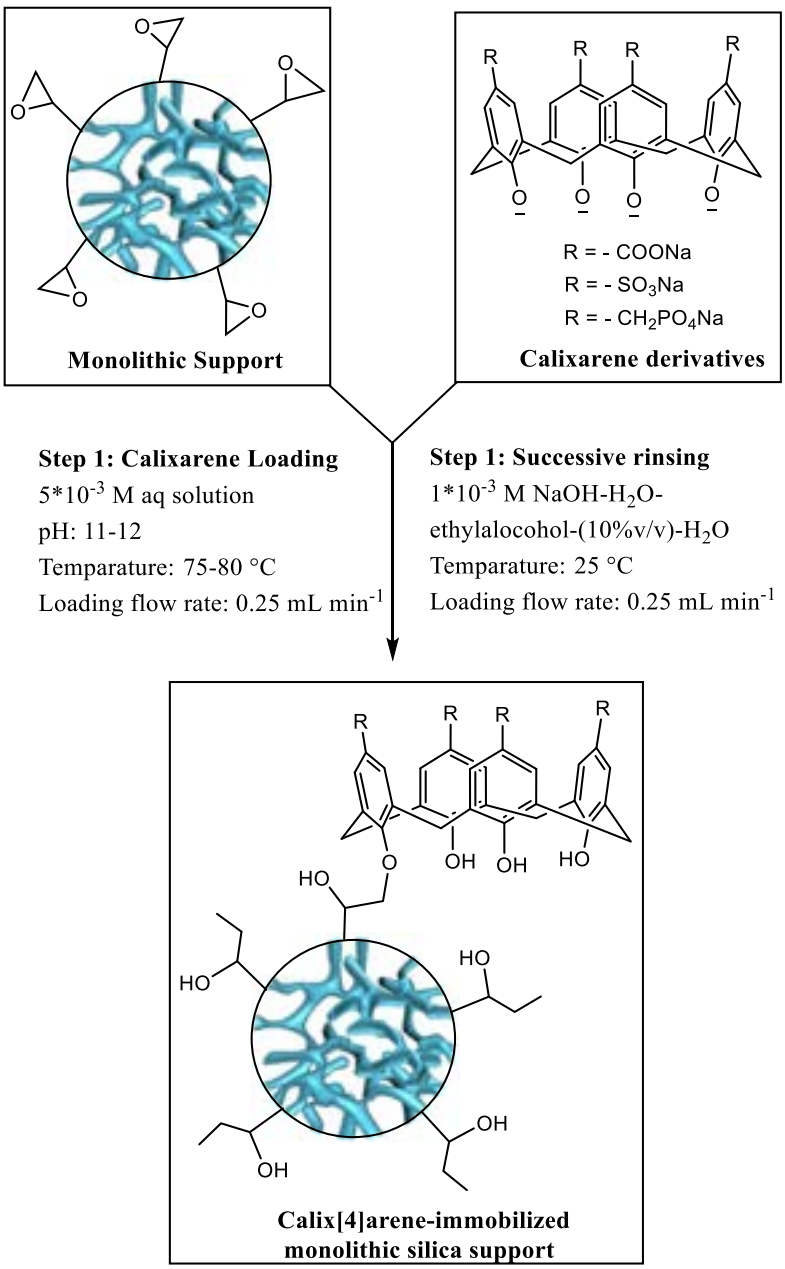

Figure 1.61 General synthesis of calixarene immobilized monolithic silica stationary phase.[150] (Reprinted with permission from Elsevier).[150]

In general, the chromatographic retention mechanism of calixarene stationary phases is not a single-mode interaction. Instead, it involves several reversible non-covalent interactions such as inclusion, hydrogen bonding, π–π interactions, van der Waals forces, dipolar–dipolar interaction, steric selectivity, and ionic selectivity. A silica-bound *p*-tert-butyl-calix[n]arene demonstrates various non-covalent host-guest interactions with the guest analyte. The *p*-tertbutyl groups and aromatic moiety of *p*-tert-butylcalix[n]arene, interacts majorly with the analyte *via* hydrophobic, π–π, and inclusion interactions. Dipolar and hydrogen bonding interactions are significant to interact the analyte with etheric oxygens of *p*-tert-butylcalix[n]arene. Organic modifiers also influence the chromatographic

retention interactions in the mobile phase, especially acetonitrile, which reduces the degree of π–π interactions, as shown in Figure 1.62 (a). Hence, in the reverse-phase chromatography mode, methanol is a common organic solvent for calixarene stationary phases.[158]

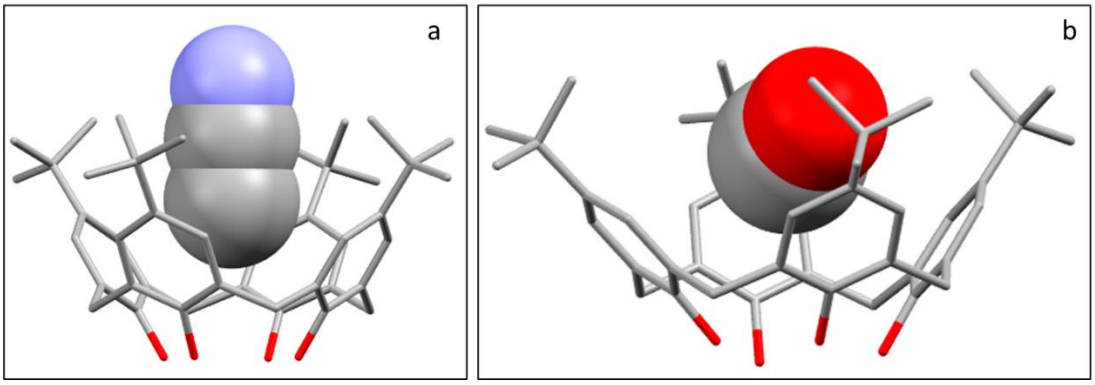

Figure 1.62 Interaction of acetonitrile (a) and methanol (b) with p-tert-butylcalix[4]arene.[158]

1.8.4 Pillar[n]arenes

In 2008, T. Ogoshi et al. reported pillar[n]arene macrocycles for the first time, as an alternative to cyclodextrin, calixarene macrocycles.[159] Pillar[n]arenes are hydrophobic tubular cavitands. The macrocycles are made up of 1,4-di-alkoxy-substituted aromatics rings linked by methylene spacer groups. The pillar[n]arene arrangement provides two functionalized upper and lower rims, as shown in Figure 1.63. The tubular structure of pillar[n]arene macrocyclic cavitands allows them to “thread” linear guests.[160]

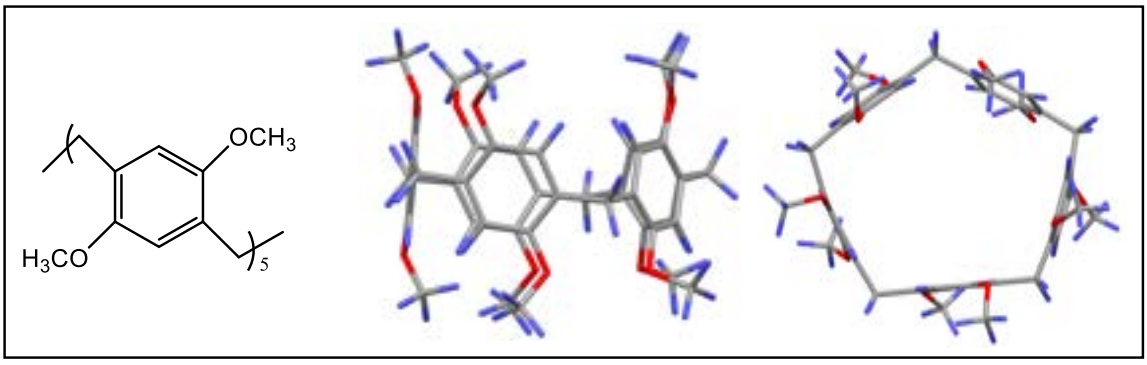

Figure 1.63. Monomer and Crystal structure of pillar[5]arene in side view and top view.[159]

Due to structural feasibility, pillar[n]arenes offer various interaction sites. The aromatic rings provide hydrophobic and π-π interactions, the hydroquinone oxygens offer hydrogen bonding, and the macrocyclic cavity holds inclusion interactions. These macrocycles have higher selectivity to the guest molecules due to their rigid structure than cyclodextrins, crown ethers, and calixarenes; the electron-rich cavity is easy to functionalize at the upper and lower rims.[160]

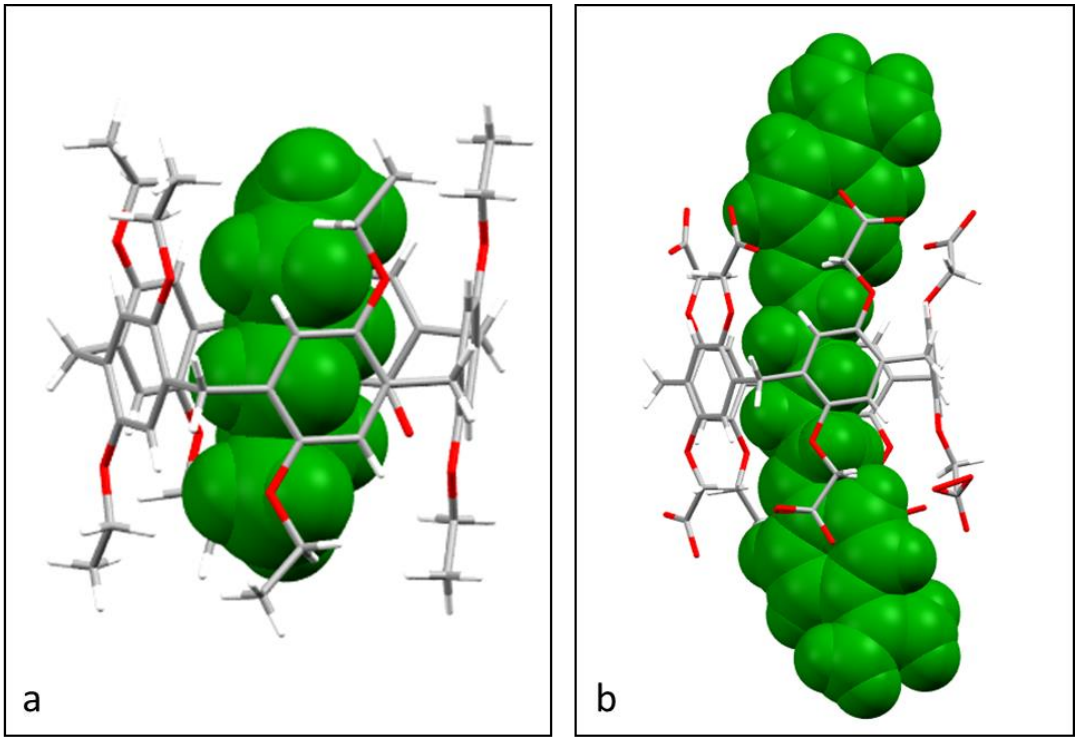

Figure 1.64 Host-guest interactions of pillar[5]arene contain hydroquinone unit with hexane (a) and carboxylated pillar[5]arene with pentamidine drug (b).[162]

Due to these characteristic host-guest features of pillar[5]arenes, these macrocyclic cavitands were functionalized on the surface of gold nanoparticles to develop electrochemical sensors. As shown in Figure 1.64, pillar[5]arene-gold organic-inorganic hybrid nanomaterials have been successfully employed to detect herbicides and isolate pesticides.[161]

Due to these specific interaction sites, which provide selective binding of pillar[n]arenes to target analytes, ease of synthesis in high yields with high purity, and ease of functionalization, pillar[n]arenes have been explored as the chiral selectors for chiral and achiral chromatography *via* silica functionalized pillar[n]arene stationary phases.

The first-ever chromatographic stationary phase based on pillar[n]arenes was synthesized by Zhang Yan *et al*. in 2017.[163] They synthesized capillary gas chromatographic stationary phases by functionalizing the silica surface with permethyl pillar[5]arene using the sol-gel coating method. This column has shown good efficiency for separating dibromo alkanes, naphthalene derivatives, and structural and geometrical isomers, compared to the commercial 5HP GC capillary column, as shown in Figures 1.65 and 1.66. The list of analytes are (1) n-undecane, (2) 1-bromooctane, (3) n-dodecane, (4) 1,4-dibromobutane, (5) 1-bromononane, (6) 1,5-dibromopentane, (7) n-tridecane, (8) 1-bromodecane, (9) 1,6-dibromohexane, (10) n-tetradecane, (11) 1,7-dibromoheptane, (12) 1-bromoundecane,

(13) n-pentadecane, (14) 1,8-dibromooctane, (15) 1-bromododecane, (16) n-hexadecane.[163]

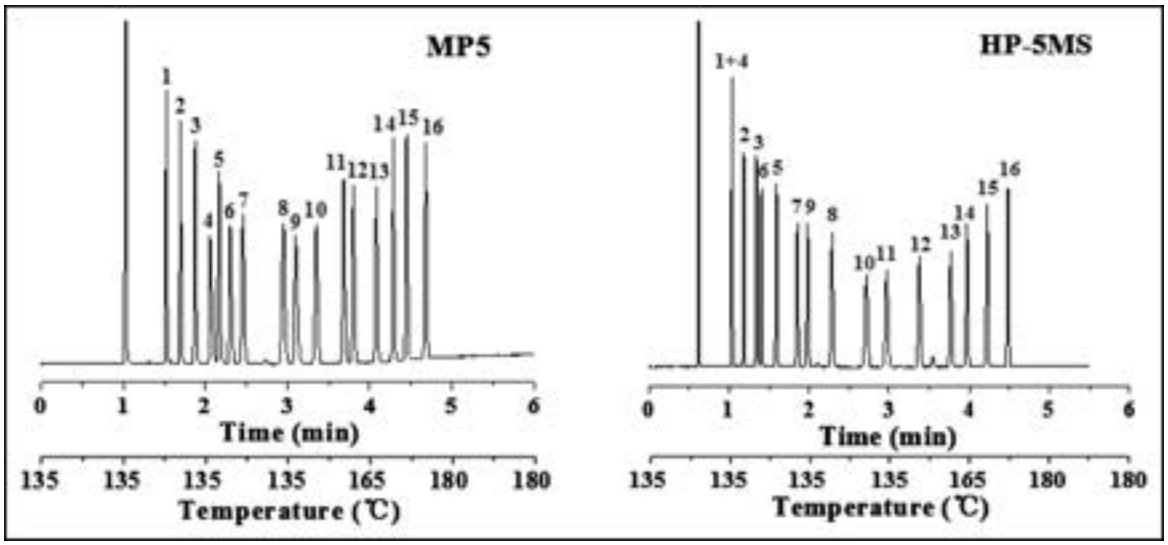

Figure 1.65 Separations of dibromo alkanes and naphthalene derivatives on the MP5 and commercial HP-5MS capillary columns. (Reprinted with permission from Elsevier, License Number 5364201078157)

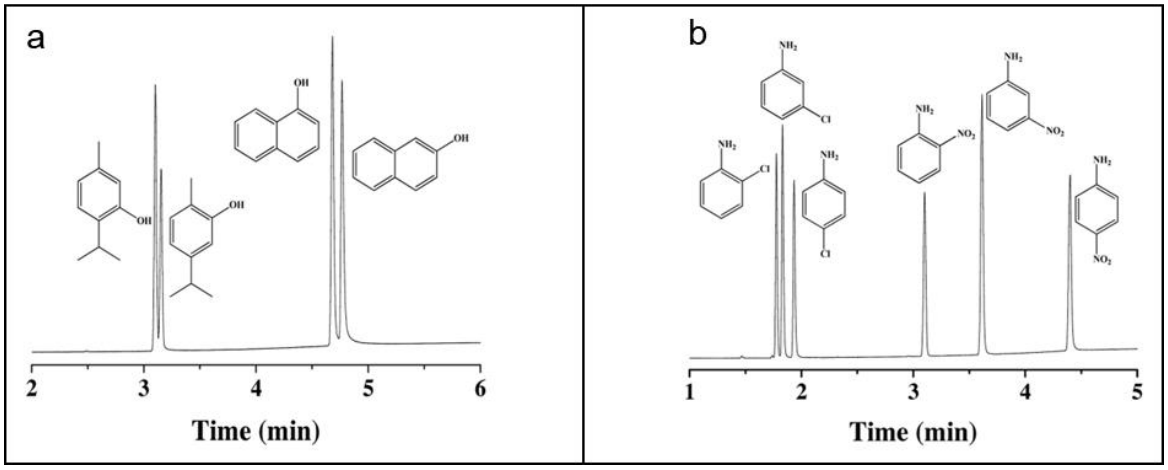

Figure 1.66 Isomeric separation of (a) thymols and naphthols and (b) o-/m-/p-chloroanilines and o-/m-/p-nitroanilines on the MP5 capillary column. (Reprinted with permission from Elsevier, License Number 5364201078157)

Subsequently, new bromoethoxypillararene (n=5,6) bound silica HPLC stationary phases were prepared and exhibited superior separation selectivity towards polyaromatic hydrocarbons (PAHs), phenols, aromatic positional isomers than that of RP-C_{18} stationary phase.[164]

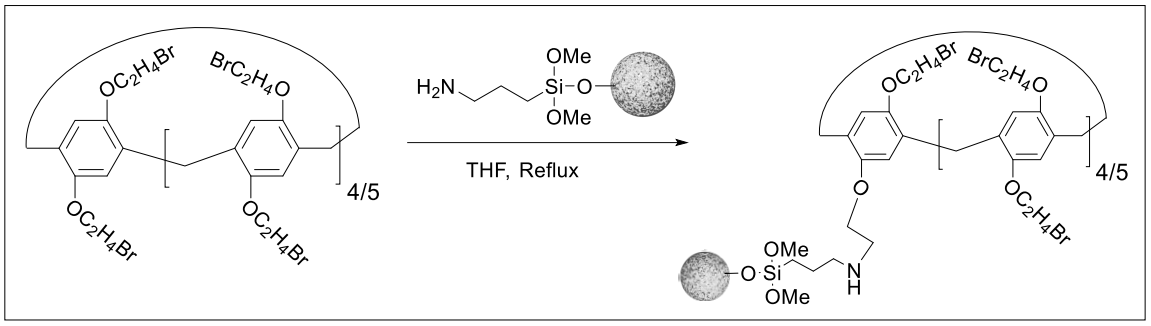

Figure 1.67 Synthesis of bromoethoxypillararene (n=5,6) bound silica HPLC stationary phases.

The chromatographic performance and separation selectivity of bromoethoxypillar[n]arene (n=5,6) bound silica HPLC stationary phases, as shown in Figure 1.67, were assessed under the reversed-phase mode using traditional RP-C_{18} *via* various analytes, such as aromatic positional isomers, polycyclic aromatic hydrocarbons, and phenols, as shown in Figure 1.68.

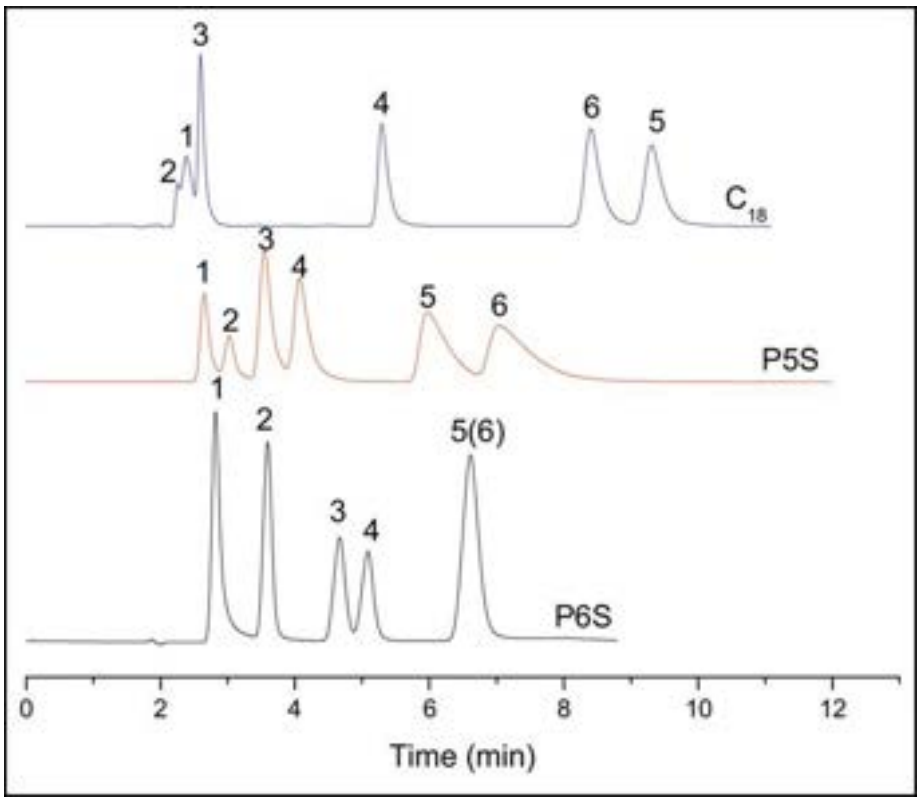

Figure 1.68 HPLC Chromatographic separation of phenols on RP-C_{18} (a), P[5]A derivative stationary phase (b), and P[6]A derivative stationary phase (c). The analytes are 2-aminophenol (1), 1,4-dihydroxybenzene (2), 1,2-dihydroxybenzene (3), phenol (4), 2-methyl phenol (5) and 3-methyl phenol (6). (Reprinted with permission from Elsevier, License Number 5364201276483)

The new P[6]A derivative stationary phase resulted in excellent separation resolution of phenols due to various supramolecular non-covalent host-guest interactions *via* hydrogen bonding, hydrophobic, inclusion, and π-π interactions. The cumulative host-guest interactions result due to various structural components of bromoethoxypillararene

macrocyclic cavitand. Subsequently, this enhanced the separation selectivity *via* various retention mechanisms. Subsequently, this pillar[n]arene bound silica chromatographic stationary phases became versatile tools to offer excellent separation potential for analyzing complex analytes.

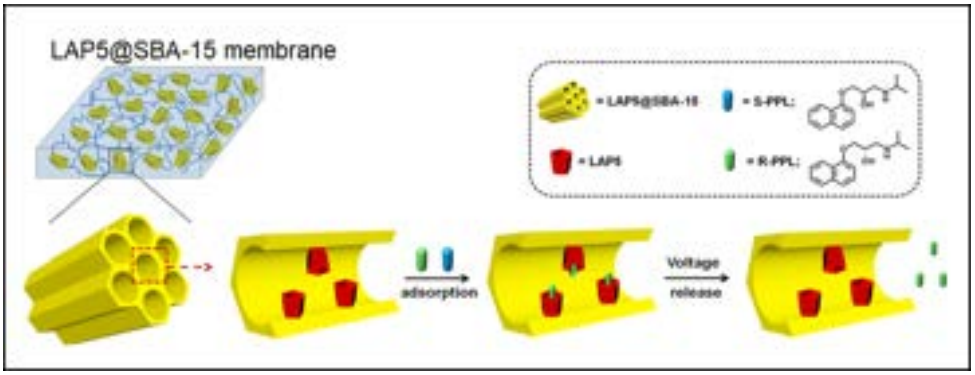

Figure 1.69. Mechanism of R-propranolol separation by the chiral L-alanine-pillar[5]arene functionalized with chiral SBA-15 membrane.[165] *(Reprinted with permission from American Chemical Society)*

Subsequently, a chiral *L*-alanine-pillar[5]arene SBA-15 embedded in a polyethersulfone (PES) membrane (Figure 1.69) has been reported to study the separation of enantiomers. The membrane demonstrated excellent chiral separation resolution for *R*-propranolol, as shown in Figure 1.70.[165]

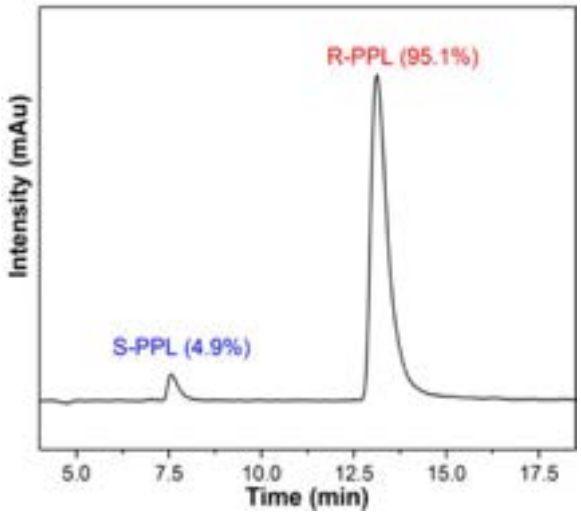

Figure 1.70 HPLC chromatogram for the separation racemic propranolol on the L-alanine-pillar[5]arene functionalized with chiral SBA-15 membrane. (Reprinted with permission from American Chemical Society)[165]

Later, a sub-microsphere monodisperse pillar[5]arene polymer solid-phase extraction column (SPE) was prepared *via* ether linkages between hydroxylated pillar[5]arene and cyanuric chloride by a single-step reaction. The SPE column has exhibited a regular spherical shape, as shown in Figure 1.71, good monodispersity, excellent chemical stability, and superior SPE extraction of trace antioxidants from food supplements.[166]

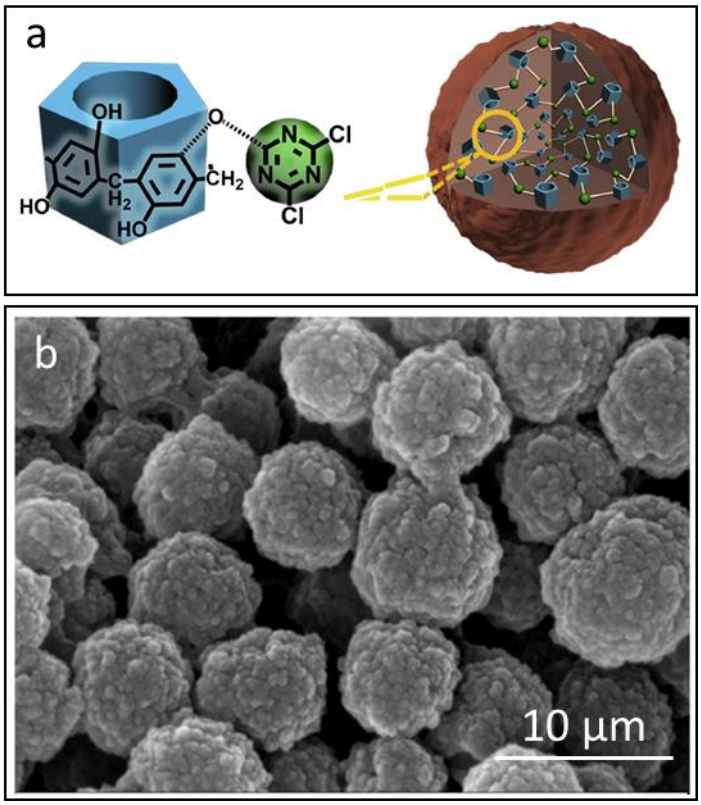

Figure 1.71. Hydroxylated pillar[5]arene polymeric sub-microsphere (a) and SEM image of sub-microsphere (b).[166] (Reprinted with permission from Elsevier)

Recently, adsorption separation strategies have been successfully employed in the pillar[5]arene nonporous adaptive crystals to separate structural and geometrical isomers. As shown in Figure 1.72, various kinds of pillar[5]arene adaptive crystals were reported, including pillar[5]arene (EtP5), perethylated pillar[6]arene (EtP6), perbromoethylated pillar[5]arene (BrP5), and perbromoethylated pillar[6]arene (BrP6).[167]

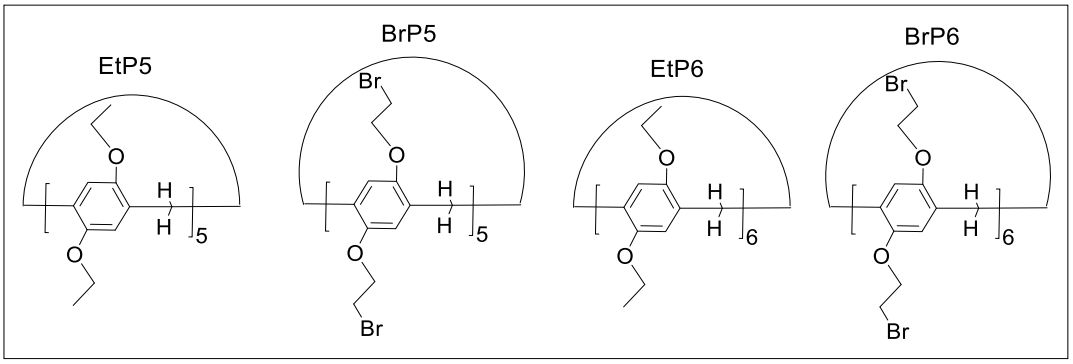

Figure 1.72 Examples of pillar[n]arene nonporous adaptive crystals.[167]

As shown in Figure 1.73, Perethylated pillar[5]arene (EtP5) adaptive nonporous crystals have shown excellent separation efficiency of *p*-chlorotoluene from an equimolar mixture of *p*-chlorotoluene/*o*-chlorotoluene without any changes in selectivity upon cycling.[167]

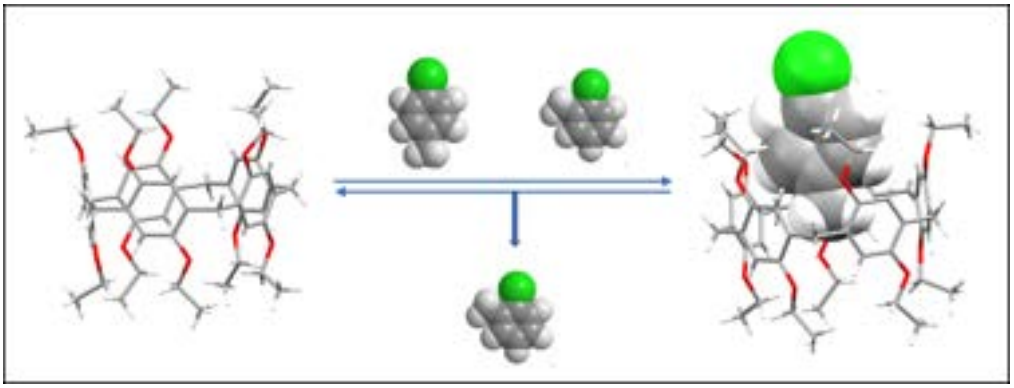

Figure 1.73 Separation of p-chlorotoluene from a mixture of p-chlorotoluene/o-chlorotoluene using Perethylated pillar[5]arene (EtP5).[167]

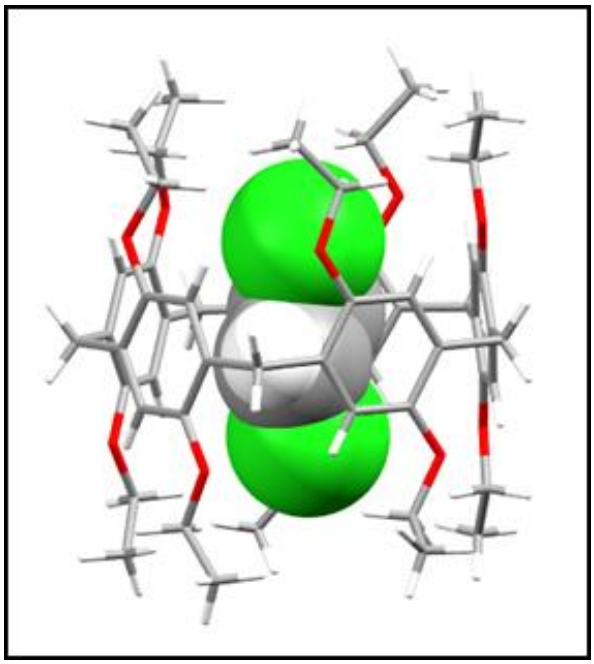

Figure 1.74 Host-guest complex of trans-dichloroethane with ethoxypillar[5]arene derivative.[168]

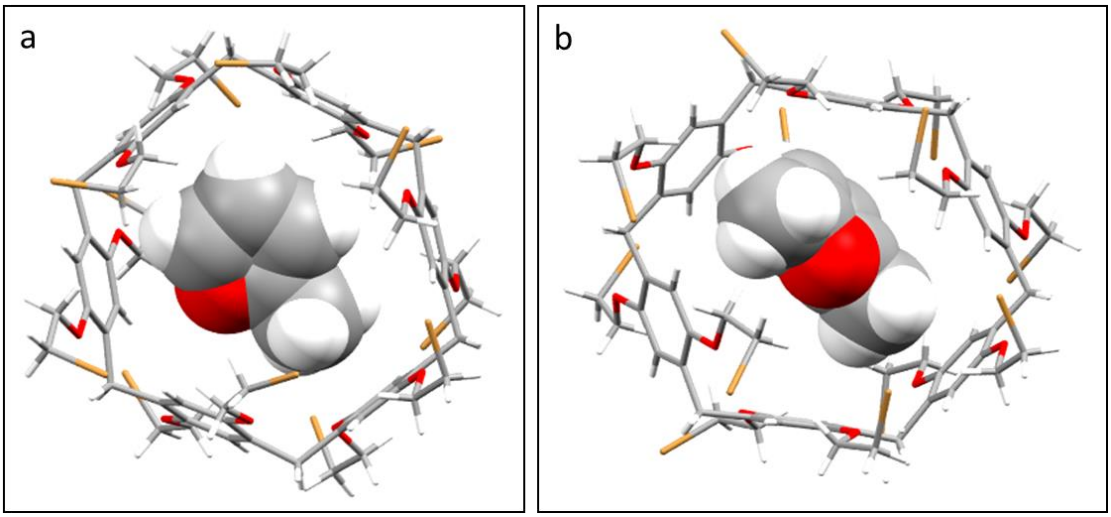

Figure 1.75 Host-Guest complexation of 2-methylfuran (a) and 2,5-dimethylfuran (b) with perbromoethylated pillar[6]arene.[169]

As shown in Figure 1.74, ethoxypillar[5]arene (EP[5]A) derivative has demonstrated superior separation resolution for *trans*-dichloroethane from the mixture of *cis*-dichloroethane and *trans*-dichloroethane.[168] In the chemical industry, the separation of 2-methylfuran (MeF) and 2,5-dimethylfuran (DMeF) from mixtures is essential. 2-methylfuran has shown remarkable separation selectivity, as shown in Figure 1.75, with perbromoethylated pillar[6]arene (BrP6) crystals.[169]

A novel silica-bound pillar[5]arene chiral stationary phase has been synthesized for enantioseparation of various racemates such as alcohols, benzoin based pesticides and triazole fungicides under normal and reversed-phase modes, as shown in Figure 1.76.

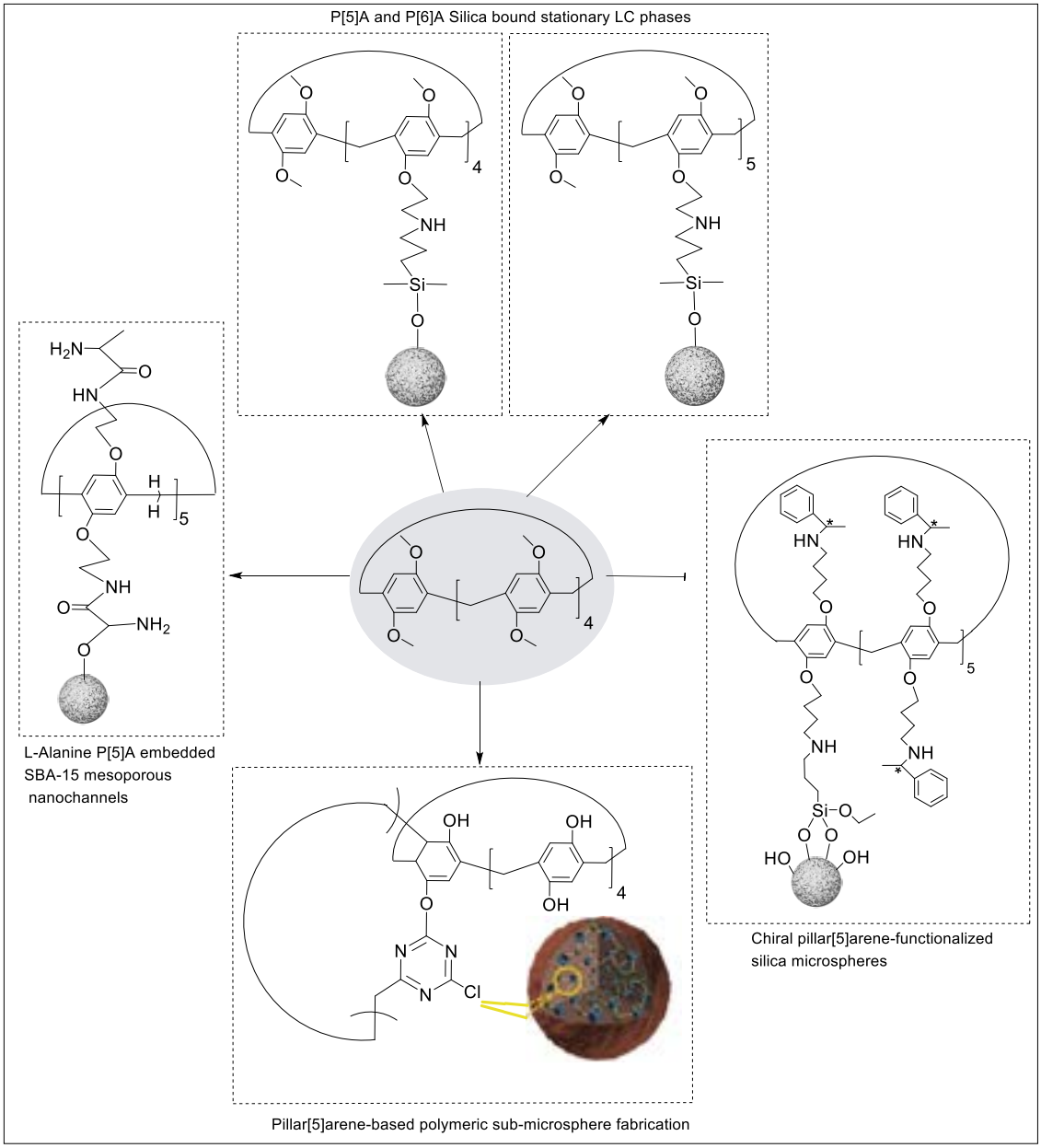

Figure 1.76. Examples of novel pillar[n]arene silica immobilized supramolecular chromatographic stationary phases.

1.9 Aims and Objectives

Reverse phase liquid chromatography (RPLC) is the most frequently used separation mode in high pressure liquid chromatography (HPLC) to separate nonpolar, weakly polar, and polar analytes. The separation of polar compounds on the reverse phase RP-C_{18} is not an easy process. However, the separation of polar analytes can be achieved by employing hydrophilic interaction LC (HILIC) columns. Mixed-mode columns, including RP-C18 and HILIC columns, are used to separate the polar analytes. The mixed-mode chromatographic columns provide increased separation selectivity, column efficiency, and column loading compared to single-mode columns.

The development of multiple novel modes of bonded chromatographic stationary phases, including utilizing macrocyclic functionalized stationary phases, is rapidly emerging as a new generation of separation tools. The ability to tune these new stationary phases goes beyond polarity and includes host-guest supramolecular interactions. Thus, pillar[5]arene, with their unique shape and easy functionalization of upper and lower rims (facilitated by non-covalent interactions with guest molecules), have attracted many researchers' attention as novel stationary phases for size exclusion chromatography.

1.9.1 Aim

The main aim of this study is to functionalize the chromatographic silica stationary phases *via* the chemical linkage of pillar[5]arene or calix[4]arene macrocycles towards selective size-exclusion chromatographic stationary phases for studying the chromatographic behaviour of xylene isomers with their impurities, a standard mixture of peptides (15-20 amino acids sequence) and a C_{60} and C_{70} fullerene mixture using flash and capillary liquid chromatography (LC) techniques. The computational *in-silico* binding energy calculations will support the chromatographic experimental results.

1.9.2 Objectives

1. Synthesis and characterization of various bromo-footed pillar[5]arene and pyrogallol[4]arene macrocycles, as sown in Figure 1.77. Microwave-assisted irradiation reactions will be used to synthesize macrocycles over conventional condensation reactions to compare reaction times and product yields. In addition, the supramolecular cavitands will be characterized by various analytical instrumental techniques.

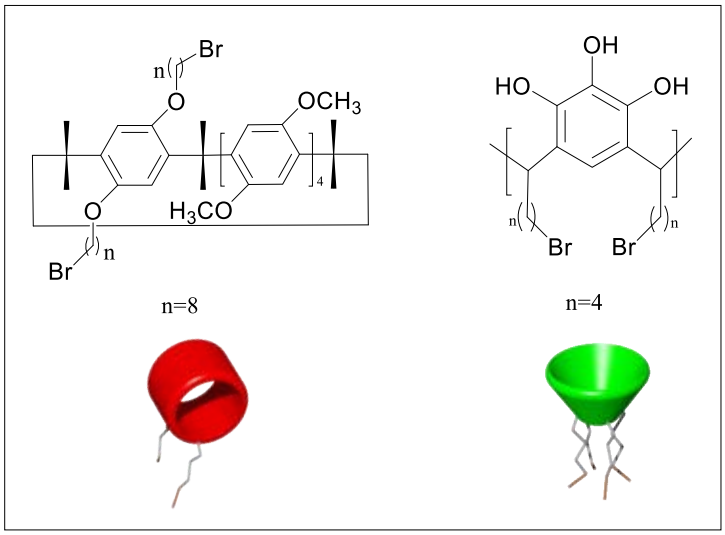

Figure 1.77 Supramolecular cavitands templates.

2. Preparation of silica-bound supramolecular chromatographic stationary phases by functionalization of activated silica with supramolecular cavitands, as shown in Figure 1.78. Thermogravimetric Analysis (TGA) and Scanning Electron Microscopy (SEM) will determine the amount of cavitands loaded on silica and structural morphologies of the synthesized stationary phase.

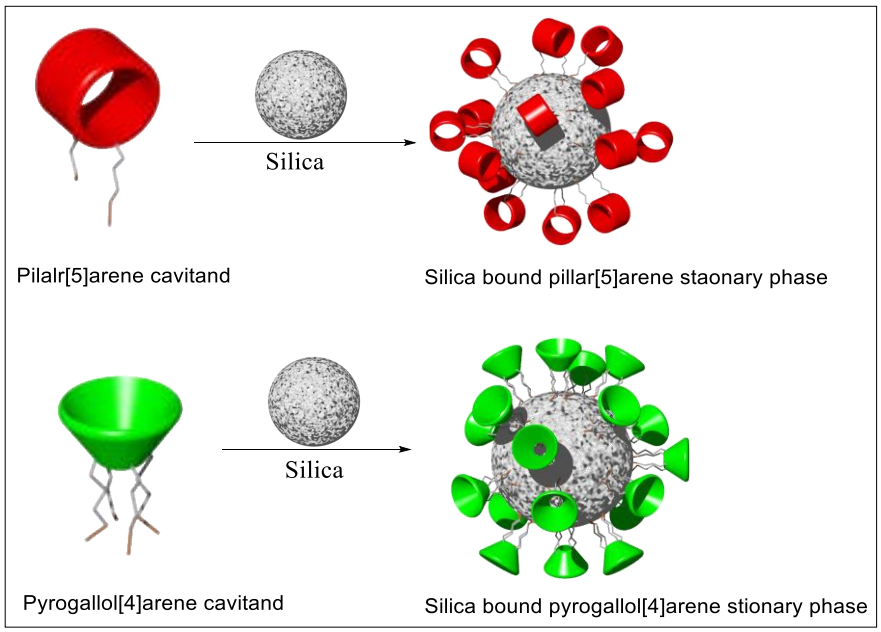

Figure 1.78 Silica bound supramolecular chromatographic stationary phases.

3. Chromatographic evaluation of silica bound supramolecular stationary phases will be carried out to separate xylene isomers from their impurities, a standard mixture of peptides (15-20 amino acids sequence) and C_{60} and C_{70} fullerene mixture.

4. Computational binding energy calculations will be performed to determine the theoretical binding energy calculations to model and visualize the spatial proximity of interacting molecules to predict retention, selectivity and elution order of analytes. This kind of strategy will also help to describe non-covalent interaction patterns triggering the supramolecular host-guest recognition interactions. All gas-phase geometry optimizations will be computed *via* Density Functional Tight Binding (DFTB) with the mio-1-1 parameter set, including the universal force field, UFF and dispersion correction as implemented in ADF version r79006 2019-10-03. In addition, solvation effects will be accounted for using the implicit Generalized Born solvation model with Solvent Accessible Surface Area (GBSA), computed using 2030 surface grid points at the same level of theory as in the gas phase.

1.10 References

1. I. Perçin, R. Khalaf, B. Brand, M. Morbidelli and O. Gezici, *J. Chromatogr. A*, 2015, **1386**, 13-21.
2. F. M. Lanças, *J. Braz. Chem*, 2003, **14**, 183-197.
3. R. Szucs, C. Brunelli, F. Lestremau and M. Hanna-Brown, *in Liquid Chromatography, ed. nonymous* , Elsevier, 2017, p. 515-537.
4. J. A. Jonsson, *Chromatographic theory and basic principles*, Dekker, New York, 1987
5. J. G. Stichlmair, *Chemical engineering and chemical process technology, unit operations-fluids and solids*, R. Pohorecki, J. Bridgewater, M. Molzahn, R. Gani and C. Gallegos, Eolss, United Kingdom, 2010, vol. 1, ch. 4, pp.68-69.
6. W. L. Luyben, *Ind Eng Chem Res*, 2012, **51**, 16427-16432; V. Gomis, R. Pedraza, O. Francés, A. Font and J. C. Asensi, *Ind Eng Chem Res*, 2007, **46**, 4572-4576.
7. M. Zougagh, M. Valcárcel and A. Rios, *Trends Analyt. Chem.*, 2004, **23**, 399-405.
8. Ž. Knez, E. Markočič, M. Leitgeb, M. Primožič, M. K. Hrnčič and M. Škerget, *Energy J.*, 2014, **77**, 235-243.
9. K. Sharif, M. Rahman, J. Azmir, A. Mohamed, M. Jahurul, F. Sahena and I. Zaidul, *J. Food Eng.*, 2014, **124**, 105-116.
10. G. Brunner*, in Gas extraction: an introduction to fundamentals of supercritical fluids and the application to separation processes*, H. Baumgartel, E. U. Franck, W. Grunbein, Springer Science & Business Media, 2013, pp.4-6.
11. A. Jones, S. Rigopoulos and R. Zauner, *Comput. Chem. Eng.,* 2005, **29**, 1159-1166.
12. H. J. M. Kramer and G. M. van Rosmalen, *in Encyclopedia of Separation Science*, ed. I. D. Wilson, Academic Press, Oxford, 2000, p. 64-84.
13. J. Chen, B. Sarma, J. M. Evans and A. S. Myerson, *Cryst. Growth Des.,* 2011, **11**, 887-895; S. Lawton, G. Steele, P. Shering, L. Zhao, I. Laird and X. Ni, *Org. Process Res.*

Dev., 2009, **13**, 1357-1363; H. Choi, N. E. Soland, B. L. Buss, N. C. Honeycutt, E. G. Tomashek, S. J. Haugen, K. J. Ramirez, J. Miscall, E. C. Tan and T. N. Smith, *Green Chem.*, 2022, **24**, 1350-1361.

14. H. G. Barth, C. Jackson and B. E. Boyes, *Anal. Chem.*, 1994, **66**, 595-620; https://www.cytivalifesciences.com/en/us/solutions/protein-research/knowledge-center/protein-purification-methods/size-exclusion-chromatography (Accessed on March 2021).
15. J. Porath and P. Flodin, *Nature*, 1959, **183**, 1657. (https://www.nature.com/articles/1831657a0.pdf)
16. J. Moore, *J. Polym. Sci., Part A: Gen. Pap.*, 1964, **2**, 835-843.
17. E. Uliyanchenko, *Anal. Bioanal. Chem*., 2014, **406**, 6087-6094; https://www.phenomenex.com.hk/Products/HPLCDetail/phenogel (accessed July 2022).
18. A. Goyon, S. Fekete, A. Beck, J. Veuthey and D. Guillarme, *J. Chromatogr. B.*, 2018, **1092**, 368-378; B. Durner, B. Scherer, T. Ehmann and F. Matysik, *ACS Appl. Polym. Mater.*, 2019, **1**, 2388-2397; S. Podzimek, *J Appl Polym Sci*, 2014, **131**. 40111
19. R. S. Feigelson, *in Handbook of Crystal Growth (Second Edition)*, ed. T. Nishinaga, Elsevier, Boston, 2015, p. 1-83.
20. L. Yu, X. Kang, L. Chen, K. Luo, Y. Jiang and X. Cao, *Materials*, 2021, **14**, 2064; X. Zhang, S. Friedrich and B. Friedrich, *J. cryst. process technol.*, 2018, **8**, 33.
21. H. Wan, J. Zhao, B. Yang, B. Xu, M. Duan, L. Kong and Y. Dai, *J. Mater. Res. Technol.*, 2020, **9**, 10366-10376.
22. M. Vogeser and C. Seger, *Clin. Biochem.*, 2008, **41**, 649-662.
23. M. Gumustas, S. Kurbanoglu, B. Uslu and S. A. Ozkan, *Chromatographia*, 2013, **76**, 1365-1427.
24. M. Vogeser and C. Seger, *Clin. Biochem.*, 2008, **41**, 649-662.
25. A. Tracqui, P. Kintz and P. Mangin, *J. Forensic Sci.*, 1995, **40**, 254-262.
26. A. J. Martin and R. L. Synge, *Biochem. J.,* 1941, **35**, 1358-1368 (DOI:10.1042/bj0351358)
27. K. M. Kalili and A. de Villiers, *J. Sep. Sci.*, 2011, **34**, 854-876.
28. H. J. Issaq, *Electrophoresis*, 2001, **22**, 3629-3638.
29. L. R. Snyder, J. J. Kirkland and J. W. Dolan, *Introduction to modern liquid chromatography*, John Wiley & Sons, 2011.
30. K. D. Bartle and P. Myers, *TrAC-Trends Anal. Chem.*, 2002, **21**, 547-557; J. C. Touchstone, *J. Liq. Chromatogr. Rel. Technol.*, 1993, **16**, 1647-1665.
31. M. Tswett, *Proc. Warsaw SOC. Natl. Sci., Biol. Sect.*, 1903, **14**, No. 6.
32. R. L. Wixom, *J. chromatogr. libr.*, 2001, **64**, 1-38; C. W. Gehrke, R. L. Wixom and E.

Bayer, *Chromatography-A Century of Discovery 1900-2000. The Bridge to The Sciences/Technology*, Elsevier, 2001.

33. L. S. Ettre, *LC-GC North America*, 2001, **19**, 506-506.
34. J. C. Moore, *J Polym Sci A.,* 1964, **2**, 835-843.
35. J. J. Kirkland, ed., *Modern Practice of Liquid Chromatography*, Wiley-Interscience, New York, 1971.
36. M. E. Swartz, *J. Liq. Chromatogr. Rel. Technol.*, 2005, **28**, 1253-1263.
37. M. W. Dong, *Modern HPLC for Practising Scientists*, John Wiley & Sons, 2006, pp. 17-24.
38. D. Guillarme, D. T. Nguyen, S. Rudaz and J. Veuthey, *Eur. J. Pharm. Biopharm.*, 2008, **68**, 430-440.
39. J. M. Miller, *Chromatography: Concepts and contracts*, Wiley, Hoboken,N.J., 2nd edn., 2005.
40. A. J. Martin and L. A. Synge RL, *Biochem. J.*, 1941, **35**, 1358-1368 (DOI:10.1042/bj0351358 [doi]).
41. E. Glueckauf, *J. Chem. Soc. Faraday Trans.*, 1955, **51**, 34-44.
42. D. DeVault, *J. Am. Chem. Soc.*, 1943, **65**, 532-540.
43. https://www.restek.com/row/technical-literature-library/articles/how-do-small-particle-size-columns-increase-sample-throughput/ (explains eddy diffusion, accessed on August 2022)
44. https://phx.phenomenex.com/lib/MDSeminar_Part1_HPLCTheory_Sep122012.pdf (explains eddy diffusion, accessed on August 2022)
45. F. Gritti and G. Guiochon, *J. Chromatogr. A*, 2012, **1228**, 2-19.
46. K. Shoykhet, K. Broeckhoven and M. W. Dong, *LC GC N. Am.*, 2019, **37**, 374.
47. M. E. Swartz, *Separation Science Re-Defined*, *LCGC Supplement*, 2005, **8**, 8-14.
48. N. Wu, J. A. Lippert and M. L. Lee, *J. Chromatogr. A*, 2001, **911**, 1-12.
49. K. Unger, D. Kumar, M. Grün, G. Büchel, S. Lüdtke, T. Adam, K. Schumacher and S. Renker, *J. Chromatogr. A*, 2000, **892**, 47-55.
50. S. Kutluay and F. Temel, *Colloids Surf. Physicochem. Eng. Aspects*, 2021, **609**, 125848.
51. A. Aqel, L. Al Wahibi, Z. A. ALOthman and A. Badjah-Hadj-Ahmed, *J. Chromatogr. A*, 2018, **1535**, 17-26.
52. S. Bocian, M. Skoczylas and B. Buszewski, *J. Sep. Sci*, 2016, **39**, 83-92.
53. X. Wang, H. Peng, J. Peng, C. Gong, Y. He, F. Chen, Y. Chen and S. Li, *Microchem. J*, 2018, **142**, 195-201.
54. Y. Yu, N. Xu, J. Zhang, B. Wang, S. Xie and L. Yuan, *ACS Appl. Mater. Interfaces.*, 2020, **12**, 16903-16911.

55. H. Xia, J. Wang, G. Chen, J. Liu, G. Wan and Q. Bai, *Microchim. Acta*, 2019, **186**, 1-8.
56. C. Boissiere, M. Kümmel, M. Persin, A. Larbot and E. Prouzet, *Adv. Funct. Mater.*, 2001, **11**, 129-135; V. Rebbin, R. Schmidt and M. Fröba, *Angew. Chem. Int. Ed.*, 2006, **45**, 5210-5214.
57. J. DeStefano, T. Langlois and J. Kirkland, *J. Chromatogr. Sci.*, 2008, **46**, 254-260; J. J. Pesek and M. T. Matyska, *J. Sep. Sci.*, 2005, **28**, 1845-1854.
58. W. H. Pirkle, J. M. Finn, J. L. Schreiner and B. C. Hamper, *J. Am. Chem. Soc.*, 1981, **103**, 3964-3966; Y. Okamoto and Y. Kaida, *J. Chromatogr. A*, 1994, **666**, 403-419; S. Hoyas, O. M. Roscioni, C. Tonneaux, P. Gerbaux, J. Cornil and L. Muccioli, *Biomacromolecules*, 2021, **22**, 2573-2581.
59. N. Wilson, J. Gilroy, J. Dolan and L. Snyder, *J. Chromatogr. A*, 2004, **1026**, 91-100; Y. Li, S. Zhang and L. Chen, *Anal. Methods.*, 2019, **11**, 3898-3909.
60. Z. Song, J. Li, W. Lu, B. Li, J. Liu, Y. Wang, Y. Wang, Z. Zhang and L. Chen, *J. Chromatogr. A*, 2021, **1656**, 462529.
61. Y. Wang, R. Wang, L. Wang, L. Wang, Y. Guo, X. Liang and S. Wang, *Analyst*, 2019, **144**, 3072-3079.
62. S. Khan, S. Hussain, A. Wong, M. V. Foguel, L. Moreira Gonçalves, M. I. Pividori Gurgo and M. d. P. Taboada Sotomayor, *React Funct Polym*, 2018, **122**, 175-182.
63. N. Tanaka, T. Tanigawa, K. Kimata, K. Hosoya and T. Arai, *J. Chromatogr. A*, 1991, **549**, 29-41.
64. J. Pesek and H. Lin, *Chromatographia,* 1989, **28**, 565-568; H. Qiu, X. Liang, M. Sun and S. Jiang, *Anal. Bioanal. Chem.*, 2011, **399**, 3307-3322; K. Tani and Y. Suzuki, *Chromatographia*, 1997, **46**, 623-627.
65. M. E. Swartz, *J. Liq. Chromatogr. Rel. Technol.*, 2005, **28**, 1253-1263.
66. The Kromasil, https://www.kromasil.com/products/classic/the_silica.php (accessed February 2022).
67. T. Zhang, Q. Zhang, J. Ge, J. Goebl, M. Sun, Y. Yan, Y. Liu, C. Chang, J. Guo and Y. Yin, *J. Phys. Chem. C*, 2009, **113**, 3168-3175; A. C. Sanchez, G. Friedlander, S. Fekete, J. Anspach, D. Guillarme, M. Chitty and T. Farkas, *J. Chromatogr. A*, 2013, **1311**, 90-97.
68. H. Qiu, X. Liang, M. Sun and S. Jiang, *Anal. Bioanal. Chem.*, 2011, **399**, 3307-3322.
69. F. Gritti, I. Leonardis, D. Shock, P. Stevenson, A. Shalliker and G. Guiochon, *J. Chromatogr. A,* 2010, **1217**, 1589-1603.
70. G. Guiochon and F. Gritti, *J. Chromatogr. A*, 2011, **1218**, 1915-1938; F. Gritti, I. Leonardis, D. Shock, P. Stevenson, A. Shalliker and G. Guiochon, *J. Chromatogr. A,* 2010, **1217**, 1589-1603.

71. https://phenomenex.blog/2017/07/25/porous-core-shell-tech/ (Accessed on August 2022)
72. The Phenomenex, https://www.phenomenex.com/Kinetex/CoreShellTechnology, (accessed February 2022); The YMC, https://www.ymc.co.jp/en/columns/ymc_meteoric_core/, (accessed February 2022); The Agilent, https://www.agilent.com/en/product/small-molecule-columns/reversed-phase-hplc-columns/infinitylab-poroshell-120, (accessed February 2022).
73. J. Ou, X. Li, S. Feng, J. Dong, X. Dong, L. Kong, M. Ye and H. Zou, *Anal. Chem.*, 2007, **79**, 639-646.
74. L. Yan, Q. Zhang, Y. Feng, W. Zhang, T. Li, L. Zhang and Y. Zhang, *J. Chromatogr. A*, 2006, **1121**, 92-98.
75. Z. Lin, F. Yang, X. He, X. Zhao and Y. Zhang, *J. Chromatogr. A*, 2009, **1216**, 8612-8622.
76. G. Yang, F. Li, L. Wang, K. H. Row, H. Liu, L. Bai, W. Cao and T. Zhu, *Chromatographia*, 2008, **68**, 27-31.
77. J. J. Kirkland, *J. Chromatogr. A*, 2004, **1060**, 9-21; W. A. Aue and C. R. Hastings, *J. Chromatogr. A*, 1969, **42**, 319-335.
78. L. R. Snyder, J. J. Kirkland and J. W. Dolan, *Introduction to Modern Liquid Chromatography*, John Wiley & Sons, 2011.
79. D. C. Locke, J. T. Schmermund and B. Banner, *Anal. Chem.*, 1972, **44**, 90-92.
80. O. Brust, I. Sebestian and I. Halász, *J. Chromatogr. A*, 1973, **83**, 15-24.
81. K. Unger, N. Becker and P. Roumeliotis, *J. Chromatogr. A*, 1976, **125**, 115-127.
82. J. M. Lehn, *Proc. Natl. Acad. Sci. U. S. A.*, 2002, **99**, 4763-4768; J.-M. Lehn, *Chem. Soc. Rev.*, 2007, **36**, 151-160.
83. J. W. Steed and J. L. Atwood, *Supramolecular Chemistry 2edn.,* John Wiley & Sons, Ltd, Chischester, UK, 2009.
84. J. A. Thoma and D. Koshland Jr, *J. Am. Chem. Soc.*, 1960, **82**, 3329-3333; J.-M. Lehn, *Pharm. Acta Helv.*, 1995, **69**, 205-211, X. Ma and Y. Zhao, *Chem. Rev.*, 2015, **115**, 7794-7839.
85. J.-M. Lehn, *Angew. Chem. Int. Ed. Engl.*, 1988, **27**, 89-112; J. W. Steed, D. R. Turner and K. Wallace, *Core concepts in supramolecular chemistry and nanochemistry*, John Wiley & Sons, West Sussex, U.K, 2007; J.-M. Lehn, M. Mascal, A. Decian and J. Fischer, *J. Chem. Soc., Chem. Commun.*, 1990, 479-481.
86. J. W. Steed and J. L. Atwood, *in Supramolecular Chemistry*, John Wiley & Sons, Ltd, New York, 2009, pp. 1-47.
87. G. W. Cave, J. Antesberger, L. J. Barbour, R. M. McKinlay and J. L. Atwood, *Angew. Chem. Int. Ed.*, 2004, **43**, 5263-5266.

88. G. W. Cave, M. C. Ferrarelli and J. L. Atwood, *Chem. Commun.*, 2005, 2787-2789.
89. K. Müller-Dethlefs and P. Hobza, *Chem. Rev.*, 1999, **100**, 143-168.
90. J. L. Atwood and A. Szumna, *J. supramol. chem.*, 2002, **2**, 479-482.
91. K. Sikligar, S. P. Kelley, G. A. Baker and J. L. Atwood, *Cryst. Growth Des.*, 2022, **22,** 2806-2811.
92. L. Trembleau and J. Rebek, *Science*, 2003, **301**, 1219-1220.
93. G. D. Andreetti, R. Ungaro and A. Pochini, *J. Chem. Soc., Chem. Commun.*, 1979, 1005-1007.
94. K. I. Assaf and W. M. Nau, *Chem. Soc. Rev.*, 2015, **44**, 394-418.
95. I. C. Jardim, L. Maldaner, J. Lourenço, L. M. Fioravanti and C. H. Collins, *J. Sep. Sci.*, 2010, **33**, 2917-2929.
96. V. Y. Gus' kov, D. A. Sukhareva, Y. Y. Gainullina, E. M. Hamitov, Y. G. Galkin and V. N. Maistrenko, *Supramol Chem.*, 2018, **30**, 940-948; A. Zhang, C. Xiao, W. Xue and Z. Chai, *Sep. Purif. Technol.*, 2009, **66**, 541-548.
97. A. Bogdanski, D. Wistuba, K. L. Larsen, U. Hartnagel, A. Hirsch and V. Schurig, *New J. Chem.*, 2010, **34**, 693-698.
98. R. Mohammadzadeh Kakhki, *J. Incl. Phenom. Macrocycl. Chem.*, 2013, **75**, 11-22.
99. Y. Xiao, S. Ng, T. T. Y. Tan and Y. Wang, *J. Chromatogr. A*, 2012, **1269**, 52-68.
100. M. Śliwka-Kaszyńska, G. Gorczyca and M. Ślebioda, *J. Chromatogr. A*, 2010, **1217**, 329-336; L. Li, S. Da, Y. Feng and M. Liu, *J. Chromatogr. A*, 2004, **1040**, 53-61; N. Li, L. J. Allen, R. G. Harrison and J. D. Lamb, *Analyst*, 2013, **138**, 1467-1474; W. Zhao, W. Wang, H. Chang, S. Cui, K. Hu, L. He, K. Lu, J. Liu, Y. Wu and J. Qian, *J. Chromatogr. A*, 2012, **1251**, 74-81.
101. C. Shi, H. Li, X. F. Shi, L. Zhao and H. Qiu, *ChemComm.*, 2022, (10.1039/D1CC06978K); W. Zhao, J. Chu, F. Xie, Q. Duan, L. He and S. Zhang, *J. Chromatogr. A,* 2017, **1485**, 44-51; Y. Zhang, Q. Lv, M. Qi and Z. Cai, *J. Chromatogr. A* 2017, **1496**, 115-121.
102. W. Zhao, J. Chu, F. Xie, Q. Duan, L. He and S. Zhang, *J. Chromatogr. A*, 2017, **1485**, 44-51.
103. G. Rounaghi and R. M. Z. Kakhki, *J. Incl. Phenom. Macrocycl. Chem.*, 2009, **63**, 117-122; R. Mohammad Zadeh Kakhki and G. Rounaghi, *J. Chem. Eng.,* 2011, **56**, 3169-3174; C. Tian, S. D. Fielden, G. F. Whitehead, I. J. Vitorica-Yrezabal and D. A. Leigh, *Nature communications*, 2020, **11**, 1-10; G. Koshkakaryan, L. M. Klivansky, D. Cao, M. Snauko, S. J. Teat, J. O. Struppe and Y. Liu, *J. Am. Chem. Soc.*, 2009, **131**, 2078-2079.

104. P. Mohapatra, D. Lakshmi, A. Bhattacharyya and V. Manchanda, *J. Hazard. Mater.*, 2009, **169**, 472-479; S. D. Fielden, D. A. Leigh, C. T. McTernan, B. Pérez-Saavedra and I. J. Vitorica-Yrezabal, *J. Am. Chem. Soc.,* 2018, **140**, 6049-6052.

105. K. Hirose, T. Nakamura, R. Nishioka, T. Ueshige and Y. Tobe, *Tetrahedron Lett.*, 2003, **44**, 1549-1551; K. Hirose, J. Yongzhu, T. Nakamura, R. Nishioka, T. Ueshige and Y. Tobe, *Chirality*, 2005, **17**, 142-148.

106. W. Lee and C. Y. Hong, *J. Chromatogr. A*, 2000, **879**, 113-120.

107. G. Dotsevi, Y. Sogah and D. J. Cram, *J. Am. Chem. Soc.*, 1975, **97**, 1259-1261.

108. T. Shinbo, T. Yamaguchi, K. Nishimura and M. Sugiura, *J. Chromatogr. A*, 1987, **405**, 145-153.

109. T. Shinbo, T. Yamaguchi, K. Nishimura and M. Sugiura, *J. Chromatogr. A*, 1987, **405**, 145-153.

110. Y. Machida, H. Nishi, K. Nakamura, H. Nakai and T. Sato, *J. Chromatogr. A*, 1998, **805**, 85-92.

111. M. H. Hyun and Y. J. Cho, *J. Sep. Sci.*, 2005, **28**, 31-38.

112. Z. Köntös, P. Huszthy, J. S. Bradshaw and R. M. Izatt, *Tetrahedron: Asymmetry*, 1999, **10**, 2087-2099.

113. K. Hirose, T. Nakamura, R. Nishioka, T. Ueshige and Y. Tobe, *Tetrahedron Lett.*, 2003, **44**, 1549-1551; K. Hirose, J. Yongzhu, T. Nakamura, R. Nishioka, T. Ueshige and Y. Tobe, *Chirality: The Pharmacological, Biological, and Chemical Consequences of Molecular Asymmetry*, 2005, **17**, 142-148; K. Hirose, J. Yongzhu, T. Nakamura, R. Nishioka, T. Ueshige and Y. Tobe, *J. Chromatogr. A*, 2005, **1078**, 35-41.

114. M. H. Hyun, G. Tan and J. Y. Xue, *J. Chromatogr. A*, 2005, **1097**, 188-191.

115. R. J. Steffeck, Y. Zelechonok and K. H. Gahm, *J. Chromatogr. A*, 2002, **947**, 301-305.

116. M. H. Hyun, S. C. Han, B. H. Lipshutz, Y. Shin and C. J. Welch, *J. Chromatogr. A*, 2001, **910**, 359-365; M. H. Hyun, S. C. Han, B. H. Lipshutz, Y. Shin and C. J. Welch, *J. Chromatogr A*, 2001, **910**, 359-365.

117. J. Yongzhu, K. Hirose, T. Nakamura, R. Nishioka, T. Ueshige and Y. Tobe, *J. Chromatogr. A*, 2006, **1129**, 201-207.

118. S. Seyhan, Y. Turgut, M. Merdivan and H. Hoşgören, *Tetrahedron: Asymmetry*, 2006, **17**, 1700-1704.

119. M. H. Hyun and Y. J. Cho, *J. Sep. Sci.*, 2005, **28**, 31-38; M. H. Hyun, J. S. Jin, S. C. Han and Y. *J. Cho, Microchem. J.,* 2001, **70**, 205-209; J. S. Jin, A. M. Stalcup and M. H. Hyun, *J. Chromatogr. A*, 2001, **933**, 83-90; M. H. Hyun, G. Tan and J. Y. Xue, *J. Chromatogr. A*, 2005, **1097**, 188-191.

120. Z. Zeng, W. Qiu, H. Xing and Z. Huang, *Anal. Sci.*, 2000, **16**, 851-854.

121. K. Kimura, H. Harino, E. Hayata and T. Shono, *Anal. Chem.*, 1986, **58**, 2233-2237; R. Saari-Nordhaus and J. M. Anderson Jr, *J. Chromatogr. A*, 2004, **1039**, 123-127.

122. J. Behr, J. Girodeau, R. C. Hayward, J. Lehn and J. Sauvage, *Helv. Chim. Acta*, 1980, **63**, 2096-2111; T. Koide and K. Ueno, *J. Chromatogr. A*, 2001, **909**, 305-315.

123. Z. Köntös, P. Huszthy, J. S. Bradshaw and R. M. Izatt, *Tetrahedron: Asymmetry*, 1999, **10**, 2087-2099.

124. M. T. Rojas, R. Koeniger, J. F. Stoddart and A. E. Kaifer, *J. Am. Chem. Soc.*, 1995, **117**, 336-343; P. R. Ashton, R. Königer, J. F. Stoddart, D. Alker and V. D. Harding, *J. Org. Chem.***,** 1996, **61**, 903-908; T. Loftsson and D. Duchêne, Int. J. Pharm., 2007, 329, 1-11; C. R. Mitchell and D. W. Armstrong, *in Chiral Separations*, Springer, 2004, p. 61-112; J. Lee, S. Lee, S. Lee and H. B. Oh, *Molecules*, 2020, **25**, 4048; L. Szente and J. Szemán, *Anal. Chem.* 2013, **85**, 8024-8030.

125. X. Wang and M. L. Brusseau, *Environ. Sci. Technol.*, 1995, **29**, 2632-2635; N. Li, L. Yang, D. Wang, C. Tang, W. Deng and Z. Wang, *Environ. Sci. Technol.*, 2021, **55**, 9181-9188; J. Wang, W. Zhang and J. Wei, *J. Mater. Chem.*, 2019, **7**, 2055-2065.

126. T. Kida, T. Iwamoto, Y. Fujino, N. Tohnai, M. Miyata and M. Akashi, *Org. Lett.*, 2011, **13**, 4570-4573.

127. W. L. Hinze, *Sep. Purif. Methods*, 1981, **10**, 159-237.

128. D. Armstrong, L. Chang, S. Chang, X. Wang, H. Ibrahim, G. Reid and T. Beesley, *J. Liq. Chromatogr. Rel. Technol.*, 1997, **20**, 3279-3295.

129. D. W. Armstrong, T. J. Ward, R. D. Armstrong and T. E. Beesley, *Science*, 1986, **232**, 1132-1135 (DOI:10.1126/science.3704640 [doi]).

130. T. Loftsson and D. Duchêne, *Int. J. Pharm.*, 2007, **329**, 1-11; C. R. Mitchell and D. W. Armstrong, *in Chiral Separations*, Springer, 2004, p. 61-112; J. Lee, S. Lee, S. Lee and H. B. Oh, *Molecules*, 2020, **25**, 4048.

131. T. Ong, R. Wang, I. W. Muderawan and S. Ng, *J. Chromatogr. A*, 2008, **1182**, 136-140; R. Wang, T. Ong and S. Ng, *J. Chromatogr. A*, 2008, **1203**, 185-192.

132. C. A. Chang, H. Abdel-Aziz, N. Melchor, Q. Wu, K. H. Pannell and D. W. Armstrong, *J. Chromatogr. A*, 1985, **347**, 51-60; J. Zhao, D. Tan, S. T. Chelvi, E. Yong, H. K. Lee and Y. Gong, *Talanta*, 2010, **83**, 286-290.

133. Z. Zhang, W. Zhang, W. Luo and J. Fan, *J. Chromatogr. A*, 2008, **1213**, 162-168; Q. Qin, S. Zhang, W. Zhang, Z. Zhang, Y. Xiong, Z. Guo, J. Fan, S. Run-Zheng, D. Finlow and Y. Yin, *J. Sep. Sci.*, 2010, **33**, 2582-2589.

134. X. Lai, W. Tang and S. Ng, *J. Chromatogr. A*, 2011, **1218**, 5597-5601; X. Lai, W. Tang and S. Ng, *J. Chromatogr. A*, 2011, **1218**, 3496-3501.

135. K. M. Kacprzak, N. M. Maier and W. Lindner, *Tetrahedron Lett.*, 2006, **47**, 8721-8726; Y. Zhang, Z. Guo, J. Ye, Q. Xu, X. Liang and A. Lei, *J. Chromatogr. A*, 2008,

1191, 188-192; H. Wang, P. Jiang, M. Zhang and X. Dong, *J. Chromatogr. A*, 2011, **1218**, 1310-1313.

136. X. Wang, H. Li, K. Quan, L. Zhao, Z. Li and H. Qiu, *J. Chromatogr. A*, 2021, **1651**, 462338.

137. Z. Zhang, M. Wu, R. Wu, J. Dong, J. Ou and H. Zou, *Anal. Chem.*, 2011, **83**, 3616-3622.

138. W. Tang and S. C. Ng, *J. Sep. Sci.*, 2008, **31**, 3246-3256.

139. D. W. Armstrong, T. J. Ward, R. D. Armstrong and T. E. Beesley, *Science*, 1986, **232**, 1132-1135.

140. X. Han, Q. Huang, J. Ding, R. C. Larock and D. W. Armstrong, *Sep. Sci. Technol.,* 2005, **40**, 2745-2759.

141. C. D. Gutsche and J. F. Stoddart, Calixarenes, 1989, 1. O. Gezici and M. Bayrakci, *J. Incl. Phenom. Macrocycl. Chem.*, 2015, **83**, 1-18.

142. G. W. Cave, J. Antesberger, L. J. Barbour, R. M. McKinlay and J. L. Atwood, *Angew. Chem. Int. Ed.*, 2004, **43**, 5263-5266; N. D. Bowley, M. Funck, D. M. Laventine, S. J. Dalgarno and G. W. Cave, *Supramol. Chem.*, 2014, **26**, 229-232; R. Puttreddy, N. K. Beyeh, R. H. Ras and K. Rissanen, *ChemistryOpen,* 2017, **6**, 417-423.

143. L. Baldini, A. Casnati, F. Sansone and R. Ungaro, *Chem. Soc. Rev.*, 2007, **36**, 254-266; M. Śliwka-Kaszyńska, K. Jaszczołt, D. Witt and J. Rachoń, *J. Chromatogr. A*, 2004, **1055**, 21-28.

144. D. J. Cram, *Angew. Chem. Int. Ed.*, 1988, **27**, 1009-1020; D. J. Cram and J. M. Cram, *Container molecules and their guests*, Royal Society of Chemistry, 1997; C. D. Gutsche, B. Dhawan, K. H. No and R. Muthukrishnan, *J. Am. Chem. Soc.*, 1981, **103**, 3782-3792; L. J. Bauer and C. D. Gutsche, *J. Am. Chem. Soc.*, 1985, **107**, 6063-6069; C. D. Gutsche, M. Iqbal and I. Alam, *J. Am. Chem. Soc.*, 1987, **109**, 4314-4320; I. Alam and C. D. Gutsche, *J. Org. Chem.*, 1990, **55**, 4487-4489; L. Li, S. Da, Y. Feng and M. Liu, *Anal. Sci.*, 2004, **20**, 561-564; G. D. Andreetti, R. Ungaro and A. Pochini, *J. Chem. Soc., Chem. Commun.*, 1979, 1005-1007.

145. E. P. Kyba, R. C. Helgeson, K. Madan, G. W. Gokel, T. L. Tarnowski, S. S. Moore and D. J. Cram, *J. Am. Chem. Soc.,* 1977, **99**, 2564-2571.

146. B. Mokhtari, K. Pourabdollah and N. Dalali, *Chromatographia*, 2011, **73**, 829-847.

147. L. Lin, C. Wu, Z. Yan, X. Yan, X. Su and H. Han, *Chromatographia*, 1998, **47**, 689-694; R. Ludwig, *Fresenius J. Anal. Chem.*, 2000, **367**, 103-128; R. Meyer and T. Jira, *Curr. Anal. Chem.*, 2007, **3**, 161-170; M. Śliwka-Kaszyńska, *Crit. Rev. Anal. Chem.*, 2007, **37**, 211-224; B. Mokhtari, K. Pourabdollah and N. Dalali, *Chromatographia*, 2011, *73*, 829-847; J. Glennon, E. Horne, K. Hall, D. Cocker, A. Kuhn, S. Harris and

M. McKervey, *J. Chromatogr. A*, 1996, **731**, 47-55; Y. Zhou, H. Li and Y. Yang, *Chin Chem Lett*, 2015, **26**, 825-828.

148. M. Śliwka-Kaszyńska, K. Jaszcołt and I. Anusiewicz, *J. Sep. Sci.*, 2009, **32**, 3107-3115; G. Delahousse, R. Lavendomme, I. Jabin, V. Agasse and P. Cardinael, *Curr. Org. Chem.*, 2015, **19**, 2237-2249.

149. K. Cabrera, *J. Sep. Sci.,* 2004, **27**, 843-852; L. Rieux, H. Niederländer, E. Verpoorte and R. Bischoff, *J. Sep. Sci.*, 2005, **28**, 1628-1641; C. Ding, K. Qu, Y. Li, K. Hu, H. Liu, B. Ye, Y. Wu and S. Zhang, *J. Chromatogr. A*, 2007, **1170**, 73-81.

150. J. Yin, L. Wang, X. Wei, G. Yang and H. Wang, *J. Chromatogr. A*, 2008, **1188**, 199-207; Guven, O. Gezici, M. Bayrakci and M. Morbidelli, *J. Chromatogr. A*, 2018, **1558**, 59-68; K. Hu, W. Zhang, H. Yang, Y. Cui, J. Zhang, W. Zhao, A. Yu and S. Zhang, *Talanta*, 2016, **152**, 392-400.

151. T. Sokoließ, U. Menyes, U. Roth and T. Jira, *J. Chromatogr. A*, 2002, **948**, 309-319.

152. L. Li, S. Da, Y. Feng and M. Liu, *J. Chromatogr. A*, 2004, **1040**, 53-61.

153. X. Xiao, Y. Feng, S. Da and Y. Zhang, *Anal. Lett.*, 2000, **33**, 3355-3372; Q. Huai and Y. Zuo, *J. Liq. Chromatogr. Rel. Technol.*, 2006, **29**, 801-814.

154. L. Li, M. Liu, S. Da and Y. Feng, *Talanta*, 2004, **63**, 433-441; Y. Xiao, X. Xiao, Y. Feng, Z. Wang and S. Da, J*. Liq. Chromatogr. Rel. Technol.*, 2001, **24**, 2925-2942.

155. Y. Xiao, X. Xiao, Y. Feng, Z. Wang and S. Da, *Talanta,* 2002, **56**, 1141-1151.

156. L. Li, S. Da, Y. Feng and M. Liu, *Talanta*, 2004, **64**, 373-379.

157. T. Sokoließ, U. Menyes, U. Roth and T. Jira, *J. Chromatogr. A*, 2000, **898**, 35-52.

158. O. Gezici and M. Bayrakci, *J. Incl. Phenom. Macrocycl. Chem.,* 2015, **83**, 1-18; 1.C. Chamseddin and T. Jira, *Chromatographia,* 2013, **76**, 449-457.

159. T. Ogoshi, S. Kanai, S. Fujinami, T. Yamagishi and Y. Nakamoto, *J. Am. Chem. Soc.*, 2008, **130**, 5022-5023.

160. N. L. Strutt, R. S. Forgan, J. M. Spruell, Y. Y. Botros and J. F. Stoddart, *J. Am. Chem. Soc.*, 2011, **133** , 5668; N. L. Strutt, H. Zhang, M. A. Giesener, J. Lei and J. F. Stoddart, *Chem. Commun.*, 2012, **48**, 1647-1649; C. Ke, N. L. Strutt, H. Li, X. Hou, K. J. Hartlieb, P. R. McGonigal, Z. Ma, J. Iehl, C. L. Stern and C. Cheng, *J. Am. Chem. Soc.*, 2013, **135**, 17019-17030.

161. T. Ogoshi, K. Kitajima, T. Aoki, S. Fujinami, T. Yamagishi and Y. Nakamoto, *J. Org. Chem.*, 2010, **75** , 3268-3273; H. Li, D. Chen, Y. Sun, Y. B. Zheng, L. Tan, P. S. Weiss and Y. Yang, *J. Am. Chem. Soc.*, 2013, **135**, 1570-1576; T. Zhou, N. Song, H. Yu and Y. Yang, *Langmuir*, 2015, **31**, 1454-1461.

162. T. Ogoshi, Y. Shimada, Y. Sakata, S. Akine and T. Yamagishi, *J. Am. Chem. Soc.*, 2017, **139**, 5664-5667; H. Butkiewicz, S. Kosiorek, V. Sashuk, M. Zimnicka and O.

Danylyuk, *Cryst. Growth Des*., 2022, **22**, 2854-2862.

163. Y. Zhang, Q. Lv, M. Qi and Z. Cai, *J. Chromatogr. A*, 2017, **1496**, 115-121.

164. W. Zhao, J. Chu, F. Xie, Q. Duan, L. He and S. Zhang, *J. Chromatogr. A,* 2017, **1485**, 44-51.

165. M. Cheng, F. Zhu, W. Xu, S. Zhang, M. K. Dhinakaran and H. Li, *ACS Appl. Mater. Interfaces*, 2021, **13**, 27305-27312.

166. R. Liang, Y. Hu and G. Li, *J. Chromatogr. A*, 2020, **1625**, 461276.

167. M. Wang, J. Zhou, E. Li, Y. Zhou, Q. Li and F. Huang, *J. Am. Chem. Soc.*, 2019, **141**, 17102-17106.

168. X. Sheng, E. Li, Y. Zhou, R. Zhao, W. Zhu and F. Huang, *J. Am. Chem. Soc.,* 2020, **142**, 6360-6364.

169. Y. Wu, J. Zhou, E. Li, M. Wang, K. Jie, H. Zhu and F. Huang, *J. Am. Chem. Soc.*, 2020, **142**, 19722-19730.

2 Chapter 2 Experimental Methodology

2.1 Materials and Instruments

All chemical reagents and solvents were purchased as analytical reagent grade, LC-MS, or GC-MS grade and used without further purification. The synthetic reactions were monitored by thin layer chromatography (TLC) plates pre-coated with silica gel (60 Å), F254, and purchased from Merck KgaA. The TLC plates were visualized *via* UV light (254, 365 nm) or iodine staining. The flash column chromatography was carried through silica gel (silica flash P60 from Fluorochem) as the stationary phase to purify synthetic reaction mixtures and crude products. ^{1}H and ^{13}C NMR spectra were recorded a Jeol 400 MHz NMR ECX-400 spectrometer at 25 °C. The chemical shift is presented in ppm and referenced by the residual solvent peak. Mass spectrometric analysis was carried out *via* a Waters MS XVEOG2XS qTOF using the direct mass spectrometric infusion spray method. Thermogravimetric analysis was performed using a Perkin Elmer thermogravimetric analyzer TGA4000 to determine the % loading of supramolecular cavitands on the surface of silica. The flash column chromatographic experiments were conducted *via* an automated PuriFlash®5.125 flash system with pre-packed or dry self-packed flash column cartridges. Interchim® silica cartridges packed with silica particles (50 µm) with a surface area of 500 m^2/g, were employed for flash column chromatographic studies. Joel JSM-7100F Field Emission Scanning Electron Microscope (SEM) was used to study the silica-bound supramolecular stationary phase's structural integrity. YMC Triart HPLC-RP_{C18} and normal silica columns were purchased from YMC Europe. MS synthetic peptide calibration mix purchased from Sciex. LC-MS/MS evaluation of new stationary phase compared with RP-C_{18} and bare silica stationary phase carried out using Eksigent ekspertTM NanoLC 425 coupled with Sciex Triple-TOFTM 5600 mass spectrometer. LC-MS/MS data processed by PeakViewTM software.

2.2 Methodology

2.2.1 Synthesis of 1,4-bis(8'-bromooctyloxy)benzene 1

Potassium carbonate (6.33 g, 0.045 mol) was added to acetonitrile (*ca* 50 ml) which is pre-dissolved with hydroquinone (1.78 g, 0.0153 mol) and 1,8-dibromooctane (11.5 ml, 0.061 mol). The reaction mixture was heated to reflux at 100 °C for 25 h, under an N_2 atmosphere. The reaction mixture was cooled, and acetonitrile was evaporated under vacuum. The solid crude product was extracted into dichloromethane (*ca* 200 mL). The

filtrate was concentrated, and the solid crude was separated by column chromatography (hexane/ethyl acetate 9:1) to afford the white solid product **1** (6.40 g, 0.01305 mol, 81 %).

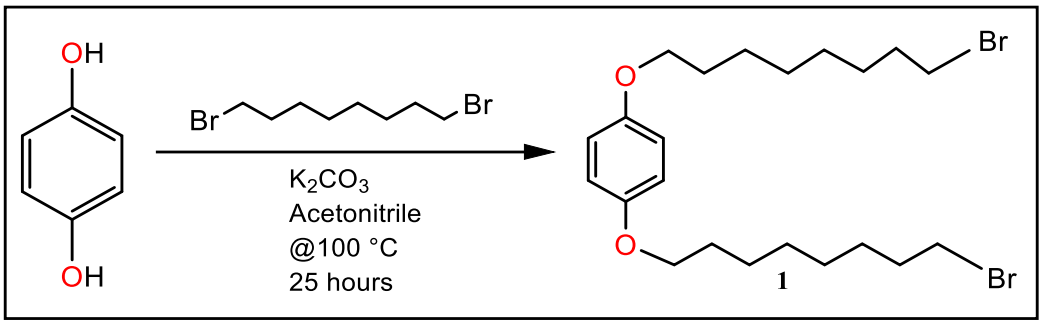

*Figure 2.1. Synthesis of 1,4-bis((8'-bromooctyl)oxy)benzene **1**.*[1]

The ^{1}H NMR spectrum of 2 :(400 MHz, $CDCl_3$) δ 6.80 (s, 4H), 3.85 (t, ^{3}J=6.8Hz, 4H) 3.42 (t, ^{3}J=6.8 Hz, 4H), 1.84 (m, 4H) 1.73 (m, 4H) 1.38 (m, 16H) ppm. ^{13}C NMR (100 MHz, $CDCl_3$, 25 °C): δ 151.6, 115.3, 68.7, 33.7, 32.6, 29.6, 28.0, 25.9, 28.6 ppm. Melting point: 82-83°C. IR vmax ATR cm^{-1} 2892, 2713, 1657, 1621,1238,1141, 981, 807 and 714

2.2.2 Synthesis of co-pillar[4+1]arene 3 by microwave irradiation

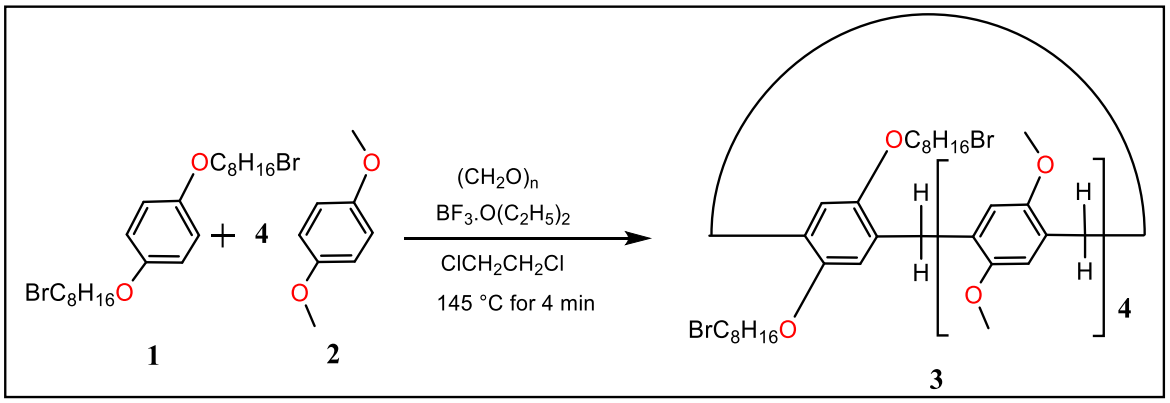

*Figure 2.2. General synthesis of co-pillar[4+1]arene **3** by microwave irradiation synthesis.*

1,4-bis(8'-bromooctyloxy)benzene **1** (1.5 g, 0.00306 mol) and 1,4-dimethoxy-benzene (g, 0.01224 mol) mixture was added to a 10-20 mL Biotage® microwave reaction vial. Later, 1,2-dichloroethane (50 mL) and paraformaldehyde (0.459 g, 0.0153 mol) were added to the above mixture and subsequent addition of $BF_3.O(C_2H_5)_2$ (1.88 mL, 0.0153 mol) before the reaction vial sealed. The mixture was pre-stirred for 30 s and heated at variable temperatures and time intervals (1-25 mins) in a Biotage Initiator 60 instrument by microwave irradiation (130 W, 2 min power cycle). 1,2-dichloromethane was evaporated from the crude reaction mixture upon cooling to room temperature. The crude solid product was triturated with acetone to give the white product. Various conditions used to optimise the synthesis of co-pillar[4+1]arene are listed in Tables 2.1-2.9

Table 2.1. Microwave synthesis of co-pillar[4+1]arene at room temperature.

No moles of **1**	No moles of **2**	Time (min)	Temperature (°C)
1	4	1	RT
		2	RT
		3	RT
		4	RT
		5	RT
		6	RT
		7	RT
		8	RT
		9	RT
		10	RT
		15	RT
		20	RT
		25	RT

Table 2.2. Microwave synthesis of co-pillar[4+1] at 50 °C.

No moles of **1**	No moles of **2**	Time (min)	Temperature (°C)
1	4	1	50
		2	50
		3	50
		4	50
		5	50
		6	50
		7	50
		8	50
		9	50
		10	50
		15	50
		20	50
		25	50

Table 2.3. Microwave synthesis of co-pillar[4+1] at 75 °C.

No moles of **1**	No moles of **2**	Time (min)	Temperature (°C)
1	4	1	75
		2	75
		3	75
		4	75
		5	75
		6	75
		7	75
		8	75
		9	75
		10	75
		15	75
		20	75
		25	75

Table 2.4. Microwave synthesis of co-pillar[4+1] at 100 °C.

No moles of **1**	No moles of **2**	Time (min)	Temperature (°C)
1	4	1	100
		2	100
		3	100
		4	100
		5	100
		6	100
		7	100
		8	100
		9	100
		10	100
		15	100
		20	100
		25	100

Table 2.5. Microwave synthesis of co-pillar[4+1] at 115 °C.

No moles of **1**	No moles of **2**	Time (min)	Temperature (°C)
1	4	1	115
		2	115
		3	115
		4	115
		5	115
		6	115
		7	115
		8	115
		9	115
		10	115
		15	115
		20	115
		25	115

Table 2.6. Microwave synthesis of co-pillar[4+1] at 125 °C.

No moles of **1**	No moles of **2**	Time (min)	Temperature (°C)
1	4	1	125
		2	125
		3	125
		4	125
		5	125
		6	125
		7	125
		8	125
		9	125
		10	125
		15	125
		20	125
		25	125

Table 2.7. Microwave synthesis of co-pillar[4+1] at 135 °C.

No moles of **1**	No moles of **2**	Time (min)	Temperature (°C)
1	4	1	135
		2	135
		3	135
		4	135
		5	135
		6	135
		7	135
		8	135
		9	135
		10	135
		15	135
		20	135
		25	135

Table 2.8. Microwave synthesis of co-pillar[4+1] at 145 °C.

No moles of **1**	No moles of **2**	Time (min)	Temperature (°C)
1	4	1	145
		2	145
		3	145
		4	145
		5	145
		6	145
		7	145
		8	145
		9	145
		10	145
		15	145
		20	145
		25	145

Table 2.9. Microwave synthesis of co-pillar[4+1] at 155 °C.

No moles of **1**	No moles of **2**	Time (min)	Temperature (°C)
1	4	1	155
		2	155
		3	155
		4	155
		5	155
		6	155
		7	155
		8	155
		9	155
		10	155
		15	155
		20	155
		25	155

There was no macrocyclic product **3** formed when the reaction was perfomed at 100 °C from 1 to 25 mins as this confirms that there ws no cyclization occurred. The ^{1}H NMR confirmed the abundance of monomeric units only. However when the temperature increases 135 °C, the formation oligomer occurred while disappearing the monomeric units. Subsequently, when the reaction conditions increased to 145 °C, the oligomers disappeared and cyclic pentamer is formed and characterized by the formation of methylene bridge at *meta* position in macrocyclized pillararene. The reaction timings were changed to study the effect of reaction time on yield of the product. The microwave reaction is optimized to produce high yield at 145 °C in 4 mins. When the reaction time increase longer time, the product starts decomposing and leaving the residual oil.

1,4-bis(8'-bromooctyloxy)benzene **1** (1.5 g, 0.00306 mol) and 1,4-dimethoxy- benzene **2** (g, 0.01224 mol) mixture was added to a 10-20 mL Biotage® microwave reaction vial containing 1,2-dichloroethane (50 mL) and paraformaldehyde (0.459 g, 0.0153 mol). Subsequently, $BF_3.O(C_2H_5)_2$ (1.88 mL, 0.0153 mol) was added to the mixture, and the reaction vial was sealed. The reaction mixture was pre-stirred for 30 seconds and subsequently heated to 145 °C for 4 min in a Biotage Initiator 60 instrument by microwave irradiation (130 W, 2 min power cycle). Later, the reaction vial was cooled to room temperature, and 1,2-dichloromethane was evaporated. The solid crude reaction mixture

was triturated with acetone and collected as a white solid product **3** *via* vacuum filtration. Yield 2.98 g (0.0027 moles, 88.5%). Melting point: 192-193 °C.

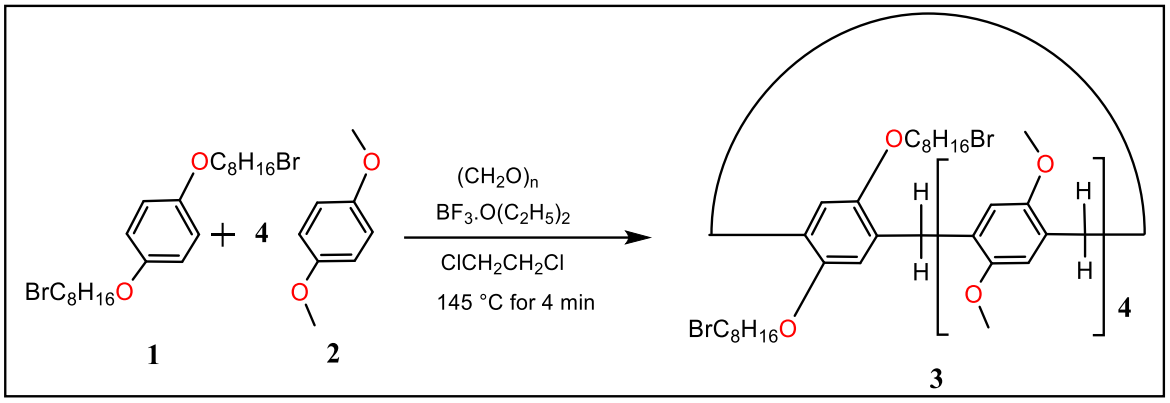

*Figure 2.3. Synthesis of co-pillar[4+1]arene **3** by microwave irradiation synthesis at 145 °C.*

The ^{1}H NMR spectrum of **3**: (400 MHz, $CDCl_3$) δ 6.62 (s, 10H), 3.91 (s, 10H), 3.79 (t, J= 7.8 Hz, 4H), 3.65 (s, 24H), 3.35 (t, J= 7.8 Hz, 4H), 1.84 (m, 4H), 1.68 (m, 4H), 1.38 (m, 8H), 1.29 (m, 8H) ppm. ^{13}C NMR (100 MHz, $CDCl_3$, 25 °C): δ 150.62, 146.71, 129.23, 128.96, 113.81, 113.56, 69.09, 56.17, 33.73, 32.65, 30.1, 29.68, 28.69, 25.91 ppm. IR vmax ATR cm^{-1} 3316, 3014, 1715,1649,1609,1241,1145, 996, 812 and 719. MS-TOF ES^{+} *m/z* calculated for $C_{59}H_{76}O_{10}Br_2$ [M+H]+: 1104.38; found: 1104.2898 and their other isotopes 1102.3054, 1103.3179, 1105.2963, 1106.2760, 1107.2970 and 1108.2913.

2.2.3 Synthesis of co-pillar[4+1]arene 3 by conventional condensation

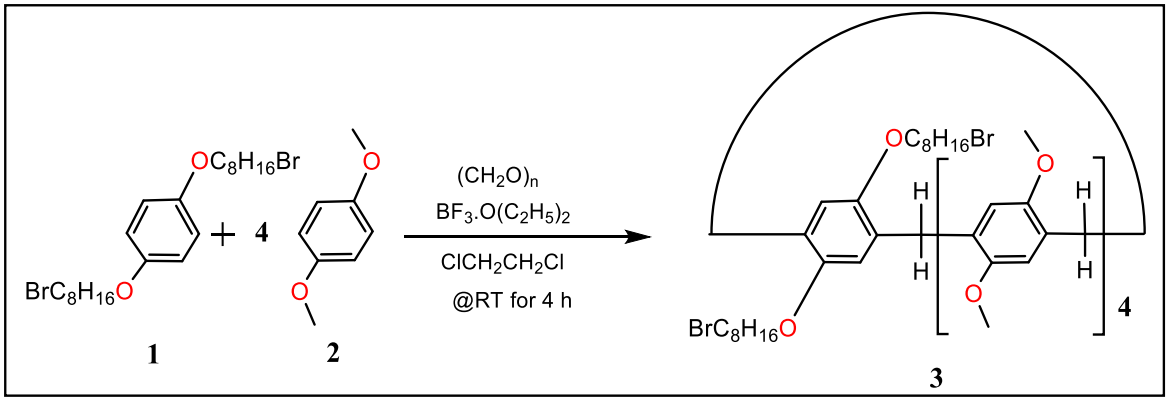

*Figure 2.4. Synthesis of co-pillar[4+1]arene **3** by a condensation method.*

1,4-bis(8'-bromooctyloxy)benzene (3.68 g, 0.0074 mol) and 1,4-dimethoxy-benzene (4.089 g, 0.0296 mol) mixture was added under nitrogen to a 250 mL round bottom flask which contains mixture of 1,2-dichloromethane (*ca.*50 mL) and paraformaldehyde (1.111 g, 0.0370 mol). Later, $BF_3.O(C_2H_5)_2$ (4.57 mL, 0.0370 mol) was injected under nitrogen and the reaction mixture was mixed for 4 hours under stirring at room temperature. The solvent was evaporated under vacuum. The crude solid residue

was triturated with acetone to offer a white solid product **3**. The yield was 2.417 g (0.002192 moles, 26.3%).

The ^{1}H NMR spectrum of **3**: (400 MHz, $CDCl_3$) δ 6.63 (s, 10H), 3.89 (s, 10H) 3.77 (t, J= 7.8 Hz, 4H), 3.65 (s, 24H), 3.41 (t, J= 7.8 Hz, 4H), 1.82 (m, 4H), 1.65 (m, 4H), 1.37 (m, 8H), 1.29 (m, 8H) ppm. ^{13}C NMR (100 MHz, $CDCl_3$, 25 °C): δ 150.68, 146.69, 129.21, 128.97, 113.82, 113.58, 69.12, 56.19, 33.72, 32.64, 30.1, 29.67, 28.69, 25.91 ppm. The melting point was recorded as 192-193 °C. IR vmax ATR cm^{-1} 3316, 3014, 1715,1649,1609,1241,1145, 996, 812 and 719. MS-TOF ES^{+} *m/z* calculated for $C_{59}H_{76}O_{10}Br_2$ [M+H]: 1104.38; found: 1104.3767 and their another isotopes 1105.3832, 1106.3834, 1107.3568, 1102.3785 and 1103.3689.

2.3 Synthesis of pyrogallol[4]arene derivative

2.3.1 Synthesis of C-hydroxybutyl-pyrogallol[4]arene 4

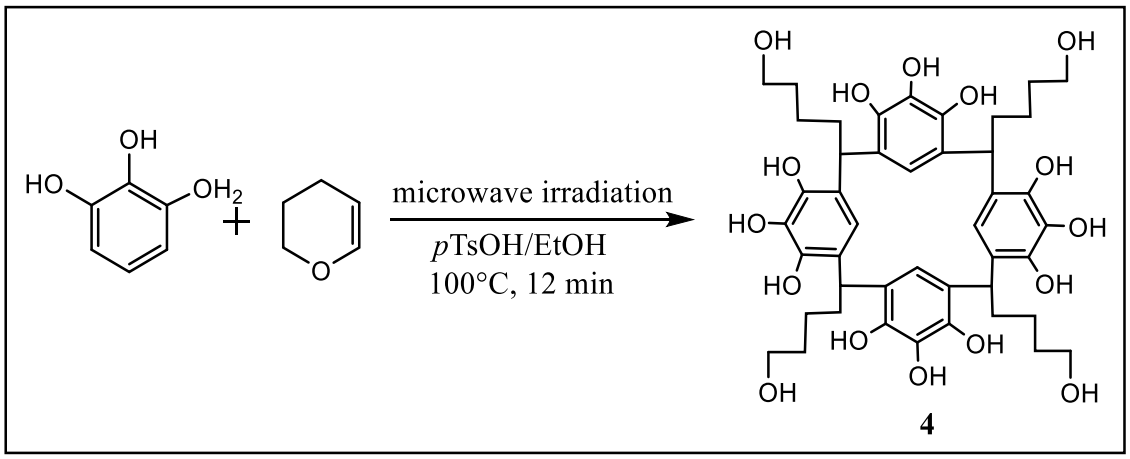

*Figure 2.5.Synthesis of C-hydroxybutyl-pyrogallol[4]arene **4**.*

C-Hydroxybutylpyrogallol[4]arene **4** was synthesized *via* the previously reported one-pot microwave-assisted irradiation reaction. In general, 2,3-dihydro-pyran (0.912 ml, 0.01 moles) and pyrogallol (1.26 g, 0.01 moles) was added to the solution of *p*-toluenesulphonic acid (0.1g, 0.58 mmol) in ethanol (*ca*. 10 mL). The reaction vial (CEM pressure vial) was sealed. The mixture was pre-stirred for 30 sec and heated to 100 °C for 12 min in a biotage Initiator 60 by microwave irradiation *via* 130 W, 2 min. power cycle. The reaction mixture vessel was cooled to room temperature. The reaction mixture was vacuum filtered and the residue was washed successively with an ethanol and water mixture (4:1, 5×60 ml). The yielded product was a white solid, and the yield was 92% (1.90 g, 3.70 mmol). The melting point was recorded as 157-159 °C

^{1}H NMR (400 MHz, d_6-Acetone) δ = 8.74 (br. s, 8H, OH), 8.18 (s, 4H, OH), 6.78 (s, 4H, Ar-H), 4.71 (s, 4H, (CH_2)OH), 4.21 (t, J= 7.8 Hz, 4H, $CHAr_2$), 3.61 (t, J= 7.8 Hz, 8H, CH_2OH),

1.89 (m, 8H, CH_2), 1.44 (m, 8H, CH_2), 1.18 (m, 8H, CH_2) ppm. ^{13}C NMR (101 MHz, d_6-Acetone) δ =139.5, 132.8 124.5, 113.5, 61.0, 39.1, 35.1, 31.7, 24.3 ppm. IR v_{max} ATR cm^{-1} 3156, 2938, 1609, 1491, 1437, 1361, 1279, 1219, 1158, 1018, 841, 516. MS -TOF *m/z* for $C_{44}H_{56}O_{16}$ calculated. 840.36, found: 840.3612 $[M]^+$.

2.3.1 Synthesis of C-bromobutylcalix[4]pyrogallolarene 5

C-Hydroxybutyl-pyrogallol[4]arene **4** (4.2 g, 5 mmol) was dissolved in CH_2Cl_2 (30 mL) and the reaction solution temperature was cooled down at 0°C under nitrogen. Subsequently, dropwise added phosphorous tribromide (2.84 mL, 30 mmol, 6.0 equiv). The reaction mixture was stirred to obtain room temperature under 1.5 h. The reaction mixture was heated at 40 °C for 5 h with stirring. The reaction mixture was then evaporated under a vacuum to collect crude oil. The resultant oil was sonicated in water (30 mL) for 15 min and vacuum filtered. The solid filtrate was vacuum dried. Product **5** was in pink colour with a yield of 64% (3.50 g, 3.2 mmol). The melting point was recorded as 164-167 °C.

^1H NMR (400 MHz, d_6-Acetone) δ = 8.64 (s, 8H, OH), 8.08 (s, 4H, OH), 6.88 (s, 4H, Ar-H, 1H), 4.13 (t, J= 7.8 Hz 4H, 7-H), 3.52 (t, J= 7.8 Hz 8H, 11-H_2), 1.84 (m, 8H, 10-H_2), 1.43 (m, 8H, 8-H_2) 1.20 (m, 8H, 9-H_2) ppm. ^{13}C NMR (101 MHz, d_6-Acetone) δ =145.1, 137.1, 127.2, 119.5, 38.2, 35.2, 33.6, 32.8, 24.8 ppm. IR v_{max} ATR cm^{-1} 3204, 2931, 2864, 1619, 1472, 1384, 1306, 1089, 1031, 978, 725. ESI-MS *m/z* calculated for $C_{44}H_{52}{}^{79}Br_4O_{12}$ was 1088.01, found: 1088.0192,1090.0216, 1092.0201, 1094.0112 and 1096.0109 $[M]^+$.

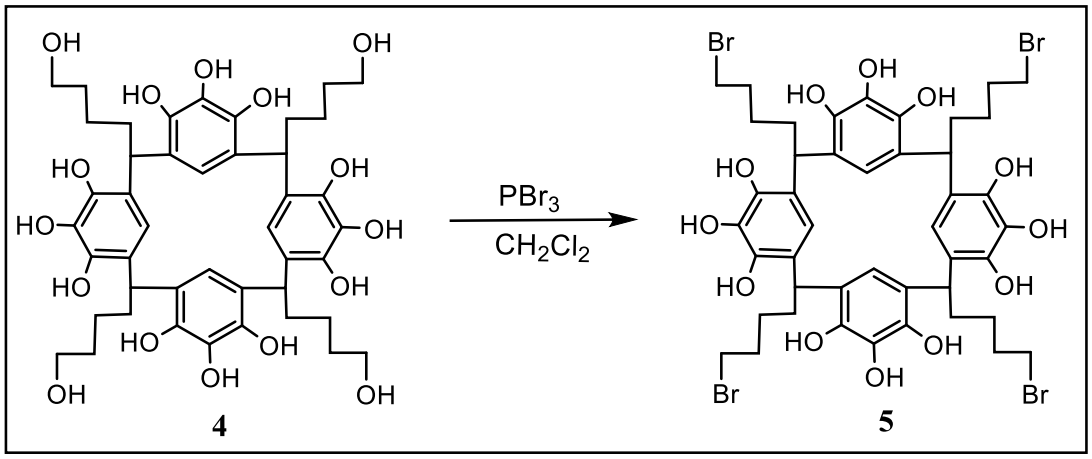

*Figure 2.6. Synthesis of C-bromobutylcalix[4]pyrogallolarene **5.***

2.4 Flash Column chromatography of co-pillar[4+1]arene stationary phase

2.4.1 Synthesis of silica-bound co-pillar[4+1]arene flash column stationary phase 6

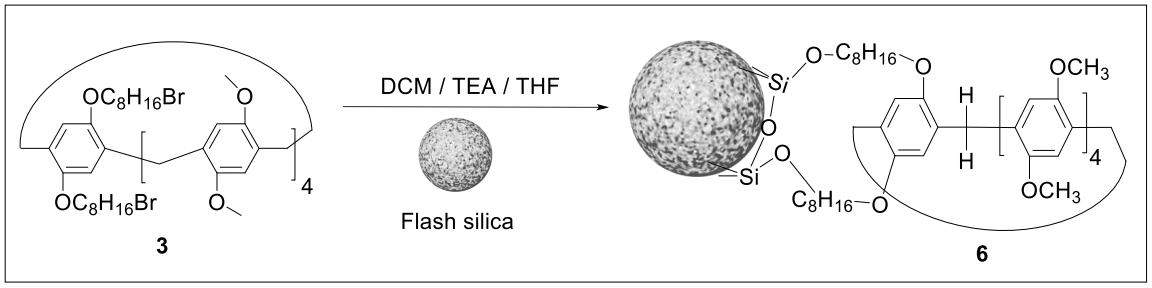

*Figure 2.7. Synthesis of silica-bound co-pillar[4+1]arene flash column stationary phase **6**.*

Interchim® flash column general purpose grade silica (irregular, 12 g, 50 µm) was stirred overnight in an equal basic solution of tetrahydrofuran and triethylamine (*ca*. 100 mL). The reaction mixture was vacuum filtered and dried at room temperature. The activated silica (12g) was reacted with the co-pillar[4+1]arene **3** by overnight stirring in acetone (*ca.* 100 mL). The stationary phase was vacuum filtered, washed with water/methanol, and dried at room temperature.

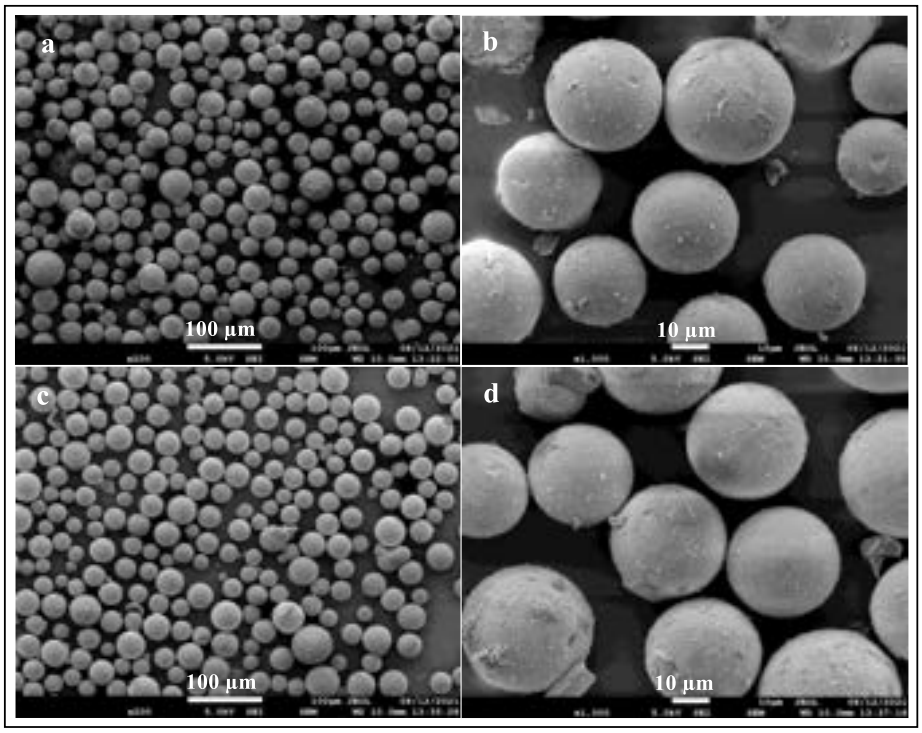

Figure 2.8 SEM images showing silica 15 µm particles at (a) 100 and (b) 10 µm magnification and silica functionalized with co-pillar[4+1]arene stationary phase particles at (c) 100 and (d) 10 µm magnification.

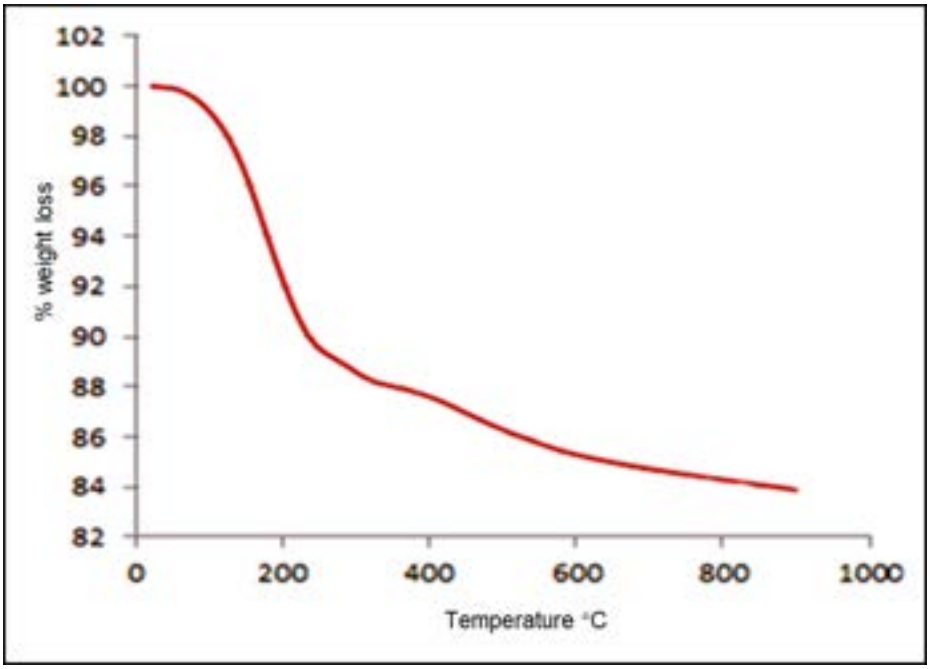

*Figure 2.9 Thermogravimetric analysis (TGA) of co-pillar[4+1]arene silica bound **6** stationary phase for flash column chromatography.*

The silica-bound co-pillar[5]arene **6** (10 mg) was removed from the sample and analyzed by thermogravimetric analysis (TGA). In brief, a silica-bound co-pillar[5]arene **6** (10 mg) was placed on an empty TGA crucible, and the temperature program was increased to 900 °C from the initial 30 °C.

2.4.2 Flash Column Conditioning

Silica-bound co-pillar[5]arene **6** gel (12 g) was dry-packed into an empty flash column (62 × 12 mm i.d.) cartridge by tapping method. The flash column was purged with cyclohexane (100%) for 15 min at 15 mL/min, ethyl acetate (100%) for 30 min at 15 mL/min, and finally with methanol (100%) for 30 min at 15 mL/min. Later the flash column was stored with methanol: water (50:50) for further chromatographic analysis.

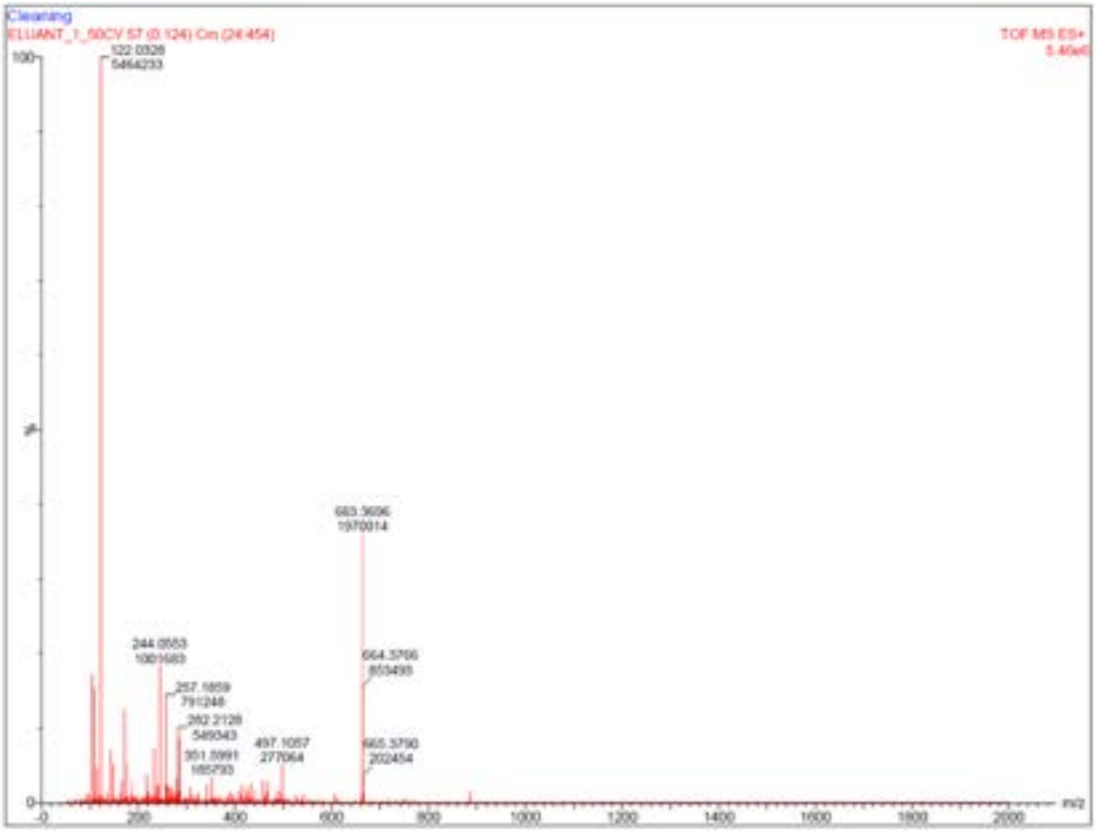

*Figure 2.10 LC-MS spectrum of mobile phase eluent from co-pillar[4+1]arene bonded-silica flash column **6** at 50 column volumes.*

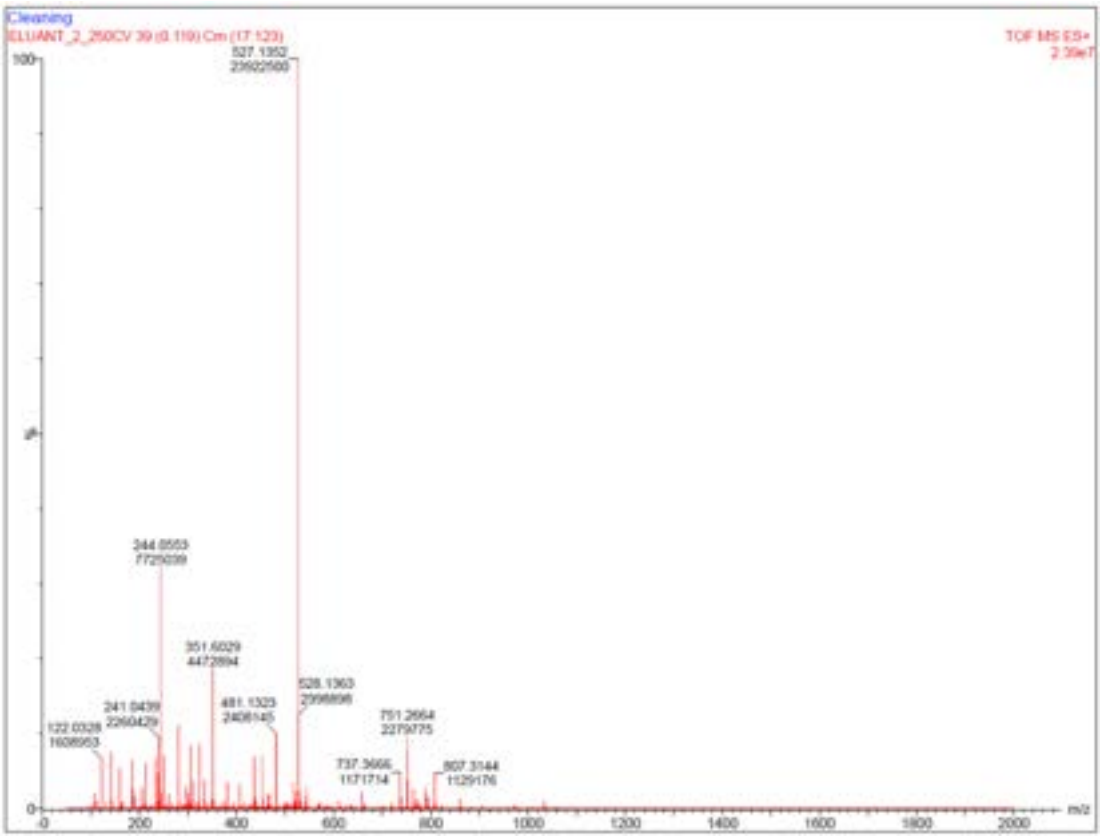

*Figure 2.11 LC-MS spectrum of mobile phase eluent from co-pillar[4+1]arene bonded-silica flash column **6** at 250 column volumes.*

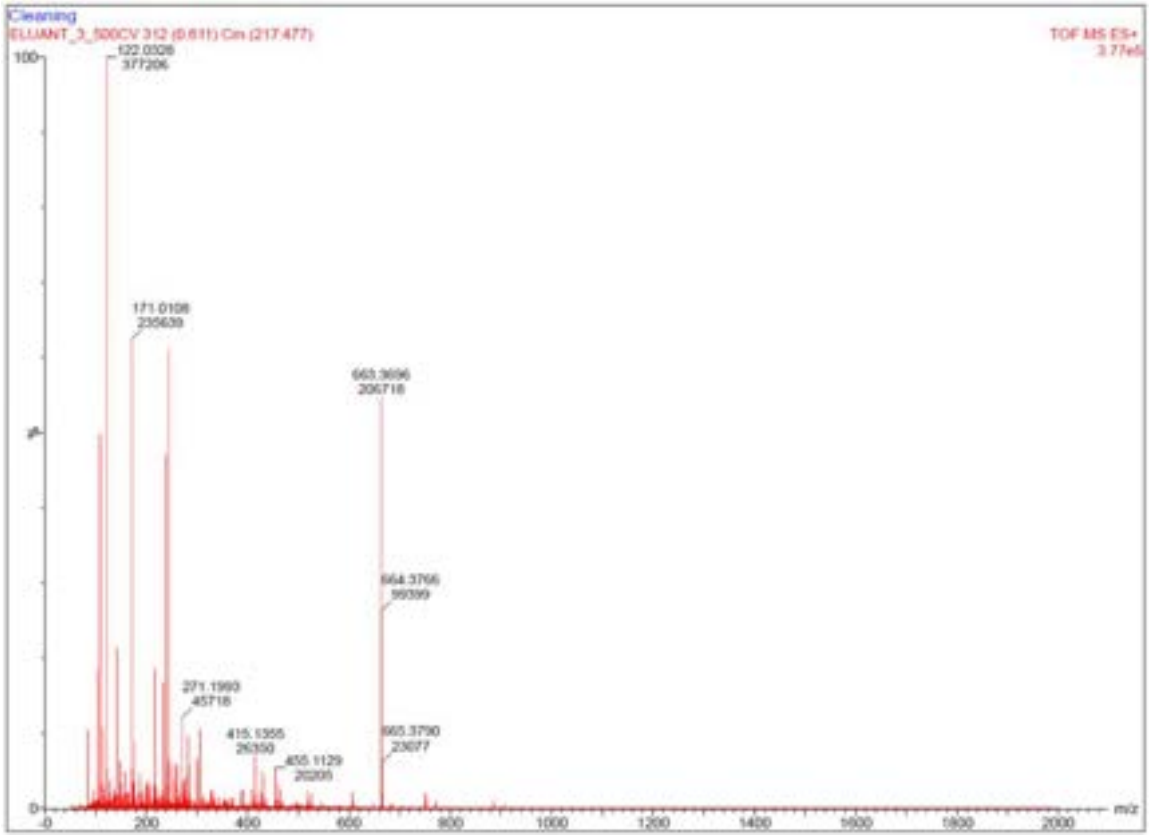

*Figure 2.12 LC-MS spectrum of mobile phase eluent from co-pillar[4+1]arene bonded-silica flash column **6** at 250 column volumes.*

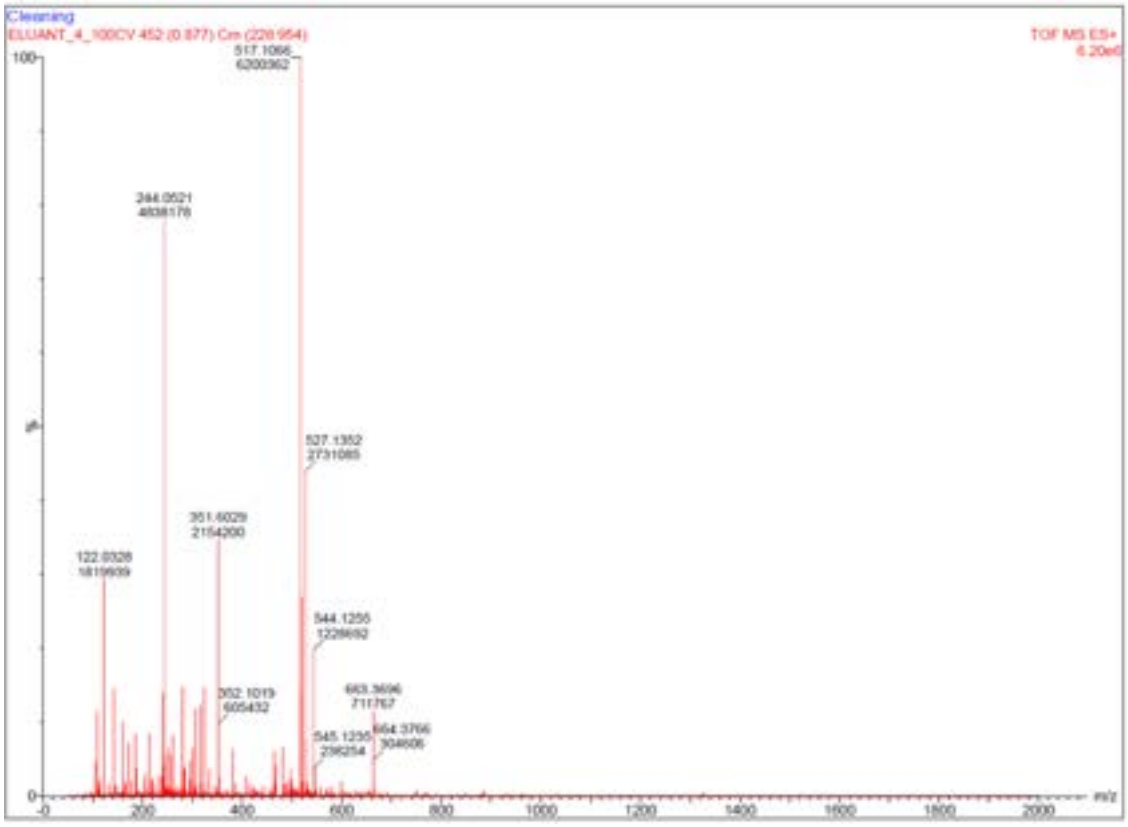

*Figure 2.13 LC-MS spectrum of mobile phase eluent from co-pillar[4+1]arene bonded-silica flash column **6** at 1000 column volumes.*

The silica-bound co-pillar[5]arene **6** flash column stationary phase stability was performed by collecting the eluent at 50, 250, 500, 750 and 1000 column volumes. The eluent at different column volumes was further subjected to the direct mass spectrometric infusion analysis to identify the elution of co-pillar[4+1]arene **3** from the silica bound co-pillar[5]arene **6**.

2.4.3 Separation of xylene isomers, toluene, and ethylbenzene on silica-bound co-pillar[5]arene 6 flash column

Flash column chromatography was performed *via* an automated PuriFlash®5.125 flash system. The column (62 × 12 mm i.d.) was equilibrated *via* in-built optimization parameters dependent on the column and particle size. In this case, the flash column was equilibrated with initial 100% ethyl acetate to 50 % and again ramped to 90% of ethyl acetate to meet mobile phase conditions to start the analysis under 12 mins. The analytes (a) *m*-xylene, (b) toluene, (c) *o*-xylene, (d) *p*-xylene, and (e) ethylbenzene were prepared by dissolving 0.5 mL of analytes in methanol: ethyl acetate (1:1). Methanol and ethyl acetate (10:90 %) was used as mobile phase under isocratic conditions with a 21 mL/min flow rate. The injection volume was 2 mL and injected automatically using Sample Loop, SS, 2ml, 1/8" tubing, Compression fittings. UV-vis detection was used to measure the 200-800 nm absorbance. The threshold fraction collection volume was set to 13 mL. The flash column fractions were collected and subjected to characterize *via* ^{1}HNMR.

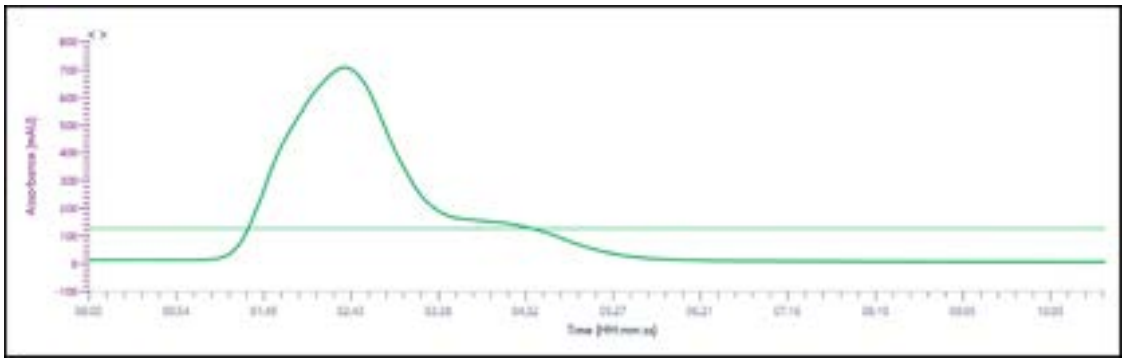

*Figure 2.14 Separation of xylene isomers, toluene, and ethylbenzene using methanol: water (80:20) on silica-bound co-pillar[4+1]arene flash column stationary phase **6**.*

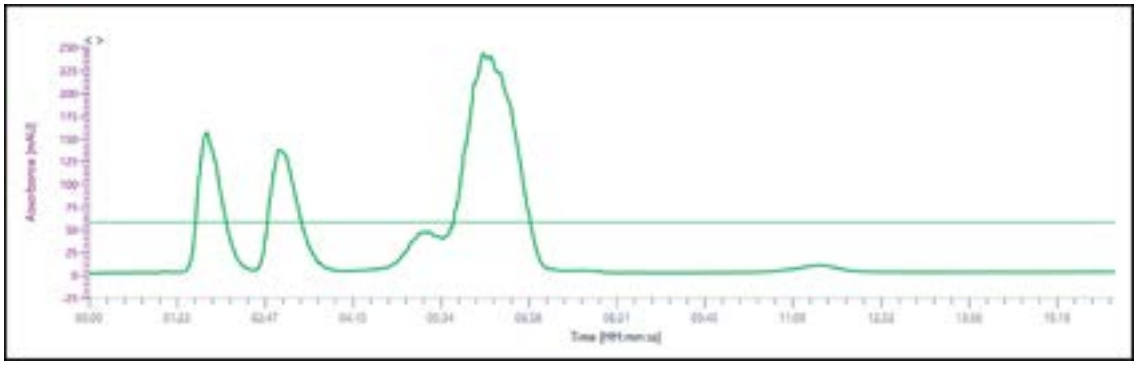

*Figure 2.15 Separation of xylene isomers, toluene, and ethylbenzene using methanol: ethyl acetate (30:70) on silica-bound co-pillar[4+1]arene flash column stationary phase **6**.*

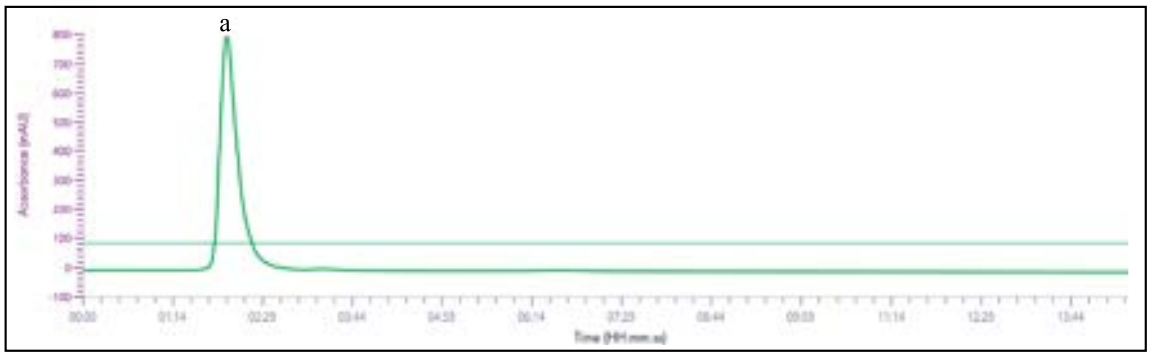

*Figure 2.16 Separation of m-xylene on silica-bound co-pillar[4+1]arene flash column cartridge **6**.*

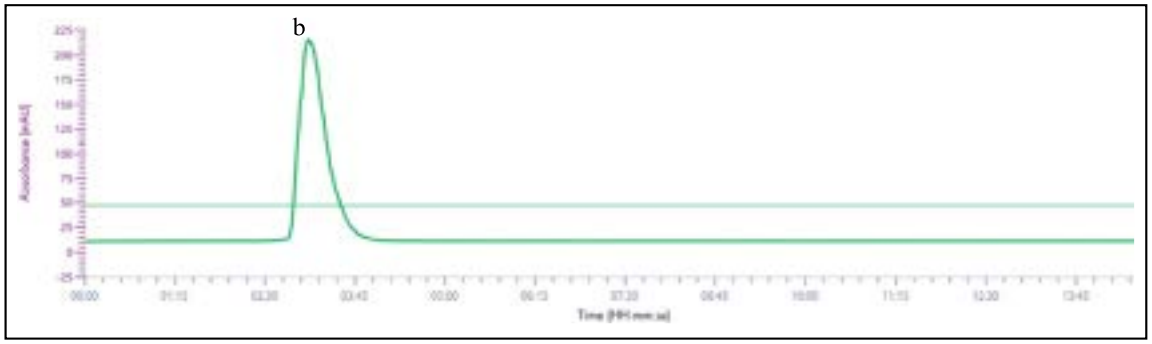

*Figure 2.17 Separation of toluene on silica-bound co-pillar[4+1]arene flash column cartridge **6**.*

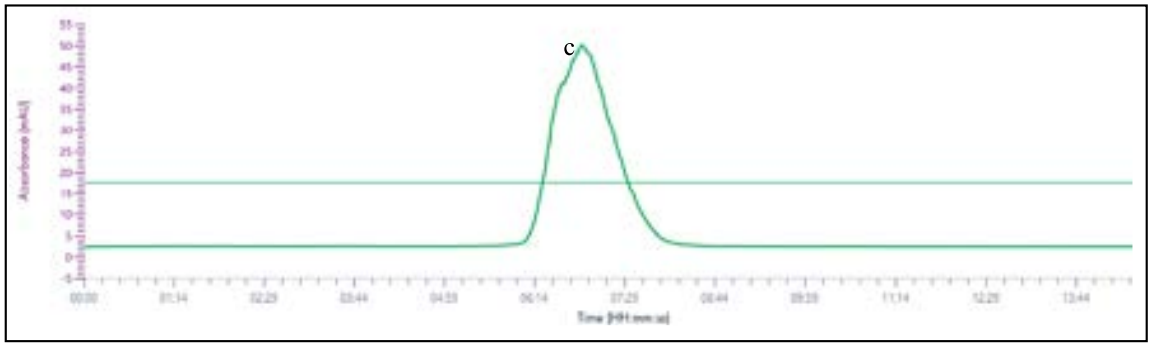

*Figure 2.18 Separation of o-xylene on silica-bound co-pillar[4+1]arene flash column cartridge **6**.*

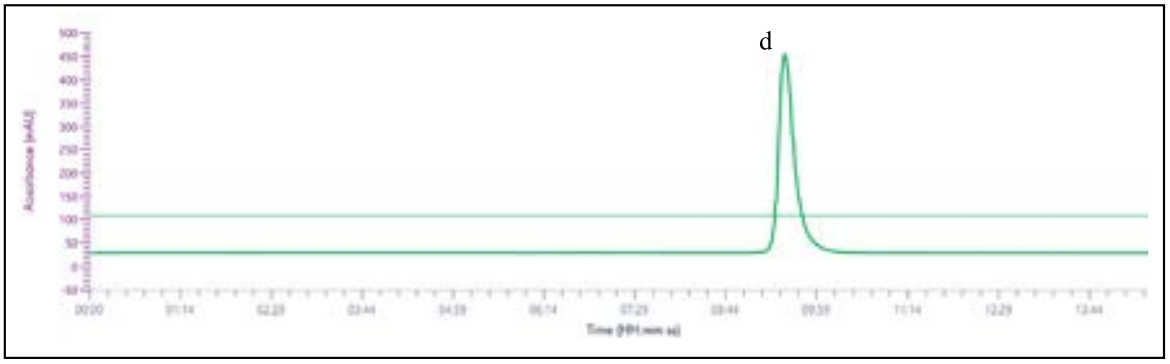

*Figure 2.19 Separation of p-xylene on silica-bound co-pillar[4+1]arene flash column cartridge **6**.*

2.4.4 Validation of silica-bound co-pillar[4+1]arene flash column stationary phase 6

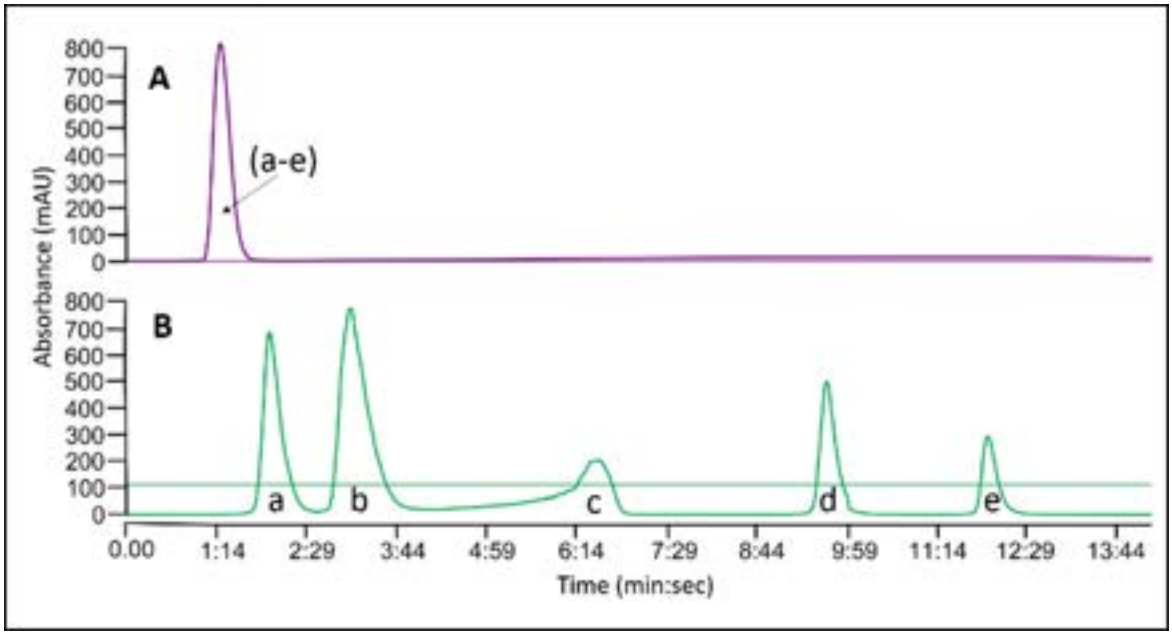

Figure 2.20 Flash column separation of Fisher Scientific xylene and toluene sample mixture; (a) m-xylene, (b) toluene, (c) o-xylene, (d) p-xylene, and (e) ethylbenzene on (A) normal phase Interchim® flash column and (B) co-pillar[4+1]arene bound-silica stationary phase.

The flash column co-pillar[4+1]arene bonded-silica gel stationary phase **6** chromatographic performance was validated against normal phase (12g, 15 µm, (62 × 12 mm i.d.) chromatographic performance under identical chromatographic conditions. The Fisher's xylene and toluene (1 mL, CAS no: 1330-20-7 and CAS number:108-88-3) was injected on normal phase, and silica bound co-pillar[4+1]arene flash stationary column phase **6** using methanol: ethyl acetate (10:90%) under isocratic mobile phase elution conditions. The eluents from both the normal phase and silica-bound co-pillar[4+1]arene flash column stationary phase **6** were analyzed and characterized by ^{1}HNMR.

2.5 Co-pillar[4+1]arene bound silica gel LC-MS stationary phase 7

2.5.1 Synthesis of silica bound co-pillar[4+1]arene LC-MS stationary phase 7

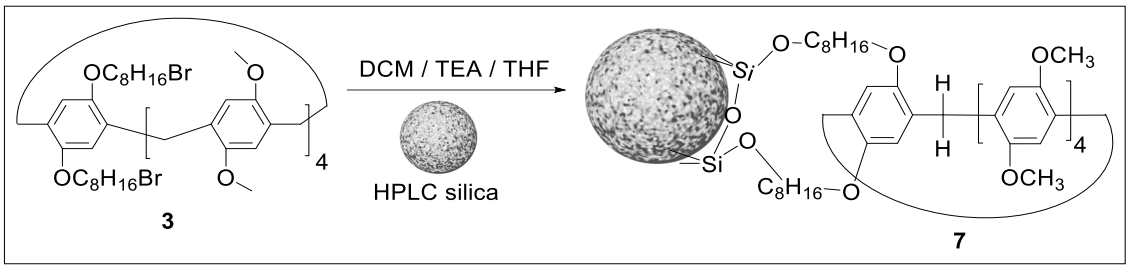

*Figure 2.21. Synthesis of silica bound co-pillar[4+1]arene LC-MS stationary phase **7.***

YMC-Japan Triart HPLC silica grade (3 g, 5 µm, and pore size 120Å) was stirred overnight in a solution of tetrahydrofuran and triethylamine (1:1, ca. 50 ml) at room temperature. The solvent mixture was evaporated under a vacuum. The solid residue dried at room temperature. Co-pillar[4+1]arene **3** (1.0 gm) was dissolved in dichloromethane (50 mL). Co-pillar[4+1]arene **3** solution was added to the dried basified silica and reacted overnight under stirring at room temperature. The silica-bound co-pillar[4+1]arene stationary phase **7** was collected after evaporation of dichloromethane under vacuum. The stationary phase **7** was washed with dichloromethane and methanol to remove unreacted materials. The stationary phase **7** was dried overnight in the fume hood at room temperature.

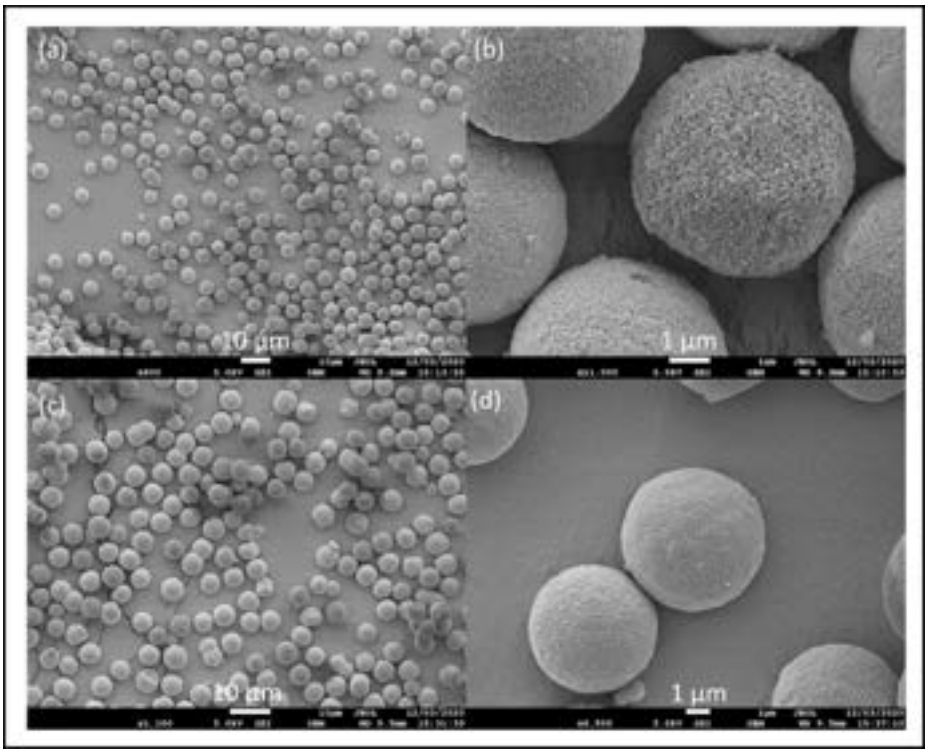

Figure 2.22 SEM images showing silica 5 µm particles at (a) 10 and (b) 1 µm magnification and silica functionalized with co-pillar[4+1]arene stationary phase particles at (c) 10 and (d) 1 µm magnification.

The silica-bound co-pillar[5]arene **7** (25 mg) was removed from the synthesized stationary phases sample and analyzed by thermogravimetric analysis (TGA). In brief, a silica-bound co-pillar[5]arene **7** (10 mg) was placed on an empty TGA crucible, and the temperature program was increased to 900 °C from the initial 30 °C.

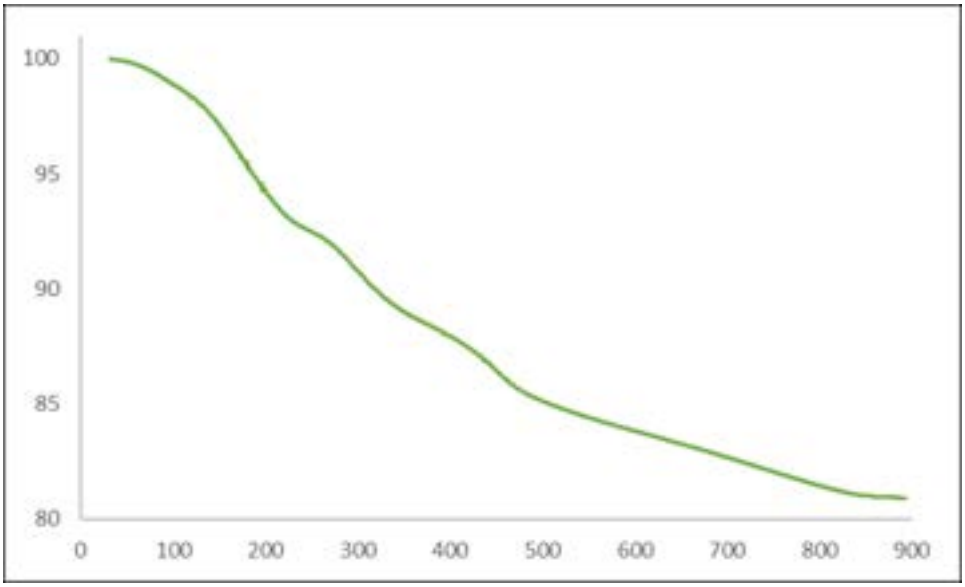

*Figure 2.23 Thermogravimetric analysis of co-pillar[4+1]arene bound-silica HPLC stationary phase **7**.*

2.5.2 Column packing of silica bound co-pillar[4+1]arene LC-MS stationary phase 7

Silica bound co-pillar[4+1]arene LC-MS stationary phase **7** was packed *via* a wet slurry packing method into a capillary LC column by YMC Europe in Japan. The capillary LC column dimensions are 12 nm, 150 x 0.3 mm with 1/32” end fitting. The packed column was conditioned with water: acetonitrile (1:1) and supplied back for chromatographic analysis studies. The newly packed capillary LC column was eluted with water: acetonitrile (1:1) to condition the column form overnight at 2 µL min^{-1}. The silica-bound co-pillar[4+11]arene **7** capillary LC stationary phase stability was performed by collecting the eluent at 1, 50 and 100 column volumes. The eluent at different column volumes was further subjected to the direct mass spectrometric infusion analysis to identify the elution of co-pillar[4+1]arene **3** from the silica bound co-pillar[5]arene **7**.

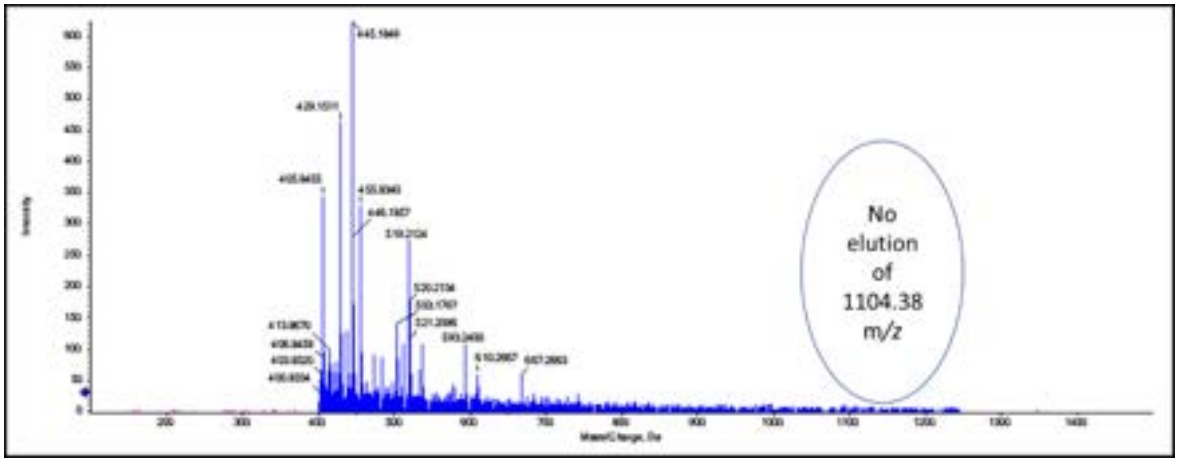

*Figure 2.24 LC-MS spectrum of eluent from silica-bound co-pillar[4+1]arene stationary phase **7** at 1 column volume.*

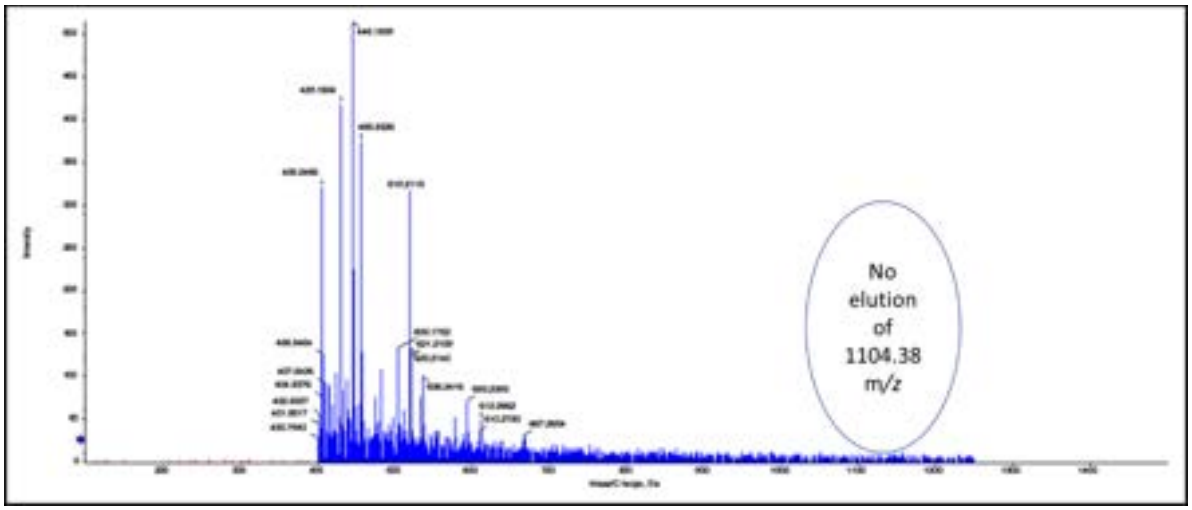

*Figure 2.25 LC-MS spectrum of eluent from silica-bound co-pillar[4+1]arene stationary phase **7** at 50 column volume.*

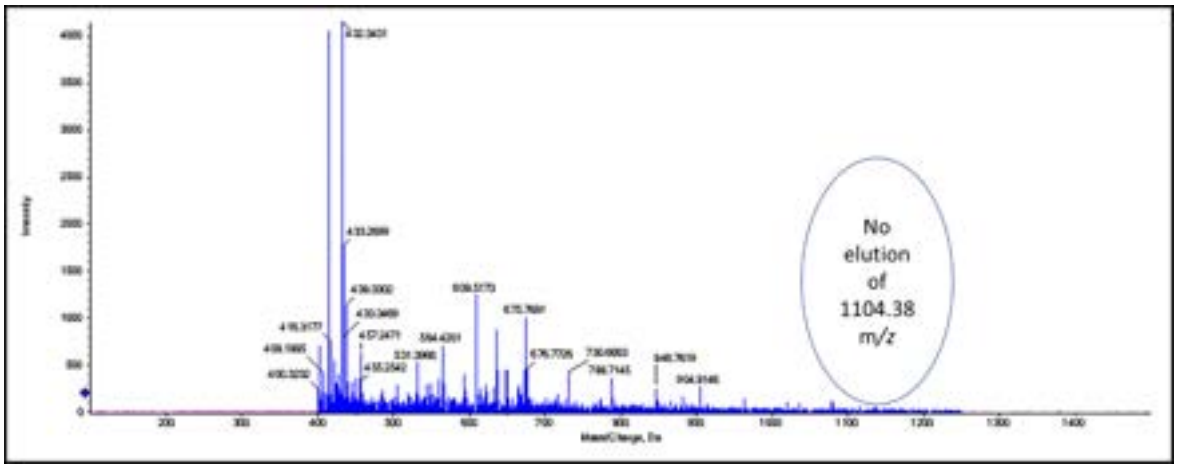

*Figure 2.26 LC-MS spectrum of eluent from silica-bound co-pillar[4+1]arene stationary phase **7** at 100 column volume.*

2.6 LC-MS/MS separation of calibration mix peptides on RP-C18, co-pillar[4+1]arene column 7, and silica normal phase

The chromatographic performance of the newly synthesized HPLC silica-bound co-pillar[4+1]arene stationary phase was evaluated using five selected peptides from a peptide calibration mix *via* LC-MS/MS, in comparison with RP-C_{18} and a normal phase silica.

Table 2.10 TripleTOF 5600+ m/z values of calibration peptides.

Peptide	MS-MS *m/z*
IGNEQGVSR	485.25302
SAEGLDASASLR	593.80053
AVGANPEQLTR	583.31360
VGNEIQYVALR	636.35273
VFTPLEVDVAK	613.34955

TOF MS^1 collision energy was set to 10 while the MS scan range was set to 400-1250. TOF MS^2 collision energy was set to 40 while the MS scan range was set to 100-1500.

2.6.1 Separation of five peptides on standard RP-C18 column

The chromatographic conditions for the separation of 5 peptides of standard PepCal calibration mix on RP-C_{18} as described below.

Column: RP-C_{18}

Flow rate: 7.5 µL min^{-1}

Injection Volume: 2 µL

Column Temperature: 30°C

Mobile Phases: solvent A: water + 0.1% formic acid

solvent B: acetonitrile + 0.1% formic acid

Analytes: IGNEQGVSR, SAEGLDASASLR, AVGANPEQLTR, VGNEIQYVALR, and VFTPLEVDVAK peptides

Concentration of Analyte: 20 fmol $µL^{-1}$

Mobile phase gradient conditions:

Time (min)	%A	%B
0.0	97	03
5.0	65	35
6.0	20	80
8.0	20	80
9.0	97	03
15	97	03

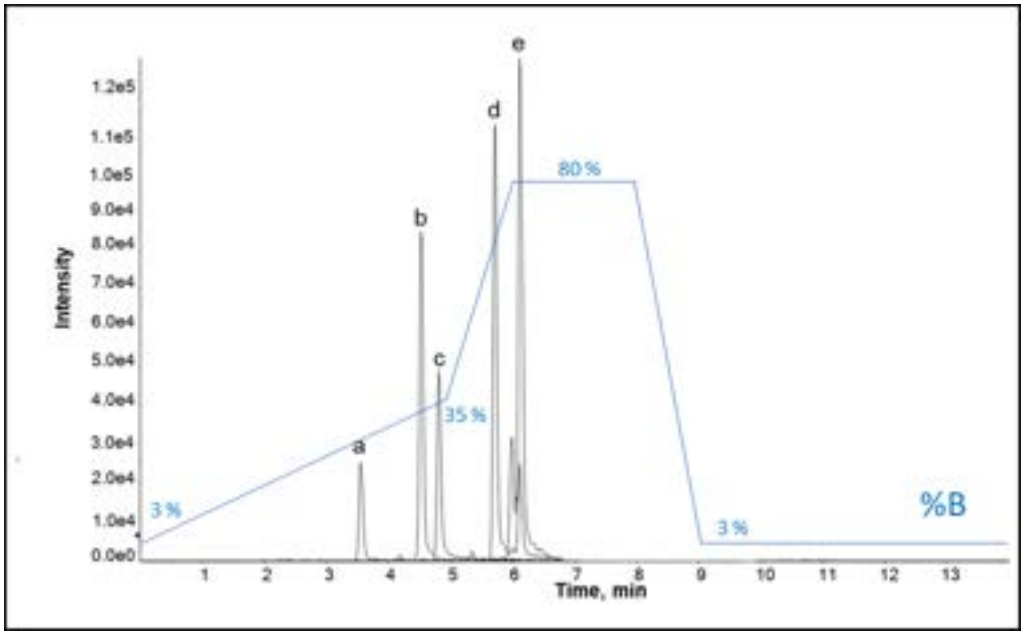

Figure 2.27 LC-MS/MS chromatographic separation of mixed peptide standard IGNEQGVSR (a), AVGANPEQLTR (b), SAEGLDASASLR (c), VGNEIQYVALR (d) and VFTPLEVDVAK (e) on RP-C_{18} silica.

2.6.2 Separation of five peptides on silica-bound co-pillar[4+1]arene stationary phase 7 using RP-C_{18} mobile phase conditions

The chromatographic conditions for separating 5 peptides of standad PepCal calibration mix on silica-bound co-pillar[4+1]arene stationary phase 7 as described below.

Column: silica-bound co-pillar[4+1]arene stationary phase **7**

Flow rate: 7.5 µL min^{-1}

Injection Volume: 2 µL

Column Temperature: 30°C

Mobile Phases: solvent A: water + 0.1% formic acid

solvent B: acetonitrile + 0.1% formic acid

Analytes: IGNEQGVSR, SAEGLDASASLR, AVGANPEQLTR, VGNEIQYVALR and VFTPLEVDVAK peptides

Concentration of Analyte: 20 fmol μL^{-1}

Mobile phase gradient conditions:

Time (min)	%A	%B
0.0	97	03
5.0	70	30
6.0	20	80
8.0	20	80
9.0	97	03
15	97	03

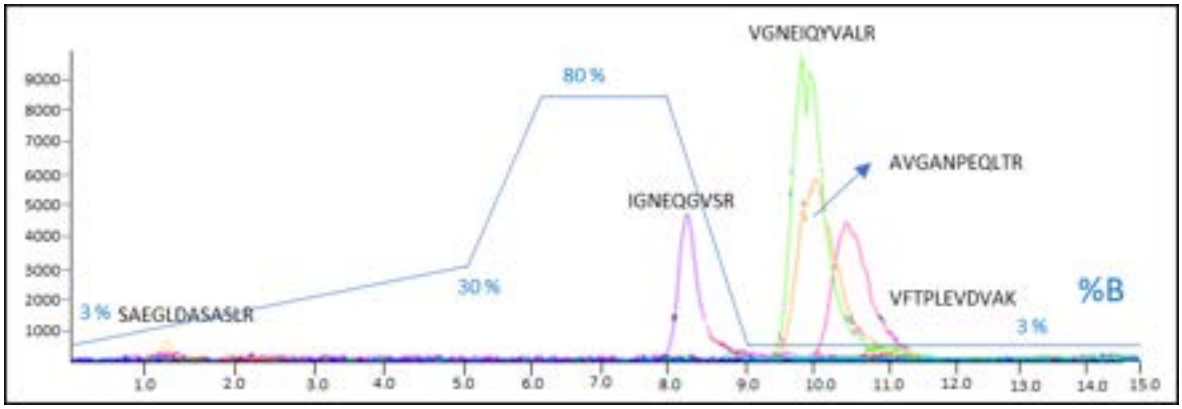

*Figure 2.28 Separation of five peptides on silica-bound co-pillar[4+1]arene HPLC column **7** using RP-C18 gradient conditions.*

2.6.3 Separation of five peptides on silica-bound co-pillar[4+1]arene stationary phase 7

The chromatographic conditions for separating 5 peptides from standard PepCal calibration mix on a silica-bound co-pillar[4+1]arene stationary phase **7** as described below.

Column: silica-bound co-pillar[4+1]arene stationary phase **7**

Flow rate: 7.5 µL min^{-1}

Injection Volume: 2 µL

Column Temperature: 30°C

Mobile Phases: solvent A: water + 0.1% formic acid

solvent B: acetonitrile + 0.1% formic acid

Analytes: IGNEQGVSR, SAEGLDASASLR, AVGANPEQLTR, VGNEIQYVALR and VFTPLEVDVAK

Concentration of Analyte: 20 fmol μL^{-1}

Mobile phase gradient conditions:

Time (min)	%A	%B
0.0	97	03
5.0	85	15
6.0	20	80
8.0	20	80
9.0	97	03
15	97	03

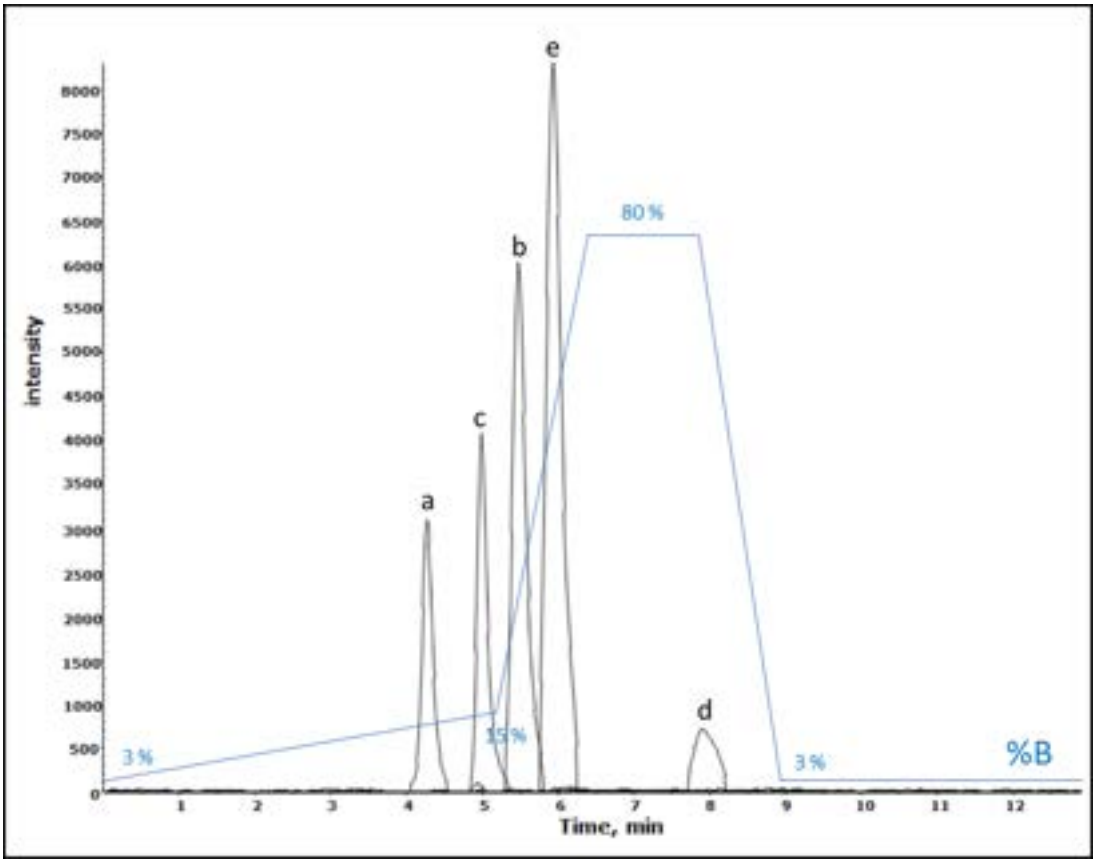

*Figure 2.29 LC-MS/MS chromatographic separation of mixed peptide standard IGNEQGVSR (a), SAEGLDASASLR (b), AVGANPEQLTR (c), VGNEIQYVALR (d) and VFTPLEVDVAK (e) on silica-bound co-pillar[4+1]arene HPLC column **7**.*

2.6.4 Separation of five peptides on RP-C18 using silica-bound co-pillar[4+1]arene 7 conditions

Column: RP-C_{18}

Flow rate: 7.5 µL min^{-1}

Injection Volume: 2 µL

Column Temperature: 30°C

Mobile Phases: solvent A: water + 0.1% formic acid

solvent B: acetonitrile + 0.1% formic acid

Analytes: IGNEQGVSR, SAEGLDASASLR, AVGANPEQLTR, VGNEIQYVALR and VFTPLEVDVAK

Concentration of Analyte: 20 fmol μL^{-1}

Mobile phase gradient conditions:

Time (min)	%A	%B
0.0	97	03
5.0	85	15
6.0	20	80

8.0	20	80
9.0	97	03
15	97	03

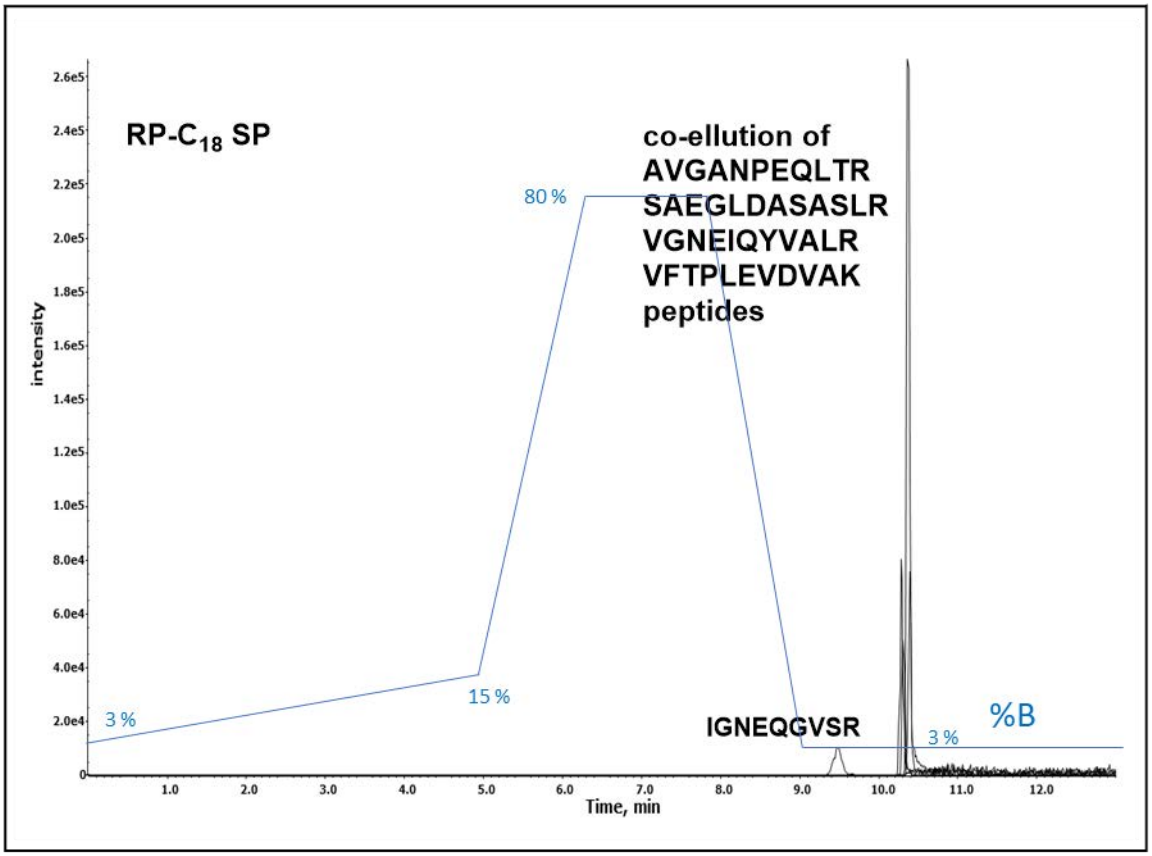

*Figure 2.30 LC-MS/MS chromatographic separation of five mixed peptides standard on RP-C_{18} using silica-bound co-pillar[4+1]arene **7** conditions.*

2.6.5 Separation of five peptides on normal phase column using silica-bound co-pillar[4+1]arene 7 conditions

Column: Normal Phase Silica

Flow rate: 7.5 µL min^{-1}

Injection Volume: 2 µL

Column Temperature: 30°C

Mobile Phases: solvent A: water + 0.1% formic acid

solvent B: acetonitrile + 0.1% formic acid

Analytes: IGNEQGVSR, SAEGLDASASLR, AVGANPEQLTR, VGNEIQYVALR and VFTPLEVDVAK

Concentration of Analyte: 20 fmol $µL^{-1}$

Mobile phase gradient conditions:

Time (min)	%A	%B
0.0	97	03
5.0	85	15
6.0	20	80
8.0	20	80
9.0	97	03
15	97	03

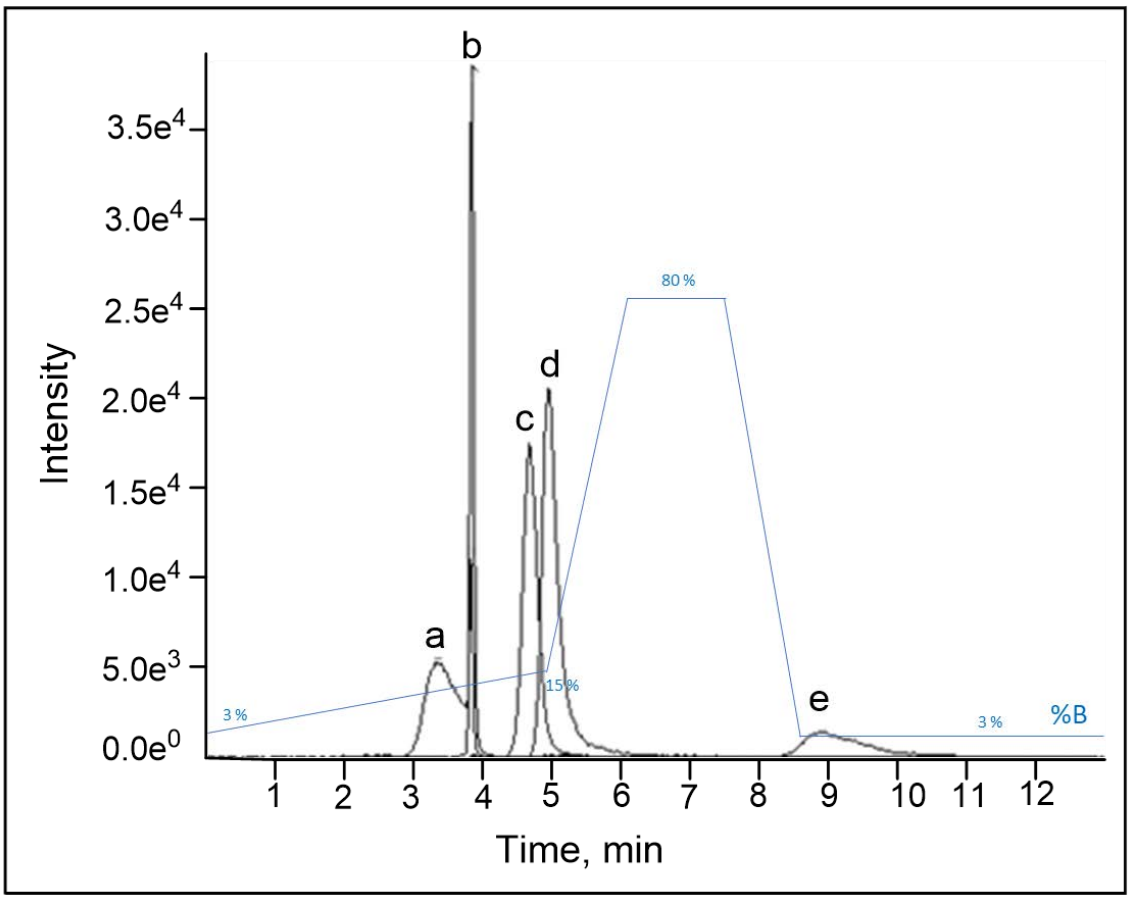

Figure 2.31 LC-MS/MS chromatographic separation of mixed peptide standard IGNEQGVSR (a), SAEGLDASASLR (b), AVGANPEQLTR (c), VGNEIQYVALR (d) and VFTPLEVDVAK (e) on normal phase silica.

2.6.6 Separation of five peptides on RP-C18, silica-bound co-pillar[4+1]arene 7 and normal phase under identical conditions

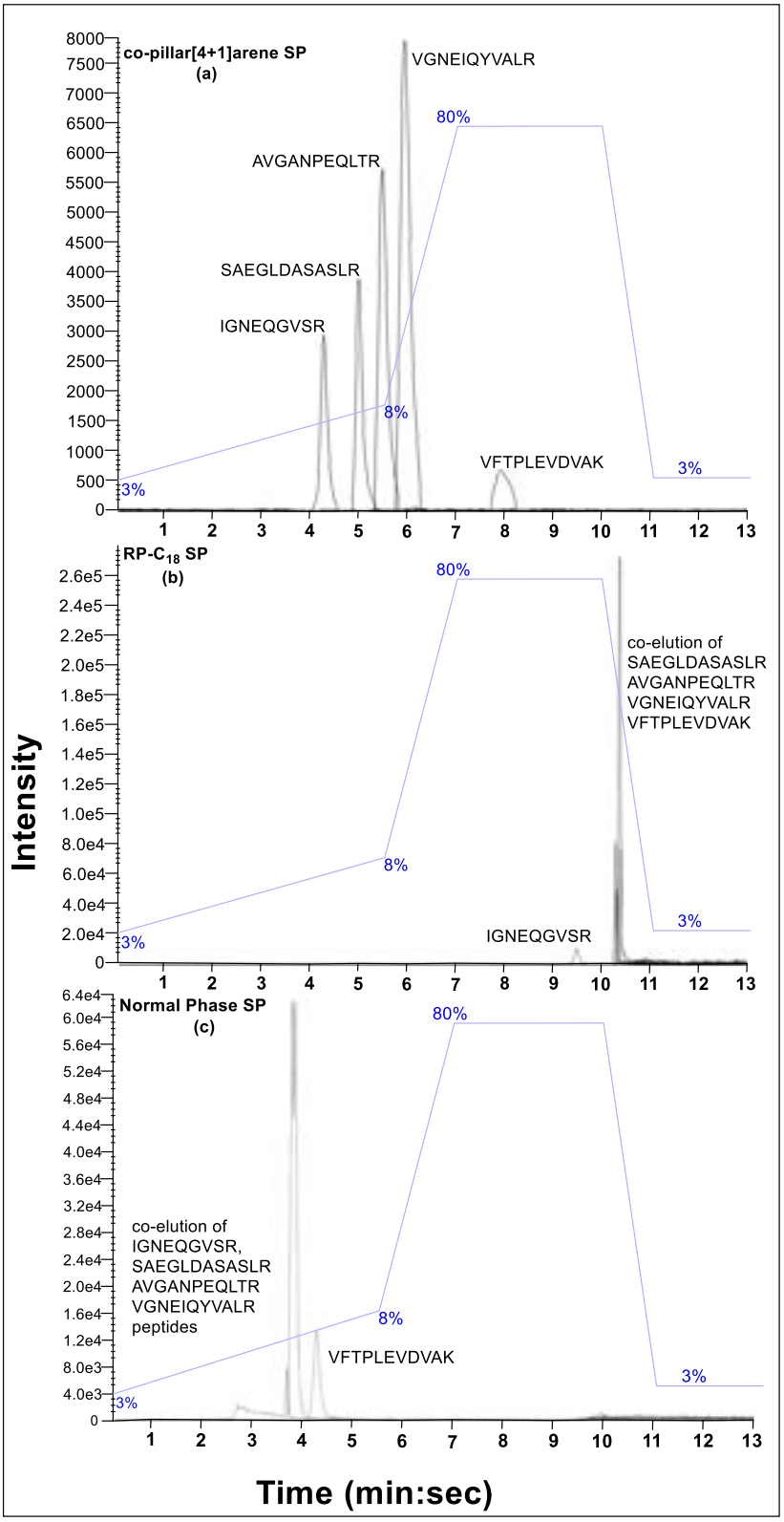

Figure 2.32 Comparison of LC-MS/MS chromatographic separation of mixed peptide standard (IGNEQGVSR, SAEGLDASASLR, AVGANPEQLTR, VGNEIQYVALR and VFTPLEVDVAK on (a) silica bound co-pillar[4+1]arene; (b) reverse phase-C18 silica; and (c) normal phase silica stationary phases.

Gradient conditions on the bare silica phase are the same as those of mobile phase gradient conditions for silica-bound co-pillar[4+1]arene stationary phase **7** column as bare silica phase has been used as the negative control.

The chromatographic conditions used for the analysis for three columns were the same and are described below.

Flow rate: RP-C18-7.5 µL min-1

Column Temperature: 30°C

Column Dimensions: 12 nm S-5 um 150 x 0.3 mm with 1/32" fitting

Mobile Phase: solvent A: water + 0.1% formic acid

solvent B: acetonitrile + 0.1% formic acid

Peptides: IGNEQGVSR, SAEGLDASASLR, AVGANPEQLTR, VGNEIQYVALR and VFTPLEVDVAK

Mobile phase gradient conditions:

Time (min)	%A	%B
0.0	97	03
5.5	92	08
7.0	20	80
10.0	20	80
11.0	97	03
13.0	97	03

2.7 Flash Column chromatography and HPLC of C-butylpyrogallol[4]arene stationary phases 8 and 9

2.7.1 Preparation of silica-bound C-butylpyrogallol[4]arene HPLC stationary phase 8

HPLC grade silica gel (1 g, AlfaAesar, CAS: 7631-86-9) was reacted overnight in a mixture of THF and TEA (1:1, 50 ml) at room temperature. The activated silica was collected after solvent removal by evaporation under vacuum and subsequently dried at room temperature. *C*-Bromobutyl-calix[4]pyrogallolarene **5** (1 g, 0.915 mmoles) was dissolved in acetone and reacted with the dried activated silica in a round-bottomed flask under constant stirring overnight at room temperature. The silica-bound *C*-butylpyrogallol[4]arene stationary phase **8** was collected after solvent evaporation under vacuum and dried at room temperature.

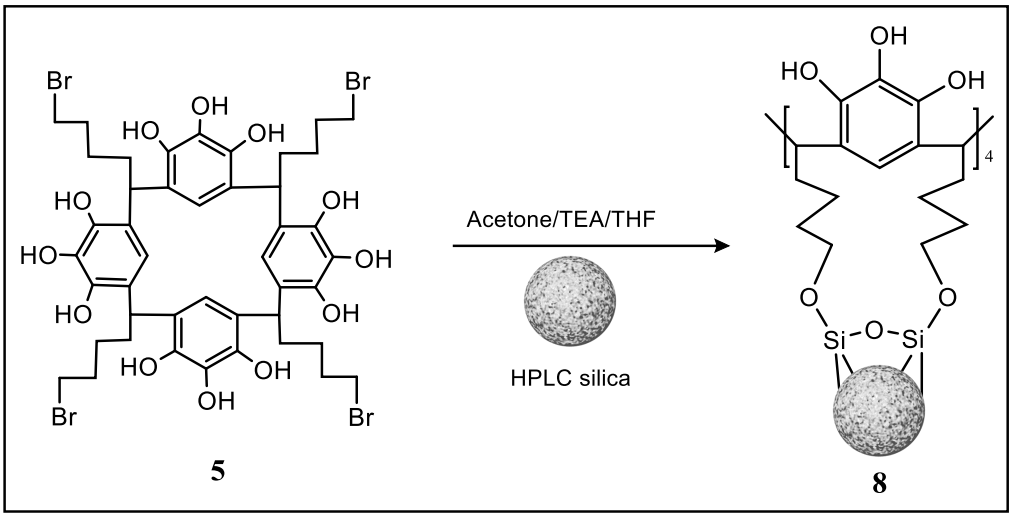

*Figure 2.33. Synthesis of silica-bound C-butylpyrogallol[4]arene HPLC stationary phase **8.***

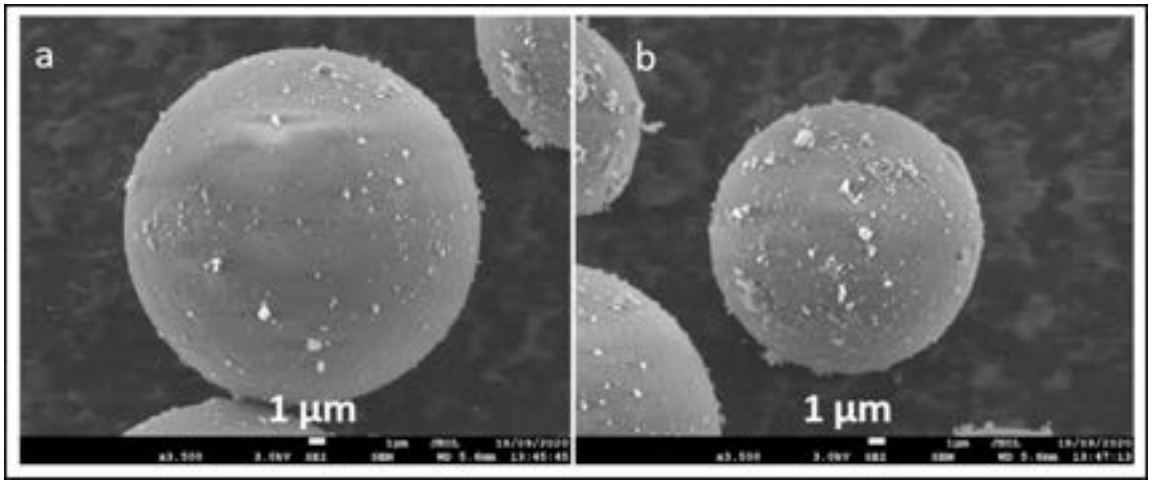

*Figure 2.34 SEM images showing unfunctionalized HPLC silica (a) and silica functionalized with C-butylpyrogallol[4]arene stationary phase particles **8** (b) at 10 and magnification.*

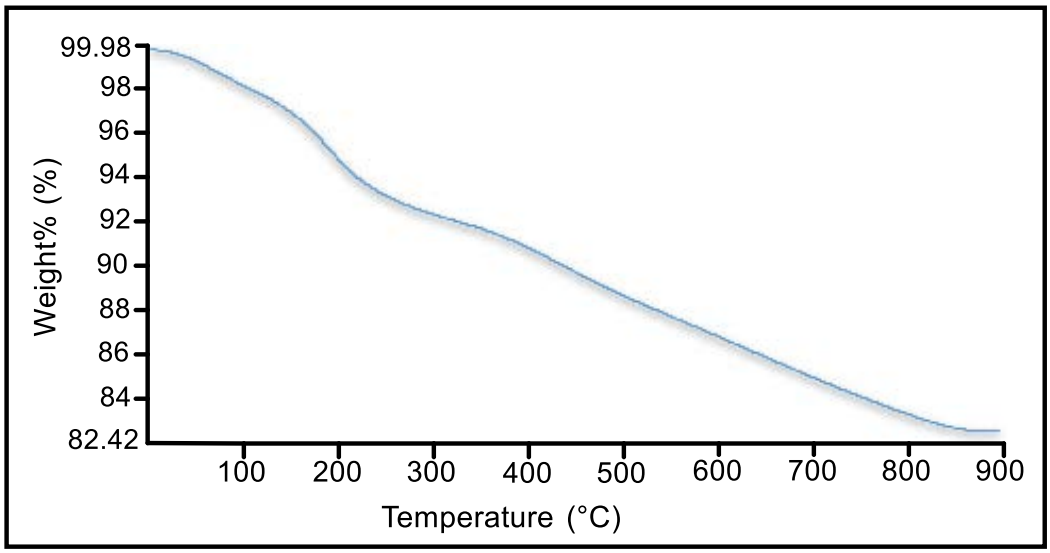

*Figure 2.35 Thermogravimetric analysis of the HPLC silica-bound C-butylpyrogallol[4]arene stationary phase **8**.*

2.7.2 Preparation of silica-bound C-butylpyrogallol[4]arene flash column stationary phase 9

Interchim® flash column Silica (12 g) was reacted overnight at room temperature in a mixture of THF and TEA (1:1, 50 ml). The activated silica was collected after solvent removal by evaporation under vacuum and subsequently dried at room temperature. *C*-Bromobutyl-calix[4]pyrogallolarene **5** (1 g, 0.915 mmoles) was dissolved in acetone (50 ml) and reacted with the dried activated silica in a round-bottomed flask under constant stirring for overnight at room temperature. The silica-bound C-butylpyrogallol[4]arene stationary phase **9** was collected after solvent evaporation under vacuum and dried at room temperature.

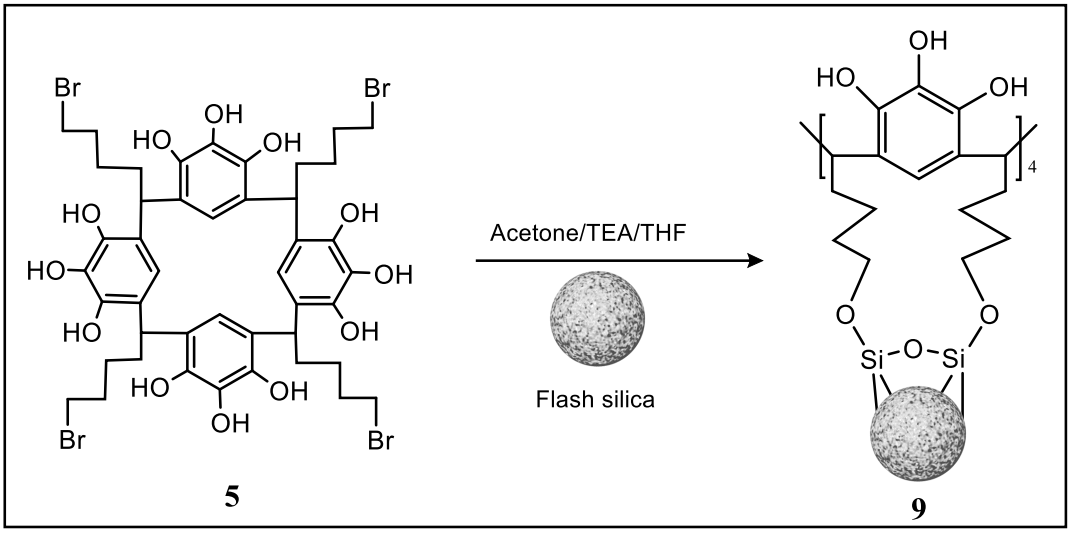

*Figure 2.36. Synthesis of silica-bound C-butylpyrogallol[4]arene flash stationary phase **9**.*

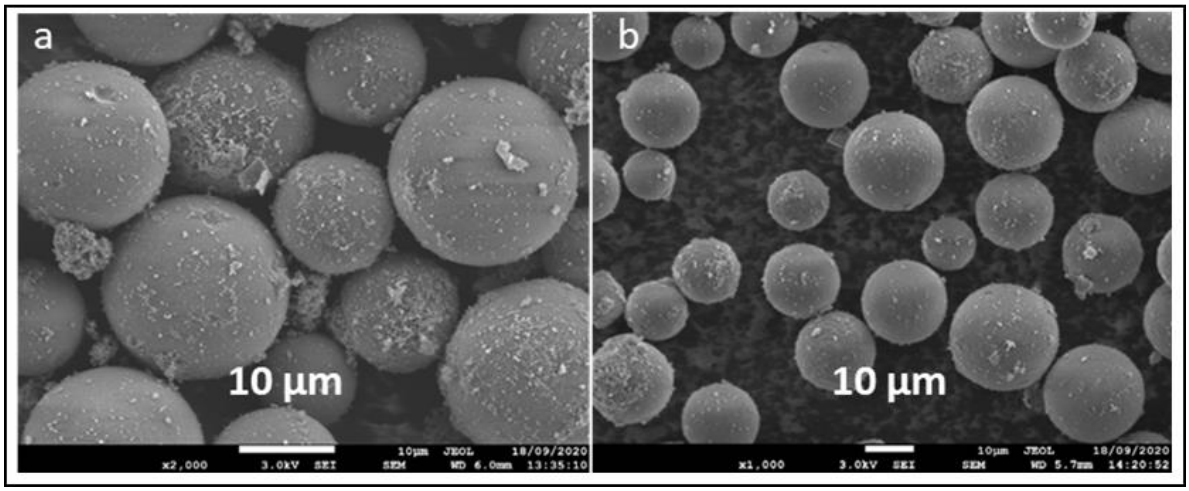

*Figure 2.37 SEM images showing unfunctionalized flash silica (a) and silica functionalized with C-butylpyrogallol[4]arene stationary phase particles **9** (b) at 10 and magnification.*

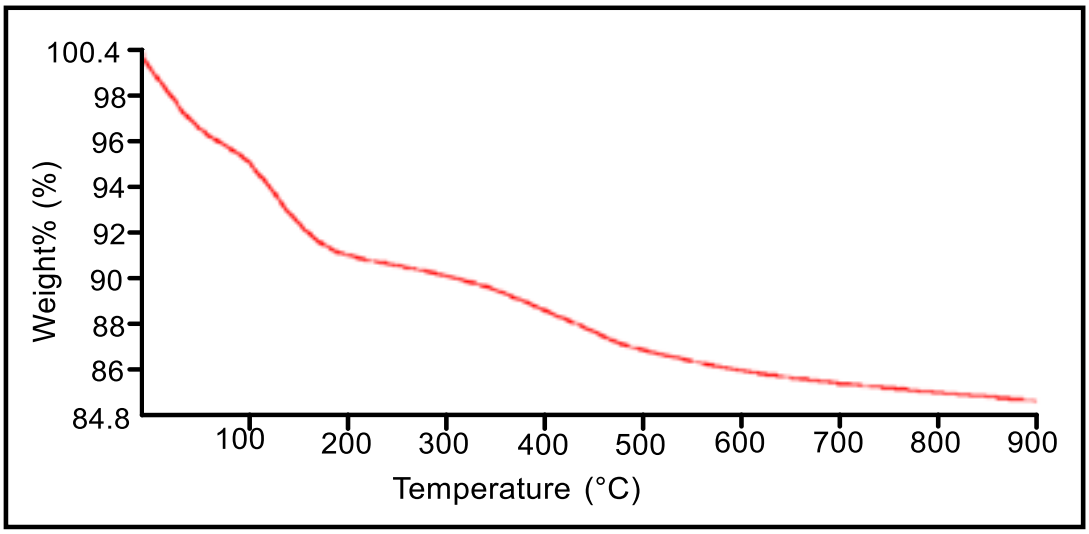

*Figure 2.38 Thermogravimetric analysis of the HPLC silica-bound C-butylpyrogallol[4]arene stationary phase **9**.*

2.7.3 Column packing

The silica bound *C*-butylpyrogallol[4]arene HPLC stationary phase **8** was packed into HPLC stainless steel tube (150 mm × 4.6 mm i.d.) *via* wet slurry packing method under a constant packing pressure (40 Mpa) using methanol as both suspension solvent and propulsion solvent. Silica-bound *C*-butylpyrogallol[4]arene flash column stationary phase **9** was dry-packed by tapping into an empty Interchim® flash column cartridge (62 mm × 12 mm i.d.).

The silica-bound *C*-butylpyrogallol[4]arene HPLC stationary phase **8** was primed with methanol: water (80:20). In contrast, silica-bound *C*-butylpyrogallol[4]arene flash column stationary phase **9** was primed with methanol: ethyl acetate (4:1) to remove unreacted organic debris.

2.7.4 HPLC separation of C60 and C70 fullerenes

The silica bound C-butylpyrogallol[4]arene HPLC stationary phase **8** was primmed and equilibrated with mobile phase methanol: water (80:20). The HPLC chromatographic separations were performed on a PerkinElmer Flexar UHPLC system (PerkinElmer, UK), containing a Flexar fx-15 UHPLC pump and an autosampler injector equipped with 20 µL PEEK sample loop along. The HPLC separations were carried out at a temperature of 25 °C with a mobile phase flow rate of 1.0 mL/min. The absorbance was detected at a wavelength of 237 nm *via* a Flexar PDA *UV* detector ranging 170-700 nm. All the chromatographic experiments were repeated five times to ensure the reliability of the obtained data.

Separation of C_{60} and C_{70} fullerenes were performed at isocratic chromatographic conditions on RP-C_{18} column silica bound C-butylpyrogallol[4]arene HPLC stationary phase **8,** and the conditions are described as bellow.

Flow rate: 1.0 mL min^{-1}

Column Temperature: ambient room temperature

Analyte Concentration: 50 µg ml^{-1} in toluene

Column Dimensions: 150mm×4.6mm i.d.,

Mobile Phase: solvent A: water + 0.1% formic acid

solvent B: acetonitrile + 0.1% formic acid

Analytes: C_{60} and C_{70} fullerenes

Elution type: Isocratic elution

Mobile phase conditions: water: methanol (40:60)

Detection wavelength: 237 nm

Run time: 10 minutes

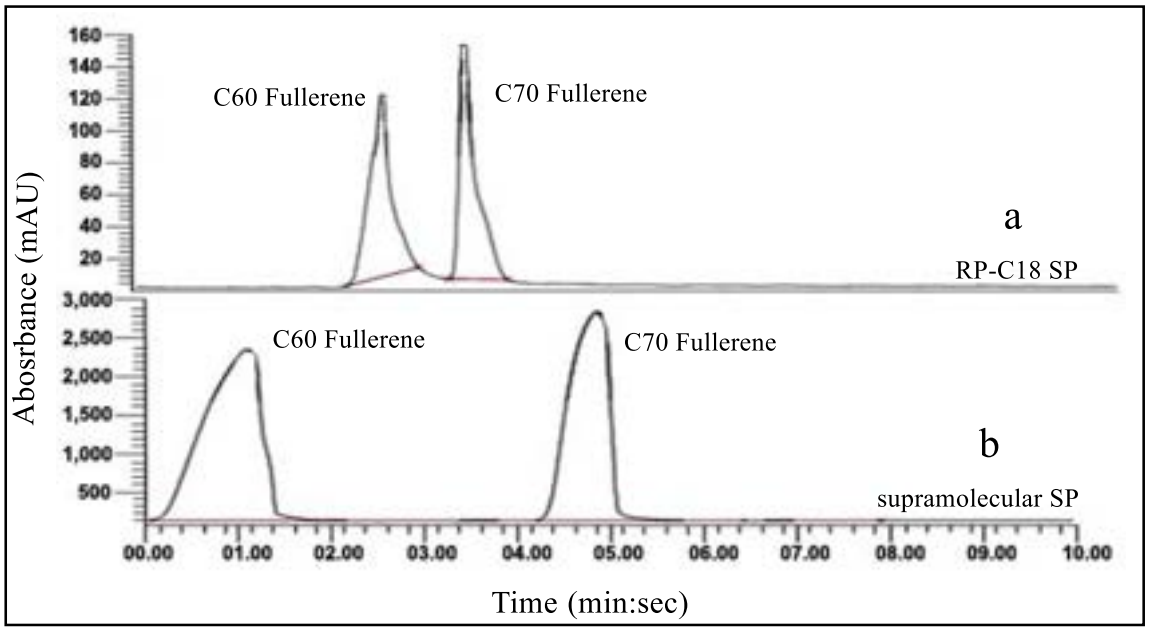

*Figure 2.39 HPLC separation of C_{60} and C_{70} fullerene standards on RP-C_{18} (a) and C-butylpyrogallol[4]arene bonded-silica column **8** (b). Run time: 10 min, column temperature: ambient room temperature.*

2.7.5 Flash column chromatographic separation of C60 and C70 fullerenes

The silica bound *C*-butylpyrogallol[4]arene flash column stationary phase **9** was equilibrated by in-built optimization conditions. The flash column **9** was equilibrated *via* in-built optimization parameters dependent on the column and particle size. In this particular case, the flash column was equilibrated with initial 95% ethyl acetate to 50 %, and toluene was ramped to 65% to meet mobile phase conditions to start the analysis under 12 mins

C_{60} and C_{70} fullerenes (50 mg) mixture was prepared in toluene (2 mL). The mixture of analytes in toluene was loaded into the column. The mobile phase used for the analysis was ethyl acetate: toluene (35:65) in isocratic conditions. The flow rate was set to 15 mL/min, and UV detection was set to 200-400 nm. Flash column chromatography was carried out via an automated PuriFlash®5.125 flash system under 15 minutes of runtime. Fraction collection volume was set to 13 mL.

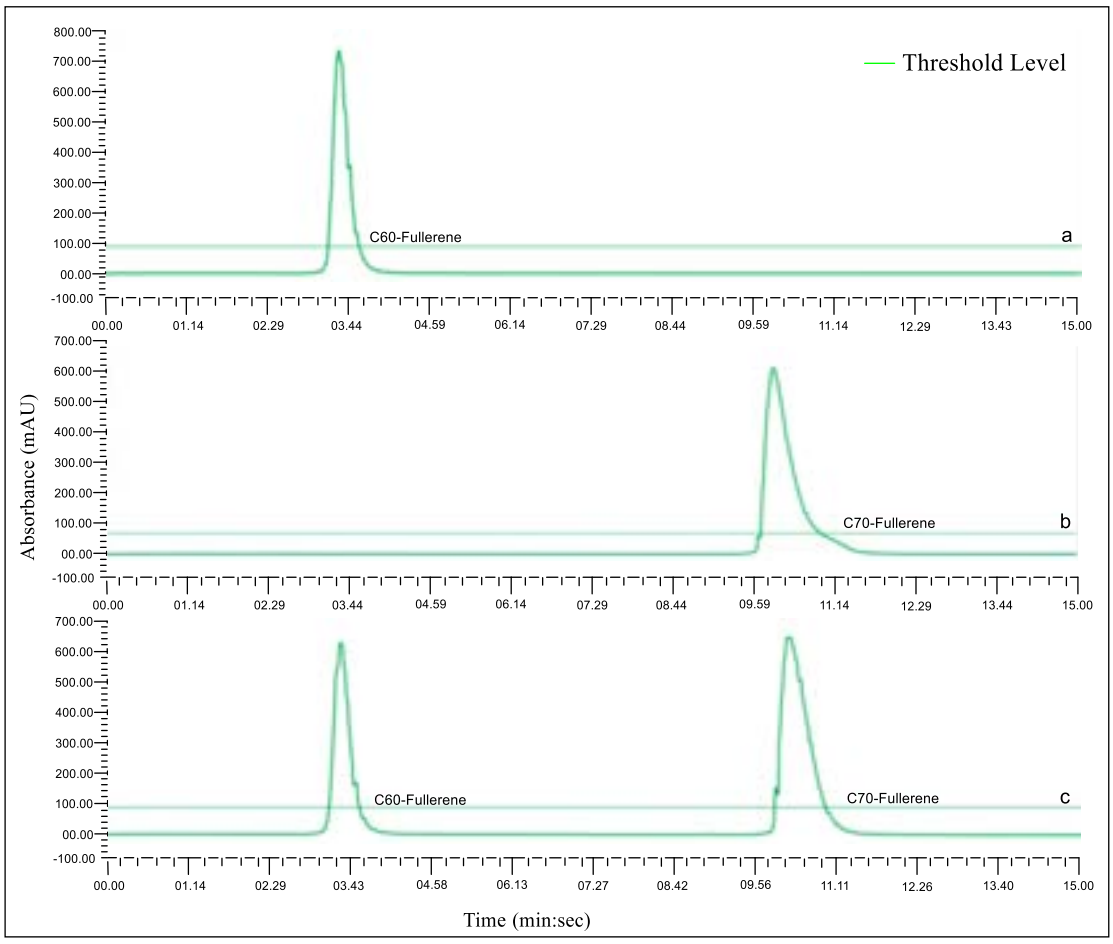

*Figure 2.40 Chromatographic separation of fullerene standards: (a) C_{60}-fullerene, (b) C_{70}-fullerene and (c) an equimolar mixture of C_{60} and C_{70}-fullerenes (c) on silica-bound C-butylpyrogallol[4]arene stationary phases **9**.*

2.8 Computational binding energy studies

2.8.1 Docking studies of xylene isomers and their impurities with pillar[5]arene

The structure of the dimethoxy-pillar[5]arene as a single molecule was obtained from a crystal structure.[3] The 500 random geometries each of ethylbenzene⊂dimethoxy-pillar[5]arene, toluene⊂dimethoxy-pillar[5]arene, *ortho*-xylene⊂dimethoxy-pillar[5]arene, *meta*-xylene⊂dimethoxy-pillar[5]arene, and *para*-xylene⊂dimethoxy-pillar[5]arene were generated using Kick[4] and optimized using Density Functional Tight Binding (DFTB) as implemented in DFTB+ 1.3. DFTB calculations utilized the 3ob-3-1 parameter set[5] and

DftD3 dispersion. The lowest possible energy structures of each guest⊂dimethoxy-pillar[5]arene were reoptimized using TPSSTPSS/Def2TZVP in Gaussian 16.[6]

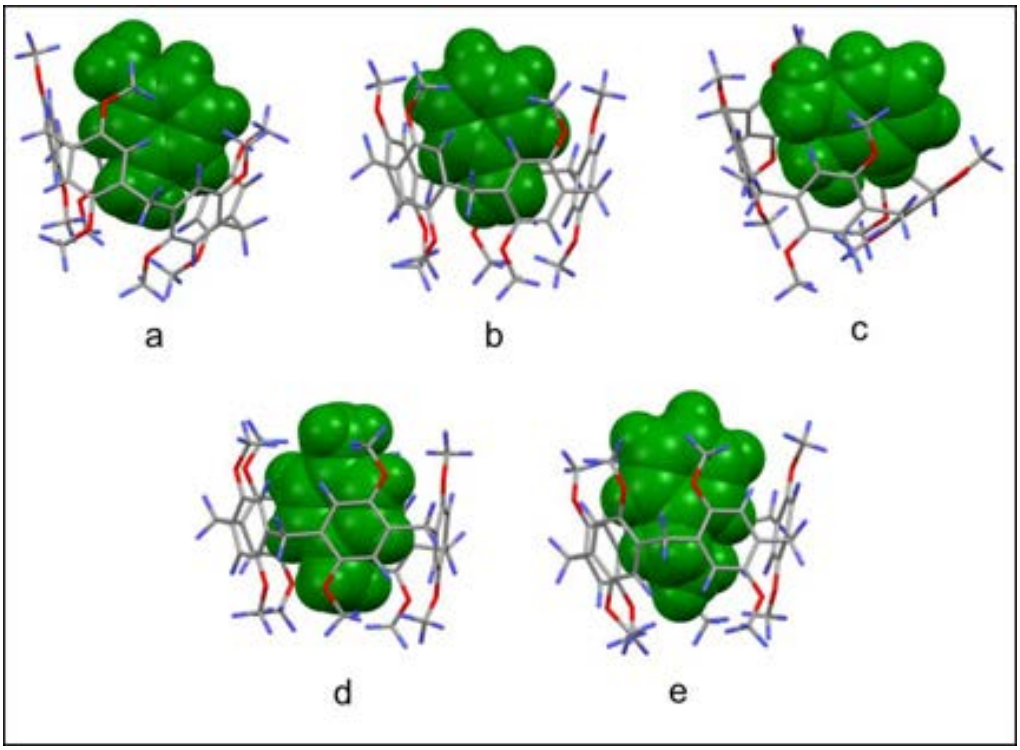

Figure 2.41 Optimized geometries of m-xylene (a), toluene (b), o-xylene (c), p-xylene (d) and ethylbenzene (e) in the dimethoxy pillar[5]arene host.

Table 2.11 Comparison between the chromatographic experimental retention times and the binding energies of toluene, ethylbenzene, and xylene isomers embedded in pillar[5]arene.

Guest	Experimental retention time (min:sec)	Binding Energy (kcal/mol)
m-Xylene	1:59	-22.19
Toluene	3:05	-22.31
o-Xylene	6:25	-23.50
p-Xylene	9:33	-25.97
Ethylbenzene	11:45	-26.74

2.8.2 *In-silico* binding motifs and binding energy calculations of peptides with pillar[5]arene

2.8.2.1 Conformer generation of peptides

To produce the different conformers for each of the peptides, the 3D linear structure of the amino acid sequence of the peptide were drawn *via* GaussView 6.0 software. The geometry of the input structure was then optimized and the optimized structure was utilized to generate the most probable conformers.[7] And the energies of conformers are within 50

Kcal mol^{-1} of this optimized structure using openbabel software. This was performed *via* the following command line argument.

“Obabel <input> -O <output> --confab –nconf 10 --score energy. Details on how to run and use openbabel can be found.[17]

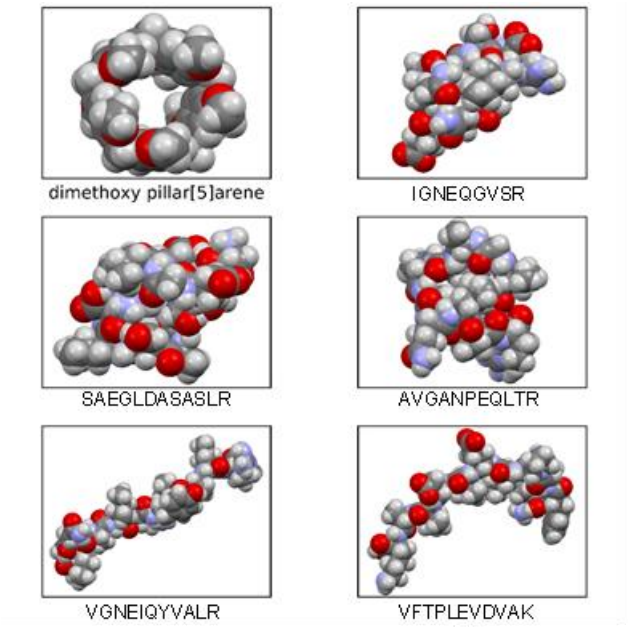

Figure 2.42 Space filled optimized structures of IGNEQGVSR, SAEGLDASASLR, AVGANPEQLTR, VGNEIQYVALR, VFTPLEVDVAK, and dimethoxy pillar[5]arene. Red: oxygen, blue: nitrogen, dark grey: carbon and light grey: hydrogen.

2.8.2.2 Generation of peptides⊂pillar[5] arene complexes

An empirical methodology generated all the peptides⊂pillar[5]arene complexes to sample all possible peptides⊂pillar[5]arene binding sites. This was achieved by manually changing each peptide conformer's location within and all around the cavity while keeping attention that all side chains and terminals of the peptides goes inside the cavity. A minimum of 50 complexes were generated for each conformer depending on the number of plausible interactions that could be sampled. These complexes' geometry was then optimized in the gas phase using DFTB/mio-1-1 with UFF corrections to dispersion as implemented in ADF version r79006 2019-10-03.[8-10] Once optimized, the 20 lowest energy complexes were selected and reoptimsed in the solvent using the implicit Generalized Born solvation model with Solvent Accessible Surface Area (GBSA). In addition, 2030 surface grid points were used to ensure smooth solvent phase geometry optimization with as minimal numerical noise as possible. These calculations were done at the same level of theory as in the gas phase. Finally, the complexes' gas and solvent phase optimized energies were used to compute the peptides⊂pillar[5]arene binding energies. This was

done using the optimized energies for each peptide conformer and the energies of the pillar[5]arene.

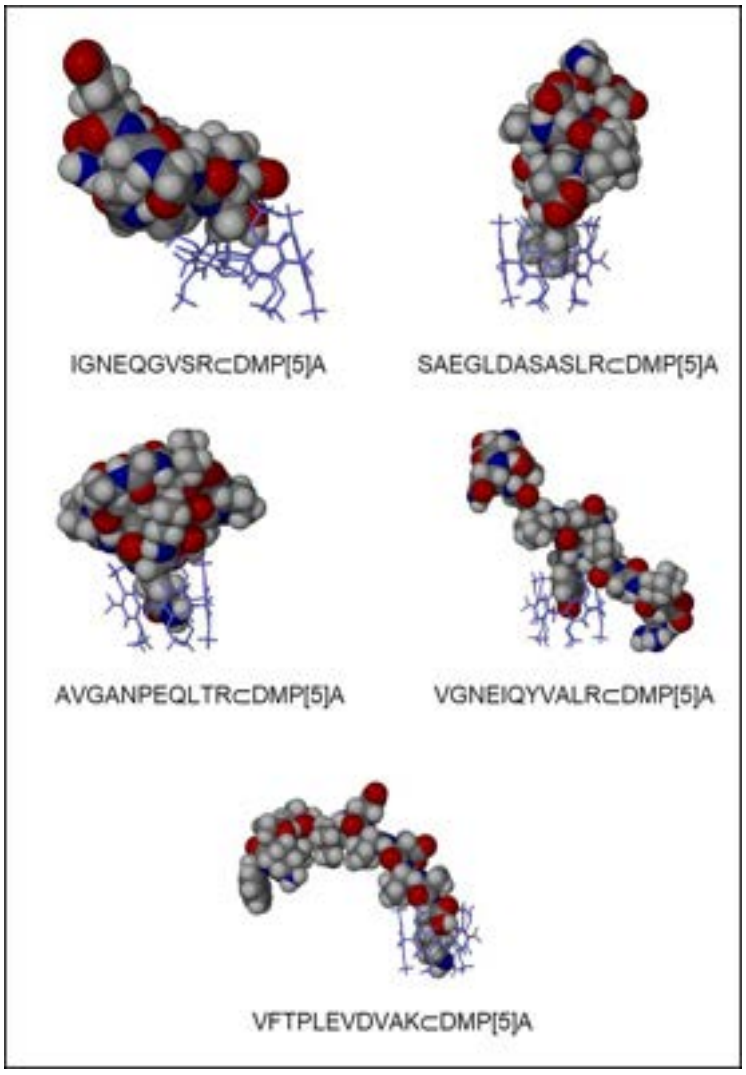

Figure 2.43 Illustration of peptide⊂dimethoxy-pillar[5]arene (DMP[5]A) interactions of IGNEQGVSR, SAEGLDASASLR, AVGANPEQLTR, VGNEIQYVALR, and VFTPLEVDVAK, embedded in pillar[4+1]arene. The space-filled molecular models represent the peptides; meanwhile, the stick represents pillar[5]arene cavity.

2.8.2.3 Distances of the most important interatomic interaction

Distances for all the significant interatomic interactions between the peptides and the cavity were calculated. These interactions correspond to interatomic bonds that are under 3.0 Å. The numbering of each one of the atoms can be visualized using any 3D molecular view *via* their 'xyz' structures provided. The interatomic distances for all the 20 complexes from each peptide conformer can be downloaded.[18]

2.8.2.4 Coordinates of all molecules

The coordinates of all the optimized structures can be downloaded.[18]

2.8.3 *In-silico* calculations of fullerenes with C-butylpyrogallol[4]arene

To measure the most possible binding motifs and energies between the fullerenes and C-butylpyrogallol[4]arene, initially, 100 fullerenes⊂*C*-butylpyrogallol[4]arene complexes were generated for each fullerene (C_{50}, C_{60}, C_{70} and C_{80}) via a semi-stochastic method to compute their host-guest interactions. In this semi-stochastic approach, a random structure generation algorithm called Kick.[11] In this method, specified molecular fragments are randomly translated in a chosen virtual box providing chemically sensible translated entities. For this study, the *C*-butylpyrogallol[4]arene cavity was considered to be the center of the virtual box with a predefined radius of 2.8 Å, which is the radius of the cavity. The fullerenes were then randomly translated into the box at different spatial positions. This was supplemented by a heuristic approach, where the coordinates of the fullerene were manually translated along with the interior of the *C*-butylpyrogallol[4]arene cavity, using Gaussview 6.0 visualizer.[12] In this process, new coordinates were obtained by inserting all regions of the optimized fullerene into the *C*-butylpyrogallol[4]arene cavity. This was done in order to ensure a broad sampling of possible fullerene⊂*C*-butylpyrogallol[4]arene complexes.

Once the 100 complexes for each fullerene were generated, a geometry optimization was performed for all these structures using Density Functional Tight Binding (DFTB) with the mio-1-1[13] parameter set including the universal force field, UFF,[14] with dispersion correction UFF- DFTB/mio-1-1 as implemented in the Amsterdam Modelling Suite AMS version adf2019.305[15]. We then selected 20 energy minima of each of these complexes and performed a vibration frequency calculation in the gas phase in order to verify that they were actual local minima on the potential energy surfaces. Once confirmed that these structures were all local minima, we performed a geometry and frequency optimization in solvent (toluene) using the implicit Generalized Born solvation model with Solvent Accessible Surface Area (GBSA) at the same level of theory as in the gas phase.[16] In addition, 2030 surface grid points were used in order to ensure smooth solvent phase geometry optimization with as little numerical noise as possible. All the structures, long-range interactions and energies of these 20 energy minima can be freely accessed.[19]

The geometry optimised gas and solvent phase Gibbs free binding energies (ΔGBE), were then computed for these 20 energy minima with the formula given in equation (2),

$$\Delta GBE = G\_complex - (G\_fullerene + G\_cavity) \quad (1)$$

where G_complex represents the Gibbs free energy of the fullerene⊂C-butylpyrogallol[4]arene complex; G_fullerene and G_cavity represent the Gibbs free

energy of the lowest energy (geometry optimised) isolated fullerene and the C-butylpyrogallol[4]arene cavity respectively *i.e.* the computed ΔGBE contain the energy contribution from deforming both the fullerene and the cavity.

Table 2.12 Gas and solvent phase DFTB/mio-1-1 Gibbs free binding energies of C_{60}⊂butylpyrogallol[4]arene and C_{70}⊂butylpyrogallol [4] arene alongside HPLC and flash column chromatographic retention times.

Guests	ΔGBE (kcal mol−1)		Experimental Chromatography	
	Gas Phase	Solvent Phase (Toluene)	HPLC (min:sec)	Flash Column (min:sec)
C_{60}-fullerene	−133.385	−123.862	1:08	03:26
C_{70}-fullerene	−135.569	−125.355	4:85	10:38

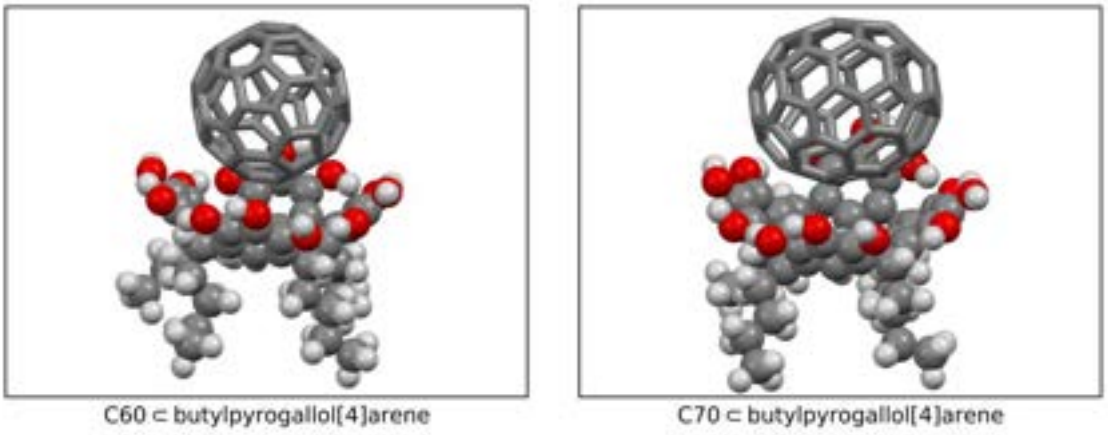

Figure 2.44 Illustration of the calculated binding modes of C_{60}⊂butylpyrogallol[4]arene and C_{70}⊂butylpyrogallol[4]arene. The red, light grey, and dark grey spheres represent oxygen, hydrogen, and carbon atoms.

2.8.4 Binding energies and modes for C60⊂RP-C18 and C70⊂RP-C18

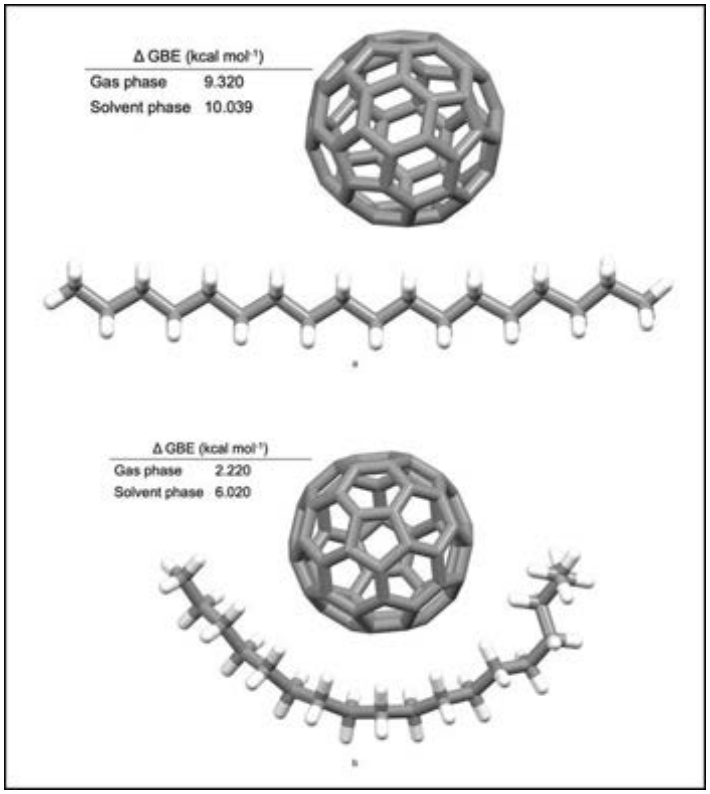

Figure 2.45 Illustration of the calculated gas and solvent phase binding energies and modes of C_{60}⊂RP-C_{18} interaction: a) represents the binding mode between the straight chain conformer of RP-C_{18} and C_{60}, and b) represents the binding mode between the curved conformer of RP-C_{18} and C_{60}.

Table 2.13 Change in electronic energy and Gibbs free binding energy of fullerene⊂RP-C18 motifs. a and b represent the binding mode of two curved conformers of RP-C_{18} with C_{70}.

Systems	Gas phase (kcal mol^{-1})		Solvent phase (kcal mol^{-1})	
	ΔE	ΔGBE	ΔE	ΔGBE
C_{60}⊂RP-C_{18}-a	-0.0153	9.320	-9.478	10.039
C_{60}⊂RP-C_{18}-b	-0.028	2.220	-12.987	6.020
C_{70}⊂RP-C_{18}-a	-0.0311	0.470	-14.315	4.0478
C_{70}⊂RP-C_{18}-b	-0.0307	0.080	-14.301	4.640

To measure the interactions between RP-C_{18} and the fullerenes, a host-guest interaction analysis was performed to compute the binding energies of C_{60}⊂ RP-C_{18} and C_{70}⊂ RP-C_{18} motifs. This was done using two conformers of RP-C18, a straight chain and a curved conformer as input structures. These computations were performed for both the gas and solvent phase using the same theory level to compute the host-guest interactions of fullerene⊂C-butylpyrogallol[4]arene complexes. The gas and solvent phase Gibbs free binding energies (ΔGBE) and electronic energies were computed.

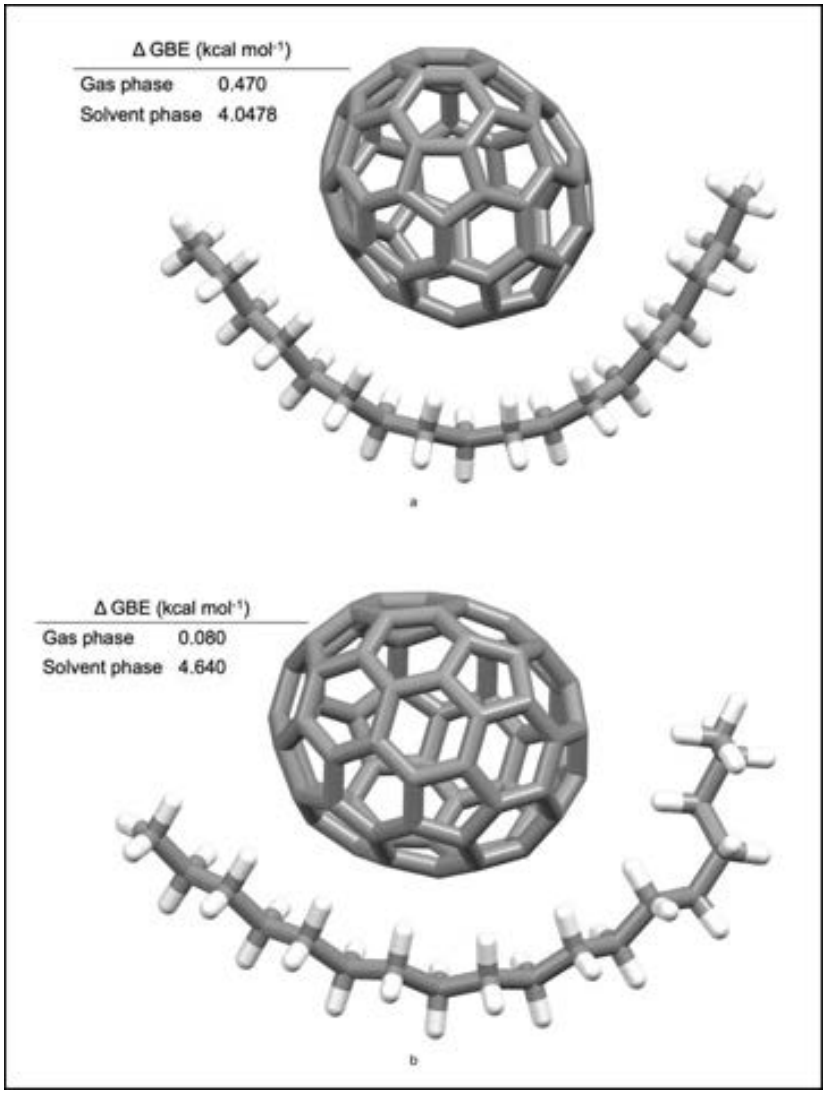

Figure 2.46 Illustration of the calculated gas and solvent phase binding energies and modes of C_{70}⊂RP-C_{18}. a and b represent the binding mode of two curved conformers of RP-C_{18} with C_{70}.

2.9 References

1. J. Chang, Q. Zhao, L. Kang, H. Li, M. Xie and X. Liao, *Macromolecules*, 2016, **49**, 2814-2820.
2. M. Funck, D. P. Guest and G. W. Cave, *Tetrahedron Lett.*, 2010, **51**, 6399-6402.
3. T. Ogoshi, S. Kanai, S. Fujinami, T. Yamagishi and Y. Nakamoto, *J. Am. Chem. Soc.*, 2008, **130**, 5022-5023.
4. M. A. Addicoat, S. Fukuoka, A. J. Page, S. Irle, *J. Comput. Chem.*, 2013, **30**, 2591-2600.
5. M. Gaus, A. Goez, M. Elstner, *J. Chem. Theory Comput.*, 2012, **9**, 338-354.
6. Gaussian 16, Revision A.02, M. J. Frisch, G. W. Trucks, H. B. Schlegel, G. E Scuseria, M. A. Robb, J. R. Cheeseman, G. Scalmani, V. Barone, G. A. Petersson, H. Nakatsuji, X. Li, M. Caricato, A. V. Marenich, J. Bloino, B. G. Janesko, R. Gomperts, B. Mennucci,

H. P. Hratchian, J. V. Ortiz, A. F. Izmaylov, J. L. Sonnenberg, D. WilliamsYoung, F. Ding, F. Lipparini, F. Egidi, J. Goings, B. Peng, A. Petrone, T. Henderson, D. Ranasinghe, V. G. Zakrzewski, J. Gao, N. Rega, G. Zheng, W. Liang, M. Hada, M. Ehara, K. Toyota, R. Fukuda, J. Hasegawa, M. Ishida, T. Nakajima, Y. Honda, O. Kitao, H. Nakai, T. Vreven, K. Throssell, J. A. Montgomery, Jr., J. E. Peralta, F. Ogliaro, M. J. Bearpark, J. J. Heyd, E. N. Brothers, K. N. Kudin, V. N. Staroverov, T. A. Keith, R. Kobayashi, J. Normand, K. Raghavachari, A. P. Rendell, J. C. Burant, S. S. Iyengar, J. Tomasi, M. Cossi, J. M. Millam, M. Klene, C. Adamo, R. Cammi, J. W. Ochterski, R. L. Martin, K. Morokuma, O. Farkas, J. B. Foresman, and D. J. Fox, Gaussian, Inc., Wallingford CT, 2016.

7. Open Babel 3.0.1, Generate multiple conformers — Open Babel 3.0.1 documentation (open-babel.readthedocs.io), (accessed on March 2022).
8. S. Grimme , J. Antony , S. Ehrlich and H. Krieg , *J. Chem. Phys.*, 2010, **132**, 154104.
9. C. Schönbeck , H. Li , B.-H. Han and B. W. Laursen , *J. Phys. Chem. B*, 2015, **119**, 6711-6720.
10. M. Elstner , D. Porezag , G. Jungnickel , J. Elsner , M. Haugk , T. Frauenheim , S. Suhai and G. Seifert , *Phys. Rev. B: Condens. Matter Mater. Phys.*, 1989, **58**, 7260.
11. M. A. Addicoat and G. F. Metha, *J. Comput. Chem.,* 2009, **30**, 57-64.
12. Dennington, R.; Keith, T.; Millam, *J. GaussView, Version 61*; Semichem Inc.: Shawnee Mission, KS, USA, 2016
13. M. Elstner, D. Porezag, G. Jungnickel, J. Elsner, M. Haugk, T. Frauenheim, S. Suhai and G. Seifert, *Physical Review B*, 1998, **58**, 7260.
14. A. K. Rappé, C. J. Casewit, K. Colwell, W. A. Goddard III and W. M. Skiff, *J. Am. Chem. Soc.*, 1992, **114**, 10024-10035.
15. G. t. Te Velde, F. M. Bickelhaupt, E. J. Baerends, C. Fonseca Guerra, S. J. van Gisbergen, J. G. Snijders and T. Ziegler, *J. Comput. Chem.*, 2001, **22**, 931-967.
16. A. V. Onufriev and D. A. Case, *Ann. Rev. Biophys.*, 2019, **48**, 275-296.
17. https://open-babel.readthedocs.io/en/latest/3DStructureGen/multipleconformers.html
18. http://doi.org/10.5281/zenodo.3995081
19. http://doi.org/10.5281/zenodo.4147306
20.

3 Chapter 3: Synthesis of supramolecular cavitands

3.1 Introduction

Supramolecular chemistry is an interdisciplinary branch of chemistry that significantly focuses on assembling molecules *via* noncovalent interactions at the nanometre scale into complex and orderly-packed molecular aggregates with specific functions.[1] Since Pedersen, Cram and Lehn won the Nobel Prize in Chemistry in 1987; supramolecular chemistry has sparked more extensive attention. Supramolecular chemistry has since been revolutionized and resulted in numerous discoveries in molecular recognition, molecular assembly, molecular machine, and other fields of chemistry. The most important of these investigations are based on constructing various supramolecular compounds. In addition, in-depth research on different methods to synthesize supramolecular cavitands, including crown ethers, cyclodextrins, cucurbits, calix[n]arenes and pillar[n]arenes has been explored to study host-guest interactions, which is one of the essential aspects of supramolecular chemistry, and its applications contributed to the development of nano-machines as "world's smallest machines" and subsequently awarded Nobel prize Chemistry 2016 for Sir Fraser Stoddart, Bernard Feringa, and Jean-Pierre Sauvage.[2]

The development of various synthetic strategies to synthesize the high yield supramolecular host homologues having different cavity sizes has extended the boundaries of supramolecular chemistry because cavity sizes play an essential role for various host-guest properties. However, the synthesis of the macrocyclic homologues with selective functional groups is usually complex in the kinetically controlled cyclization process. Therefore, the use of template compounds is necessary for the selective synthesis of particular macrocyclic homologues, which controls the cyclization process thermodynamically.[3]

Calixarene owing to their 3D surface and conformationally rigid structure, as shown in Figure 3.1, and its degree of ambiguity, has been used extensively as a building block for molecular sensing, catalysis, drug carrier, nanoscience and separation sciences due to its accessibility and easier functionalization at both the upper or lower ends of the molecular structure within the possible building blocks.[4] Furthermore, selective functionalization of calixarenes occurs by either alkylation of the phenolic hydroxyl groups at the lower rim or by selective dealkylation of the *para*-alkyl groups. As a result, many elegant calix[n]arene-based receptors have synthesized in high yields over the past years.[4]

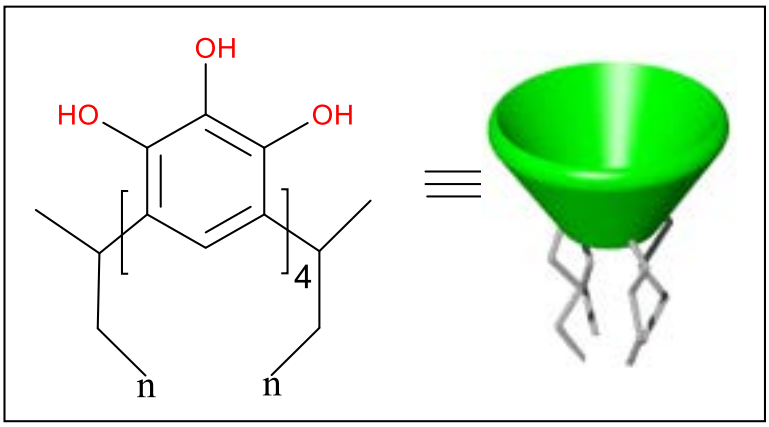

Figure 3.1. C-Alkylpyrogallolcalix[4]arenes.

Following the first report of pillar[5]arene macrocycles in 2008[5], various new synthetic routes have been rapidly developed to elucidate essential properties of pillar[5]arenes with anticipated chemical or physical properties, such as shape and reaction mechanism, host-guest properties, and their versatile functionality as shown in Figure 3.2. Furthermore, these developments contributed significantly to developing pillar[5]arene chemistry and their subsequent applications in various fields, including artificial membrane transport systems, controlled drug delivery systems, biomedical imaging, biosensors, separation and storage materials, and surface chemistry based on host-guest interactions.[6]

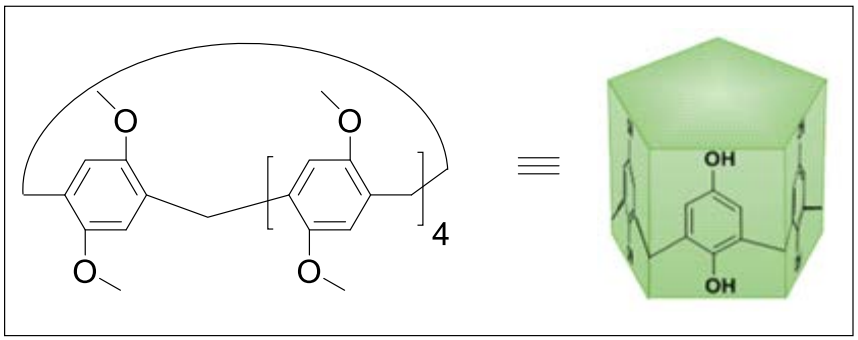

Figure 3.2. Graphical representation pillar[5]arene (Reprinted with permission from American Chemical Society).[18]

Pillar[n]arenes have numerous exceptional advantages compared with other traditional macrocyclic hosts. Firstly, the ease of synthesis and selective functionalization of 10 substituent groups as shown in Figure 3.3. Secondly, they can disperse freely in different solutions after chemical modification, including water, dichloromethane, and acetone. Lastly, the rigid electron-rich cavity enabled pillararenes as ideal candidates to construct supramolecular aggregates based on host-guest complexation.[7]

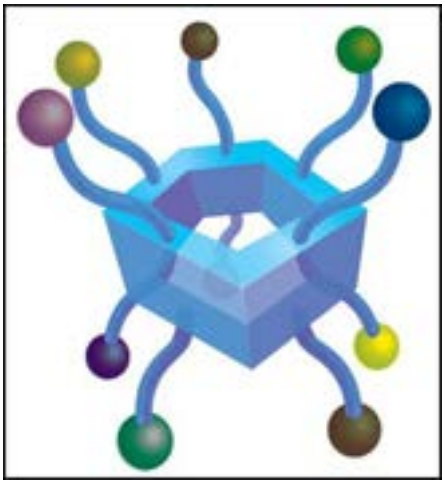

Figure 3.3. Graphical representation pillar[5]arene owing upper and lower rim functional groups.[8] (Reprinted with permission from American Chemical Society).

Position-selective functionalization of 10 substituent groups of pillar[5]arene by various organic synthetic approaches enabled the construction of the number of mono-, di-, tetra-, penta- and, per-functionalized pillar[5]arenes, as well as cases with two substituents on phenyl ring (phenylene substitution) and rim-differentiated pillar[5]arene supramolecular assemblies as shown in Figure 3.4.[8]

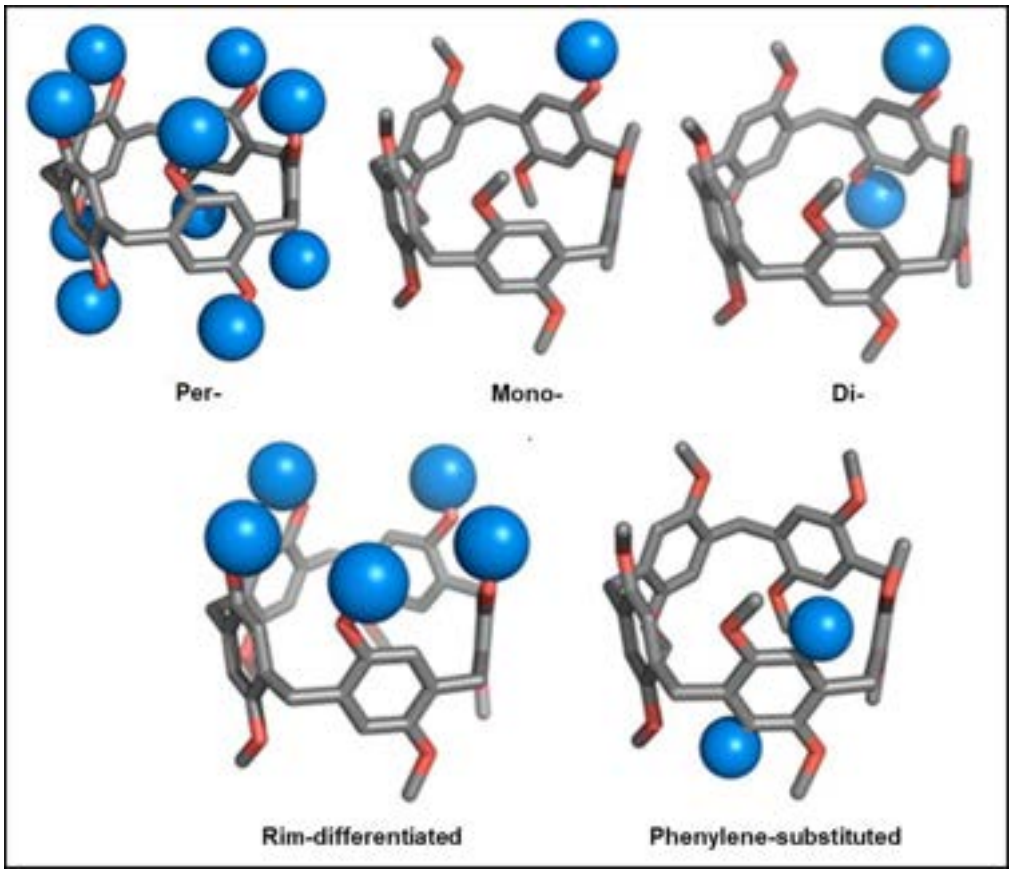

Figure 3.4 Various types of functionalized pillar[5]arenes.[8] (Reprinted with permission from American Chemical Society)

3.1.1 Homo-cyclooligomerization

The condensation reaction between 1,4-dimethoxybenzene and paraformaldehyde using the Lewis acid $BF_3{\cdot}O(C_2H_5)_2$, resulted in a dimethoxy pillar[5]arene with a yield of 22%, as shown in Figure 3.5. However, adding an excess of three equivalent of paraformaldehyde to 1,4-dimethoxybenzene synthesized the dimethoxypillar[5]arene in a higher yield of 71%. This method also requires less time, but the reaction is moisture sensitive.[9]

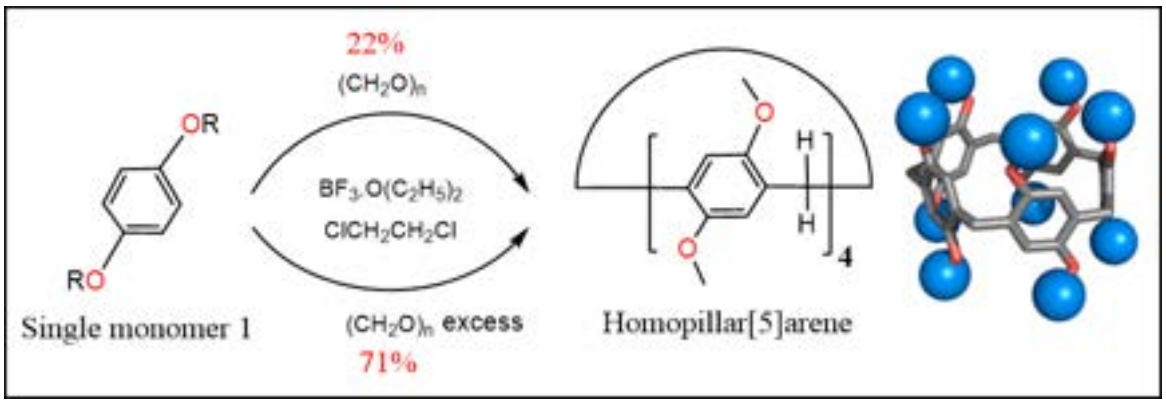

Figure 3.5. Synthesis of dimethoxypillar[5]arene via homo-cyclooligomerization.

The solvent system plays an important role in synthesizing pillar[n]arenes. Dichloroethane (DCE) and chlorocyclohexane are suitable solvent templates for the synthesis of pillar[5]arenes and pillar[6]arenes. Linear dihaloalkane DCE fits well into the pillar[5]arene cavity as the cavity size of pillar[5]arenes is *ca*. 5.5 Å, and acts as the template for the synthesis of the pillar[5]arene, indicating a thermodynamically controlled cyclization process. Various Lewis acids were tested, including H_2SO_4, $FeCl_3$, $AlCl_3$, $TiCl_4$ and $SnCl_4$, but BF_3OEt_2 gave the cleanest yield of the pillar[5]arene macrocycles. Various monomers have been investigated for synthesis pillar[n]arenes, such as 1,4-dialkoxy-2,5-bis(alkoxymethyl)benzene, 2,5-dialkoxybenzyl alcohols, and 2,5-dialkoxybenzyl bromide.[10]

3.1.2 Co-cyclooligomerization

Three methods for synthesizing difunctionalized pillararene derivatives have been reported to construct co-pillar[n+1]arene macrocycles, such as co-cyclization, oxidation-reduction, and *in-situ* cyclization and deprotection. In 2010, Huang *et al*. reported the first synthesis of a copillar[5]arene *via* co-cyclization of 1,4-dimethoxybenzene and four moles of symmetric 1,4-di-n-butyloxybenzene, resulting in less than 10% yield as shown in Figure 3.6.[11]

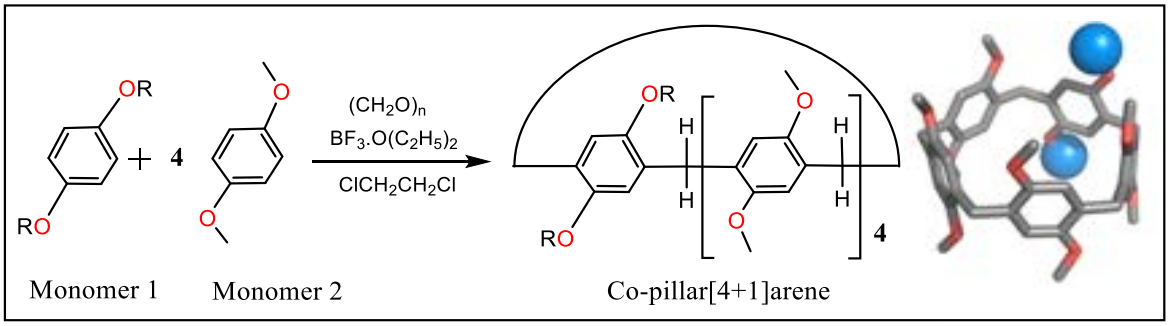

Figure 3.6. General synthesis of co-pillar[4+1]arene via different monomer units.

The 4:1 mixture also forms a copillar[5]arene, containing four dimethoxybenzene groups and one di-n-butoxybenzene group, in 16% yield. X-ray crystallography showed the compounds to have all the aromatic rings in the pseudo-D_5 confirmation.[11]

Currently, there are two possible approaches to synthesizing copillar[n+1]arenes: selective modification of pillararenes and co-cyclo oligomerization of different monomers. The ratio of the repeating monomer units in the final copillar[n+1]arenes can be tuned by differing the starting ratio of the two monomers. Otherwise, several by-products could be produced.[11]

3.2 Results and Discussion

Despite the rapid emergence and utilization of pillar[n]arene and pillar[n]arene derivatized macrocyclic building blocks, the original synthesis remained unchanged. However, several attempts have been made to improve the yield of pillar[n]arenes while studying the effect of Lewis acid catalyst and ratios of monomeric units.

Microwave irradiation has emerged as a versatile tool for organic synthesis and is used for its ability to reach high temperatures rapidly *via* electromagnetic waves. In microwave irradiation, the microwaves are principally electromagnetic waves contains electric and magnetic field. The dipole field of the materials will adjust to be in line with the oscillating electric field of the microwave when the microwave energy passes through the reaction materials. However, there will be not sufficient time for the molecules to be in line with the oscillating electrical field (2.45 GHz). Subsequently, the continuous readjustment of molecules leads to loss of energy *via* molecular friction and loss of dielectric. In this process the released amount of heat is dependent on capability of molecules to readjust with the oscillating electrical filed, which often termed as “microwave dielectric heating effect”.[19]

Traditionally, heating temperatures above the reflux conditions are used *via* pressure sealing systems in microwave reactors. Subsequently, these enables the higher

temperatures in short time. The rate at which the reaction time decreases with increased temperature explained by the Arrhenius law as stated in equation 3.1.

$$K = Ae^{\frac{-Ea}{RT}} \quad (1)$$

Where,

K = Rate constant
A= Pre-exponential factor
E_a= Activation energy
R = Universal gas constant
T = Absolute temperature

The reaction time is decreased to half with every increase of 10 °C. The microwave reactors can be able to reach 300 °C and contain a maximum pressure threshold (435 psi).[19] In traditional methods, the heat transfer rate to the reaction solution is achieved *via the* wall of the reaction vessel. However, this process is slow and ineffective in developing temperature gradients and subsequent development of side reactions. Microwave reactors have more advantages compared to traditional heating methods. In microwaves, the energy is applied directly to the molecules, which can heat the reaction mixture to the pre-programmed temperature conditions within minutes. By utilizing microwave irradiation, the reaction times can often be significantly reduced; therefore, the energy efficiency is greatly increased. Herein we demonstrate the use of microwave-induced synthesis to prepare a novel co-pillar[4+1]arene.[12]

3.2.1 Synthesis of Co-pillar[4+1]arene 3

3.2.1.1 Microwave irradiation synthesis

The general procedure consists of premixing 1:4 quantities of 1,4-bis(8'-bromooctyloxy)benzene and 1,4-dimethoxy-benzene in 1,2-dichloroethane with paraformaldehyde (5 moles) using the catalyst $BF_3.O(C_2H_5)_2$, as shown in Figure 3.7. Next, the reaction vessel is sealed and subjected to microwave irradiation for various time intervals at different temperatures using a CEM Discovery SP instrument. Finally, the dichloromethane solvent was evaporated under the vacuum. The crude product was collected as a pure product by trituration with acetone upon cooling.

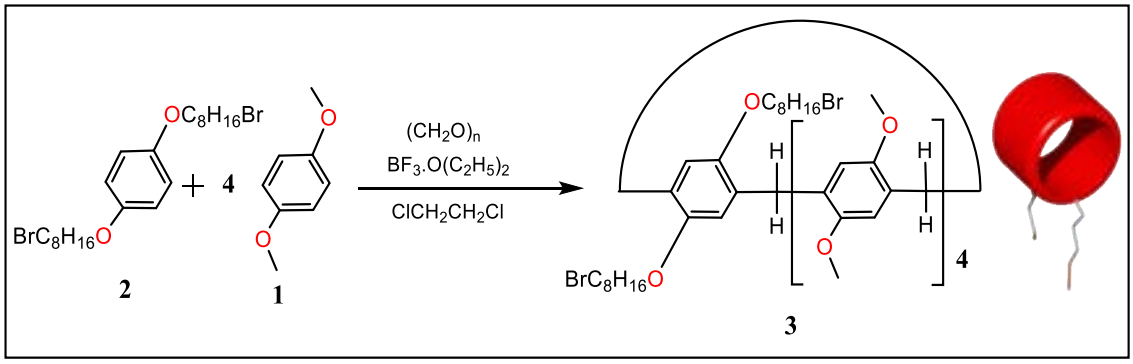

Figure 3.7. General scheme for microwave synthesis of co-pillar[4+1]arene ***3.***[12]

The microwave synthesis of co-pillar[4+1]arene macrocycle **3** was performed at room temperature at different time intervals of 1, 2, 3, 4, 5, 6, 7, 8, 9, 10, 15, 20, and 25 mins. Initially, when the two monomeric units **1** and **2** reacted in a 4:1 ratio together at room temperature with aldehyde under $BF_3.O(C_2H_5)_2$ catalyst, no aromatic -CH_2- linkage was found, and the presence of a major paraformaldehyde peak in the ^{1}H NMR spectrum was observed along with two monomeric units signals. This observation indicates no cyclization between two monomeric units at the para position occurred. Furthermore, the reaction colour changed to green upon adding catalyst $BF_3.O(C_2H_5)_2$. Similarly, the microwave irradiation reaction was performed between two monomeric units **1** and **2** in a 4:1 ratio at various temperature conditions, including 50, 75, 100, 115, 125, 135, 145 and 155 °C, with reaction times from 1 to 25 mins.

Compound **3** was successfully synthesized at 145 °C in under 4 mins *via* the $BF_3{\cdot}O(C_2H_5)_2$-catalysed condensation of monomeric units **1** and **2** (in a 1:4 molar ratio) with paraformaldehyde (5 mole equivalents) under nitrogen. Furthermore, the expected colour change was observed upon adding the above Lewis acid catalyst to the dark greenish colour. Finally, co-pillar[4+1]arene macrocycle **3** was triturated with acetone. White solid co-pillar[4+1]arene macrocycle **3** was collected at 88% yield under a vacuum after cooling the reaction.

Isolation of co-pillar[4+1]arene macrocycle **3** from the crude product was challenging during the synthesis. Therefore, several attempts were made to separate co-pillar[4+1]arene macrocycle **3** using flash column chromatography using both normal phase and reverse phase stationary with various solvent systems. Initially, the separation of co-pillar[4+1]arene crude product *via* automated flash column performed using various ratios of petroleum ether: hexane, hexane: chloroform, petroleum ether: ethyl acetate. However, there was no success in isolating co-pillar[4+1]arene macrocycle **3** from the crude product. This could be due to lack of interactions with the flash column normal stationary phase. Later recrystallization was also used to isolate co-pillar[4+1]arene

macrocycle **3**, which ended up with unresolved crude product **3**. Finally, a trituration method implemented to isolate the product **3** using acetone. When acetone was added to a crude product, the solid white product is obtained at the bottom of the solvent acetone. The solid white product was collected under vacuum filtration and characterized by ^{1}H and ^{13}C NMR and direct infusion mass spectrometry.

The ^{1}H NMR spectrum of co-pillar[4+1]arene macrocycle **3** gave a singlet at 6.62 ppm corresponding to the aromatic protons, a singlet at 3.65 ppm corresponding to methyl protons of Ar-OCH_3, and triplets at 3.79 and 3.35 ppm corresponding to the Ar-O-CH_2 and Br-CH_2- from the aliphatic chains. The bridging methylene protons occur at 3.91 ppm. This confirmed successful cyclization. The microwave irradiation reaction was successful, with an increased yield to 88% in under four minutes. Additionally, the work-up procedure has been reduced to simple trituration while controlling the reaction conditions and using a sealed vessel. When the temperature reached 155 °C, the reaction mixture turned black from dark greenish colour, indicating that the mixture of monomeric units **1** and **2** were found to have decomposed.

Traditional synthetic methods of producing pillar[5]arene and pillar[5]arene derivatives typically take 3-48 hours with only moderate yields. Following the initial 16% low-yielding synthesis of copillar[4+1]arene by the Huang group in 2010, the race was on to find an improved synthetic protocol route. Meier *et al.* replaced the traditional BF_3 etherate catalyst with $FeCl_3$ in CH_2Cl_2 and demonstrated an increased yield of 50-85% in 4-24 hours. Latterly, there has been a desire by supramolecular chemists to adopt green methodologies for the synthesis of pillar[n]arenes and co-pillar[n]arenes to reduce the reaction time while increasing reaction yields.[12] Despite the more significant problems of steric crowding interfering with its synthesis, the copillar[5]arene formed through the 4:1 reaction between 1,4-dimethoxybenzene and 1,4-di-n-octyloxybenzene gives a much higher yield of 27%. Huang also prepared a copillar[5]arene based on dimethoxy pillar[5]arene in which one 1,4-dimethoxybenzene group was substituted with 1-methoxy-4-(octyloxy)benzene. The modest yield of 9% was worth the work as the compound was able to form supramolecular polymers.

When compared, the yield of co-pillar[4+1]arene macrocycle **3** synthesized *via* microwave-assisted irradiation is more effective than that of the previously reported methods for pillar[n]arenes by T. Ogoshi, co-pillar[n+1]arenes by Huang.[5,11]

3.2.1.2 Traditional condensation synthesis

In order to validate the new microwave green synthetic approach for making co-pillar[4+1]arene macrocycle **3** in high yield, the same condensation reaction was repeated

using traditional methodologies.[13] The reagents were heated under reflux at ambient pressure for 4 hours, as shown in Figure 3.8. Finally, the co-pillar[4+1]arene macrocycle **3** was isolated from the reaction mixture by triturating with acetone in a 26.3% yield.

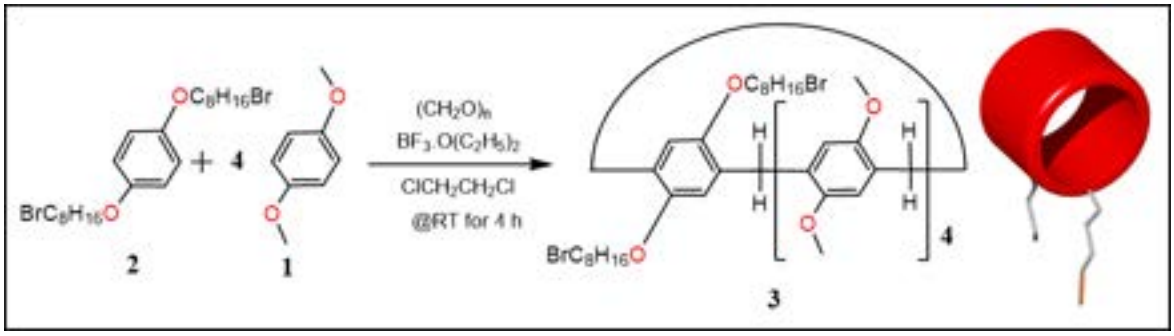

*Figure 3.8. Synthesis of co-pillar[4+1]arene **3** via condensation method.*

3.2.2 Synthesis of *C*-bromo-butylpyrogallol[4]arene 5

C-Alkylpyrogallol[4]arenes are a subgroup of calixarene macrocycles, which share two key features. The first is they comprise twelve hydroxy groups at the upper rim of their cup-like structure, which results in many hydrogen-bonding interactions. Second is the alkyl groups that radiate from the spheroidal assembly, ranging in length from ethyl to undecyl.[14] This abundance of potential hydrogen bonding sites led to the synthesis of several pyrogallol[n]arene derivatives to study chromatographic applications of pyrogallol[n]arenes in the field of separation science.[15]

3.2.2.1 Synthesis of *C*-butanolpyrogallol[4]arene 4

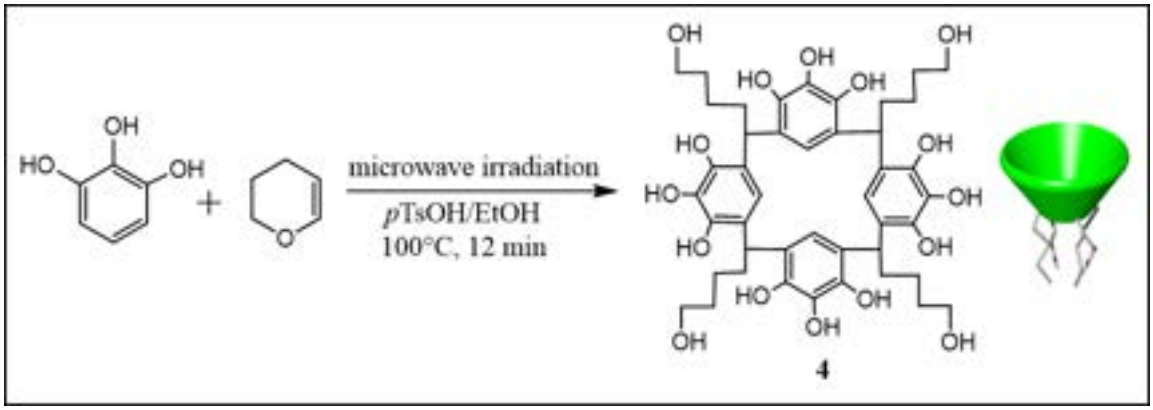

*Figure 3.9. Syntehsis of C-butanolpyrogallol[4]arene **4**.[16]*

C-hydroxybutylpyrogallo[4]arene **4** was prepared from pyrogallol and 2,3-dihydropyran implementing microwave irradiation using the previously reported microwave-assisted synthesis of macrocycles, as shown in Figure 3.9.[16] In general, 2,3-dihydropyran was added to a pyrogallol and p-toluenesulphonic acid solution in ethanol contained in a sealed

CEM pressure vial. The mixture was pre-stirred (30 sec.) and heated (100 °C) in a Biotage Initiator 60 instrument by microwave irradiation (130 W, 2 min. power cycle, total of 12 min.). After cooling to room temperature, the precipitate was collected by vacuum filtration and washed successively with an ethanol and water mixture. The NMR chemical shifts for macrocycle **4** were consistent with the previously reported values.[16]

3.2.2.2 Synthesis of *C*-bromobutyl pyrogallol[4]arene 5

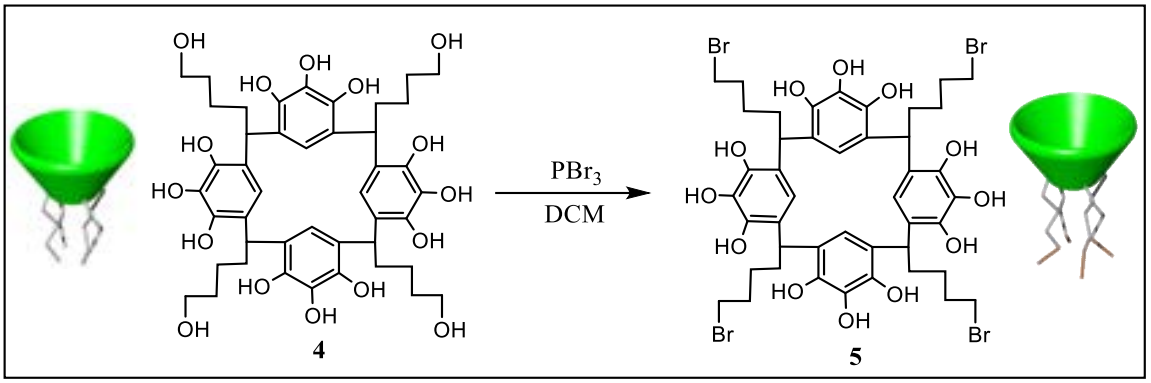

*Figure 3.10. Synthesis of C-bromobutyl pyrogallol[4]arene **5**.*[17]

C-hydroxybutylpyrogallo[4]arene **4** was converted to the tetrabromo derivative pyrogallol[4]arene **5** with phosphorus tribromide, as shown in Figure 3.10. *C*-4-Hydroxybutyl-pyrogallol[4]arene **4** in dichloromethane was cooled to 0 °C under nitrogen. Phosphorus tribromide was added dropwise to the reaction mixture, and the reaction mixture was stirred until it reached room temperature (1.5 hr.). Next, the reaction mixture was stirred at 40 °C for 5 hr. The reaction mixture was then evaporated under vacuum. The resulting oil was sonicated in water (30 mL) for 15 minutes, filtered, and dried under vacuum to obtain a pink solid in 64 % yield.[17]

The ^{1}H NMR for *C*-bromobutylpyrogallol[4]arene **5** revealed the presence of two singlet signals for hydroxy protons in 1:2 ratio in the downfield region, the multiplet signals for the rest of the aliphatic side chain protons are in good agreement with the proposed structure. ^{13}C NMR confirmed four aromatic carbons. The mass spectrometric analysis (ESI-MS) of **5** confirmed the presence of the molecular ion as five isotopic m/z peaks, $[M]^+$ to $[M+8]^+$, in an appropriate ratio for a tetrabromo compound. ESI-MS m/z calculated for $C_{44}H_{52}{}^{79}Br_4O_{12}$ was 1088.0187, found: 1088.0192, 1090.0216, 1092.0201, 1094.0112 and 1096.0109 $[M]^+$.[17]

In conclusion, The rapid synthesis of the macrocycles using this microwave technique has enabled the synthesis of macrocycle co-pillar[4+1]arene **3** in a high yield of 88.5% under 4 mins compared to the yield of 26.3% by the traditional condensation

reaction method. Similarly, *C*-bromobutyl pyrogallol[4]arene **5** is synthesized under a high yield of 65% from *C*-butanolpyrogallol[4]arene **4** synthesized by microwave-assisted irradiation methodology. In implementing a microwave irradiation green technique, the energy required and the waste production are considerably reduced compared to the traditional open vessel condensation synthesis macrocycles.

3.3 References

1. L. Guo, J. Du, Y. Wang, K. Shi and E. Ma, *J. Incl. Phenom. Macrocycl. Chem.,* 2020, **97**, 1-17.
2. C. Sathiyajith, R. R. Shaikh, Q. Han, Y. Zhang, K. Meguellati and Y. Yang, *Chem.Commun.*, 2017, **53**, 677-696.
3. K. Yang, Y. Pei, J. Wen and Z. Pei, *Chem.Commun.*, 2016, **52**, 9316-9326; P. J. Cragg and K. Sharma, *Chem. Soc. Rev.*, 2012, **41**, 597-607.
4. A. Isik, M. Oguz, A. Kocak and M. Yilmaz, *J. Incl. Phenom. Macrocycl. Chem.*, 2022, 1-11; D. Schlüter, K. R. Korsching and V. A. Azov, *Eur. J. Org. Chem.,* 2021, **2021**, 4469-4476; J. P. Buttress, D. P. Day, J. M. Courtney, E. J. Lawrence, D. L. Hughes, R. J. Blagg, A. Crossley, S. E. Matthews, C. Redshaw and P. C. Bulman Page, *Langmuir*, 2016, **32**, 7806-7813.
5. T. Ogoshi, S. Kanai, S. Fujinami, T. Yamagishi and Y. Nakamoto, *J. Am. Chem. Soc.*, 2008, **130**, 5022-5023.
6. T. Ogoshi, T. Yamagishi and Y. Nakamoto, *Chem. Rev.*, 2016, **116**, 7937-8002.
7. K. Yang, Y. Pei, J. Wen and Z. Pei, *Chem.Commun.*, 2016, **52**, 9316-9326.
8. N. L. Strutt, H. Zhang, S. T. Schneebeli and J. F. Stoddart, *Acc. Chem. Res.*, 2014, **47**, 2631-2642.
9. T. Ogoshi and T. Yamagishi, *Eur. J. Org. Chem.*, 2013, **2013**, 2961-2975.
10. T. Ogoshi, N. Ueshima, T. Akutsu, D. Yamafuji, T. Furuta, F. Sakakibara and T. Yamagishi, *Chem.Commun.*, 2014, **50**, 5774-5777.
11. Z. Zhang, B. Xia, C. Han, Y. Yu and F. Huang, *Org. Lett.*, 2010, **12**, 3285-328.
12. S. Mekapothula, M. A. Addicoat, D. J. Boocock, J. D. Wallis, P. J. Cragg and G. W. Cave, *Chem.Commun.*, 2020, **56**, 1792-1794.
13. L. Liu, D. Cao, Y. Jin, H. Tao, Y. Kou and H. Meier, *Org. Biomol. Chem.*, 2011, **9**, 7007-7010.
14. G. W. Cave, J. Antesberger, L. J. Barbour, R. M. McKinlay and J. L. Atwood, *Angew. Chem. Int. Ed.*, 2004, **43**, 5263-5266; M. W. Heaven, G. W. Cave, R. M. McKinlay, J. Antesberger, S. J. Dalgarno, P. K. Thallapally and J. L. Atwood, *Angew. Chem. Int. Ed.*, 2006, **45**, 6221-6224.
15. G. W. Cave, S. J. Dalgarno, J. Antesberger, M. C. Ferrarelli, R. M. McKinlay and J. L.

Atwood, *Supramol. Chem.*, 2008, **20**, 157-159; Bassil, D. B. Bassil, S. J. Dalgarno, G. W. Cave, J. L. Atwood and S. A. Tucker, *J. Phys. Chem. B*, 2007, **111**, 9088-9092.
16. M. Funck, D. P. Guest and G. W. Cave, *Tetrahedron Lett.*, 2010, **51**, 6399-6402.
17. S. Mekapothula, A. Wonanke, M. A. Addicoat, D. J. Boocock, J. D. Wallis and G. W. Cave, *Int. J. Mol. Sci.*, 2021, **22**, 5726.
18. C. B. Rodell, J. E. Mealy and J. A. Burdick, *Bioconjug. Chem.*, 2015, **26**, 2279-2289.
19. https://cem.com/en/benefits-of-microwave-reactions (Accessed November 2022)

4 Chapter 4: Silica-bound supramolecular chromatographic separation of xylene isomers and their impurities

4.1 Introduction

Developing new functional materials that reduce the environmental impact of chemical processing is essential with the growing global demand for petrochemical feedstocks. Improving the efficiency of the separation and refining of organic geometrical xylene isomers and their impurities are particularly important, given the large volumes of these compounds used as starting materials in the chemical industry. For example, *p*-xylene is an important raw material for synthesizing polyethylene terephthalate (PET) resins for beverage bottles, and polybutylene terephthalate (PBT); *o*-xylene is utilized to produce phthalic anhydride, and *m*-xylene to synthesize isophthalic acid.[1] Even though ethylbenzene, benzene, and toluene are the by-products of catalytic reforming processes, benzene and toluene are isolated as pure components during the second separation of aromatic complexes, which transforms reformates into intermediates, *i.e.,* benzene, toluene, and a mixture of ethylbenzene and xylenes, often termed as the BTEX group. Moreover, ethylbenzene exists as an impurity of xylene isomers. Henceforth, the development of energy-efficient separation of xylene isomers and their impurities with high purity is therefore significantly needed.[2,3]

Refineries utilize solvent extraction to separate benzene, toluene, and C_8 fractions from BTEX. However, due to the similar solubilities of isomers in the most common solvents, it is challenging to separate xylene isomers by solvent extraction.[4] Even though distillation, including azeotropic and extractive distillation, has been traditionally used to separate benzene derivatives, it is not pertinent to separate the xylene isomers due to the requirement of many theoretical plates (150 for *o*-xylene and 360 for *m*-xylene and *p*-xylene), and high energy costs.[5] Industrially, *p*-xylene is isolated widely by fractional distillation owing to lower melting points. However, low temperature or high pressure is challenging to achieve the eutectic point during the crystallization process, and the product recovery is only 60-70%.[6]

In the past decades, highly selective and energy-efficient selective adsorption using porous materials, *i.e.*, zeolites, metal-organic frameworks (MOFs), porous coordination polymers (PCPs), and covalent organic frameworks (COFs), have been widely used in the industry to separate xylene isomers. In addition, these materials have been used extensively to separate gases, drugs, and hydrocarbons.[7-10] An efficient zeolite-derivated simulated

moving bed (SMB) chromatographic technology was reported in the 1960's and currently accounts more than 75% of industrial *p*-xylene separation worldwide. In the SMB separation process, zeolites and derivatives are packed as solid adsorbents into columns to separate xylene mixtures.[11] Subsequently, several porous materials have been applied as solid adsorbents to separate xylene isomers, such as carbon materials,[12] silica gel,[13] microporous organic polymers (MOPs),[14] MOFs,[15] metal-organic complexes,[16] covalent-organic frameworks (COFs),[17] and hydrogen-bonded organic frameworks (HOFs) as shown in the Figure 4.1.[18] However, almost all porous absorbent materials struggled with low repeatability and reproducibility due to loss of porosity or transformation because of the low thermal stability of porous adsorbents. Subsequently, the development of various highly energy-efficient technologies and materials has sparked researchers' attention.

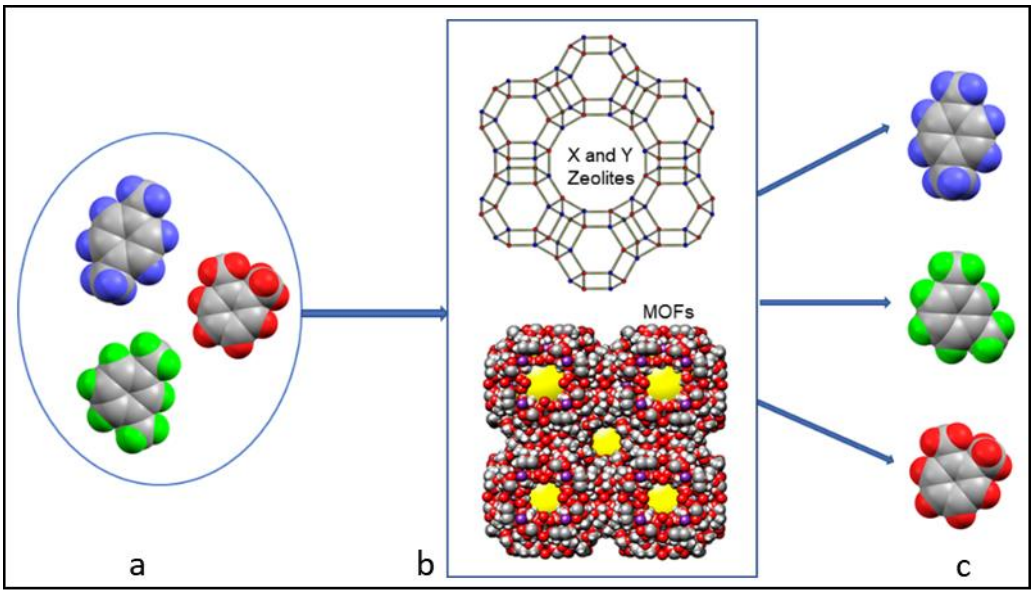

Figure 4.1. Graphical representation of xylene isomers separation by zeolites and MOFs. Xylene mixture (a), cation-exchanged faujasite (FAU)-type zeolites and Zinc-based MAF-X8 (b), and separated individual xylene isomers. p-xylene (blue), *o*-xylene (red), and *m*-xylene (green)

A subclass of porous materials called intrinsically porous molecular materials[19] consisting of organic macrocycles and cages with specific guest-accessible intrinsic cavities has been developed. These isolated porous materials range from distinct porous molecules to highly ordered crystalline structures, including cyclodextrins,[20] calixarenes,[21] cucurbiturils,[22] trianglamine,[23] pillararenes,[24] and porous organic cages.[25] Due to non-covalent host-guest interactions, these materials can absorb guest molecules in solid, liquid, solution, and even gas phases.

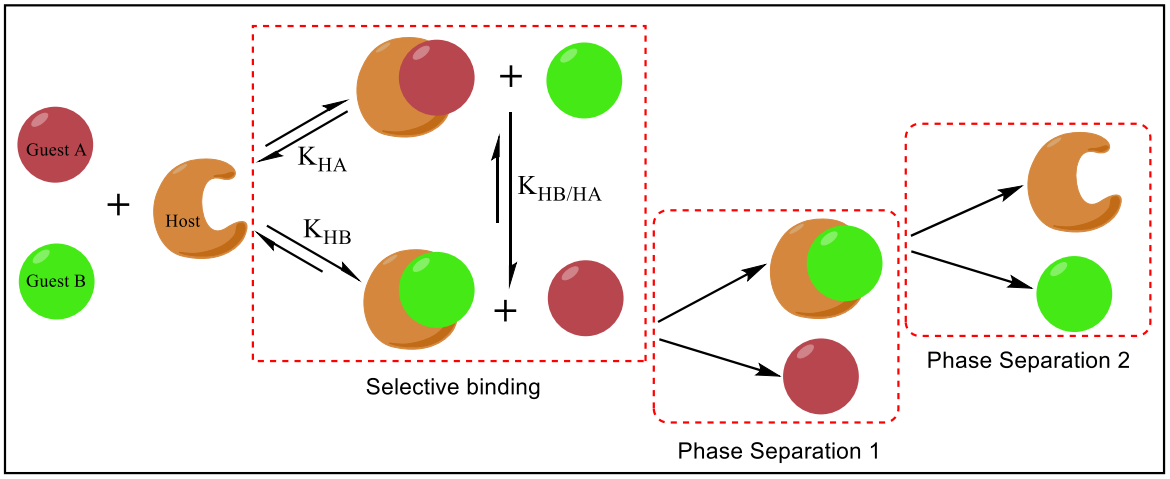

Figure 4.2. Macrocyclic host separation of guest molecules (Assuming Guest B has a stronger binding affinity with the guest). KHA and KHB are binding constants.

Supramolecular host-guest interactions between functional groups and size complementarity have been widely used to bind specific geometric isomers selectively, as shown in Figure 4.2.[26.] While this approach to separation *via* stepwise complexation and crystallization is feasible for particular isomers, it is inherently limited to single geometric isomers. It, therefore, has limited application for *in-situ* separation of multiple sets of isomers.[27] Several research groups have reported the synthesis and separation applications of combining the supramolecular host-guest properties of the bowl-like calix[*n*]arene or cyclodextrin macrocycles, bound to chromatographic silica.[28] These novel stationary phases have demonstrated good potential for separating hydrocarbons.

Since discovering pillararenes, several research groups have reported the extensive study of host-guest properties using hydrocarbons and alkylaromatic compounds. For example, Yang et al. reported a biphenyl-extended pillar[6]arene for effective selective inclusion of toluene and *m*-xylene in the solid state.[29] Haung et al. and other research groups have also reported the pillararene crystals for effective gas storage and hydrocarbon separation,[30] e.g. a perethylated pillar[6]arene crystal to purify styrene from a mixture of styrene and ethylbenzene;[31] a perethylated pillar[5]arene crystal to separate1-pentene over its positional isomer 2-pentene;[32] a perethylated pillar[n]arene crystal (n = 5, 6), which successfully used separate xylene isomers.[33]

Due to the unique structural features of pillar[n]arenes and their demonstrated host-guest supramolecular non-covalent interactions for aromatic hydrocarbons and their positional isomers, has been constructed herein, as a silica-bound co-pillar[4+1]arene flash column chromatographic stationary phase to demonstrate the chromatographic retention behaviour of xylene isomers and their impurities. The experimental chromatographic results were supported by computational binding energy calculations.

4.2 Results and Discussion

4.2.1 Synthesis of silica bound co-pillar[4+1]arene stationary phase 6

Co-pillar[4+1]arene **3** was successfully functionalized on the surface of chromatographic activated silica (Interchim general purpose grade) *via* a modified procedure, as shown in Figure 4.3. The chromatographic silica specifications are particle size 50 µm, and pore size 500 Å and are suitable for flash column chromatography. First, the activation of silica was performed *via the* treatment of silica in a 1:1 ratio of basic solution of triethylamine (TEA) and tetrahydrofuran (THF). The stationary phase **6** was then separated from the solution by vacuum filtration. Finally, the stationary phase **6** was washed with water/methanol to remove unreacted chemical debris and allowed to dry at room temperature.

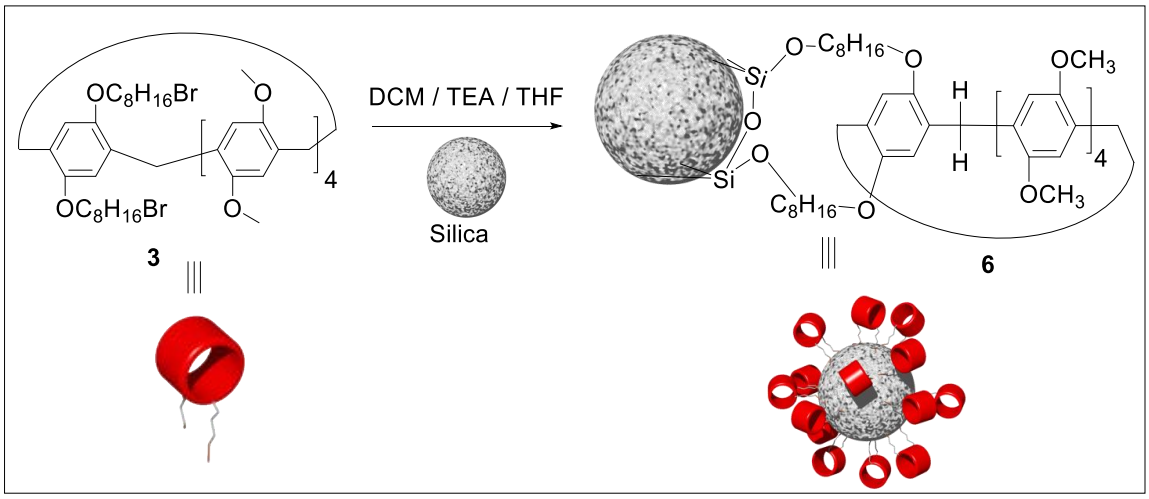

*Figure 4.3. Synthesis of silica-bound co-pillar[4+1]arene stationary phase **6.***

4.2.2 Characterization of stationary phase 6

After successfully synthesizing the silica-bound co-pillar[4+1]arene flash column chromatographic stationary phase **6,** thermogravimetric analysis was performed to characterize the amount of co-pillar[4+1]arene **3** on the surface of flash column chromatographic silica. The thermogravimetric analysis was performed starting at an initial 50 °C, increasing to 900 °C with 20 °C increments per minute. Two main weight loss regions were observed (Figure 4.4). First, the initial weight loss starting from 100 °C to 150 °C can be attributed to the 4% loss of residual water, both on the surface of the silica and embedded within the host cavitand. The second weight-loss indicated decomposition of the functionalized co-pillar[4+1]arene **3** from 200-900 °C. Thermogravimetric analysis studies confirmed the mass loading of the co-pillar[4+1]arene **3** macrocycle on silica surface at 16% w/w, as shown in Figure 4.4.

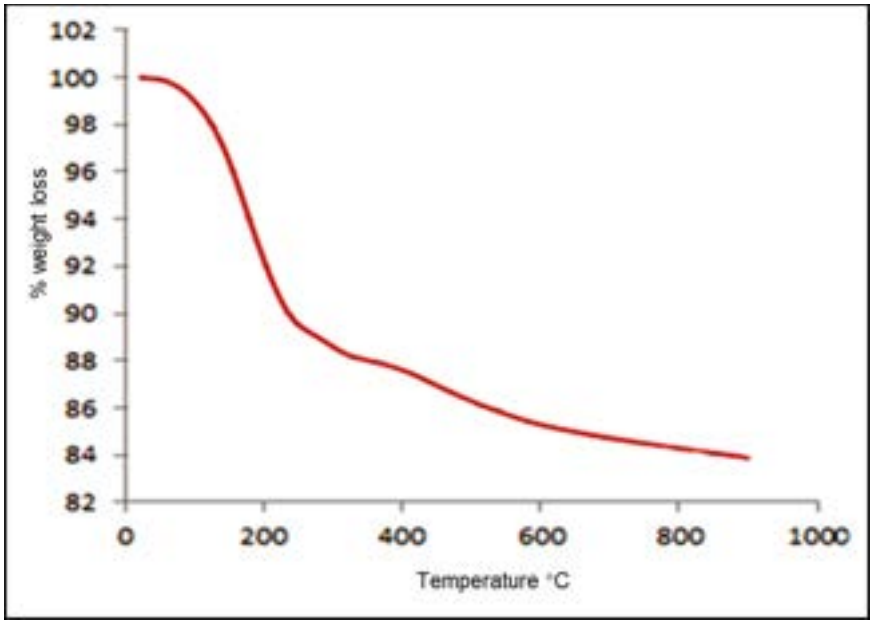

Figure 4.4. Thermogravimetric analysis (TGA) of silica for flash column chromatography.

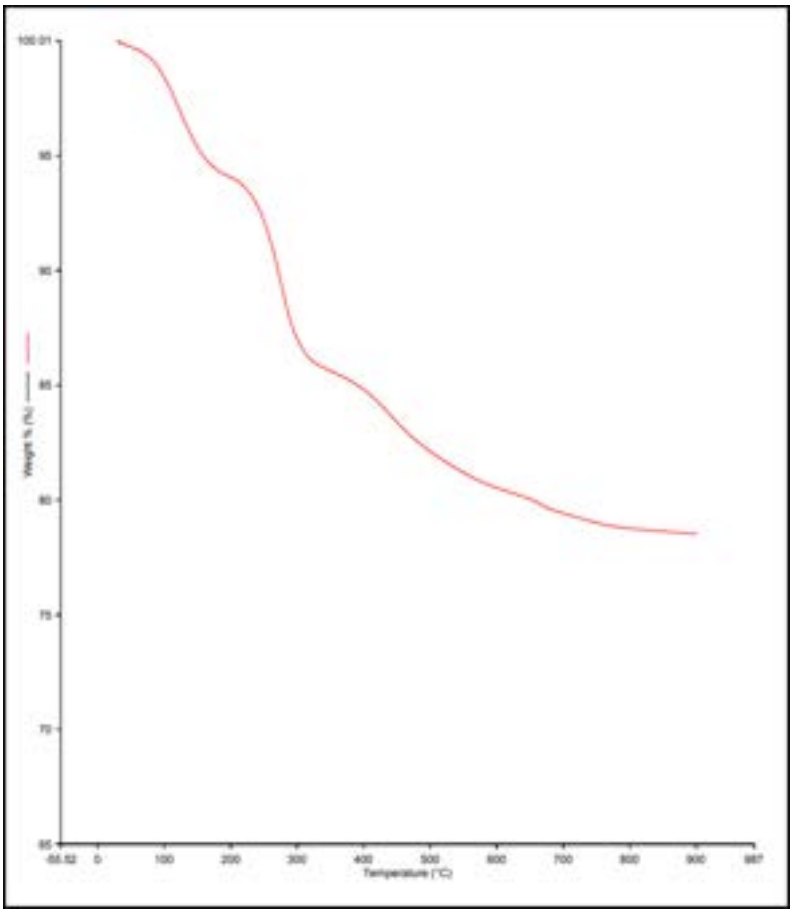

*Figure 4.5 Thermogravimetric analysis (TGA) of co-pillar[4+1]arene silica bound **6** stationary phase for flash column chromatography.*

4.2.3 Column packing and conditioning of stationary phase 6

Co-pillar[4+1]arene bonded-silica gel **6** (12 g) was dry-packed into an empty flash column cartridge (62 × 12 mm i.d.) with continuous tapping and primed with cyclohexane (100%), ethyl acetate (100%), and finally with methanol (100%) to remove unreacted chemical components or debris. The flash column was stored with methanol:water (80:20).

To validate the stability of silica-bound co-pillar[4+1]arene flash column stationary phase **6**, a mobile phase with methanol: water (80:20) was eluted through the flash column stationary phase **6.** First, the flash column eluents were collected after multiple column volumes. Then, they were directly infused on a mass spectrometer to identify the elution of co-pillar[5]arene from the silica-bound co-pillar[5]arene during various column volumes. However, there was no observation of co-pillar[4+1]arene **3** in the mass spectra, which confirms that there was no leaking of co-pillar[4+1]arene **3** from silica-bound co-pillar[4+1]arene flash column stationary phase **6** even after 1000 column volumes as shown in Figures 4.6 and 4.9.

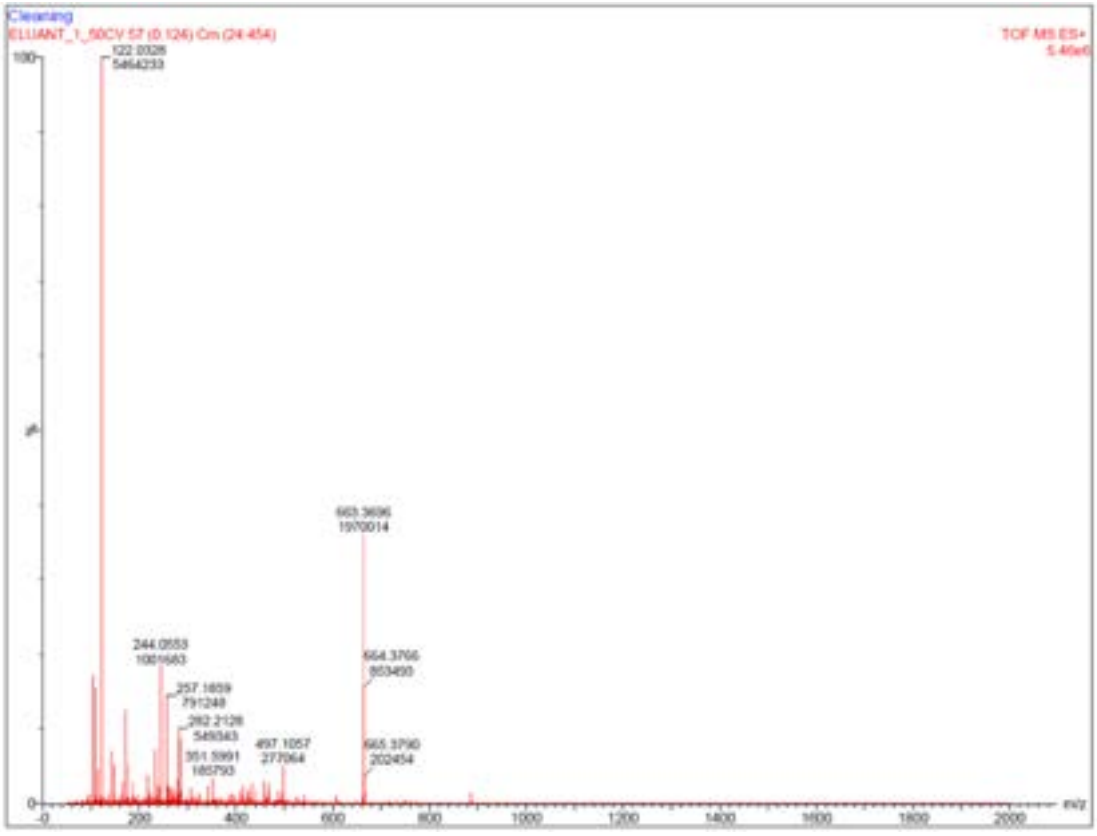

*Figure 4.5. LC-MS spectrum of mobile phase eluent from co-pillar[4+1]arene bonded-silica flash column **6** at 50 column volumes.*

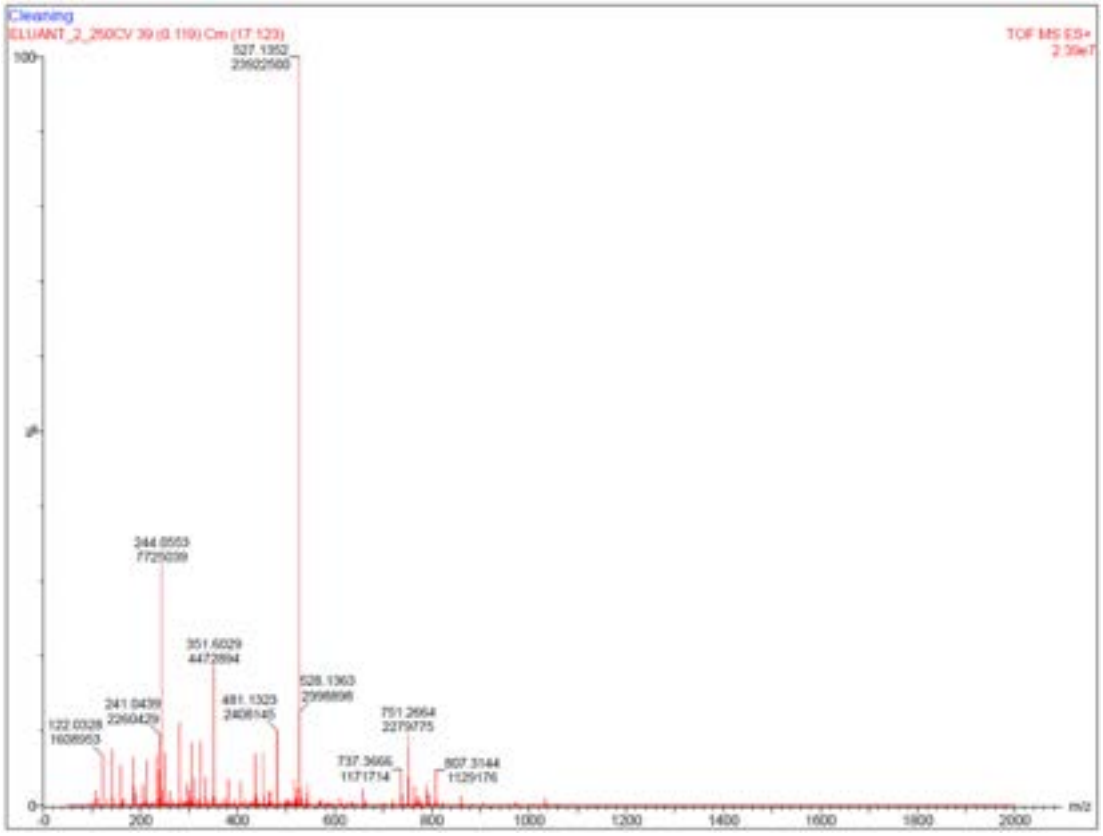

*Figure 4.6 LC-MS spectrum of mobile phase eluent from co-pillar[4+1]arene bonded-silica flash column **6** at 250 column volumes.*

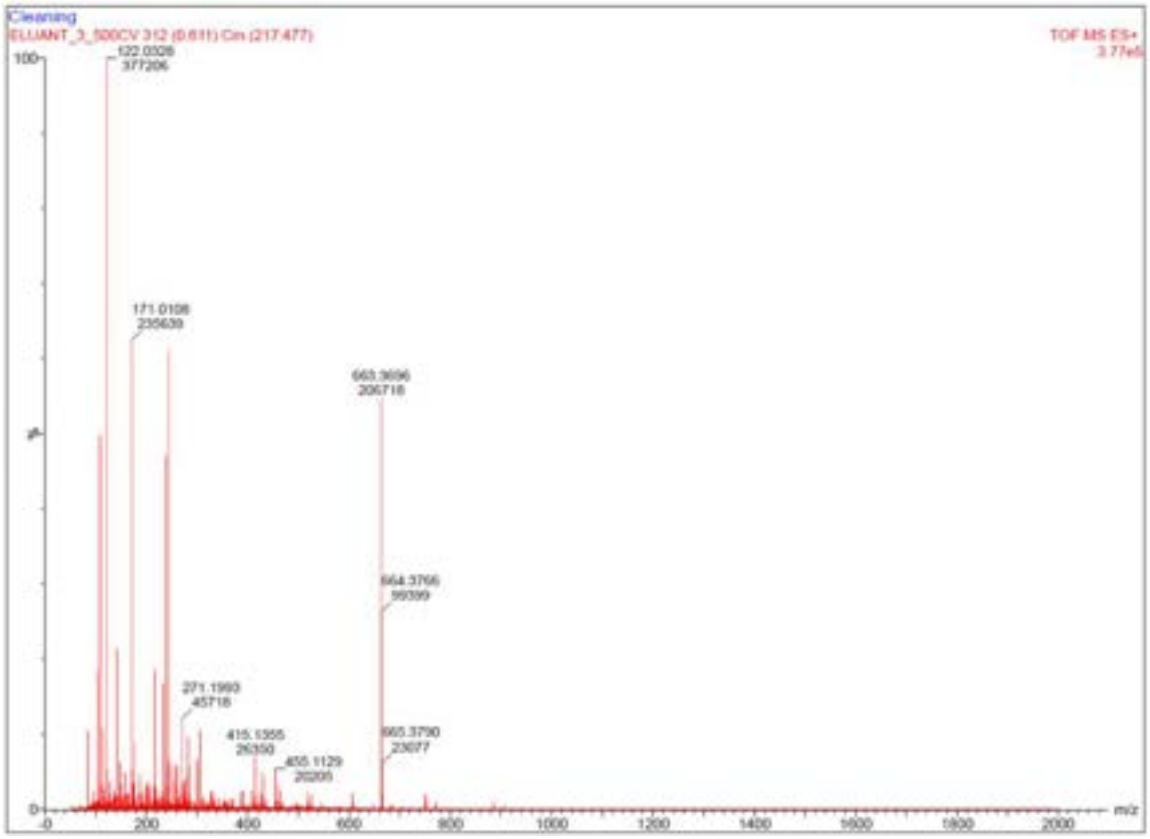

*Figure 4.7 LC-MS spectrum of mobile phase eluent from co-pillar[4+1]arene bonded-silica flash column **6** at 500 column volumes*

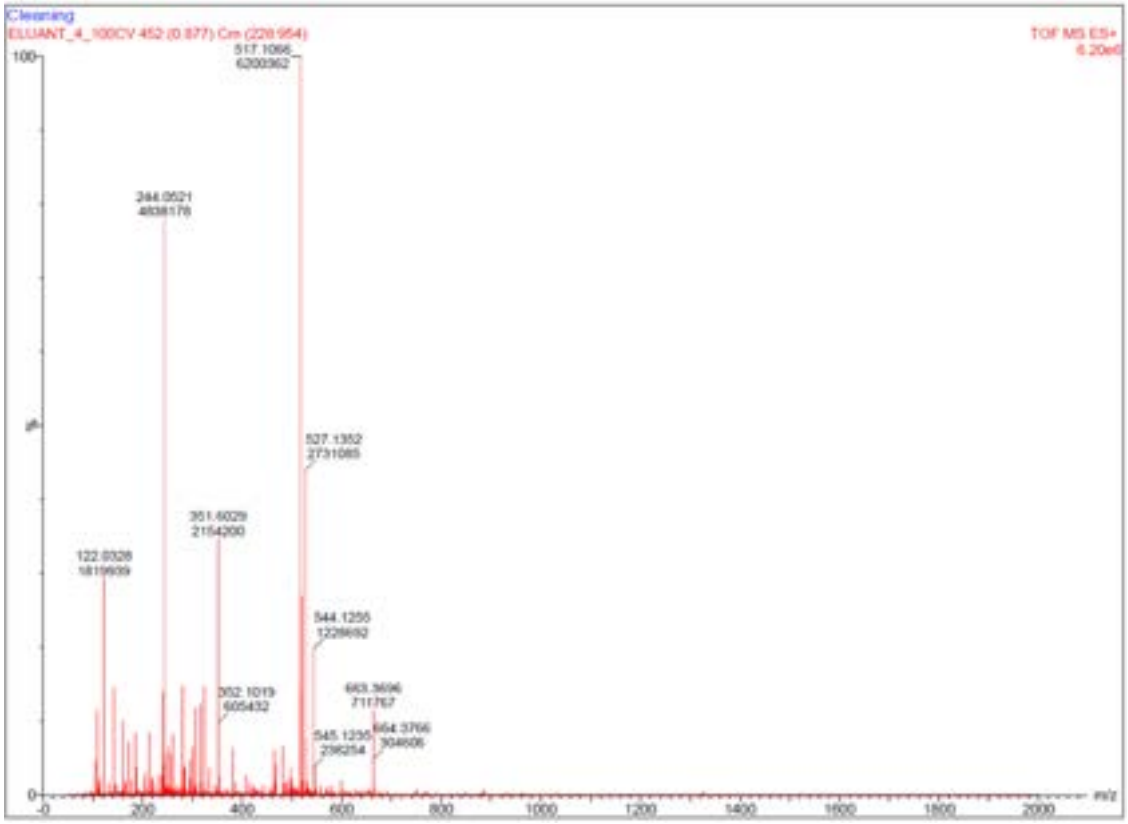

*Figure 4.8. LC-MS spectrum of mobile phase eluent from co-pillar[4+1]arene bonded-silica flash column **6** at 500 and 1000 column volumes.*

4.2.4 Separation of individual xylene isomers on flash column stationary phase 6

The primary approach to the flash column chromatographic separation of xylene isomers and their impurities toluene and ethylbenzene on silica-bound co-pillar[4+1]arene stationary phase **6,** was carried out to optimize the mobile phase conditions to achieve a symmetrical peak shape. As shown in Table 4.1, several mobile phase combinations have been studied under isocratic conditions to optimize the mobile phase conditions.

Table 4.1. Mobile phase combinations and solvent ratios for method development.

Mobile phase	Solvent ratios
Methanol:water	80:20
Methanol:water	90:10
Methanol:water	70:30
Methanol:water	60:40
Acetonitrile:water	90:10
Acetonitrile:water	60:40
Methanol:ethyl acetate	90:10
Methanol:ethyl acetate	70:30

Methanol:ethyl acetate	50:50
Methanol:ethyl acetate	30:70
Methanol:ethyl acetate	10:90

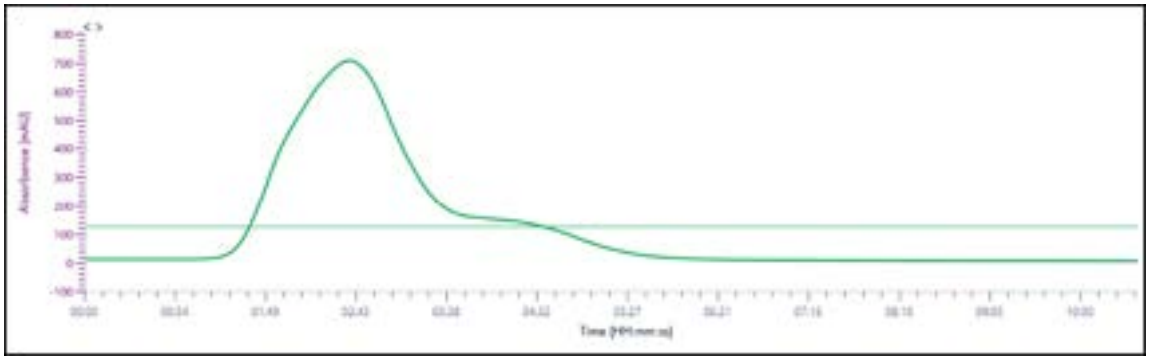

Figure 4.9. Separation of xylene isomers, toluene, and ethylbenzene using methanol: water (80:20).

When the method development for the separation of xylene isomers was studied using a mobile phase with varying concentrations of methanol:water or acetonitrile:water, there was no significant observation of the chromatographic separation of xylene isomers and impurities. Instead, they resulted in a broad single peak, as shown in Figure 4.10.

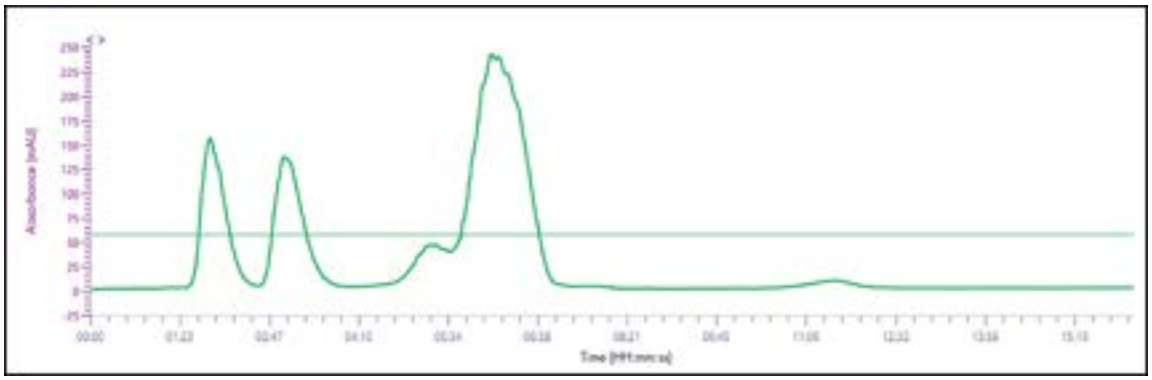

Figure 4.10. Separation of xylene isomers, toluene, and ethylbenzene using methanol: ethyl acetate (30:70).

As shown in Figure 4.11, toluene and *o*-xylene were eluted as single components from the mixture of xylene isomers on the co- pillar[4+1]arene silica flash cartridge **6** (12 g) using mobile phase methanol: ethyl acetate (30:70) under isocratic conditions. However, *m*-xylene and *p*-xylene were eluted as a single unresolved mixture of analytes. Therefore, the mobile phase conditions methanol: ethyl acetate (30:70) under isocratic conditions have not resolved all isomers and toluene as individual components; chromatographic peaks were observed for all components in the chromatogram as shown in Figure 4.11.

These chromatographic mobile phase conditions served as stepping stones to optimize the peak symmetry while changing the concentration of ethyl acetate, which would affect

the peak symmetry. As a result, the ethyl acetate concentration rose to 90% in the mobile phase as methanol: ethyl acetate (10:90) to optimize the chromatographic behaviour of isomers and their impurities.

The individual xylene isomers and toluene (2 mL) were loaded onto the silica-bound co-pillar[4+1]arene flash column cartridge **6** *via* an optimized mobile phase isocratic elution of methanol/ethyl acetate (21 10:90, 15 min). The mobile phase flow rate was set to 21 mL/min. In addition, the fraction collection volume was set to 13 mL. In-built advance mode optimization conditions equilibrated the silica-bound copillar[4+1]arene flash column **6** while UV detection was performed between 200-800 nm.

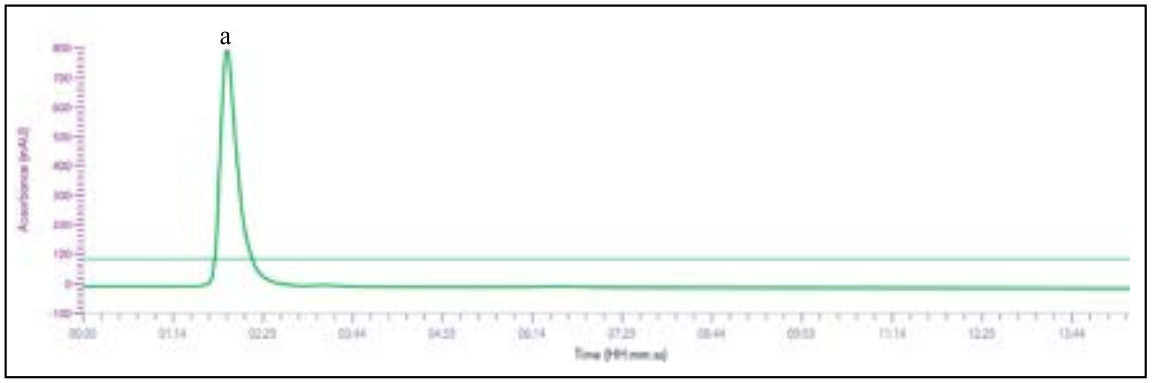

*Figure 4.11. Separation of m-xylene (a) on silica-bound co-pillar[4+1]arene flash column cartridge **6**.*

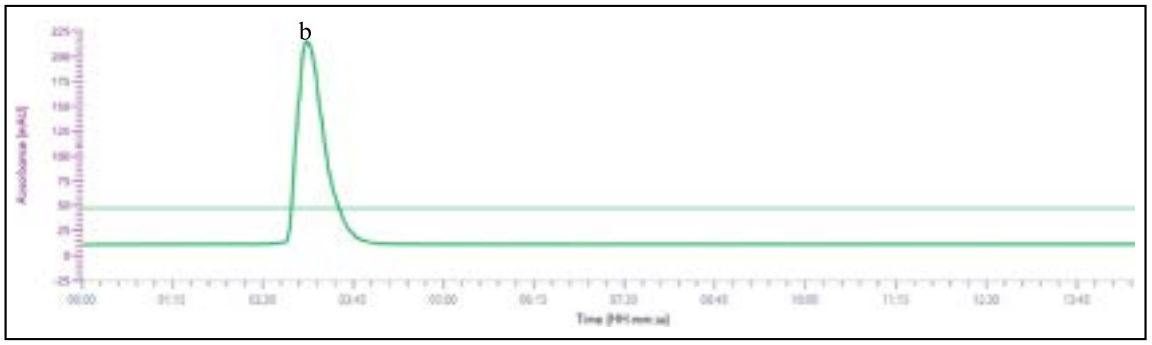

*Figure 4.12. Separation of toluene (b) on silica-bound co-pillar[4+1]arene flash column cartridge **6**.*

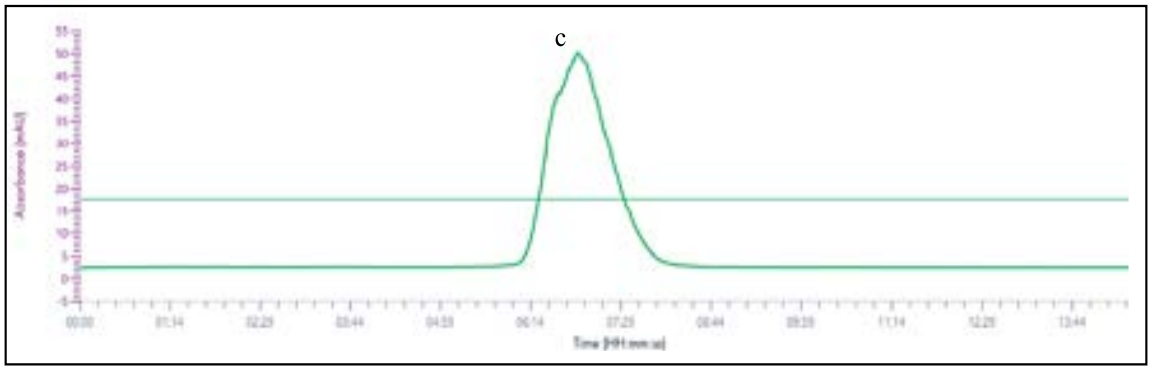

*Figure 4.13. Separation of o-xylene (c) on silica-bound co-pillar[4+1]arene flash column cartridge **6**.*

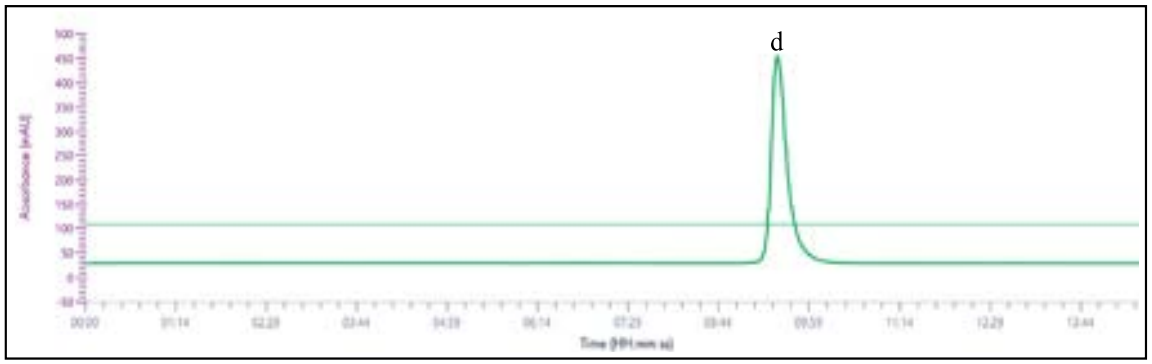

*Figure 4.14. Separation of p-xylene (d) on silica-bound co-pillar[4+1]arene flash column cartridge **6**.*

As a result, the individual m-xylene (a), toluene (b), o-xylene (c), and p-xylene (d) were eluted symmetrically from the silica-bound co-pillar[4+1]arene **6** flash column (12 g) in under 15 mins, and their retention times can be seen in the following Figures 4.12-4.15. Finally, the separation of xylene isomers and their impurities as individual components were achieved with the optimized mobile phase conditions of methanol: ethyl acetate (10:90). Then, all the fractions were collected and analyzed by the ^{1}H-NMR, as shown in Figures 4.16-4.19.

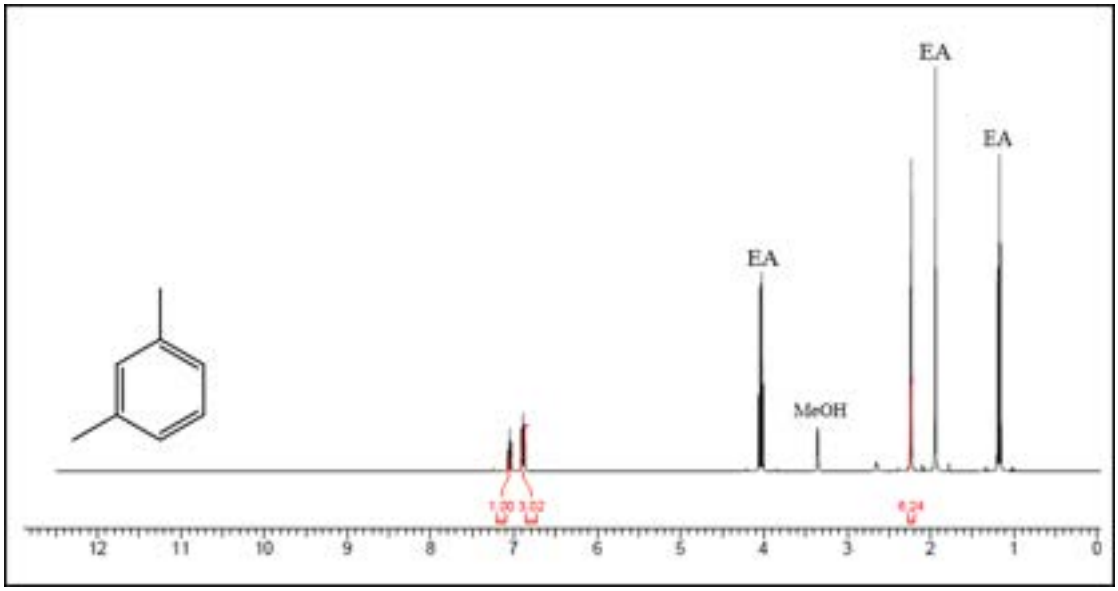

*Figure 4.15. ^{1}H NMR spectrum (400 MHz, chloroform-d, room temperature) of m-xylene fraction from co-pillar[4+1]arene stationary phase **6**. (EA is Ethylaceate and MeOH is methanol)*

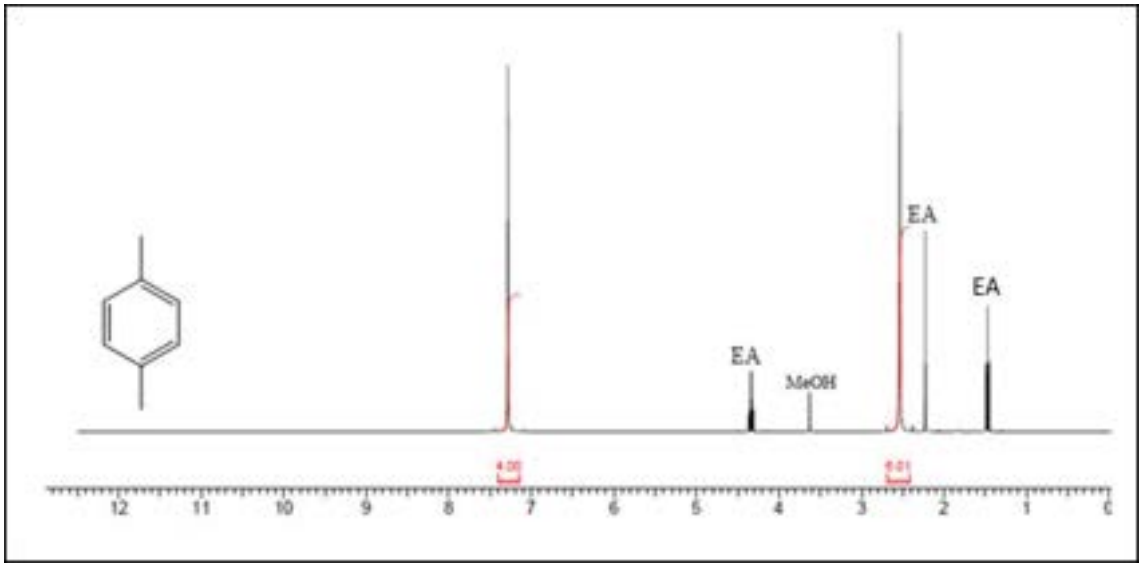

*Figure 4.16. ^{1}H NMR spectrum (400 MHz, chloroform-d, room temperature) of p-xylene fraction from co-pillar[4+1]arene stationary phase **6**. (EA is Ethylaceate and MeOH is methanol)*

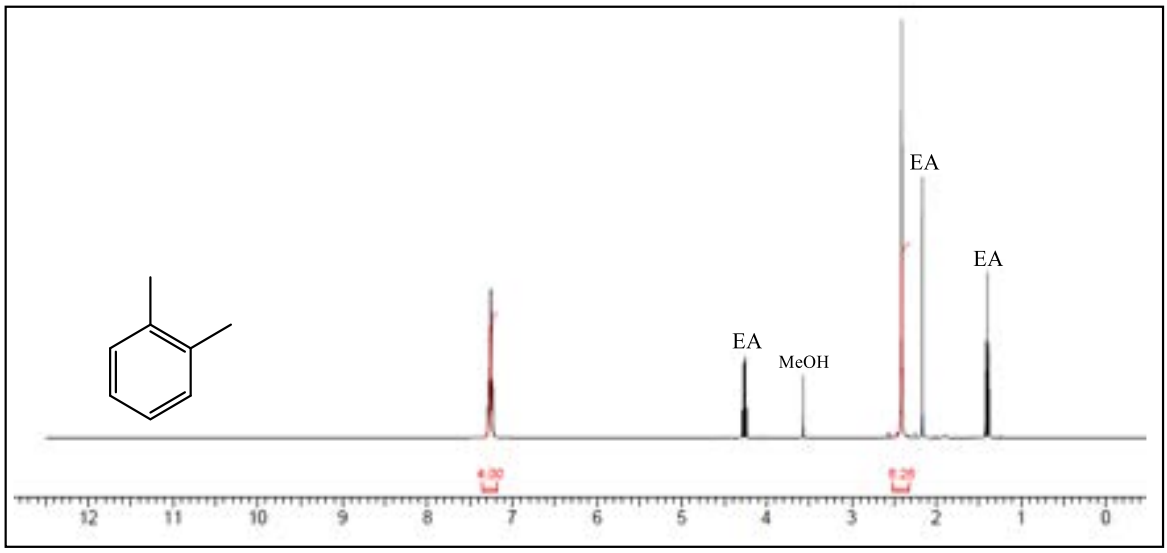

*Figure 4.17. ^{1}H NMR spectrum (400 MHz, chloroform-d, room temperature) of o-xylene fraction from co-pillar[4+1]arene stationary phase **6**. (EA is Ethylaceate and MeOH is methanol)*

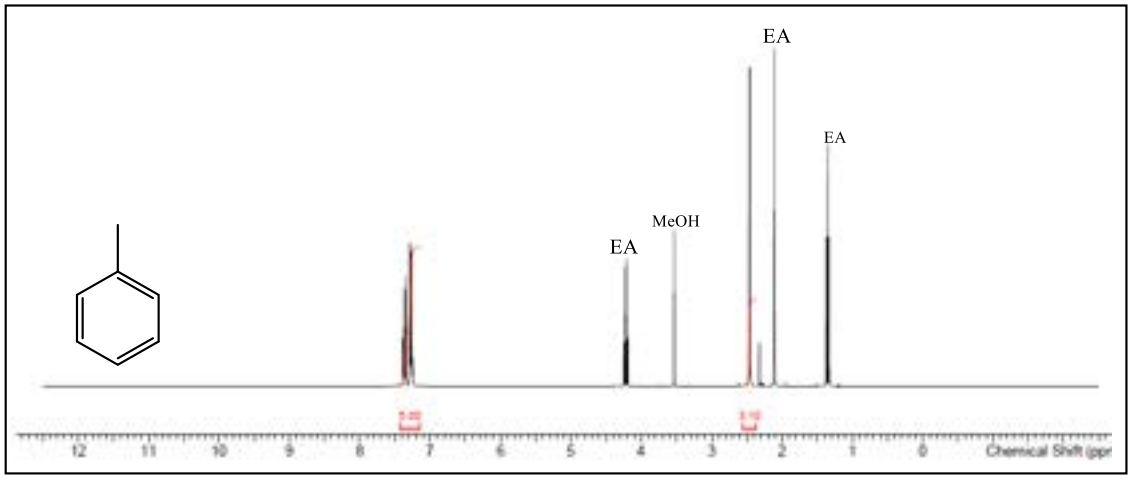

*Figure 4.18. ^{1}H NMR spectrum (400 MHz, chloroform-d, room temperature) of o-xylene fraction from co-pillar[4+1]arene stationary phase **6**. (EA is Ethylaceate and MeOH is methanol)*

4.2.5 Validation of the developed method

In order to validate the newly developed silica-bound co-pillar[4+1]arene stationary phase **6**, chromatographic separation was performed to separate the mixture of xylenes, ethylbenzene (1.0 mL, Fisher Scientific CAS number: 1330-20-7, 100-41-4), and toluene (1.0 mL, Fisher Scientific CAS number: 108-88-3) on both normal phase Interchim® flash column (12 g) and the silica-bound co-pillar[4+1]arene flash column **6** (12 g) using the optimized method under isocratic mobile phase elution (methanol/ethyl acetate, 10:90, at 21 mL min^{-1}, 15 min) as shown in Figure 4.20.

The normal phase flash column resulted in a single sharp peak which eluted all five eluents together, as shown in Figure 4.20A. However, the co-pillar[4+1]arene bound-silica

4 flash column separated out the mixture into five discreet bands (together as shown in Figure 4.20B), which were collected and analyzed by ^{1}H-NMR. As a result, the elution order of the Fisher Scientific xylene and toluene sample mixture was observed to be; m-xylene (a), toluene (b), o-xylene (c), p-xylene (d), and ethylbenzene (e) as shown in Figure 4.20B. The elution order of the Fisher Scientific xylene and toluene sample mixture was in line with the elution order of individual standard xylene isomers and their impurities, such as ethylbenzene and toluene.

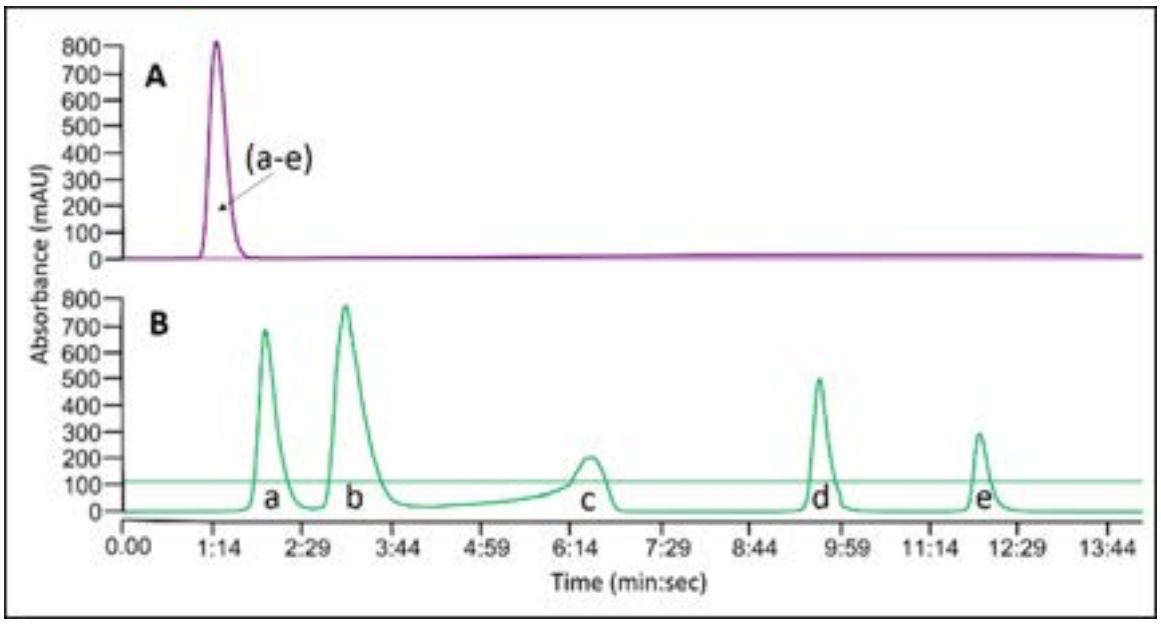

Figure 4.19. Flash column separation of Fisher Scientific xylene and toluene sample mixture; (a) m-xylene, (b) toluene, (c) o-xylene, (d) p-xylene, and (e) ethylbenzene on (A) normal phase Interchim® flash column and (B) co-pillar[4+1]arene bound-silica stationary phase.

The xylene isomers eluted from the co-pillar[4+1]arene bound-silica **6** flash column were quantified *via* ^{1}H-NMR and observed to be in line with the supplier certificate of analysis. The ratios of *m*-xylene, *o*-xylene, *p*-xylene and ethylbenzene were 45%, 24%, 20% and 10%. The eluents from the Fisher Scientific xylene and toluene sample mixture were identified, and reported as *m*-xylene (a), toluene (b), *o*-xylene (c), and *p*-xylene (d) in Figures 4.21-4.26. In addition, it was noted that the *o*-xylene isomer resulted in a broader peak shape compared to the other isomers.

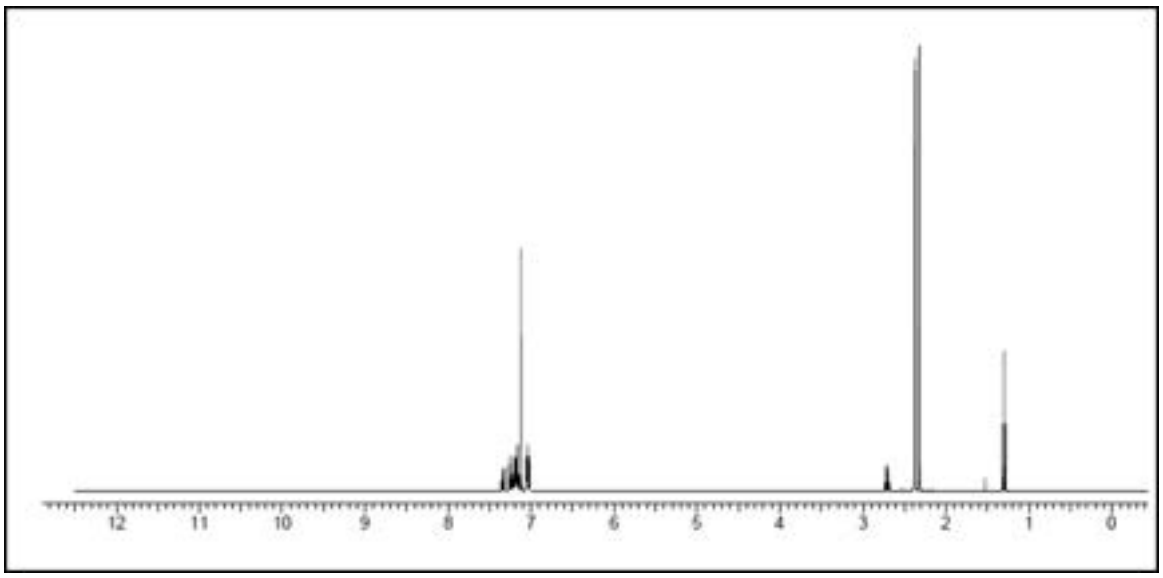

Figure 4.20. ^{1}H NMR spectrum (400 MHz, chloroform-d, room temperature) of xylene mixture fraction from normal phase.

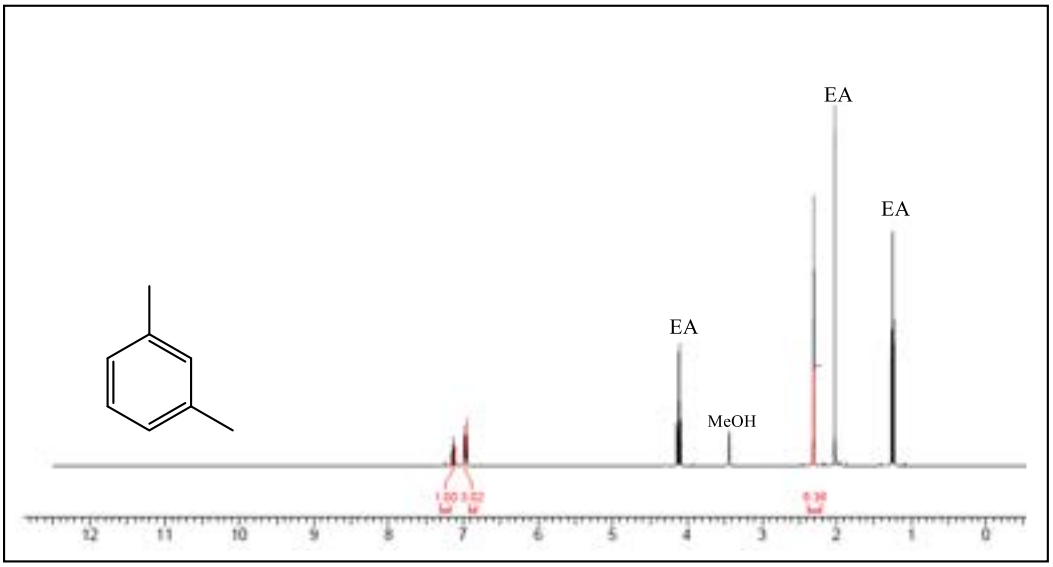

Figure 4.21. ^{1}H NMR spectrum (400 MHz, chloroform-d, room temperature) of fraction 1 from the mixture of Fisher Scientific's xylene and toluene and confirmed as m-xylene. (EA is Ethylaceate and MeOH is methanol)

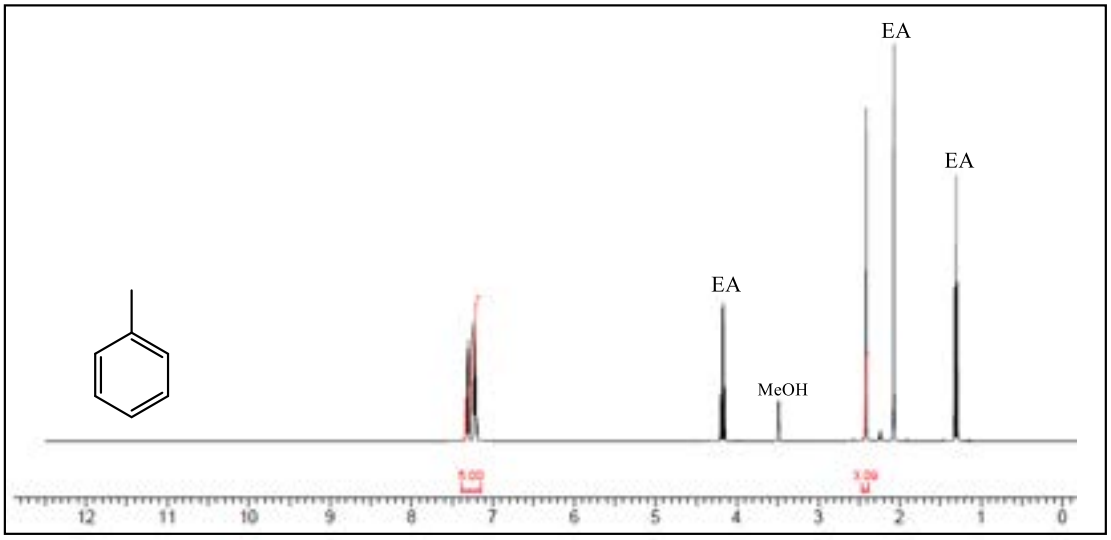

Figure 4.22. ^{1}H NMR spectrum (400 MHz, chloroform-d, room temperature) of fraction 2 from the mixture of Fisher Scientific's xylene and toluene and confirmed as toluene. (EA is Ethylaceate and MeOH is methanol)

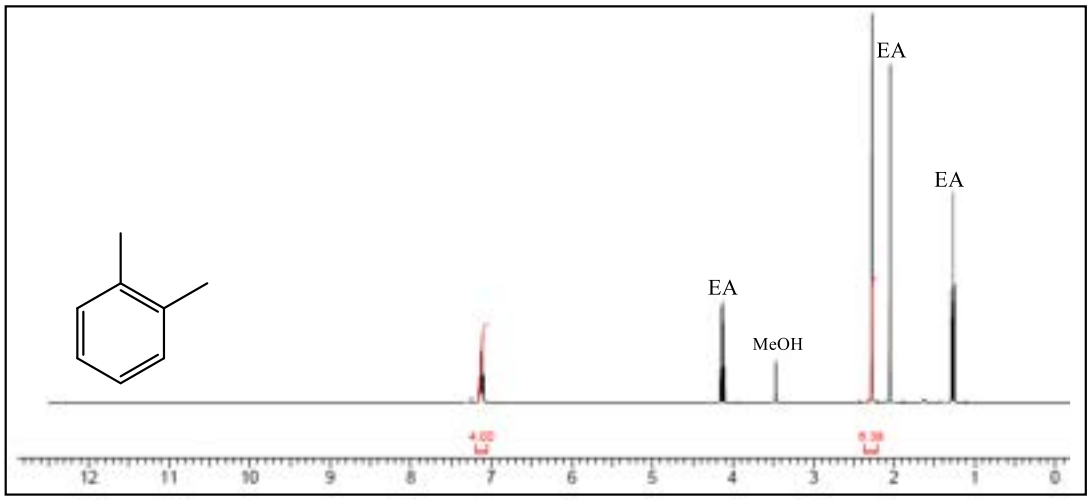

Figure 4.23. ^{1}H NMR spectrum (400 MHz, chloroform-d, room temperature) of fraction 3 from the mixture of Fisher Scientific's xylene and toluene and confirmed as o-xylene. (EA is Ethylaceate and MeOH is methanol)

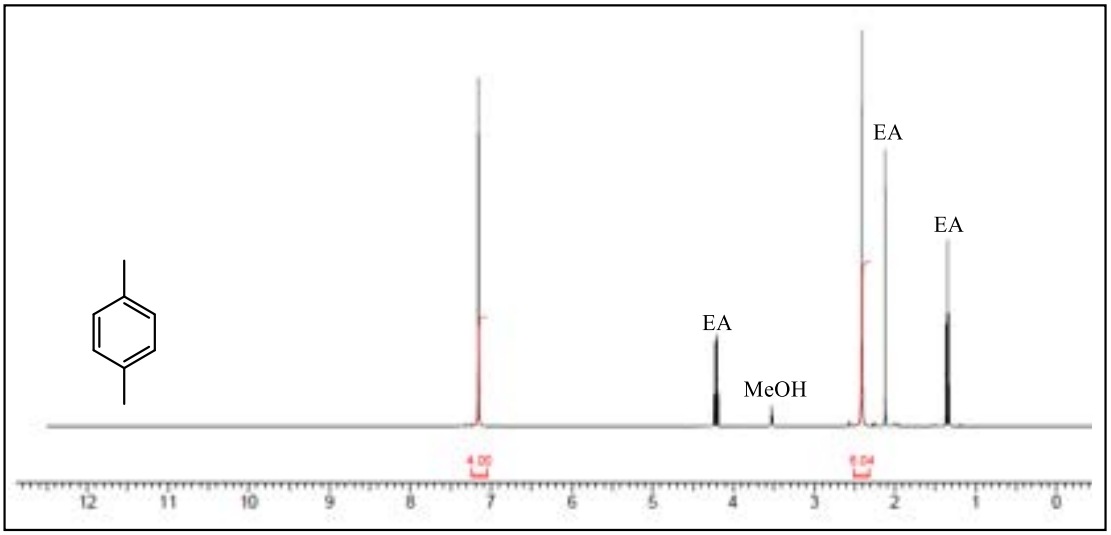

Figure 4.24. ^{1}H NMR spectrum (400 MHz, chloroform-d, room temperature) of fraction 4 from the mixture of Fisher Scientific's xylene and toluene and confirmed as p-xylene. (EA is Ethylaceate and MeOH is methanol)

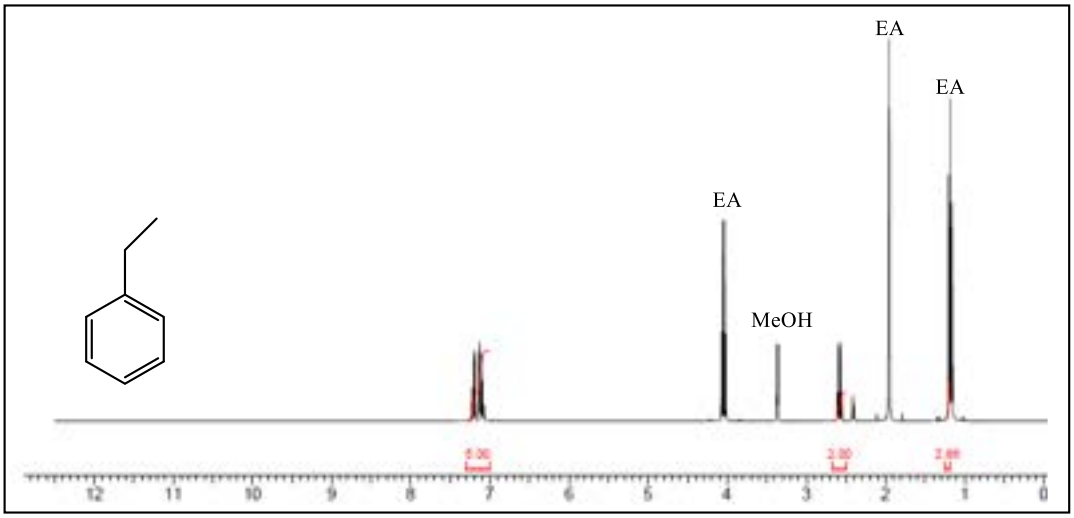

Figure 4.25. ^{1}H NMR spectrum (400 MHz, chloroform-d, room temperature) of fraction 5 from the mixture of Fisher Scientific's xylene and toluene and confirmed as ethylbenzene. (EA is Ethylaceate and MeOH is methanol)

4.2.6 Computational binding energy calculations

To support the experimental chromatographic separation results, which resulted from the host-guest interactions, we further performed *in-silico* studies of the binding energies of three xylene isomers, toluene, and ethylbenzene in the pillar[5]arene host to explore the interactions of analytes with stationary phase ligand. The binding energies of toluene, ethylbenzene, and the three xylene isomers in the cavity of the pillar[5]arene molecule were calculated using the Density Functional Tight Binding (DFTB) method implemented in DFTB+ version 1.3.[35] 500 initial starting geometries were generated using the Kick3 stochastic structure generator to determine the likely binding motifs for each

molecule@pillar combination and optimized using the 3ob-3-1 parameter set including -D3 dispersion, as shown in Figure 4.27.[36]

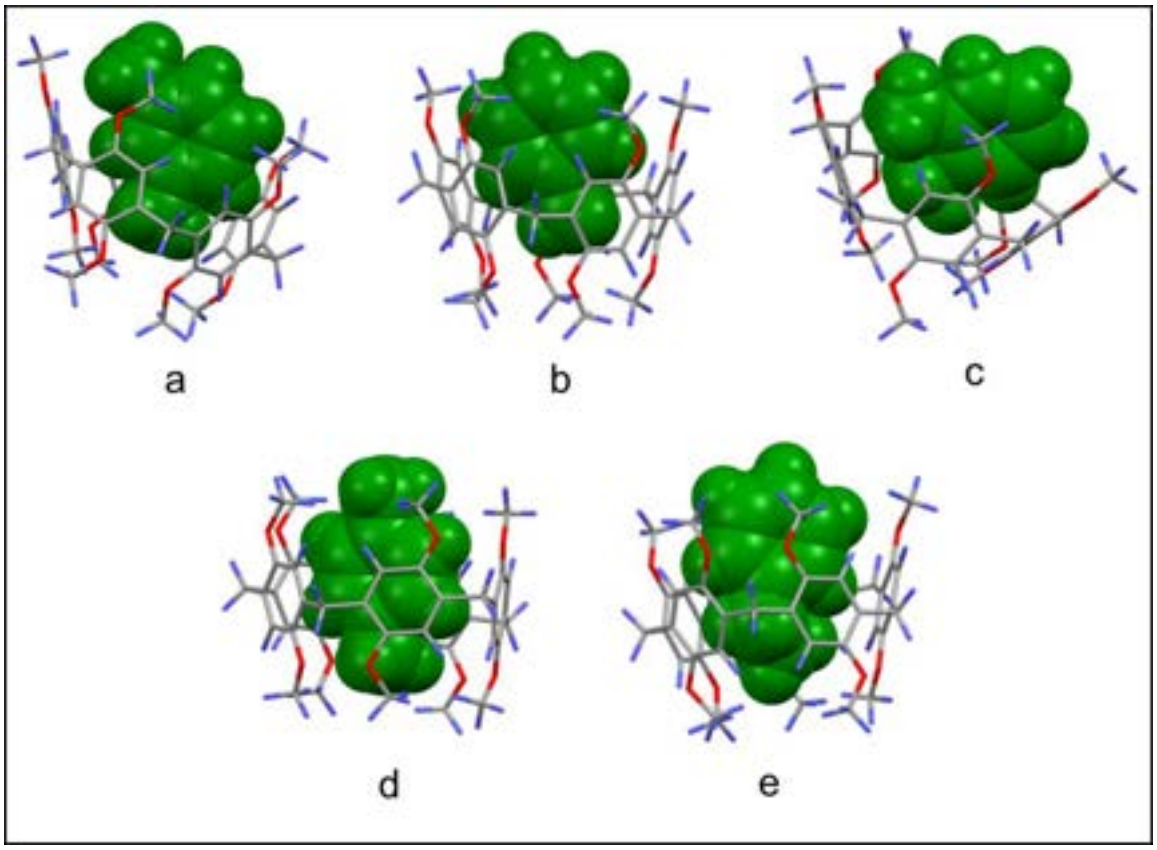

Figure 4.26. Optimized geometries of m-xylene (a), toluene (b), o-xylene (c), p-xylene (d) and ethylbenzene (e) in the dimethoxy pillar[5]arene host.

Table 4.2. Comparison between the chromatographic experimental retention times and the binding energies of toluene, ethylbenzene, and xylene isomers embedded in pillar[5]arene.

Guest	**Experimental retention time (min:sec)**	**Binding Energy (kcal/mol)**
m-Xylene	1:59	-22.19
Toluene	3:05	-22.31
o-Xylene	6:25	-23.50
p-Xylene	9:33	-25.97
Ethylbenzene	11:45	-26.74

The results of the binding energy study, shown in Table 4.2, perfectly correlate with the experimental chromatographic separation results. Ethylbenzene with a calculated *in-silico* binding energy (-26.74 kcal/mol) demonstrated the highest retention time towards the chromatographic separation *via* host-guest interactions, while m-xylene (-22.19 kcal/mol) with the lowest binding energy, eluted most rapidly from the chromatographic flash column.

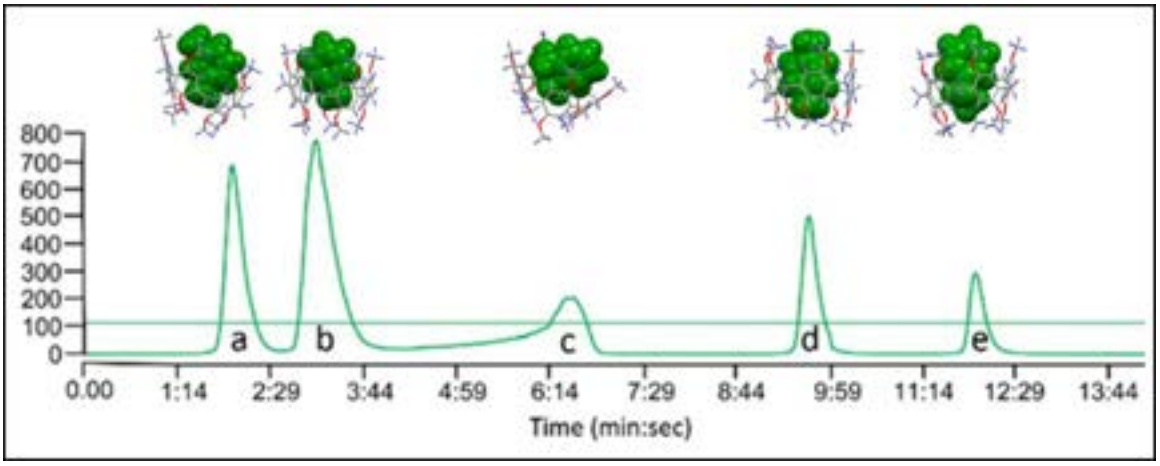

Figure 4.27. Experimental chromatographic separation v/s optimized geometries of the host-guest interactions. Optimized geometries of m-xylene (a), toluene (b), o-xylene (c), p-xylene (d), and ethylbenzene (e) in the dimethoxy pillar[5]arene host.

When observing the optimized geometries of the host-guest interactions and experimental chromatographic results, as shown in Figure 4.28, it is deceptive that the *ortho*-xylene isomer (C) significantly distorts the pillar[5]arene cavity from a tube-like morphology into a boat-like conformer (Figure 24C). As it binds the guest, this conformational transformation of the host molecule results in a kinetic distributional change that slows down the uptake and release of the o-xylene guest and subsequently leads to a broader peak shape in the chromatogram.

T. Ogoshi *et al.,* have studied extensive research on the shape selectivity of Pillar[n]arenes and their derivatives varying in different cavity cavities. For example, they have reported the molecular separation of xylene isomers on adsorptive crystals of perthylated pillar[5]arenes (PEP[5]A) and perethylated pillar[6]arenes (PEP[6]A) to understand the effect of cavity size on host-guest selectivity of xylene isomers with pillararene cavity. The perethylated pillar[6]arene demonstrated excellent adsorption towards the *p*-xylene from a mixture of xylene isomers *via* host-guest complexation in both the solution and solid states. The selective adsorption is due to the conformational adaptability of flexible perethylated pillar[6]arene cavity upon the guest molecules, such as xylene isomers, adsorb during the host-guest complexation. The flexibility of the cavity was studied *via* computational conformational energy, crystallography, and solid-state NMR studies. Moreover, the cumulative selective adsorptive separation and guest-induced structural adaptability are similar to the flexible MOFs.[37]

In *m*-xylene⊂perthylated pillar[6]arene complex, two oppositive aromatic rings are perpendicular to their neighboring aromatic rings. Due to these structural deformations, the pillar[6]arene cavity cannot accommodate the *m*-xylene in the cavity. p-xylene⊂perthylated pillar[6]arene host-guest complex was stabilized via offset π–π stacking interactions

between *p*-xylene and the two aromatic rings of the cavity, as shown in Figure 4.29. Interestingly, the *ortho*-substituted methyl groups of *o*-xylene were fit in the center of the disordered cavity.[37]

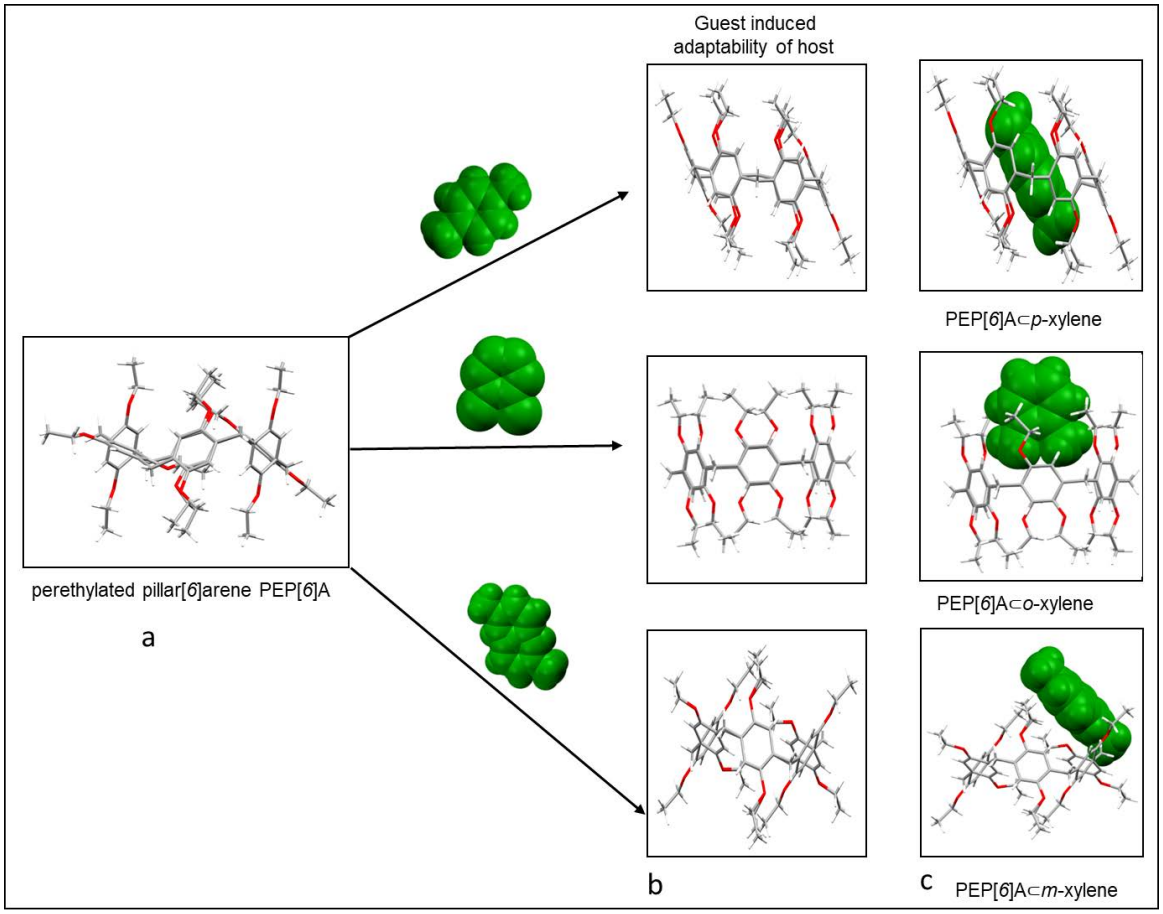

Figure 4.28 Crystal structure of perethylated pillar[6]arene (a), conformational adaptability of the cavity during host-guest complexation (b), and host-guest complexes of xylene isomers with perethylated pillar[6]arene cavity (c).

Subsequently, they further extend to study the effect of perethylated pillar[5]arene cavity size on the conformational disordering during host-guest complexation of xylene isomers with the perethylated pillar[5]arene. The perethylated pillar[5]arene conformed bowl-shaped cavity with *p*-xylene*. P-xylene is accommodated partially with aromatic pillars of the cavity*. Subsequently, one of the methyl groups of *m*-xylene was directed toward the center of the cavity. In contrast, the other methyl group was led away from the cavity. Surprisingly, there was no host-guest complexation of *o*-xylene with the perehtylated pillar[5]arene cavity, as shown in Figure 4.30.[37]

Though the separation of xylene isomers is carried out *via* porous materials such as zeolites, COFs, MOFs, and adaptive crystals of pillar[5]arene, the silica-bound co-pillar[4+1]arene is very easy to synthesize compared to the other pillar[n]arene derivatives, has good stability compared to MOFs, COFs. Moreover, the new stationary phase cavitand

can transform the confirmational changes, as observed with *o*-xylene changing the pillar-shaped cavity to boat-like confirmation.

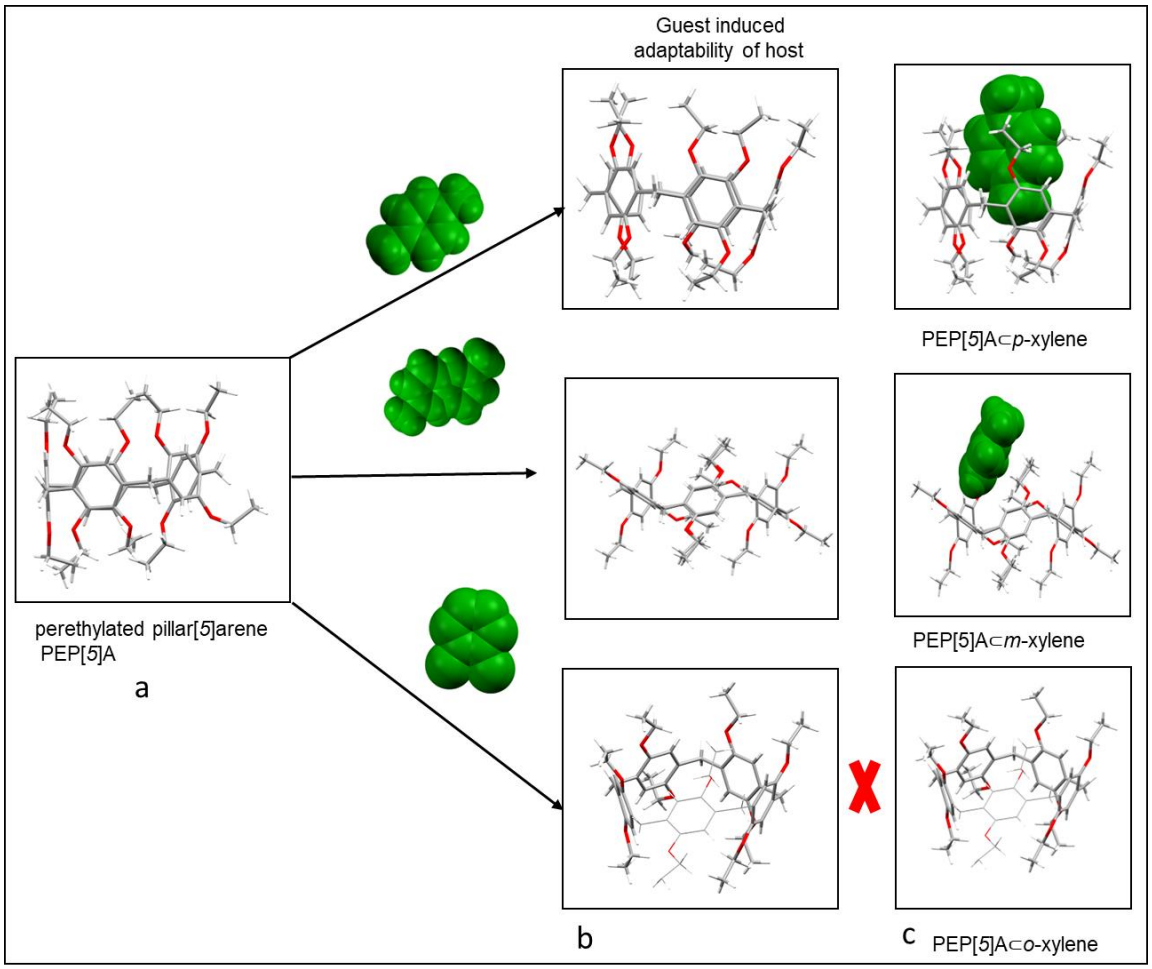

Figure 4.29 Crystal structure of perethylated pillar[5]arene (a), conformational adaptability of the cavity during host-guest complexation (b), and host-guest complexes of xylene isomers with perethylated pillar[5]arene cavity (c).

In conclusion, the silica-bound co-pillar[4+1]arene flash column chromatographic stationary phase **6** has been prepared for the first time *via* direct attachment of co-pillar[4+1]arene **3** to activated chromatographic silica. Moreover, the newly synthesized silica-bound co-pillar[4+1]arene **6** was characterized successfully using analytical techniques such as thermogravimetric analysis to study the mass loading of co-pillar[4+1]arene **3** on the surface of silica. And, the stability of silica-bound co-pillar[4+1]arene **6** was studied *via* mass spectrometric analysis of mobile phase eluents at different column volumes.

Finally, silica-bound co-pillar[4+1]arene stationary phase **6** was successfully utilized for the chromatographic separation of individual xylene isomers with optimized mobile phase conditions. Additionally, a comparative chromatographic experimental study was performed to validate the chromatographic behavior of xylene isomers and their

impurities on the normal phase Interchim® flash silica column (12 g), and on the silica-bound co-pillar[4+1]arene flash column **6** under the same chromatographic mobile phase conditions. Besides, i*n-silico* studies indicate differential bindings for the different xylene isomers to the pillar[5]arene. Thus, the co-pillar[4+1]arene **3** will enhance the ability of the separation and refining of aromatic hydrocarbons. It also plays an essential industrial application where the bulk volume of aromatic hydrocarbons is mainly utilized as starting materials in the chemical industry.

4.3 References

1. Y. Yang, P. Bai and X. Guo, *Ind Eng Chem Res*, 2017, **56**, 14725-14753.
2. T. Udaya Bhaskara Rao and T. Pradeep, *Angew. Chem. Int.*, 2010, **49**, 3925-3929.
3. H. Mohameed, B. A. Jdayil and K. Takrouri, *Chem. Eng. Process.: Process Intensif.*, 2007, **46**, 25-36.
4. M. Sharma, P. Sharma and J. N. Kim, *RSC Adv.*, 2013, **3**, 10103-10126.
5. M. Lusi and L. J. Barbour, *Angew. Chem.*, 2012, **124**, 3994-3997.
6. *US Pat.,* US8293963B2, 2012.
7. J. Li, R. J. Kuppler and H. Zhou, *Chem. Soc. Rev.*, 2009, **38**, 1477-1504.
8. J. Navarro-Sanchez, A. I. Argente-Garcia, Y. Moliner-Martinez, D. Roca-Sanjuan, D. Antypov, P. Campins-Falco, M. J. Rosseinsky and C. Marti-Gastaldo, *J. Am. Chem. Soc.*, 2017, **139**, 4294-4297; J. Li, J. Sculley and H. Zhou, *Chem. Rev.*, 2012, **112**, 869-932.
9. R. Lin, S. Xiang, H. Xing, W. Zhou and B. Chen, *Coord. Chem. Rev.*, 2019, **378**, 87-103.
10. M. L. Jue, D. Koh, B. A. McCool and R. P. Lively, *Chem. Mater.*, 2017, **29**, 9863-9876.
11. M. F. Hasan, E. L. First and C. A. Floudas, *Chem. Eng. Sci.*, 2017, **159**, 3-17.
12. Z. Wu, Y. Yang, B. Tu, P. A. Webley and D. Zhao, *Adsorption*, 2009, **15**, 123-132; M. Rana, R. B. Reddy, B. B. Rath and U. K. Gautam, *Angew. Chem.*, 2014, **126**, 13741-13745.
13. A. Kiselev, A. Aratskova, T. Gvozdovitch and Y. I. Yashin, *J. Chromatogr. A*, 1980, **195**, 205-210.
14. C. Lu, S. Liu, J. Xu, Y. Ding and G. Ouyang, *Anal. Chim. Acta*., 2016, **902**, 205-211.
15. Y. Yang, P. Bai and X. Guo, *Ind. Eng. Chem. Res.*, 2017, **56**, 14725-14753; J. M. Holcroft, K. J. Hartlieb, P. Z. Moghadam, J. G. Bell, G. Barin, D. P. Ferris, E. D. Bloch, M. M. Algaradah, M. S. Nassar and Y. Y. Botros, *J. Am. Chem. Soc.*, 2015, **137**, 5706-5719; X. Li, J. Wang, N. Bai, X. Zhang, X. Han, I. Da Silva, C. G. Morris, S. Xu, D. M. Wilary and Y. Sun, *Nat. Commun.*, 2020, **11**, 1-10; J. A. Gee, K. Zhang, S. Bhattacharyya, J. Bentley, M. Rungta, J. S. Abichandani, D. S. Sholl and S. Nair, *J.*

Phys. Chem. C, 2016, **120**, 12075-12082; X. Wu, W. Wei, J. Jiang, J. Caro and A. Huang, *Angew. Chem. Int. Ed.*, 2018, **57**, 15354-15358; X. Cui, Z. Niu, C. Shan, L. Yang, J. Hu, Q. Wang, P. C. Lan, Y. Li, L. Wojtas and S. Ma, *Nat. commun.*, 2020, **11**, 1-8; A. Torres‐Knoop, R. Krishna and D. Dubbeldam, *Angew. Chem.*, 2014, **126**, 7908-7912.

16. N. Sun, S. Wang, R. Zou, W. Cui, A. Zhang, T. Zhang, Q. Li, Z. Zhuang, Y. Zhang and J. Xu, *Chem. Sci. J.*, 2019, **10**, 8850-8854; M. Lusi and L. J. Barbour, *Angew. Chem.*, 2012, **124**, 3994-3997; M. du Plessis, V. I. Nikolayenko and L. J. Barbour, *J. Am. Chem. Soc.*, 2020, **142**, 4529-4533.
17. J. Huang, X. Han, S. Yang, Y. Cao, C. Yuan, Y. Liu, J. Wang and Y. Cui, *J. Am. Chem. Soc.*, 2019, **141**, 8996-9003.
18. S. H. Kim, J. H. Park, E. M. Go, W. Kim and S. K. Kwak, *J. Ind. Eng. Chem.*, 2020, **85**, 276-281.
19. G. Zhang, B. Hua, A. Dey, M. Ghosh, B. A. Moosa and N. M. Khashab, *Acc. Chem. Res.*, 2020, **54**, 155-168.
20. G. Y. Du, J. Shen, T. Sun, H. Y. Sun, C. C. Shi and A. Y. Hao, *Colloids Surf. A: Physicochem. Eng. Asp.*, 2012, **414**, 120-124.
21. S. Peng, Q. He, G. I. Vargas-Zúñiga, L. Qin, I. Hwang, S. K. Kim, N. J. Heo, C. Lee, R. Dutta and J. L. Sessler, *Chem. Soc. Rev.*, 2020, **49**, 865-907.
22. S. Lim, H. Kim, N. Selvapalam, K. Kim, S. J. Cho, G. Seo and K. Kim, *Angew. Chem.*, 2008, **120**, 3400-3403.
23. A. Chaix, G. Mouchaham, A. Shkurenko, P. Hoang, B. Moosa, P. M. Bhatt, K. Adil, K. N. Salama, M. Eddaoudi and N. M. Khashab, *J. Am. Chem. Soc.*, 2018, **140**, 14571-14575.
24. K. Jie, Y. Zhou, E. Li and F. Huang, *Acc. Chem. Res.*, 2018, **51**, 2064-2072; J. Wu and Y. Yang, *Angew. Chem. Int. Ed.*, 2021, **60**, 1690-1701.
25. T. Tozawa, J. T. Jones, S. I. Swamy, S. Jiang, D. J. Adams, S. Shakespeare, R. Clowes, D. Bradshaw, T. Hasell and S. Y. Chong, *Nat. Mater.*, 2009, **8**, 973-978; B. Moosa, L. O. Alimi, A. Shkurenko, A. Fakim, P. M. Bhatt, G. Zhang, M. Eddaoudi and N. M. Khashab, *Angew. Chem. Int. Ed.*, 2020, **59**, 21367-21371.
26. H. Takaba and J. D. Way, *Ind. Eng. Chem. Res.*, 2003, **42**,1243 -1252.
27. R. El Osta, A. Carlin-Sinclair, N. Guillou, R. I. Walton, F. Vermoortele, M. Maes, D. de Vos and F. Millange, *Chem. Mater.*, 2012, **24** 2781-2791.
28. M. Śliwka-Kaszyńska and M. Ślebioda, *J. Sep. Sci.*, 2014, **37**, 543-550; K. Hu, J. Liu, C. Tang, C. Wang, A. Yu, F. Wen, W. Zhao, B. Ye, Y. Wu and S. Zhang, *J. Sep. Sci.*, 2012, **35**, 239-247; W. Nowik, M. B. De Bellaistre, A. Tchapla and S. Héron, *J.*

Chromatogr. A., 2011, **1218**, 3636-3647.

29. B. Gao, L. Tan, N. Song, K. Li and Y. Yang, *Chem. Commun.*, 2016, **52**, 5804-5807.
30. L. Tan, Y. Zhu, H. Long, Y. Jin, W. Zhang and Y. Yang, *Chem. Commun.*, 2017, **53**, 6409-6412; Z. V. Singh, L. Tan, M. G. Cowan, Y. Yang, W. Zhang, D. L. Gin and R. D. Noble, *J. Membr. Sci.*, 2017, **539**, 224-228.
31. K. Jie, M. Liu, Y. Zhou, M. A. Little, S. Bonakala, S. Y. Chong, A. Stephenson, L. Chen, F. Huang and A. I. Cooper, *J. Am. Chem. Soc.*, 2017, **139**, 2908-2911.
32. K. Jie, Y. Zhou, E. Li, R. Zhao, M. Liu and F. Huang, *J. Am. Chem. Soc.*, 2018, **140**, 3190-3193.
33. K. Jie, M. Liu, Y. Zhou, M. A. Little, A. Pulido, S. Y. Chong, A. Stephenson, A. R. Hughes, F. Sakakibara and T. Ogoshi, *J. Am. Chem. Soc.*, 2018, **140**, 6921-6930.
34. X. Ren, K. Zhang, D. Gao, Q. Fu, J. Zeng, D. Zhou, L. Wang and Z. Xia, *J. Chromatogr. A.*, 2018, **1564**, 137-144.
35. B. Aradi, B. Hourahine and T. Frauenheim, *J. Phys. Chem. A*, 2007, **111**, 5678-5684.
36. M. A. Addicoat, S. Fukuoka, A. J. Page and S. Irle, *J. Comput. Chem.*, 2013, **34**, 2591-2600; M. Gaus, A. Goez and M. Elstner, *J. Chem. Theory Comput.*, 2012, **9**, 338-354.; S. Grimme, J. Antony, S. Ehrlich and H. Krieg, *J. Chem. Phys.*, 2010, **132**, 154104.
37. K. Jie, M. Liu, Y. Zhou, M. A. Little, A. Pulido, S. Y. Chong, A. Stephenson, A. R. Hughes, F. Sakakibara and T. Ogoshi, *J. Am. Chem. Soc.*, 2018, **140**, 6921-6930.

5 Chapter 5: A supramolecular cavitand for selective chromatographic separation of peptides

5.1 Introduction

Proteomics is a branch of science that concerns the analysis of the total present in the cells. These include identifying, characterization, and quantifying protein components in the cells, tissues, and whole organism. The global analysis of proteins in biological systems.[1] Proteomics usually employs mass spectrometry (MS) to probe protein spatial distribution, response to environmental stimuli, and the differences between their morphology in diseased and non-diseased states. Following either a top-down or bottom-up proteolytic digestion, conventional gel and liquid chromatography-based separations are typically utilized before MS characterization to resolve the proteome better.[1]

Routinely, high-resolution liquid chromatography (LC) separation, coupled in-line with mass spectrometry, is the central component of a bottom-up proteomics platform due to its sensitivity and productivity.[2] Over the past decade, there have been significant developments in LC separations, such as improved mass spectrometer acquisition speeds, and mass accuracy.[3,4] These combined developments have contributed to the exponential progress of proteomics over the last decade.[5] However, even with such progress, the most advanced proteomics workflows still cannot map an entire proteome from a single analysis. The rate limiting factor in practical proteomics is currently the chromatographic separation, which still depends on generic alkyl, covalently functionalized, stationary phases e.g. C_{18}.[6] Advances in modern chromatographic techniques aim toward increasing peak capacity via the utilization of ultra-pressure liquid chromatography (UPLC) packing materials,[7] such as core-shell silica,[8] and instrumentational development such as multi-dimensional chromatographic techniques.[9]

Despite the significant progress in modern chromatographic techniques, there is still an increasing need for universal chromatographic stationary phases with the potential to separate a broad range of analytes selectively. Reverse phase liquid chromatography, RPLC, is the most frequently used High-Pressure Liquid Chromatography, HPLC, the mode for separating nonpolar, weakly polar, and polar compounds. However, separating highly polar compounds on RPLC columns is far from easy; this can be overcome by employing hydrophilic interactions on LC (HILIC) columns. In HILIC mode, water is adsorbed on the surface of the polar stationary phase, made up of silica, amino, amide, cationic, and zwitterionic. Subsequently, the surface residual silanol groups become a

water-rich layer on the surface of the stationary silica phase. Subsequently, polar analytes portioned between the mobile phase and water-rich layers to provide hydrogen donor interactions among polar analytes and electrostatic interactions under high organic acetonitrile in the mobile phase eluent. Henceforth, the separation of analytes occurs due to the degree of the analyte's polarity and partition between the two phases. However, the complete mechanism of separation in HILIC mode is still a complex process.

RPLC/HILIC mixed-mode columns are typically used to separate nonpolar, weakly, moderately, and highly polar compounds in a single column.[10] When compared with the conventional single-mode stationary phases, mixed-mode stationary phases hold the merits of high separation selectivity, high separation efficiency, and high loading capacity.[11,12] The development of novel mixed-mode bonded stationary chromatographic phases, including the utilization of macrocyclic functionalized stationary phases, is rapidly emerging as a new generation of separation tools.[4,5] The ability to tune these new stationary phases goes beyond polarity and includes host-guest supramolecular interactions.[13,14] To design new chromatographic stationary phases, we have incorporated supramolecular macrocycles onto the stationary phase, providing enhanced separation via non-covalent host-guest molecular recognition.[15,16]

A recent study reported a new high-yield microwave-assisted synthesis of co-pillar[4+1]arene incorporating two bromo-octyl substituents.[16] The co-pillar[4+1]arene cavitand was covalently functionalized to flash column grade chromatographic silica, to deliver a chromatographic stationary phase which demonstrated selective separation of xylene isomers and their impurities from a commercial xylene mixture *via* flash column chromatography. To illustrate the versatility of this novel class of pillar[n]arene bound chromatographic stationary phases, this work was extended further to explore their potential within the field of proteomics. Furthermore, pillar[5]arene and pyrogallol[4]arene macrocycles (calixarenes) have been widely studied over the last 10 years for their host-guest chemistry. Their phenolic cores have enabled chemists to functionalize them towards bespoke receptors readily. While much of this work has been studied in the solid-state (x-ray) and solution (NMR), there is no *in-silico* data in the literature.

Henceforth, this chapter demonstrates a molecular binding model experiment that evaluate the host-guest interactions of a library of peptides with the dimethoxy-pillar[5]arene macrocycle. These *in-silico* studies were realized experimentally by synthesizing a co-pillar[4+1]arene HPLC grade stationary phase, and subsequent LC-MS/MS separation and characterization of a standard calibration mix peptides (Sciex PepCal mix). These

assessments serve as proof of principle for further exploration of silica-bound co-pillar[4+1]arene stationary phase in separating biomolecules.

5.2 General Methodology

5.2.1 Computational methodology

The probable implementation of a macrocyclic dimethoxy-pillar[5]arene as a possible chromatographic stationary phase was evaluated by computing host-guest interactions for a series of peptides (10-15 amino acid sequence) selected from a standard Sciex PepCal mixture (Sciex UK Limited). The sequence for the five peptides used in this study was IGNEQGVSR, SAEGLDASASLR, AVGANPEQLTR, VGNEIQYVALR, and VFTPLEVDVAK. Abbreviations for each amino acid in the peptide are shown in Figure 5.1

A semi-stochastic approach was employed to determine the five peptides' likely binding motifs and energies.[17] Due to the size and flexibility of the peptides, geometry optimizations were possible, but vibrational frequency calculations were considered unfeasible.[18] Due to the multiple rotatable bonds present in each peptide unit, there is a vast conformational space that can be sample by these peptides. For this reason, an ensemble of low energy (< 50 kcal mol^{-1}) conformers of each peptide were generated using Open Babel.[30] Each end of each peptide conformer was then docked into the pillar[5]arene cavity using a semi-stochastically approach wherein a minimum of 50 peptide⊂dimethoxy-pillar[5]arene complexes were generated for each peptide. Geometries of each peptide⊂dimethoxy-pillar[5]arene complex were optimized in the gas phase. The 20 energy minima complexes were selected for each conformer and reoptimized in implicit solvent (acetonitrile). The peptide⊂dimethoxy-pillar[5]arene binding energies (BE) were then computed for these 20 energetic minima with the formula given in equation (1),

$$BE = \mathrm{Ec} - (\mathrm{Ep} + \mathrm{Em}) \quad (1)$$

where E_c represents the energy of the peptide⊂dimethoxy-pillar[5]arene complex for each conformer, E_p and E_m represent the energies of the isolated peptide and the macrocyclic dimethoxy-pillar[5]arene, respectively. All gas-phase geometry optimizations were computed using Density Functional Tight Binding (DFTB) with the mio-1-1 parameter set, including the universal force field (UFF) dispersion correction as implemented in ADF version r79006 2019-10-03.[19-21] Solvation effects were accounted for using the implicit Generalized Born solvation model with Solvent Accessible Surface Area (GBSA), computed using 2030 surface grid points at the same level of theory as in the gas phase. Optimized coordinates for all gas and solvent phase systems can freely be downloaded.[32]

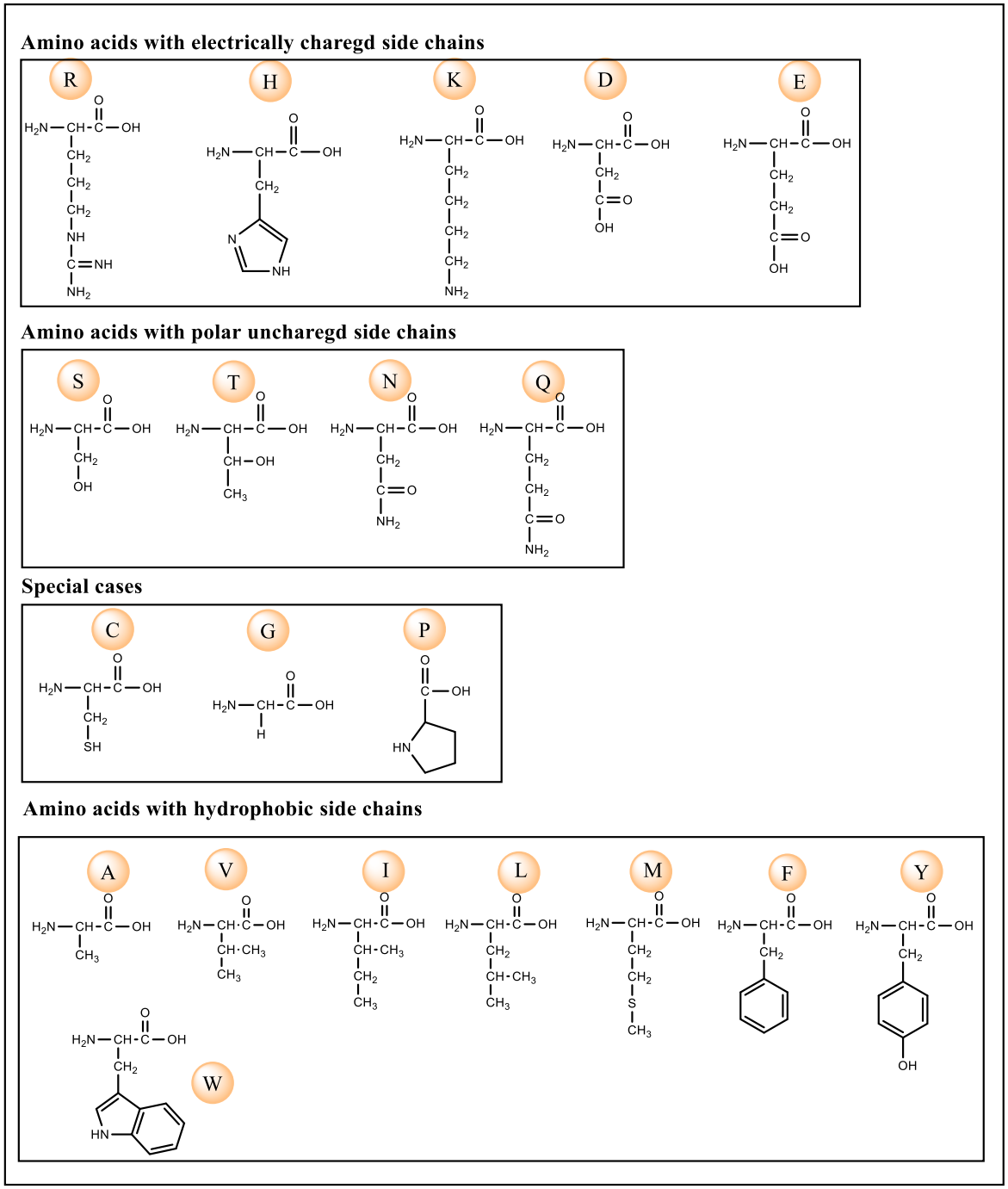

Figure 5.1 Abbreviations of amino acids.

5.2.2 Experimental section

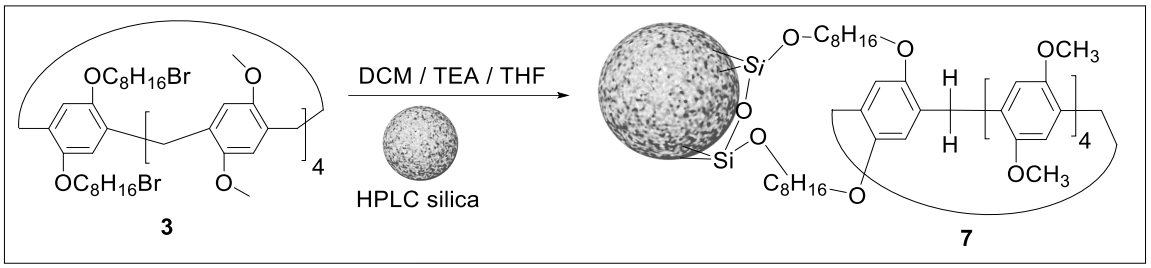

*Figure 5.2. Synthesis of silica bound co-pillar[4+1]arene LC-MS stationary phase **7.***

To validate the computational studies, the co-pillar[4+1]arene **3** was synthesized according to our previously reported microwave-assisted protocol, as shown in Figure 5.2.[16] Subsequently, co-pillar[4+1]arene **3** was attached covalently to HPLC grade chromatographic silica particles (5 µm particle size, YMC Europe) with a mass loading of the co-pillar[4+1]arene **3** at 19 % w/w for the HPLC stationary phase as shown in Figure 5.9 as determined by thermogravimetric analysis (TGA). The morphological characterization of the functionalized silica was assessed *via* Scanning Electron Microscopy (SEM). The silica functionalized co-pillar[4+1]arene stationary phase **7** material was packed *via* a wet slurry packing method in a capillary column (1/32" fitting, 150 x 0.3 mm) using the YMC-Europe in-house column packing protocol. To condition the co-pillar[4+1]arene stationary phase **7** and assess the stability of covalent attachment to the surface of silica, the column was eluted with over 100 column volumes using water: acetonitrile 1:1, 0.1% formic acid. After that time, the macrocycle remained fully attached, with no change in resolution or efficiency. This is in line with traditional RP-C_{18} silica, and we routinely store these columns with 0.1% formic acid in water: acetonitrile (30:70).

Chromatographic conditions were as follows: Solvent A - water + 0.1% formic acid; Solvent B - acetonitrile + 0.1% TFA) at a flow rate of 7.5 µL/min, runtime 13 min. Gradient elution: Solvent B- 3% ramped to 8% in 5.5 minutes; to 80% in 7 min and isocratic to 11 min and re-equilibrated at 13 min (97:3, H_2O:ACN).

5.3 Results and Discussion

5.3.1. Computational results

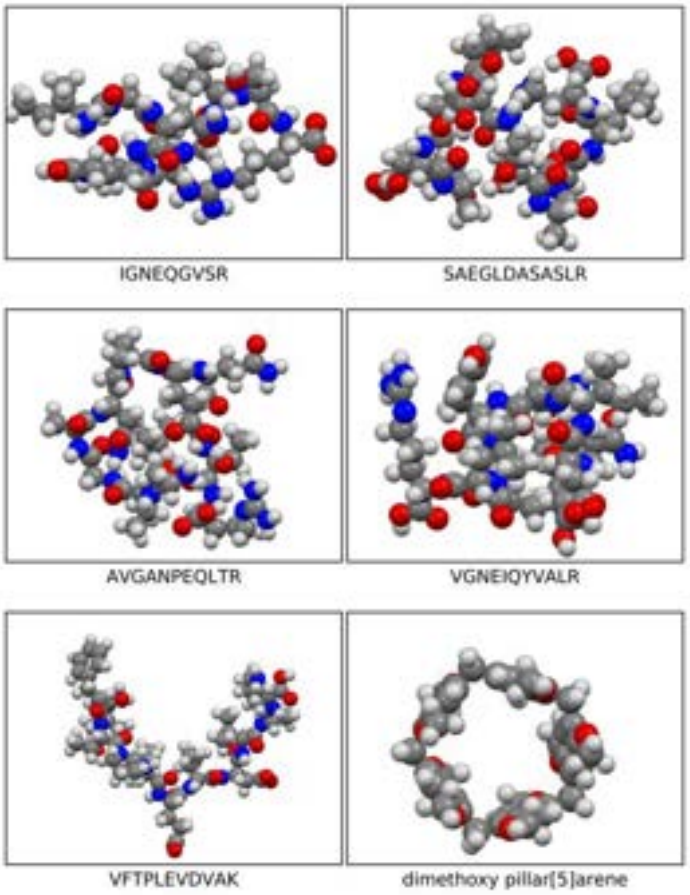

Figure 5.3. Space filled optimized structures of IGNEQGVSR, SAEGLDASASLR, AVGANPEQLTR, VGNEIQYVALR, VFTPLEVDVAK, and dimethoxy pillar[5]arene. Red: oxygen, blue: nitrogen, dark grey: carbon and light grey: hydrogen.

The morphologies of the geometry-optimized dimethoxy-pillar[5]arene cavity and the five peptides are illustrated in Figure 5.3. The strengths of the host-guest interactions were posited to depend on the intramolecular interactions within the peptides, which lead to their corresponding morphologies. However, this study did not try to provide answers to the thermodynamic question corresponding to the balance between the various intramolecular forces that dictate the structures of the peptides, nor to the kinetic question of the different folding routes in each peptide. Nonetheless, it has been shown from previous studies that folding in peptides is determined by the amino acid sequence and is governed by intramolecular hydrogen bonding interactions as well as other long-range forces, including van der Waals interactions.[22,23]

The three conformers of peptide VFTPLEVDVAK interact effectively with the cavity, with either the glutamic acid or valine units occupying the cavity, as shown in Figure 5.4.

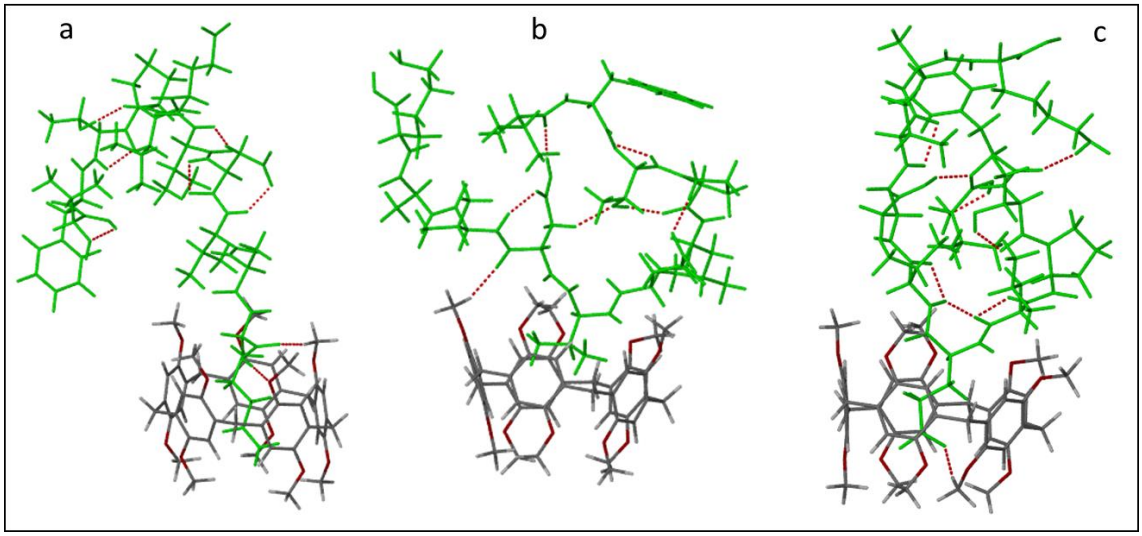

Figure 5.4 Hydrogen bonding interactions between the pillar[5]arene and VFTPLEVDVAK conformers blue (a), green (b), and orange (c). all the peptide conformers are represented in green colour for better visibility.

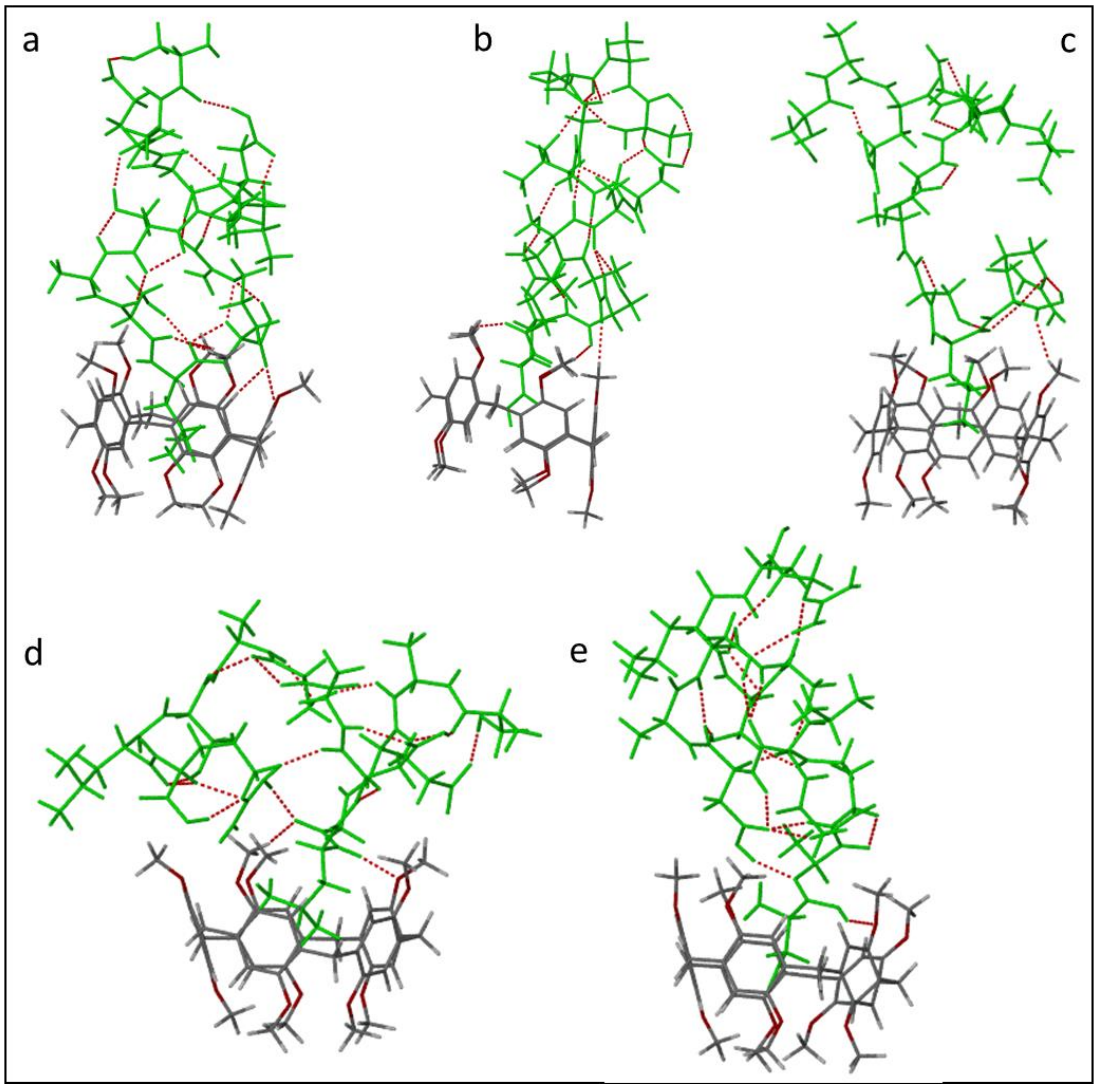

Figure 5.5 Hydrogen bonding interactions of Hydrogen bonding interactions between the pillar[5]arene and SAEGLDASASLR conformers blue (a), green (b), orange (c), red (d), and yellow (e). all the peptide conformers are represented in green colour for better visibility.

The conformers of peptides SAEGLDASASLR, AVGANPEQLTR, and VGNEIQYVALR were all predicted to have relatively weaker interactions with the cavity, as shown in Figures 5.5, 5.6, and 5.7. In peptide SAEGLDASASLR, the binding energies span approximately 25 kcal mol^{-1}. The strongest interactions with the cavity are *via* either the leucine adjacent to the terminal arginine (Figure 5.5a) or in the case of conformers binding using the terminal serine, a strong interaction is also observed with the lip of the cavity, without the peptide penetrating the cavity (Figure 5.5d).

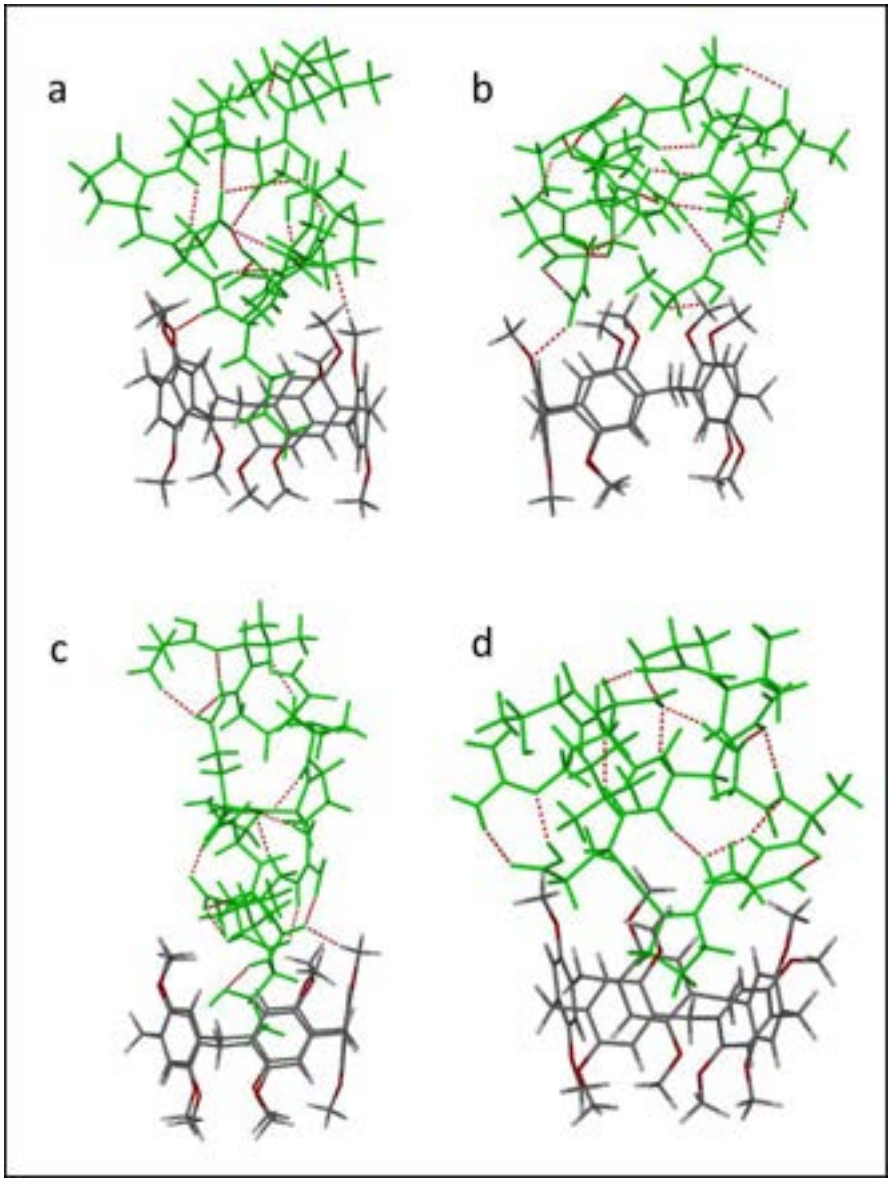

Figure 5.6 Hydrogen bonding interactions of Hydrogen bonding interactions between the pillar[5]arene and AVGANPEQLTR conformers blue (a), green (b), orange (c), and red (d). all the peptide conformers are represented in green colour for better visibility.

In peptide AVGANPEQLTR, the strongest binding interactions were observed with either the central proline (5.6 d) or the threonine residues (5.6 c). The interaction *via* the alanine was found to be less stable.

Peptide VGNEIQYVALR predominantly interacts with the cavity via its terminal valine and the adjacent glycine residues (5.7 a). However, strong interactions were also found with the glutamic acid (5.7 b).

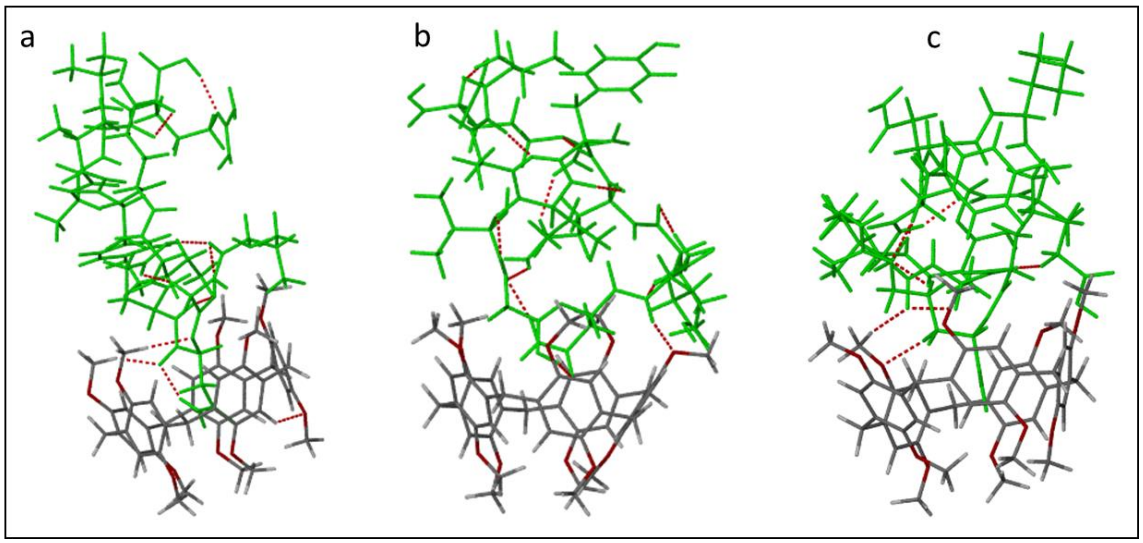

Figure 5.7 Hydrogen bonding interactions of Hydrogen bonding interactions between the pillar[5]arene and VGNEIQYVALR conformers blue (a), green (b), orange (c), and red (d). all the peptide conformers are represented in green colour for better visibility.

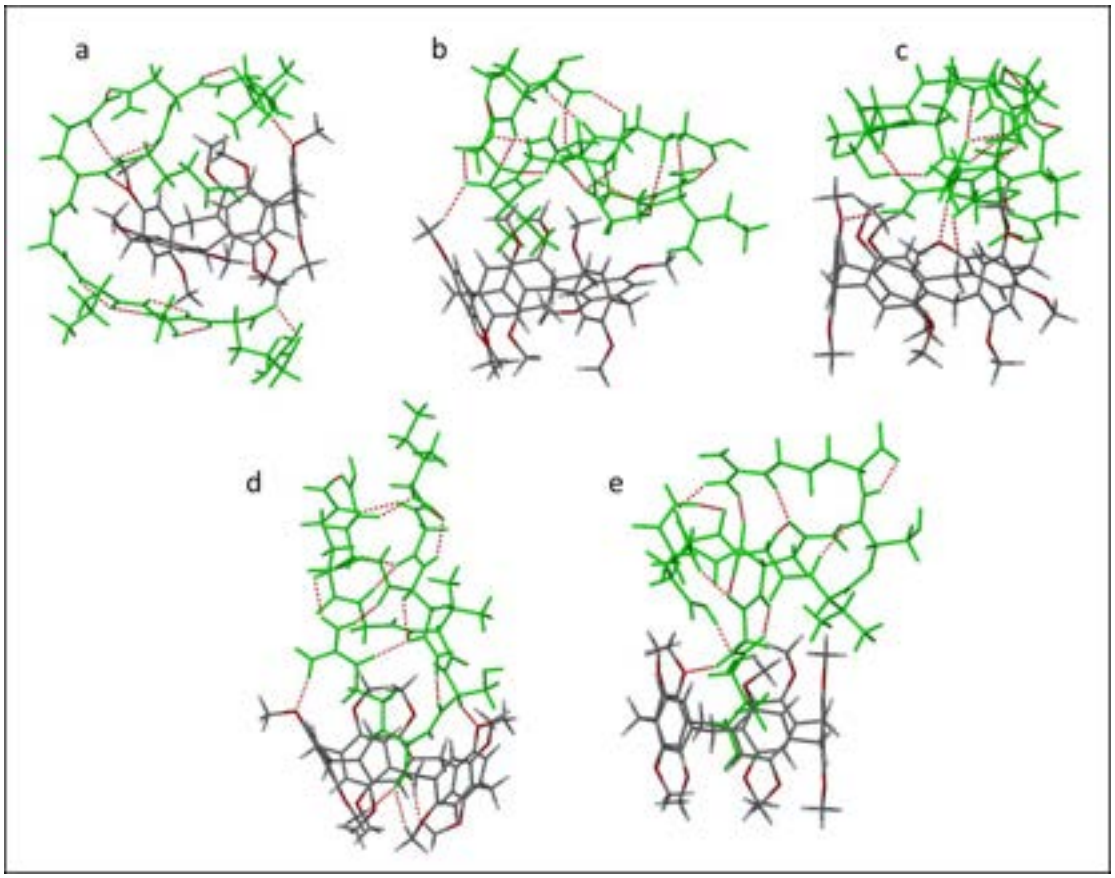

Figure 5.8 Hydrogen bonding interactions of Hydrogen bonding interactions between the pillar[5]arene and IGNEQGVSR conformers blue (a), green (b), orange (c), red (d), and yellow (e). all the peptide conformers are represented in green colour for better visibility.

IGNEQGVSR, strong binding energies were found when the glutamic acid penetrates the cavity and permits the remainder of the peptide to interact with the outside of the cavity, as shown in Figure 5.8 a. However, most conformers (Figure 5.8 b, c, d and e) of this peptide interact weakly with the cavity.

The interactions of amino acids from each peptide conformers with the cavity of pillar[5]arene were detailed in Table 5.1. Each colour indicates a different peptide conformer, as shown in Figure 5.14, structures of each conformer.[32]

Table 5.1. Specific amino acid interaction units between cavity and peptides for solvated phase.

Peptides	Description of specific interacting units of each conformer with the cavity				
	Blue	Orange	Green	Red	Yellow
IGNEQGVSR	The glutamic acid (E) unit is fully inserted into the cavity.	The Isoleucine unit (I) at the head of the peptide is fully inserted into the cavity.	The carboxylate unit found on the terminal arginine unit (R) is partially inserted into the cavity.	The Isoleucine unit (I) at the head of the peptide is fully inserted into the cavity.	The Isoleucine unit (I) at the head of the peptide is fully inserted into the cavity.
SAEGLDASASLR	The terminal leucine (L) unit closest to the arginine (R) unit is fully inserted into the cavity.	The terminal leucine (L) unit closest to the arginine (R) unit is halfway inserted into the cavity.	None of the amino acid units are inserted into the cavity. All interactions are at the exterior of the cavity.	The terminal leucine (L) unit closest to the arginine (R) unit is fully inserted into the cavity.	The Serine unit (S) at the head of the peptide is halfway inserted into the cavity.
AVGANPEQLTR	Proline (P) unit halfway inserted in the cavity.	The threonine unit (T), closest to the arginine (R) is halfway inserted into the cavity.	The Alanine-valine (A-V) peptide bond is partially inserted into the cavity.	Proline (P) unit halfway inserted into the cavity.	-
VGNEIQYVALR	The valine and the glycine head (V-G) are inserted in the cavity.	Here the Valine (V) at the head is halfway inserted in the cavity.	Glutamic acid (E) fully inserted in the cavity.	-	-
VFTPLEVDVAK	The glutamic acid (E) unit is fully inserted into the cavity.	The glutamic acid (E) unit is fully inserted into the cavity.	The Valine (V) unit, which is closest to the glutamic acid (L-E-V), is fully inserted into the cavity.	-	-

5.3.2. Characterization of the silica-bound co-pillar[4+1]arene HPLC column 7

Co-pillar[4+1]arene **3** was attached to HPLC grade chromatographic silica particles (5 µm particle size, YMC Europe) with a mass loading of the co-pillar[4+1]arene **3** at 19 % w/w for the HPLC stationary phase as determined *via* thermogravimetric analysis (TGA) as shown in the Figure 5.9.

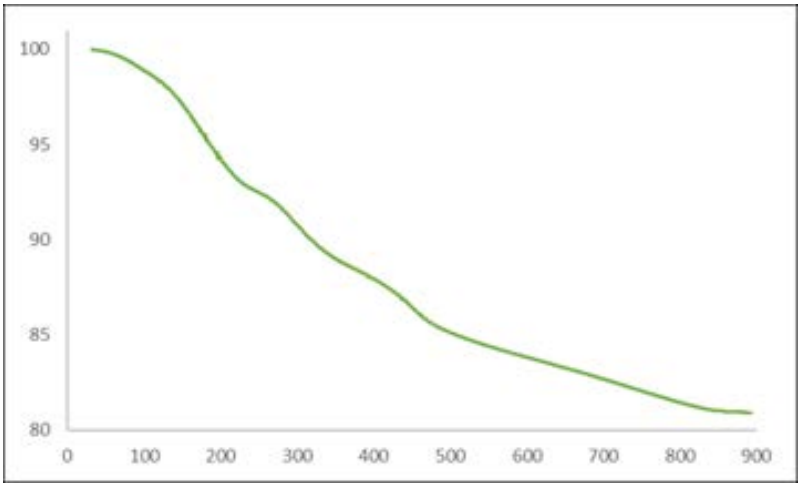

*Figure 5.9 Thermogravimetric analysis of co-pillar[4+1]arene bound-silica HPLC stationary phase **7**.*

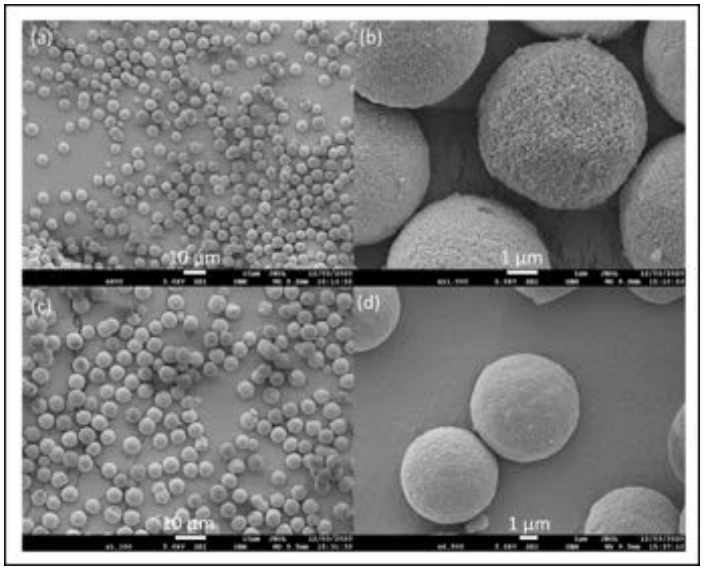

Figure 5.10. SEM images showing silica 5 µm particles at (a) 10 and (b) 1 µm magnification and silica functionalized with co-pillar[4+1]arene stationary phase particles at (c) 10 and (d) 1 µm magnification.

The morphological features of the modified silica with co-pillar[4+1]arene **7** were evaluated *via* Scanning Electron Microscopy (SEM) and the morphology of this modified silica was observed to be comparable to the starting spherical silica particles, as shown in Figure 5.10. The functionalized silica-bound co-

pillar[4+1]arene HPLC column stationary phase **7** was observed to have smooth surfaces deprived of any structural flaws and preserved well-defined cavities; necessary for the free flow of mobile phase and analytes.[24] Consequently, exhibit low back pressure was observed during the conditioning of the column and chromatographic evaluation process.

5.3.3. Column packing and conditioning of the silica-bound co-pillar[4+1]arene HPLC column 7

Co-pillar[4+1]arene bonded silica gel HPLC stationary phase **7** was packed into an HPLC column using a wet slurry packing method by YMC Europe with column dimensions of 12 nm S-5 µm 150 x 0.3 mm with 1/32" fitting. After packing the column, it was conditioned with water: acetonitrile (1:1) and supplied back for chromatographic studies. Before chromatographic experiments, the newly packed HPLC columns were flushed with water: acetonitrile (1:1) to condition the column. The eluents were collected at different column volumes to identify the elution of co-pillar[5]arene **3** from the silica-bound co-pillar[5]arene HPLC stationary phase **7**. As shown in Figures 5.11-5.13, there was no observation of co-pillar[4+1]arene eluting from the column even after 100 column volumes.

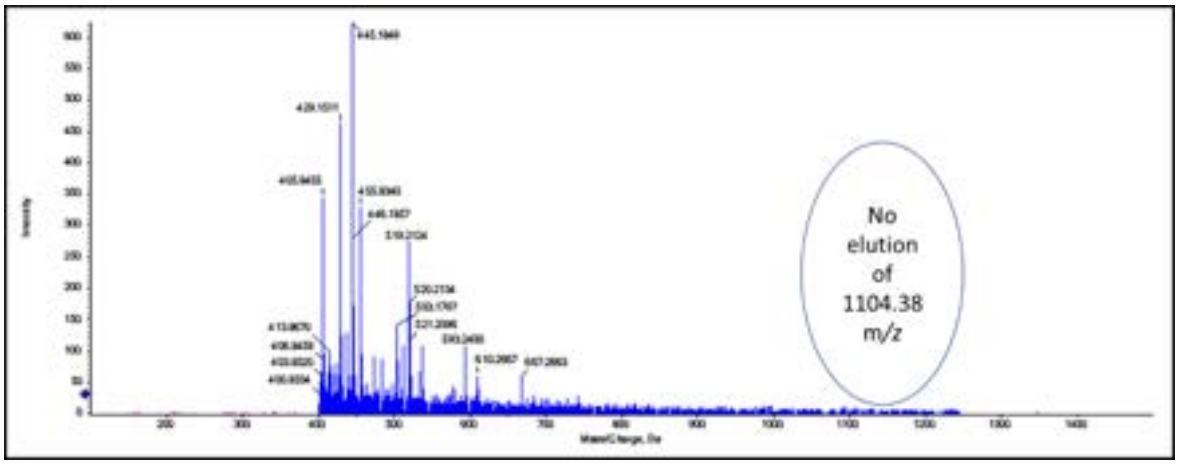

Figure 5.11. LC-MS spectrum of eluent from silica-bound co-pillar[4+1]arene stationary phase at 1 column volume.

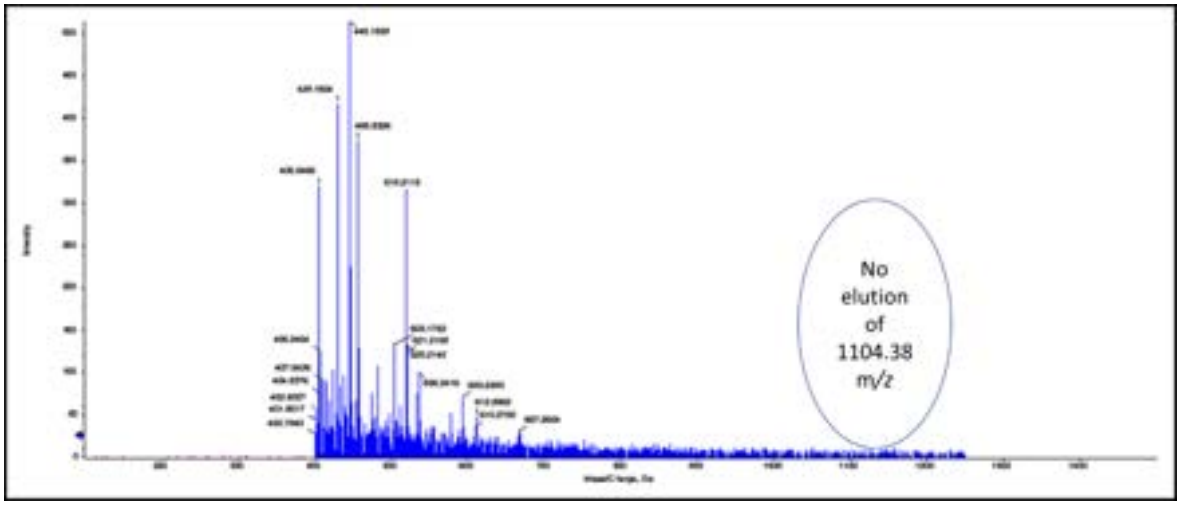

Figure 5.12. LC-MS spectrum of eluent from silica-bound co-pillar[4+1]arene stationary phase at 50 column volumes.

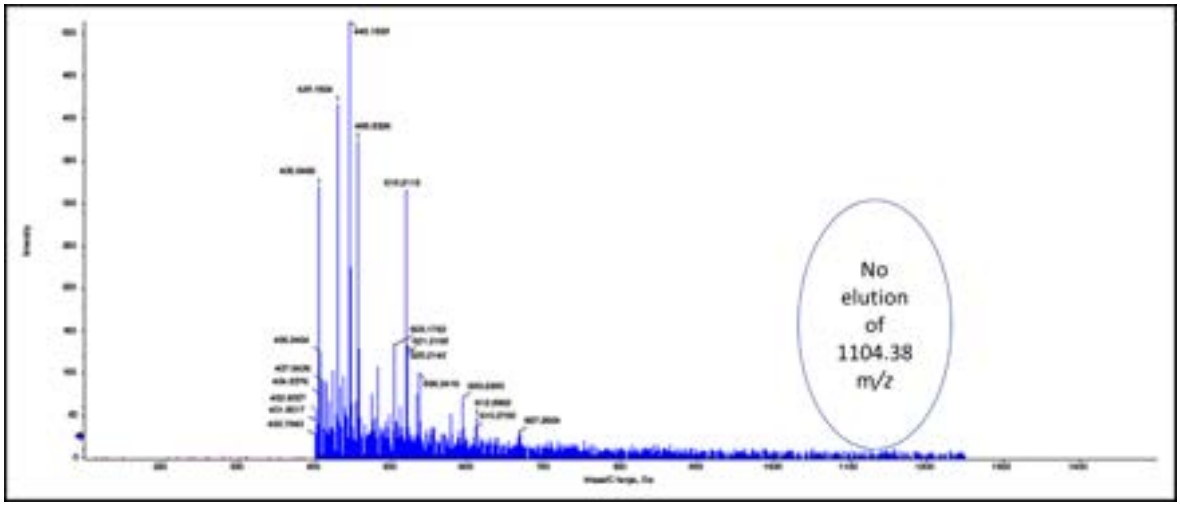

Figure 5.13. LC-MS spectrum of eluent from silica-bound co-pillar[4+1]arene stationary phase at 100 column volumes.

5.3.4. Separation of standard five PepCal peptides

After the conditioning of the new HPLC column **7** with mobile phase consisting of water: acetonitrile 1:1, 0.1% formic acid, the retention performance of the silica functionalized co-pillar[4+1]arene stationary phase **7** was screened under reverse phase mode conditions, utilizing a mobile phase gradient to assess the chromatographic behaviour of the five peptide mixture. Identical capillary columns (1/32" fitting, 150 x 0.3 mm) consisting C_{18} (YMC Triart RP-C_{18}, 5 µm particle size silica column) and normal phase silica (5 µm particle size silica, packed by YMC-Europe) were used a compare a the co-pillar[4+1]arene modified stationary phase **7**. In addition, normal phase silica was used to assess whether the co-pillar[4+1]arene functionalized silica was degrading or leaching from the HPLC column **7**.

5.3.4.1 Separation of five peptides on RP-C_{18} column

The peptide mixture (2 µL, 20 fmol/µL) was loaded onto the RP-C_{18} column. The peptides were eluted on the RP-C_{18} column using gradient mobile phase conditions (water: acetonitrile, 3-35% over 5 min and ramped to 80%, as shown in Table 5.2 and detected *via* mass spectrometry (Sciex Triple-TOFTM 5600). All five IGNEQGVSR, SAEGLDASASLR, AVGANPEQLTR, VGNEIQYVALR, and VFTPLEVDVAK peptides were eluted between 3.4 and 7.0 min on the commercial reverse phase C_{18} column, as shown in Figure 10. However, SAEGLDASASLR and AVGANPEQLTR peptides were eluted with very similar retention times on the RP- C_{18} column while IGNEQGVSR resolved completely. Similarly, VGNEIQYVALR and VFTPLEVDVAK peptides were co-eluted on the same column. Even though the peptides eluted together, the chromatographic peaks were resolved in a symmetrical shape, as seen in Figure 5.14.

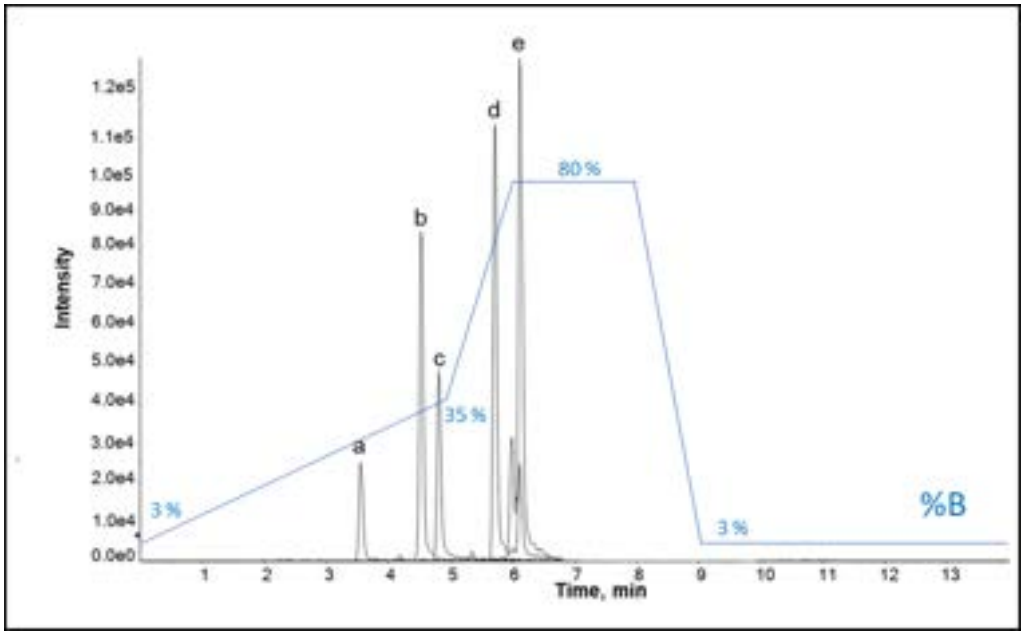

Figure 5.14. LC-MS/MS chromatographic separation of mixed peptide standard IGNEQGVSR (a), SAEGLDASASLR (b), AVGANPEQLTR (c), VGNEIQYVALR (d) and VFTPLEVDVAK (e) on RP-C_{18} silica.

Table 5.2. Mobile phase gradient conditions on RP-C_{18} column.

Time (min)	%A	%B
0.0	97	03
5.0	65	35
6.0	20	80
8.0	20	80
9.0	97	03

15	97	03

5.2.4.1 Separation of five peptides on silica-bound co-pillar[4+1]arene HPLC column 7 using RP-C_{18} gradient conditions

In order to optimize the gradient mobile phase conditions to separate IGNEQGVSR, SAEGLDASASLR, AVGANPEQLTR, VGNEIQYVALR, and VFTPLEVDVAK peptides on silica-bound co-pillar[4+1]arene HPLC column **7,** RP-C_{18} mobile phase gradients were used to understand the chromatographic behaviour of IGNEQGVSR, SAEGLDASASLR, AVGANPEQLTR, VGNEIQYVALR, and VFTPLEVDVAK peptides on HPLC column **7** using the mobile phase gradients, as shown in the Table 5.3. The peptides IGNEQGVSR, SAEGLDASASLR, AVGANPEQLTR, VGNEIQYVALR, and VFTPLEVDVAK were retained on the silica-bound co-pillar[4+1]arene HPLC column **7** column. However, the resolution of five peptides was poor with RP-C_{18} mobile phase gradient conditions, as shown in Figure 5.15. Furthermore, there are significant host-guest peptides interactions with co-pillar[4+1]arene cavity. Henceforth, the mobile phase gradients that are suitable to the silica-bound co-pillar[4+1]arene HPLC column **7** column had to be developed to retain and resolve the peptides on the newly developed HPLC column **7**.

Table 5.3. Mobile phase RP-C_{18} gradient conditions on silica-bound co-pillar[4+1]arene HPLC column 7 column.

Time (min)	%A	%B
0.0	97	03
5.0	70	30
6.0	20	80
8.0	20	80
9.0	97	03
15	97	03

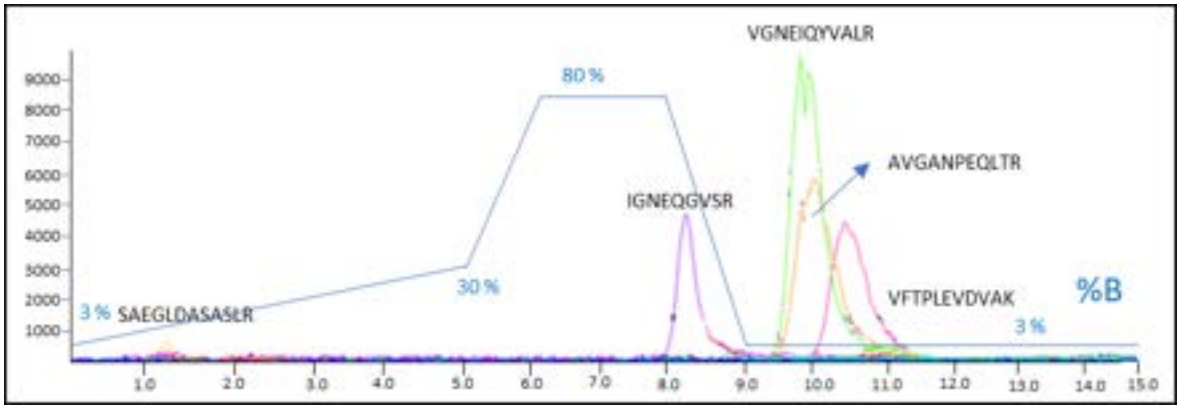

*Figure 5.15. Separation of five peptides on silica-bound co-pillar[4+1]arene HPLC column **7** using RP-C18 gradient conditions.*

5.3.4.3 Separation of five peptides on silica-bound co-pillar[4+1]arene HPLC column 7

The same peptide mixture (2 µL, 20 fmol/µL) was loaded onto the silica-bound co-pillar[4+1]arene HPLC column **7** with a flow rate of 7.5 µL min^{-1} at a column temperature of 30°C. The peptides were eluted on column **7** using optimized gradient mobile phase conditions (water: acetonitrile, 3-15% over 5 min and ramped to 80% in 6 min, as shown in Table 5.4). All five IGNEQGVSR, SAEGLDASASLR, AVGANPEQLTR, VGNEIQYVALR, and VFTPLEVDVAK peptides were eluted between 3.5 and 9.0 min on the silica-bound co-pillar[4+1]arene HPLC column **7** column, as shown in Figure 5.16. The order of elution was changed. The significant observation on silica-bound co-pillar[4+1]arene HPLC column **7** is that SAEGLDASASLR peptide eluted after AVGANPEQLTR peptide eluted. Furthermore, VFTPLEVDVAK was retained more than peptide VGNEIQYVALR and were resolved well on the silica-bound co-pillar[4+1]arene HPLC column **7**, as shown in Figure 5.16. This substantial change in the retention order confirmed the significant supramolecular host-guest interactions between the peptides and co-pillar[4+1]arene cavity.

*Table 5.4. Mobile phase gradient conditions on silica-bound co-pillar[4+1]arene HPLC column **7** column.*

Time (min)	%A	%B
0.0	97	03
5.0	85	15
6.0	20	80
8.0	20	80
9.0	97	03
15	97	03

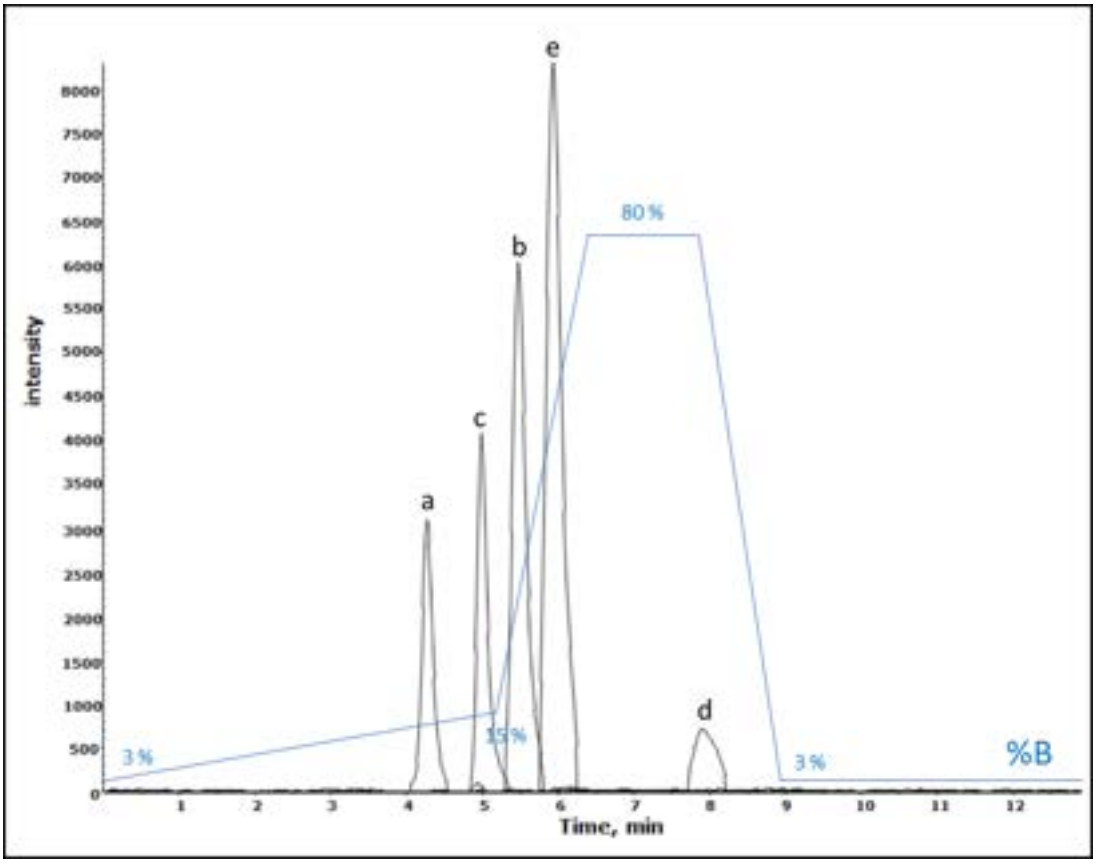

*Figure 5.16. LC-MS/MS chromatographic separation of mixed peptide standard IGNEQGVSR (a), SAEGLDASASLR (b), AVGANPEQLTR (c), VGNEIQYVALR (d) and VFTPLEVDVAK (e) on silica-bound co-pillar[4+1]arene HPLC column **7**.*

5.3.4.4 Separation of 5 peptides on a normal phase silica column

Normal phase silica was used to evaluate whether the co-pillar[4+1]arene **3** was degrading or leaching from the co-pillar[4+1]arene functionalized silica **7** column. The mobile phase gradients conditions of co-pillar[4+1]arene functionalized silica **7** column, as shown in Table 5.4. Standard IGNEQGVSR and SAEGLDASASLR peptides were eluted together, while AVGANPEQLTR and VGNEIQYVALR peptides were eluted together, as shown in Figure 5.17. In addition, the VFTPLEVDVAK peptide was resolved at base level detection. These preliminary chromatographic studies confirm that the retention of peptides on co-pillar[4+1] arene-bound silica HPLC column **7** is different from that of peptides on RP-C_{18} and the normal phase silica column.

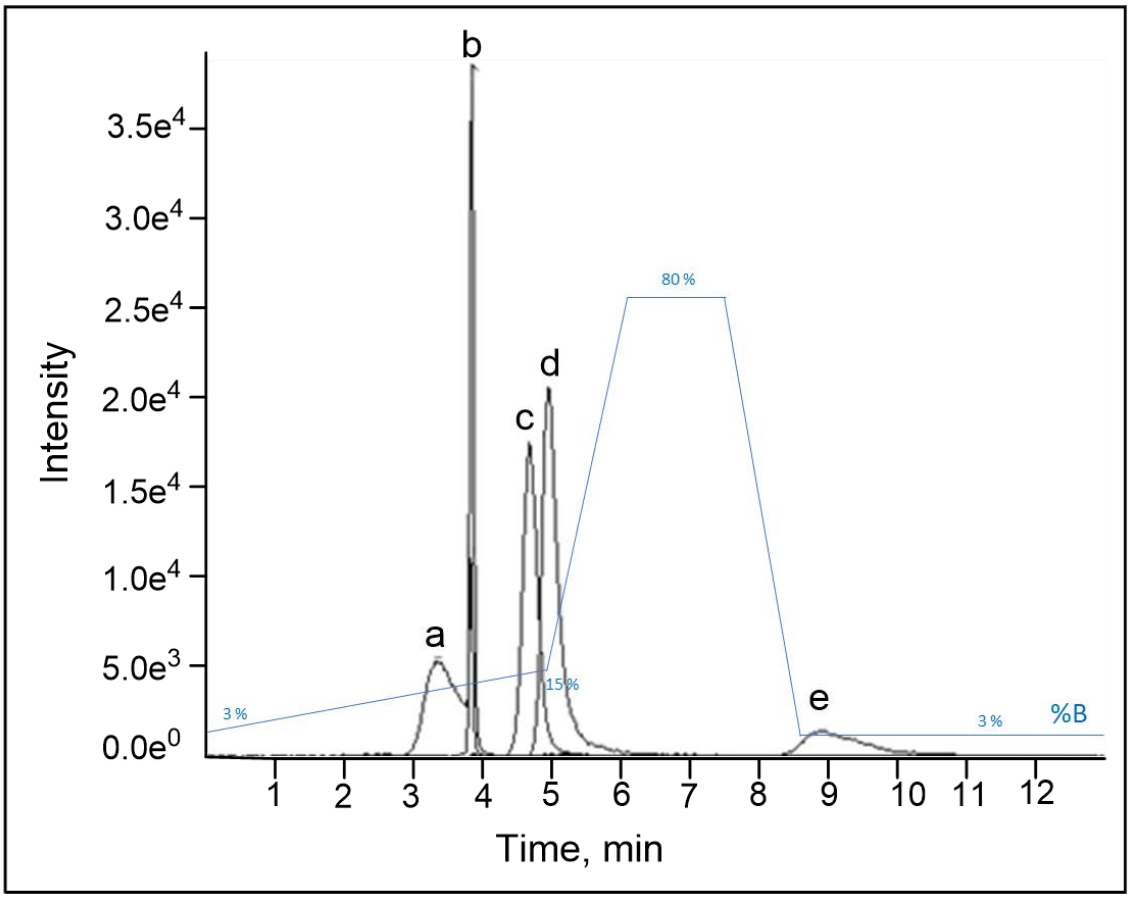

Figure 5.17. LC-MS/MS chromatographic separation of mixed peptide standard IGNEQGVSR (a), SAEGLDASASLR (b), AVGANPEQLTR (c), VGNEIQYVALR (d) and VFTPLEVDVAK (e) on normal phase silica.

5.3.4.5 Separation of five peptides on RP-C_{18}, silica-bound co-pillar[4+1]arene HPLC column 7, and normal phase under ideal gradient conditions.

All five peptides were eluted between 9.28 and 10.31 minutes on the commercial reverse phase C_{18} column, as shown in Figure 5.18. Nevertheless, only the IGNEQGVSR peptide was resolved, while the SAEGLDASASLR, AVGANPEQLTR, VGNEIQYVALR, and VFTPLEVDVAK peptides eluted all together and could not be resolved. Furthermore, on the commercially packed normal phase column, the VFTPLEVDVAK peptide was fully resolved, but the IGNEQGVSR, AVGANPEQLTR, SAEGLDASASLR, and VGNEIQYVALR peptides co-eluted between 2.6-4.1 min.

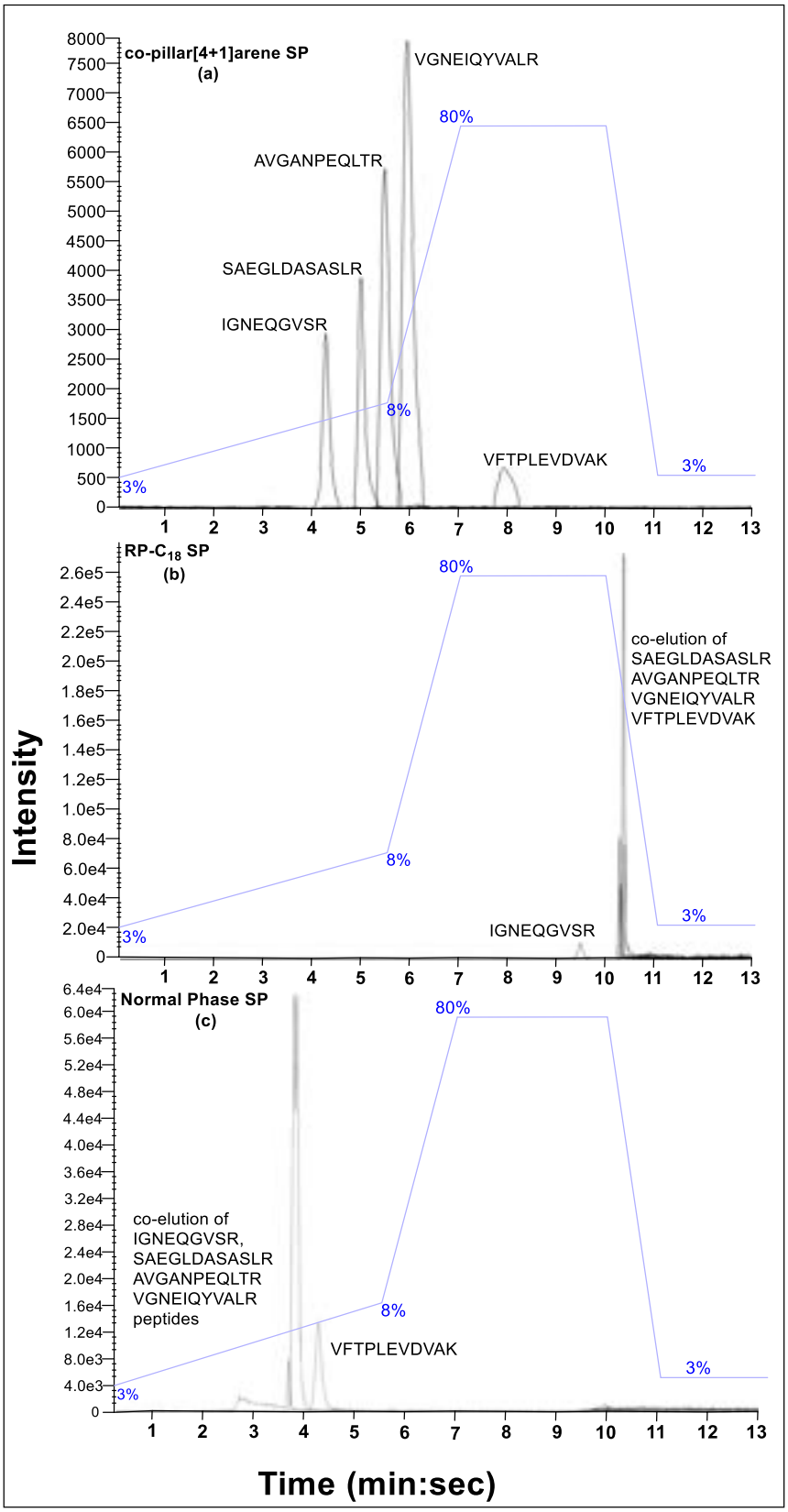

Figure 5.18. Comparison of LC-MS/MS chromatographic separation of mixed peptide standard (IGNEQGVSR, SAEGLDASASLR, AVGANPEQLTR, VGNEIQYVALR and VFTPLEVDVAK on (a) silica bound co-pillar[4+1]arene; (b) reverse phase-C18 silica; and (c) normal phase silica stationary phases.

However, when the same peptide standard mixture was eluted on the new supramolecular column 7, all the peptides were individually resolved between 4.0-8.5 min, such as IGNEQGVSR 4.0-4.4 min, SAEGLDASASLR 4.8-5.4 min, AVGANPEQLTR 5.4-5.8 min, VGNEIQYVALR 5.7-6.3 min and VFTPLEVDVAK 7.7-8.2 min). Chromatographic conditions were as follows: Solvent A – water + 0.1% formic acid; Solvent B – acetonitrile + 0.1% TFA at a flow rate of 7.5 µL min^{-1}, runtime 13 min. Gradient elution: Solvent B – 3% ramped to 8% in 5.5 minutes; to 80% in 7 min and isocratic to 11 min and re-equilibrated at 13 min.

5.3.5. Synthetic relevance

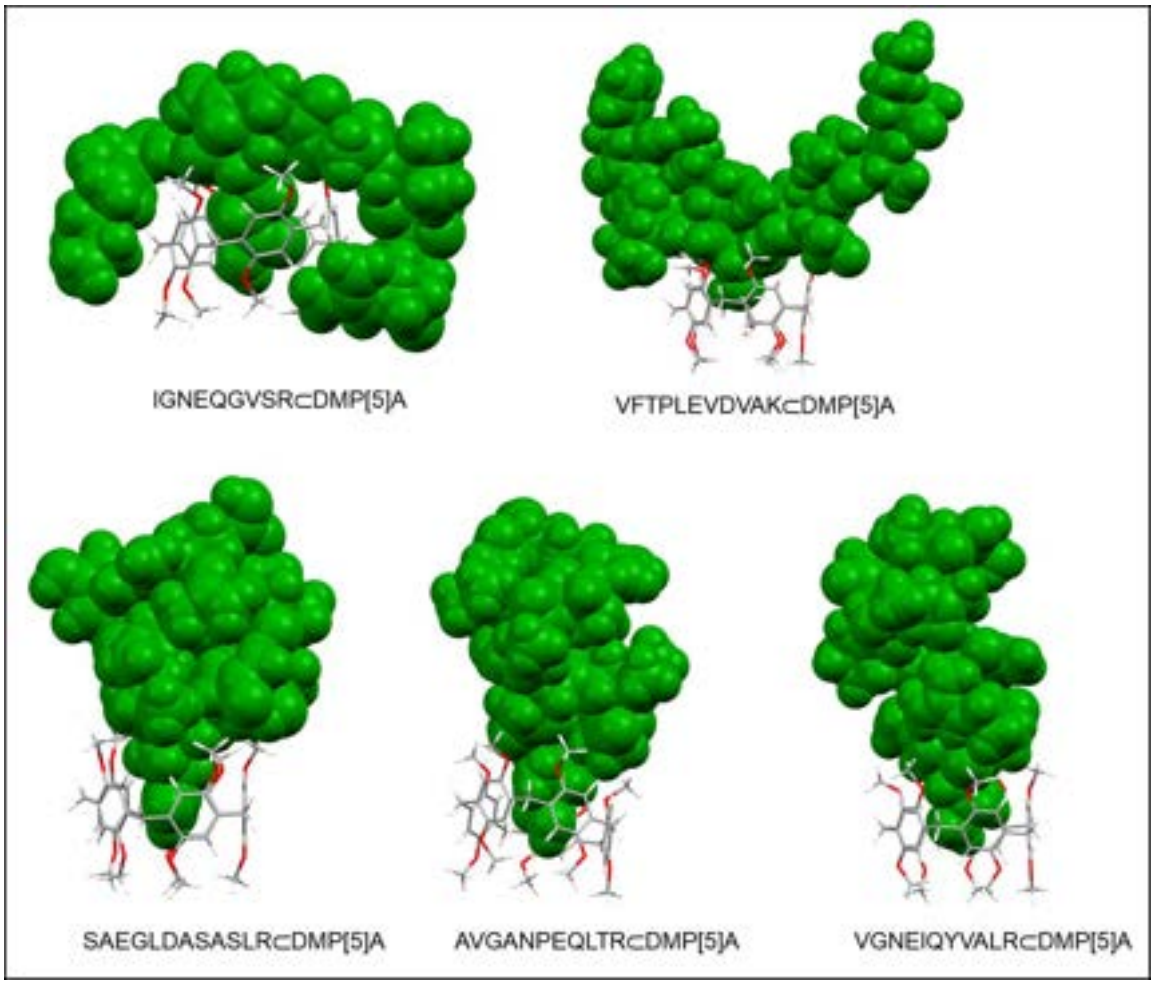

Figure 5.19 Illustration of peptide⊂dimethoxy-pillar[5]arene (DMP[5]A) interactions of IGNEQGVSR, SAEGLDASASLR, AVGANPEQLTR, VGNEIQYVALR, and VFTPLEVDVAK, embedded in pillar[4+1]arene. The space-filled molecular models represent the peptides meanwhile, the stick represents pillar[5]arene cavity.

The elution order of the peptides is in line with the *in-silico* computational binding energy predictions. For example, all conformers calculated of VFTPLEVDVAK, bind strongly to the cavity with binding energies between -20 and -50 kcal mol^{-1}, as shown in Figure 5.4. This prediction of consistently strong interaction between the peptide and cavity was supported experimentally as this peptide was observed to possess the highest

retention time of 7.93 minutes, as shown in Figure 5.19. Furthermore, the glutamic acid residue penetrates the cavity fully in the strongest binding modes (blue and orange dots in Figure 5.20). The neighbouring leucine and valine residues form weak hydrogen bonds with the lip of the cavity. In contrast, in the weaker binding modes (green dots in Figure 5.14), the smaller valine residue penetrates the cavity, which is responsible for the weaker interaction. Details of the most essential long-range intermolecular interactions, broken down by interaction type of all the studied peptides.[31]

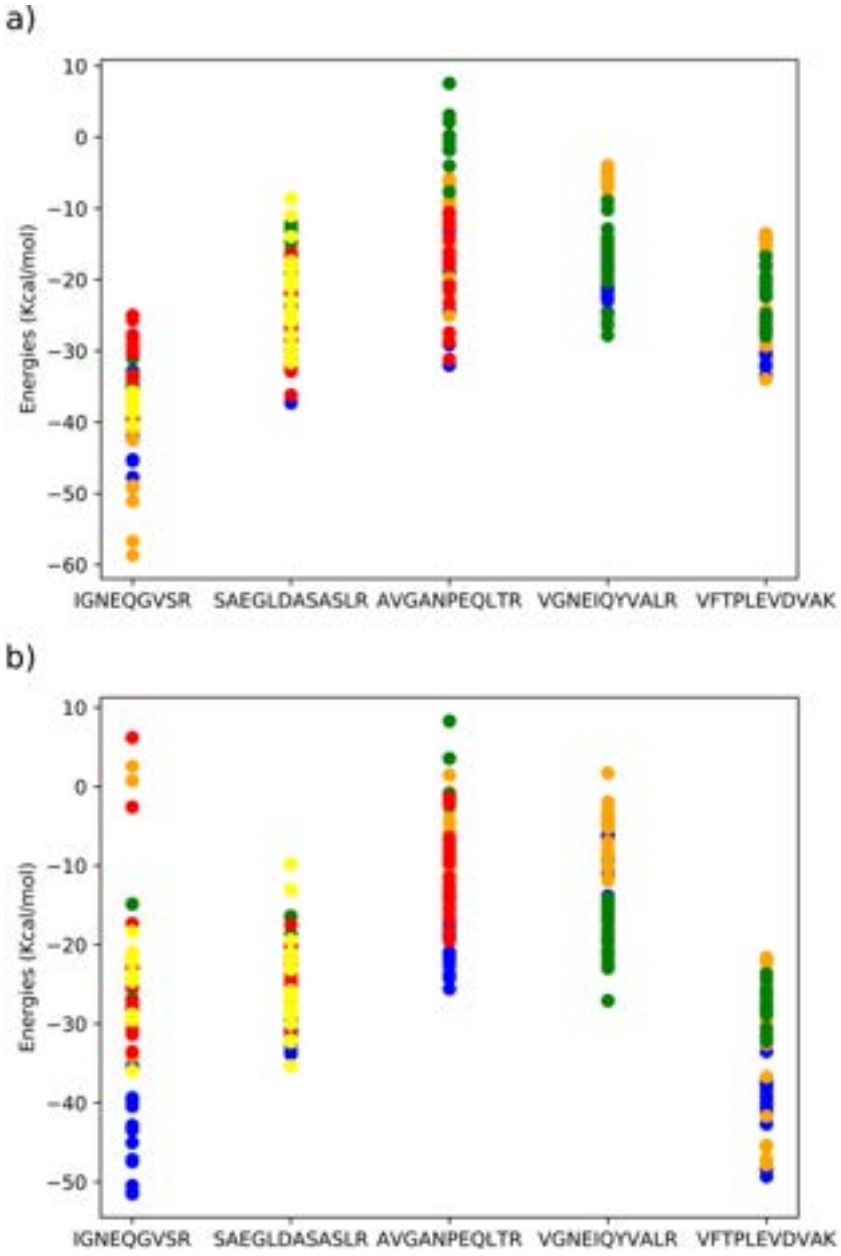

Figure 5.20. DFTB mio-1-1 binding energies of peptides⊂dimethoxypillar[5]arene in a) gas phase, b) implicit acetonitrile solvent. Each colour indicates a different peptide conformer.

The retention times of AVGANPEQLTR and VGNEIQYVALR also correlate well with the range of binding energies for these peptides. Peptide SAEGLDASASLR, is predicted to

bind more strongly to the cavity (-10 to -35 kcal mol^{-1}), the conformer structures insert either the terminal serine (yellow dots in Figure 5.20) or the arginine-adjacent leucine residue (orange, blue and red dots in Figure 5.20). However, several optimizations (green dots in Figure 5.20) resulted in the peptide not penetrating the cavity at all, suggesting that while strong binding is possible between this peptide and cavity, it is less likely to be observed, which aligns with the relatively low retention time of this peptide, as shown in Figure 5.5

The peptide with the lowest retention time, IGNEQGVSR has one binding mode in common with VFTPLEVDVAK, where the glutamic acid residue is inserted into the cavity (blue dots in Figure 5.20), and several hydrogen bonds are formed between the remainder of the peptide and the lip of the cavity.

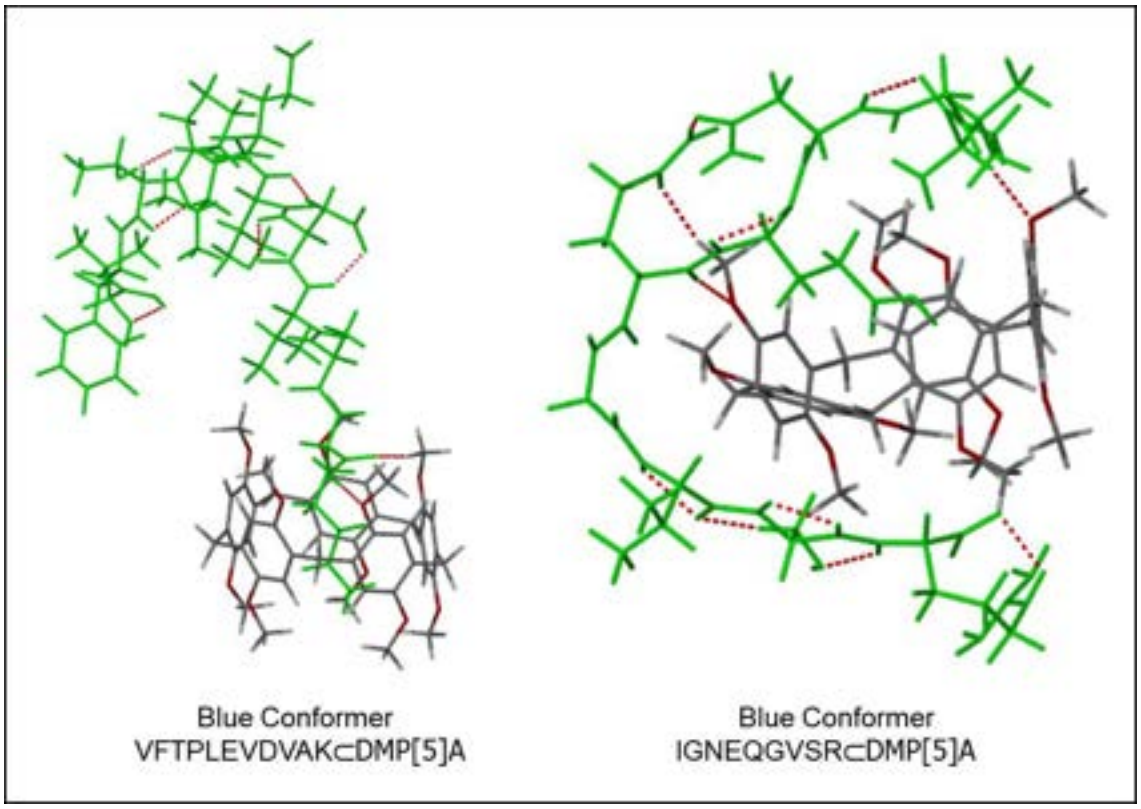

Figure 5.21 Entry of glutamic acid residue from peptide IGNEQGVSR and VFTPLEVDVAK into DMP[5]A cavity.

However, all other calculated conformers of this peptide interact weakly with the cavity using either the terminal arginine (green dots) or isoleucine residues (red, orange and yellow dots in Figure 5.20). Given the specificity of the conformer required to insert the glutamic acid residue and the number of peptide-cavity interactions required to achieve the strong binding energy, this mode of interaction is unlikely to contribute to the experimentally observed weak retention.

5.3.6. Chromatographic resolution and peak symmetry

Under ideal conditions, a chromatographic peak will be symmetrical and follow a Gaussian curve distribution. Though, experimental peaks are more asymmetric in shape, often exhibiting some degree of tailing. Peak tailing can therefore be characterized by the tailing factor (TF).[25] A value of TF = 1.00 corresponds to perfectly symmetrical peaks. An increase in peak tailing thus results in poorer separation. Major peak tailing can be significantly unfavourable for both separation and quantification. The data from Figure 5.18 demonstrates that the new silica bound co-pillar[4+1]arene column **7** meets the experimental prerequisite for routine separation for all peaks as shown in Table 5.8 (TF<2). Even though a resolution Rs>2 is advantageous in chromatographic separation, this is not practical for larger peak areas.

Peptides IGNEQGVSR and VFTPLEVDVAK were significantly resolved on the supramolecular column 7 with a resolution of 6.09. By comparison, the RP-C_{18} column was only capable of a resolution of 5.66, as shown in Figure. 5.18a under the ideal conditions. The peak resolutions of SAEGLDASASLR-AVGANPEQLTR, SAEGLDASASLR-VGNEIQYVAL, and AVGANPEQLTR-VGNEIQYVALR peptides on the supramolecular column **7** were 1.20, 2.24 and 1.26 min respectively, as shown in Table 5.6, compared to 0.29, 0.88 and 1.32 min from the RP-C_{18} column. Hence, the silica-bound co-pillar[4+1]arene column **7** shows better resolution than the RP-C_{18} column across the standard peptide mix. In theory, there is no correlation between % loading and separation resolution between 5% to 18% w/w; however, this will be the subject of further studies. It is worth noting that this stationary phase was observed to be effective in the pure organic solvent while resolving xylene isomers and their impurities on a flash column variant of this silica-bound supramolecular flash column chromatographic stationary phase **6**.[16]

5.3.6.1 Peak Width

*Table 5.5. Chromatographic data and peaks table on silica-bound co-pillar[4+1]arene stationary phase **7**.*

Chromatographic data and peaks table on silica-bound co-pillar[4+1]arene stationary phase 7						
Peptides	Retention time (min)	Peak area	Start time (min)	End time (min)	Width at base (min)	Width at 50% (min)
IGNEQGVSR	4.27	32675	3.83	4.71	0.87	0.23
SAEGLDASASLR	4.99	44967	4.64	6.00	1.36	0.22
AVGANPEQLTR	5.48	87843	5.10	6.55	1.45	0.26
VGNEIQYVALR	5.94	145069	5.46	7.29	1.83	0.28
VFTPLEVDVAK	7.94	23811	7.23	8.67	1.44	0.48

Table 5.6 Chromatographic data and peaks table on RP-C_{18} stationary phase.

Chromatographic data and peaks table on RP-C_{18} stationary phase						
Peptides	Retention time (min)	Peak area	Start time (min)	End time (min)	Width at base (min)	Width at 50% (min)
IGNEQGVSR	9.43	77773	9.28	9.65	0.37	0.12
AVGANPEQLTR	10.29	224733	10.20	10.42	0.22	0.04
SAEGLDASASLR	10.31	139460	10.24	10.43	0.19	0.04
VGNEIQYVALR	10.37	848562	10.29	10.73	0.44	0.04
VFTPLEVDVAK	10.39	199718	10.31	10.47	0.28	0.08

5.3.6.2 Chromatographic separation resolution data

The peak width at 50% (FWHM) and retention times of 5 peptides were substituted in the resolution equation to calculate the resolution of 5 peptides on silica bound co-pillar[4+1]arene stationary phase **7** and RP-C_{18} stationary phase.[26]

$$\text{Resolution R} = 1.18 \times \left[\frac{tr_2 - tr_1}{w0.5_{h1} + w0.5_{h2}}\right]$$

*Table 5.7 Chromatographic separation resolution of peptide standards on co-pillar[4+1]arene stationary phase **7** and RP-C_{18} stationary phase.*

Peptides comparison	Resolution of Chromatogram	
	co-pillar[4+1]arene stationary phase **7**	RP-C_{18} stationary phase
IGNEQGVSR and VFTPLEVDVAK	6.09	5.66
SAEGLDASASLR & AVGANPEQLTR	1.20	0.29
SAEGLDASASLR & VGNEIQYVAL	2.24	0.88
AVGANPEQLTR & VGNEIQYVALR	1.26	1.32

5.3.6.3 Peak asymmetry data

The peak asymmetry [27] of chromatographic peaks on co-pillar[4+1]arene stationary phase and RP-C_{18} stationary phase was calculated according to Sciex recommended formula as the experiment was carried out using Analyst® Software provided by Sciex.

Peak asymmetry (A_s) $= \left[\frac{peak\ end\ time - retention\ time}{retention\ time - peak\ start\ time}\right] = \frac{b}{a}$

*Table 5.8 Chromatographic peak asymmetry on co-pillar[4+1]arene stationary phase **7** and RP-C_{18} stationary phase.*

Peptide	Co-pillar[4+1]arene silica bound stationary phase **7**	RP-C_{18} stationary phase
IGNEQGVSR	1.00	1.46
SAEGLDASASLR	2.88	1.44
AVGANPEQLTR	2.81	2.00
VGNEIQYVALR	2.81	4.50
VFTPLEVDVAK	1.02	1.00

5.3.6.4 Peak tailing data

The peak tailing of chromatographic peaks on co-pillar[4+1]arene stationary phase **7** and RP-C_{18} stationary phase was calculated according to the following formula.

$$\text{Peak tailing} = \frac{(a+b)}{2a}$$

*Table 5.9 Chromatographic peak tailing on co-pillar[4+1]arene stationary phase **7** and RP-C_{18} stationary phase.*

Peptide	Co-pillar[4+1]arene silica bound stationary phase **7**	RP-C_{18} stationary phase
IGNEQGVSR	1.00	1.23
SAEGLDASASLR	1.94	1.22
AVGANPEQLTR	1.92	1.50
VGNEIQYVALR	1.90	2.75
VFTPLEVDVAK	0.99	1.00

We previously tried to conduct a binding study with individual amino acids and the 1,4-dimethoxypillar[5]arene macrocycle. However, we unable to find a solvent system that would work for both the host and guest molecules. It is worth noting that Ogoshi, NL Strutt and many others modified both upper and lower rim with different functional moieties wherein the host and guest species were observed to be soluble in the same solvent.[29]

In conclusion, computational supramolecular host-guest binding energies have been successfully used to design and predict a new class of chromatographic stationary phases towards the efficient and effective separation of peptides that are highly significant in proteomic studies. This work will facilitate sample preparation before mass spectrometric analysis and lead to bespoke chromatographic systems that can be designed in silico to optimize the separation of physiological salts and peptides directly from trypsin digested proteins.

5.4 References

1. a) K. Hixson, D. Lopez-Ferrer, E. Robinson, L. Paša-Tolić, *Encyclopedia of Spectroscopy and Spectrometry* 2017, 766-773; b) N. L. Anderson and N. G. Anderson, *Electrophoresis* 1998, **19**, 1853-1861.
2. Z. Fang, Y. Z. Baghdady, K. A. Schug, S. M. Chowdhury, *J. Proteome Res.* 2019, **18**, 1916-1925.
3. a) Y. Yang, H. Chen, M. A. Beckner, P. Xiang, J. J. Lu, C. Cao, S. Liu, *Anal. Chem.* 2018, **90**, 10676-10680; b) P. Yu, S. Petzoldt, M. Wilhelm, D. P. Zolg, R. Zheng, X. Sun, X. Liu, G. Schneider, A. Huhmer, B. Kuster, *Anal. Chem.* 2017, **89**, 8884-8891; c) Y. Wang, S. V. Olesik, *Anal. Chem.* 2018, **91**, 935-942.
4. a) Q. Hu, R. J. Noll, H. Li, A. Makarov, M. Hardman, R. Graham Cooks, *J. Mass Spectrom.* 2005, **40**, 430-443; b) G. L. Andrews, B. L. Simons, J. B. Young, A. M. Hawkridge, D. C. Muddiman, *Anal. Chem.* 2011, **83**, 5442-5446; c) N. M. Riley, C. Mullen, C. R. Weisbrod, S. Sharma, M. W. Senko, V. Zabrouskov, M. S. Westphall, J. E. Syka, J. J. Coon, *J. Am. Soc. Mass Spectrom.* 2016, **27**, 520-531.
5. M. Kim, A. Pandey, *Proteomics* 2012, **12**, 530-542.
6. K. M. Grinias, J. M. Godinho, E. G. Franklin, J. T. Stobaugh, J. W. Jorgenson, *J. Chromatogr. A* 2016, **1469**, 60-67.
7. a) R. M. Wimalasinghe, Z. S. Breitbach, J. T. Lee, D. W. Armstrong, *Anal. Bioanal. Chem.* 2017, **409**, 2437-2447; b) P. Tsai, T. Sung, C. Chong, S. Huang, S. Chen, *Anal. Methods.* 2018, **10**, 4756-4764; c) A. F. Gargano, L. S. Roca, R. T. Fellers, M. Bocxe, E. Domínguez-Vega, G. W. Somsen, *Anal. Chem.* 2018, **90**, 6601-6609.
8. H. S. Berg, K. E. Seterdal, T. Smetop, R. Rozenvalds, O. K. Brandtzaeg, T. Vehus, E. Lundanes, S. R. Wilson, *J. Chromatogr. A* 2017, **1498**, 111-119.
9. A. L. Capriotti, C. Cavaliere, A. Cavazzini, F. Gasparrini, G. Pierri, S. Piovesana, A. Laganà, *J. Chromatogr. A* 2017, **1498**, 176-182.
10. H. Aral, K. S. Çelik, R. Altındağ and T. Aral, *Talanta*, 2017, **174**, 703-714.
11. K. Hu, Y. Zhang, J. Liu, K. Chen, W. Zhao, W. Zhu, Z. Song, B. Ye and S. Zhang, *J. Sep. Sci.*, 2013, **36**, 445-453.
12. S. Ray, M. Takafuji and H. Ihara, *J. Chromatogr. A*, 2012, **1266**, 43-52.
13. J. Lu, W. Zhang, Y. Zhang, W. Zhao, K. Hu, A. Yu, P. Liu, Y. Wu and S. Zhang, *J. Chromatogr. A,* 2014, **1350**, 61-67.
14. S. Chelvi, J. Zhao, L. Chen, S. Yan, X. Yin, J. Sun, E. Yong, Q. Wei and Y. Gong, *J. Chromatogr. A*, 2014, **1324**, 104-108.
15. a) M. Śliwka-Kaszyńska and M. Ślebioda , *J. Sep. Sci.,* 2014, **37**, 543-550; b) K. Hu , J. Liu , C. Tang, C. Wang, A. Yu, F. Wen, W. Zhao, B. Ye, Y. Wu and S. Zhang, *J.*

Sep. Sci., 2012, **35**, 239-247; d) W. Nowik, M. B. De Bellaistre, A. Tchapla and S. Héron, *J. Chromatogr. A,* 2011, **1218**, 3636-3647.

16. S. Mekapothula, M. A. Addicoat, D. J. Boocock, P. Cragg, J. D. Wallis and G. W. V. Cave, *Chem. Commun.*, 2020, **56**, 1792-1794.
17. M. A. Addicoat and G. F. Metha, *J. Comput. Chem.*, 2009, **30**, 57-64.
18. J. Kleinjung and F. Fraternali, *Curr Opin Struct Biol.,* 2014, **25**, 126-134.
19. S. Grimme, J. Antony, S. Ehrlich and H. Krieg, *J. Chem. Phys.,* 2010, **132**, 154104.
20. C. Schönbeck, H Li, B.-H Han and B. W. Laursen, *J. Phys. Chem* B, 2015, **119**, 6711-6720.
21. M. Elstner, D. Porezag, G. Jungnickel, J. Elsner, M. Haugk, T. Frauenheim, S. Suhai and G. Seifert, *Phys. Rev. B*:*Condens. Matter Mater. Phys.,* 1989, **58**, 7260.
22. S. S. Sung, *Protein Sci.*, 2015, **24**, 1383-1388.
23. K. A. Dill, S. B. Ozkan, M. S. Shell & T. Weikl, Annu. Rev. Biophys., 2008, **37**, 289-316.
24. a) J. DeStefano, T. Langlois and J. Kirkland, *J. Chromatogr. Sci.*, 2008, **46**, 254-260; b) T. Hara, H. Kobayashi, T. Ikegami, K. Nakanishi and N. Tanaka, *Anal. Chem.,* 2006, **78**, 7632-7642; c) J. Kirkland, *Anal. Chem.,* 1992, **64**, 1239-1245; d) R. E. Majors, *Anal. Chem.*, 1972, **44**, 1722-1726.
25. (a) About Resolution, Part 1: SHIMADZU (Shimadzu Corporation), https://www.shimadzu.com/an/hplc/support/lib/lctalk/resol-1.html, accessed May 2020. (b) How Is Peak Asymmetry Caluclated in Analyst® Software Quantitate Mode? https://sciex.com/support/knowledge-base-articles/how-peak-asymmetry-value-caluclated-in-analyst-quant-mode, accessed May 2020. (c) “Peak Tailing in HPLC”, https://www.crawfordscientific.com/technical/chromatography-blog/hplc-chromatography-tips/hplc-troubleshooting/peak-tailing-in-hplc, accessed may 2022.
26. "About Resolution, Part 1 : SHIMADZU (Shimadzu Corporation)", can be found under https://www.shimadzu.com/an/hplc/support/lib/lctalk/resol-1.html, 2022.
27. "How Is Peak Asymmetry Caluclated in Analyst® Software Quantitate Mode?", can be found under https://sciex.com/support/knowledge-base-articles/how-peak-asymmetry-value-caluclated-in-analyst-quantmode, 2022.
28. (a) N. Gospodinova and E. Tomsik, *Prog. Polym. Sci.*, 2015, **42**, 33-47; (b) J. S. Mugride , G. Szigethy , R. G. Bergman and K. N. Raymond , *J. Am. Chem. Soc.*, 2010, **132**, 16256-16264.
29. (a) T. Ogoshi , M. Hashizume , T. Yamagishi and Y. Nakamoto , *Chem. Commun.*, 2010, 46, 3708-3710; (b) N. L. Strutt , R. S. Forgan , J. M. Spruell , Y. Y. Botros and J. F. Stoddart , *J. Am. Chem. Soc.*, 2011, **133**, 5668-5671.

30. N. M. O'Boyle, M. Banck, C. A. James, C. Morley, T. Vandermeersch and G. R. Hutchison, *J. Cheminformatics*, 2011, **3**, 1-14.
31. https://zenodo.org/record/3995081#.ZCWS2crMK70.
32. https://www.rsc.org/suppdata/d0/nj/d0nj03555f/d0nj03555f1.pdf.

6 Chapter 6: Silica-bound supramolecular chromatographic separation of C_{60} and C_{70} fullerenes

6.1 Introduction

There has been a constant growing scientific and industrial attention to fullerenes since they were introduced in 1985. They have extraordinary electronic and in optoelectronic properties, charge transferability, efficient singlet oxygen sensitizing ability, robust electron acceptor character, and superconductivity upon doping with alkali metals.[1-2] These specific characteristic features drive fullerenes, and their derivatives have been used in the construction of biosensors,[3-4] skin preparation and cosmetics,[5-6] and a wide range of other medical applications.[7-8] Fullerenes-based nanomaterials have excellent potential for a plethora of biomedical applications but are restricted by the high cost and difficulties in purification. This difficulty arises from the similarities in the structure of fullerenes, particularly the exclusive sp^2 carbon atoms of the fullerenes connected in hollow ball-shaped structures as shown in Figure 6.1.[9]

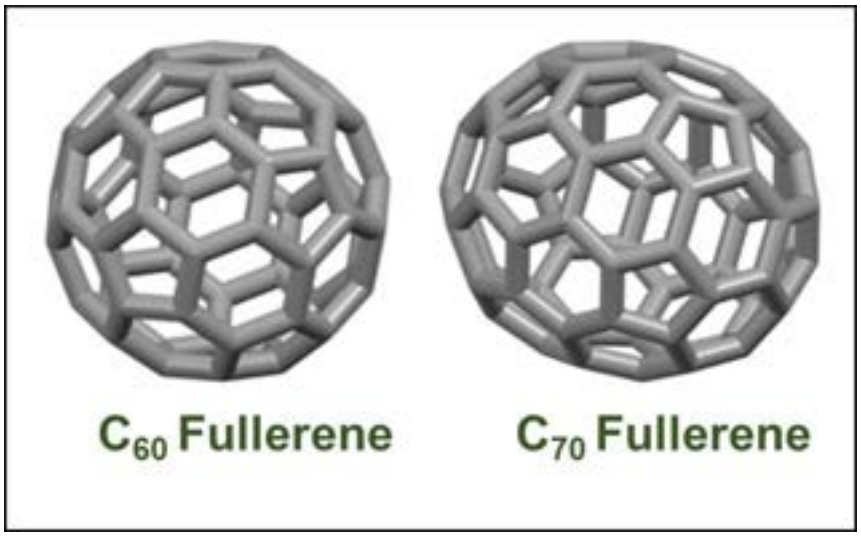

Figure 6.1.Structures of C_{60}-fullerene and C_{70}-fullerene.

The most generally utilized techniques for the separation and purification of fullerenes are crystallization,[10] complexations[11] and chromatographic techniques.[12] Furthermore, each method has its merits and demerits; for example, complexation methods require pre-engineered molecules, which are costly and difficult to recycle. On the other hand, crystallization is time-consuming and lacks facile means for automation.

Several novel liquid chromatographic stationary phases have been designed and constructed for the successful separation and isolation of fullerenes. For example,

activated carbon for separation of C_{60}/C_{70} fullerene mixtures,[13] and metal-organic frameworks (MOFs) for separation of a eight different fullerenes from the mixture of C_{60} to C_{84}.[14] There are several reverse-phase stationary phases available for the separation of pristine fullerenes (C_{60}, C_{70}, C_{76}, C_{78}, $C_{82,}$ and C_{84}), i.e., silica functionalized with C_{18} chains,[15] humic acids,[16] tetraphenylporhyrin,[17] metal-organic frameworks (MOFs),[18] and pyrenebutyric acid.[19] Although several silica-functionalized chromatographic columns bearing various functional moieties are available commercially, optimization is performed empirically and permits only the separation of fullerenes on a qualitative scale.[20] The progression in the LC separation and purification of fullerenes is dependent on the nature of the stationary phase. Therefore, many studies have explored the utilization of specific organic selectors, consisting of one or multiple interaction sites as stationary phases for the LC separation of fullerite.[13-19]

The development of novel supramolecular cavitands as specific selectors to provide host-guest systems, facilitated *via* non-covalent interactions, is one of the significant essential goals of supramolecular chemistry.[21-22] Calix[n]arenes are referred to as third-generation supramolecular cavitands, discovered after crown ethers and cyclodextrins. Calix[n]arenes possess cavities and demonstrate versatile complexation abilities with guest molecules.[23-24] Calix[n]arenes have become excellent tools in analytical chemistry due to their characteristic guest recognition features and their ability to form a reversible complex with neutral and charged molecules.[25-27] Primary efforts have been made to purify and separate fullerenes *via* supramolecular cavitands such as cyclodextrins,[28-29] calixarene macrocycles,[30] and porphyrin nano-barrels.[31] Furthermore, the selective extraction and precipitation of C_{70} over C_{60} have successfully been attained *via* *p*-halohomooxacalix[3]arenes and calix[5]arene.[32] However, this approach is limited due to the significant struggle encountered in the release and recovery of fullerenes from the complex mixture. Various host-guest interaction mechanisms, such as hydrophobic, π–π interactions, hydrogen bonding, and inclusion interactions, were exploited in the separation process mediated by supramolecular systems. These supramolecular silica-bound chromatographic stationary phases offer multiple-mode of interactions to the analytes compared to the traditional chromatographic stationary phases that include normal or reverse phases.[32]

In this chapter 6, it is described how the supramolecular cavitand *C*-bromo-butylpyrogallol[4]arene **5** from *C*-hydroxybutylpyrogallol[4]arene **4** itself was synthesized *via* a previously reported high yield microwave irradiation reaction.[33] Subsequently, *C*-bromobutylpyrogallol[4]arene **5** was covalently functionalized on the surface of

chromatographic silica gel particles. The new stationary phases **8** and **9** were evaluated to study the chromatographic behaviour of C_{60} and C_{70}-fullerenes *via* flash column chromatography and high-pressure liquid chromatography (HPLC) techniques compared with a traditional RP-C_{18} stationary phase. Furthermore, an *in-silico* study was performed to gauge further the host-guest interactions between the butylpyrogallol[4]arene stationary phase **5** and the two C_{60} and C_{70}-fullerenes.[34]

6.2 Results and Discussion

C-Alkylpyrogallol[4]arenes (PgCn) are a subgroup of calixarene macrocycles, which carry two major key characteristic features. Primarily, they consist of twelve hydroxy groups at the upper rim of the calixarene cavity, leading to several hydrogen-bonding interactions. Second is the four pendant alkyl groups that radiate from the spheroidal assembly, which traditionally range in length from ethyl to undecyl, as shown in Figure 6.2.[35-36] This plethora of potential hydrogen bonding sites led to the synthesis of several pyrogallol[n]arene derivatives to explore the chromatographic applications of silica-bound pyrogallol[n]arenes and also various applications in separation science.[37-38]

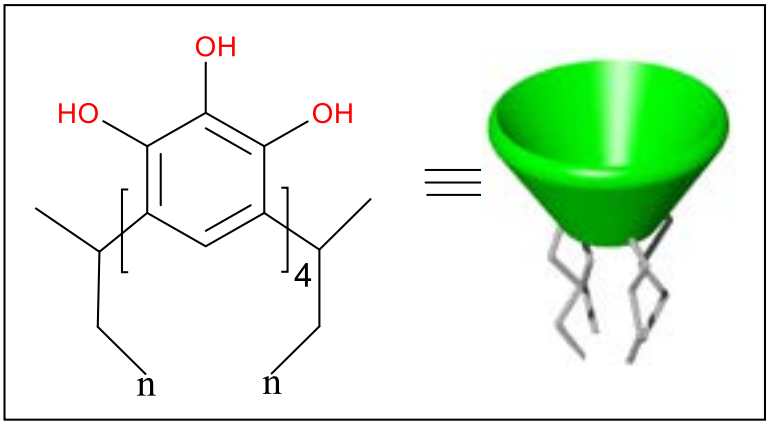

Figure 6.2. C-Alkylpyrogallol[4]arenes (PgCn).

6.2.1. Synthesis of *C*-butylpyrogallol[4]arene 5

As discussed in Chapter 3, *C*-Hydroxybutylpyrogallo[4]arene **4** was prepared from pyrogallol and 2,3-dihydropyran under microwave irradiation[33] and converted to the tetrabromo derivative **5** with phosphorus tribromide in 64% yield, as shown in Figure 6.3. First, *C*-hydroxybutyl-pyrogallol [4]arene **4** in DCM was cooled down to 0°C under nitrogen. Subsequently, phosphorous tribromide was added dropwise. The reaction mixture was stirred for 1.5 hours and allowed to reach room temperature. Next, the reaction mixture was heated at 40 °C for 5 h. under stirring. The reaction mixture was then evaporated under a vacuum to collect a crude oil. The resultant crude oil was sonicated in water (30

mL) for 15 min and vacuum filtered. Finally, the solid filtrate was vacuum dried. Product **5** was a light pink colour with a yield of 64%. The mass spectrometric analysis (ESI-MS) of **5** confirmed the existence of the five m/z peaks, $[M]^+$ to $[M+8]^+$, in a proper ratio for a tetrabromo compound **5** (appendix).[34]

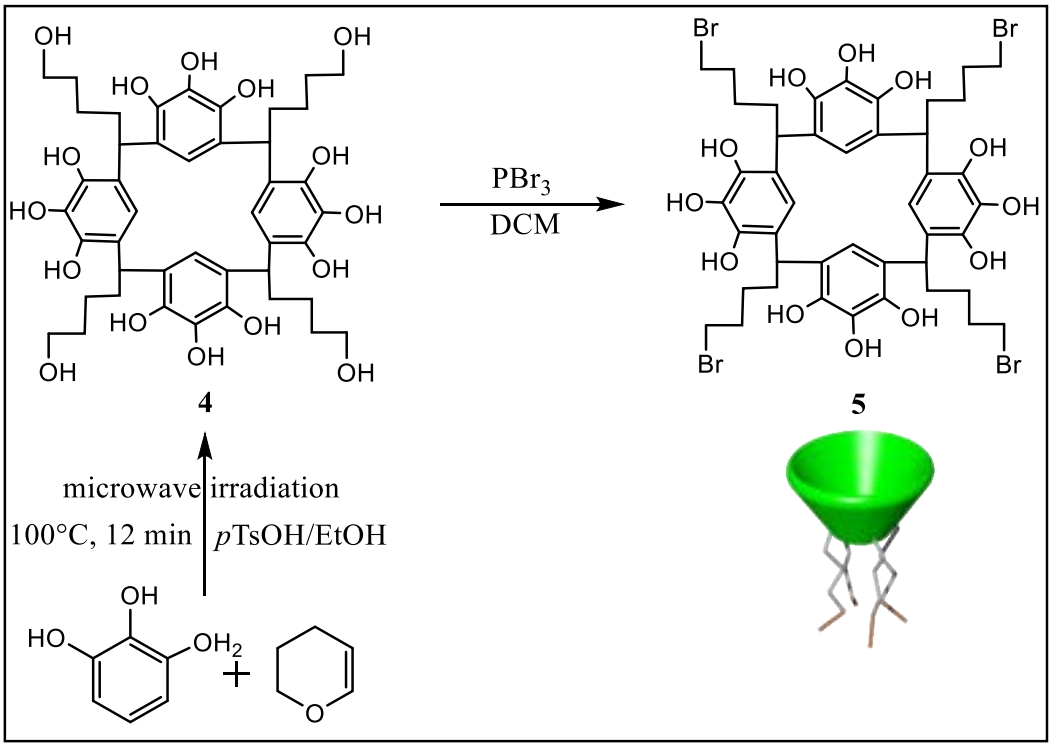

Figure 6.3. Synthesis of C-butylpyrogallol[4]arene ***5.***

The ^{1}H NMR for *C*-bromobutylpyrogallol[4]arene **5** was in line with the expected signals, including two singlet signals for aromatic hydroxy protons in the downfield region, triplet signals for the proton at the bridging position, and the multiplet signals for the methylene protons next to bromine. In addition, the multiplet signals for the rest of the aliphatic side chain protons are in line with the proposed structure, as shown in Figure 6.4.

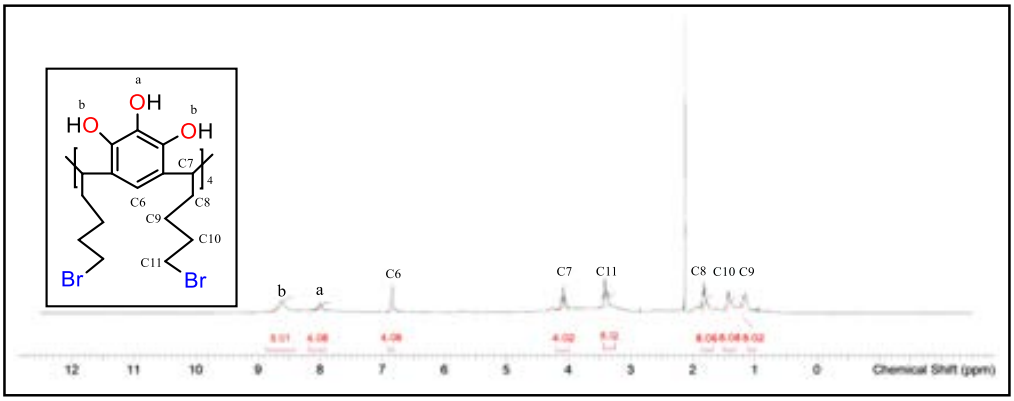

Figure 6.4. ^{1}H NMR spectrum (400 MHz, d_6-DMSO, room temperature) of C-bromobutylpyrogallol[4]arene ***5****.*

6.2.2. Synthesis of silica-bound *C*-butylpyrogallol[4]arene stationary phase 8 and 9

The *C*-butylpyrogallol[4]arene silica-bound HPLC stationary phase is represented as phase **8**, while *C*-butylpyrogallol[4]arene silica-bound flash stationary phase is reported as phase **9,** as shown in Figures 6.5 and 6.6 respectively, as discussed in Chapter 3.

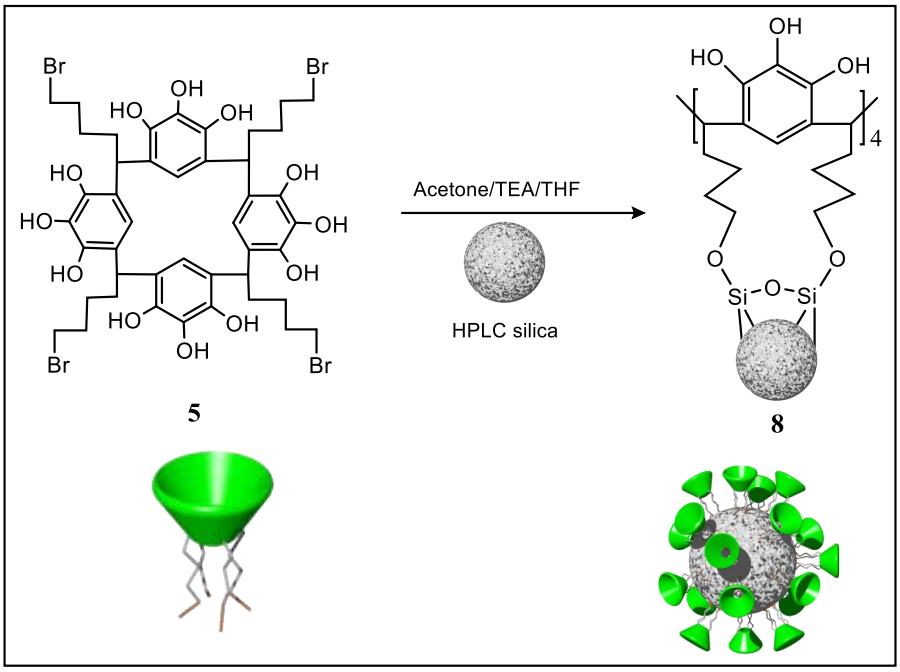

*Figure 6.5. Silica-bound C-butylpyrogallol[4]arene bonded chromatographic stationary phase for HPLC **8**.*

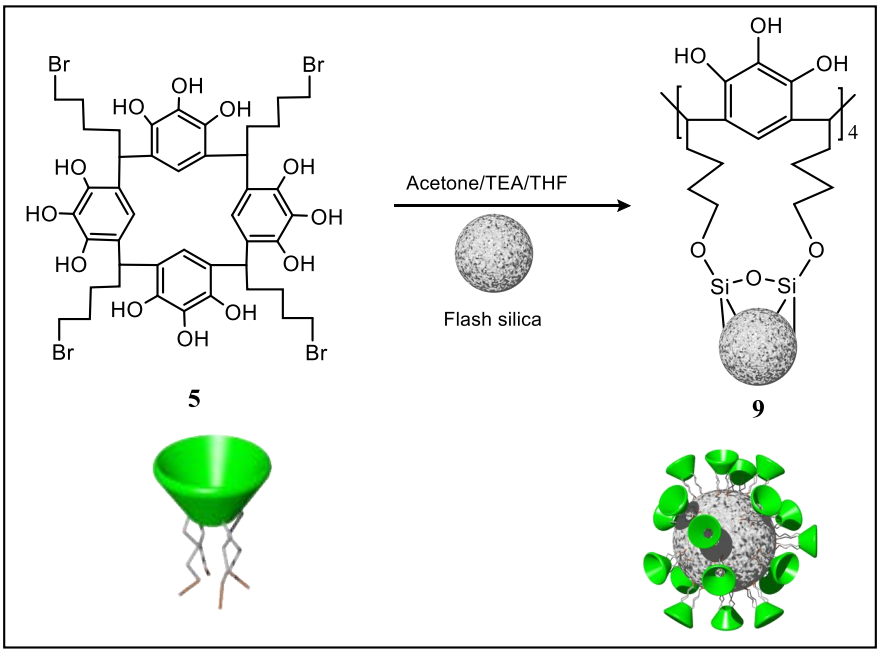

*Figure 6.6. Silica-bound C-butylpyrogallol[4]arene bonded flash column chromatography **9.***

C-Bromobutylpyrogallol[4]arene **5** was covalently attached to the surface of chromatographic silica for HPLC and flash column *via* the earlier reported method as shown in Figures 6.5 and 6.6.[21-22.] To give the HPLC chromatographic stationary phase **8** and the flash column stationary phase **9** have resulted. Next, the chromatographic stationary phases **8** and **9** were purged with methanol: acetone (70:30) to eliminate unreacted pyrogallol[4]arene cavitand. Finally, both stationary phases **8** and **9** were dried at room temperature. The specifications for silica used to functionalize with *C*-butylpyrogallol[4]arene for HPLC **8** and flash column chromatography **9** are reported in Table 6.1.[34]

Table 6.1. Chromatographic silica specifications for flash column chromatography and HPLC.

Chromatograp-hic Technique	Shape of Silica Gel	Particle Size (µm)	Surface Area (m^2/g)	Pore Volume (cc/g)	Pore Size
Flash column	spherical	50	500	0.70	500
HPLC	spherical	5	120	0.95	70

6.2.3. Characterization of the silica-bound *C*-butylpyrogallol[4]arene stationary phases 8 and 9

The silica-bound *C*-butylpyrogallol[4]arene stationary phases **8** and **9** were characterized *via* thermogravimetric analysis (TGA) to determine the loading of *C*-butylpyrogallol[4]arene **5** and by scanning electron microscopy (SEM) to analyze the structural, morphological characterization of uncoated silica and *C*-butylpyrogallol[4]arene-bound silicas **8** and **9**.[34]

In brief, the thermogravimetric analysis (TGA) studies were carried out over a temperature range from 25 to 900 °C with an increment of 10 °C per minute, as shown in Figure 6.7. The TGA characterization results confirmed the mass loading of the *C*-butylpyrogallol[4]arene **5** on the surface of the functionalized silica at 17.5% (0.01613 M) for the HPLC stationary phase **8** and at 14.1% (0.00792 M) for the flash column chromatography phase **9**, as shown in Figure 6.7.[34]

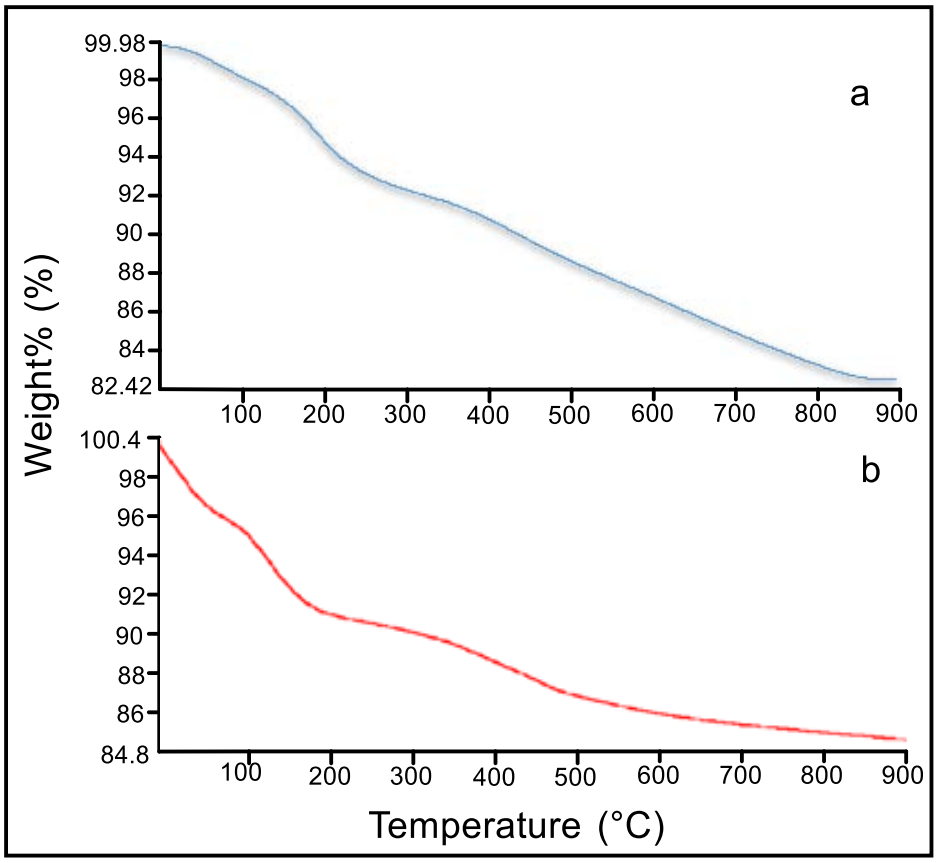

*Figure 6.7. Thermogravimetric analysis of the silica-bound C-butylpyrogallol[4]arene stationary phases: (a) HPLC grade **8** and (b) flash column chromatography grade **9**.*

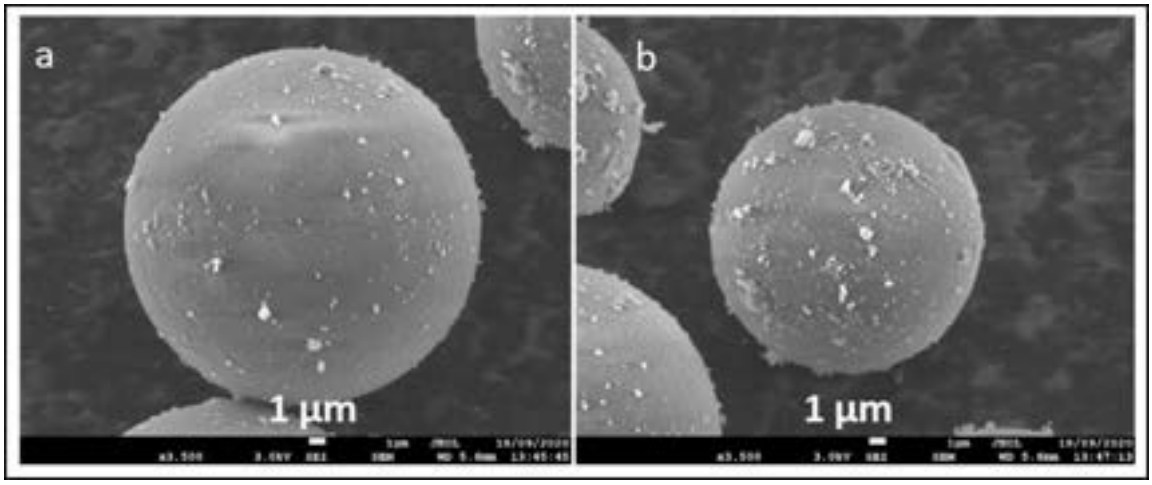

*Figure 6.8. SEM images showing unfunctionalized flash silica (a) and silica functionalized with C-butylpyrogallol[4]arene stationary phase particles **8** (b) at 10 and magnification.*

The structural integrities of the silicas functionalized with *C*-butylpyrogallol[4]arene **5** for HPLC and flash chromatography, **8** and **9**, were assessed via scanning electron microscopy (SEM) and demonstrated to be similar to the initial spherical silica particles, as shown in Figures 6.8 and 6.9. Furthermore, they appear to have smooth surfaces without

cracks or well-defined cavities, which are essential for free-flow of the mobile phase and analytes.[39-42] Subsequently, remarkable low-back pressure was observed during the conditioning of the columns and chromatographic evaluation processes.[34]

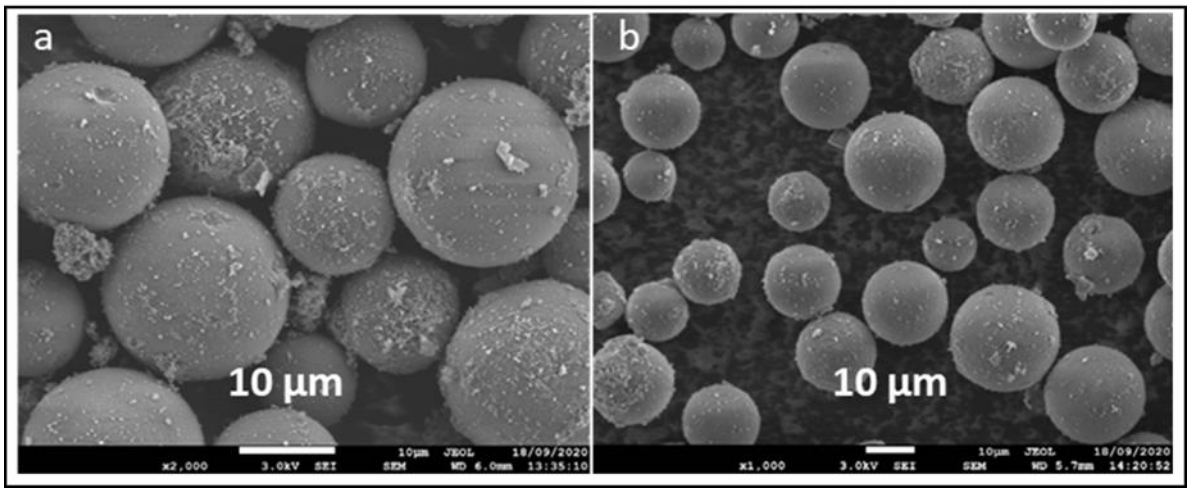

*Figure 6.9. SEM images showing unfunctionalized HPLC silica (a) and silica functionalized with C-butylpyrogallol[4]arene HPLC stationary phase particles **9** (b) at 1 µm magnification.*

6.2.4. Supramolecular chromatographic separation of C_{60} and C_{70}-fullerenes

The HPLC silica functionalized with *C*-butylpyrogallol[4]arene **8** was slurry packed into a stainless-steel HPLC column (150 × 4.6 mm i.d.) *via* a wet slurry packing method using methanol as the displacing agent at a constant pressure of 34.5 MPa. The flash column variant of the stationary phase material **9** was dry-packed into a flash column cartridge (12 gm, 62 mm × 12 mm i.d.) *via a* continuous tapping method.[34]

6.2.4.1. HPLC Separation of C_{60} and C_{70}-Fullerenes

Since the discovery of fullerenes, reverse-phase chromatography RP-C_{18} is the major chromatographic techniques to separate the fullerene shoot.[34] To advance the new developments, several *p*-butyl pyrogallol[4]arenes have been extensively explored for the isolation of fullerenes *via* host-guest complexation, such as *p*-butyl-calix[8]arene,[30] 5-nitro-11,17,23,29-tetramethylcalix[5]arene,[43] and *p*-tert-butylcalix[6]arene bearing one *O*-butanoic acid side chain.[44] In addition, a variety of chromatographic phases have been reported to separate fullerene mixtures, including Lewis base modified magnesia–zirconia,[45] monomeric type C_{30} stationary phase,[46] ligand-modified silica stationary phases, such as p-nitrobenzoic acid and naphthyl-acetic acid silica;[47] a core-shell biphenyl stationary phase,[48] pyrenebutyric acid bonded silica,[49] porphyrins iimmobilizedsilica,[50] heavy atom containing silica[51] and Phenomenex Cosmosil Buckyprep.[52]

However, the silica-bound calixarene chromatographic stationary phases and other modified LC stationary phases have restricted use in the tedious isolation and purification of the fullerene mixture. This is due to the necessity of a chromatographic column with fast analysis and improved sample loading capacity.[33,34]

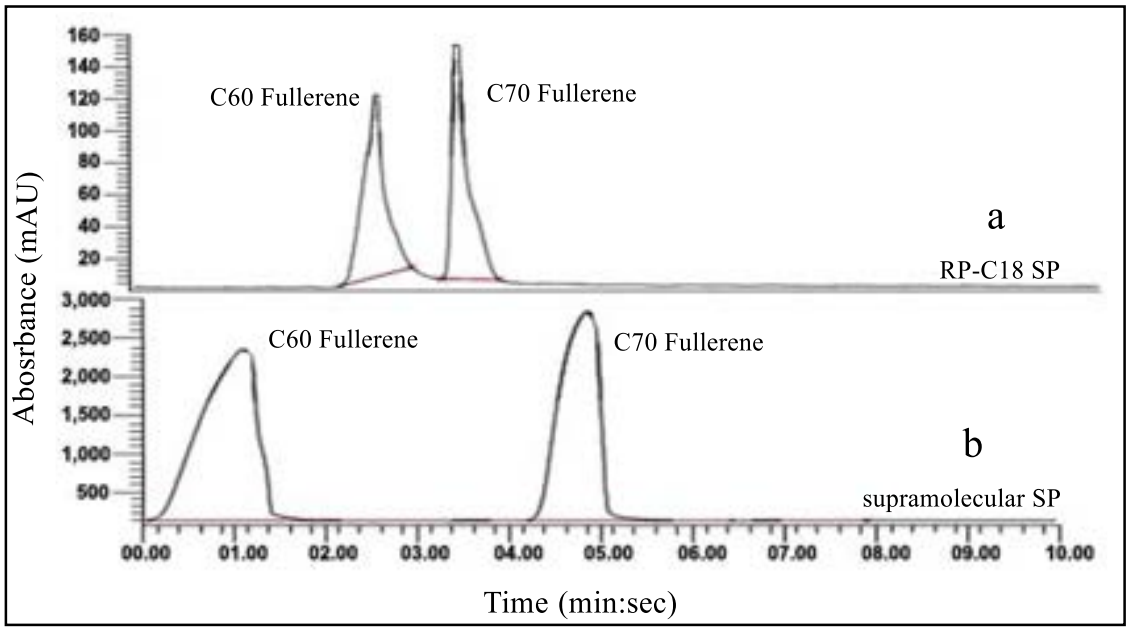

*Figure 6.10.HPLC separation of C_{60} and C_{70} fullerene standards on RP-C_{18} (a) and C-butylpyrogallol[4]arene bonded-silica column **8** (b). Run time: 10 min, column temperature: ambient room temperature.*

The newly synthesized HPLC silica-bonded C-butylpyrogallol[4]arene stationary phase **8** was primed with equimolar ratios of water:methanol at 0.1 mL/min overnight to condition the column, to remove the unreacted materials, and subsequently to condition the column **8** for further chromatographic separation of a C_{60} and C_{70} fullerene mixture. C_{60} and C_{70} fullerenes were employed as probes for the study of the chromatographic evaluation of the silica-bonded *C*-butylpyrogallol[4]arene HPLC stationary phase **8**, and their chromatographic performance was subsequently compared with a traditional RP-C_{18} column (150 × 4.6 mm i.d.), as shown in Figure 6.10a, under reverse phase mode conditions. As shown in Figure 10a, a 2 µL injection volume of C_{60} and C_{70} fullerenes (50 µg) dissolved in toluene (1 mL) was separated on a traditional RP-C_{18} column *via* isocratic elution using a modified mobile phase (water:methanol, 40:60). The mobile phase flow rate was operated at 1.0 mL min^{-1} and a photodiode array (PDA) detector used to measure the absorbance at a wavelength of 237 nm.[52] These chromatographic conditions resulted in C_{60} and C_{70} fullerenes elution at 2.52 and 3.35 min on the RP-C_{18} column, as shown in Figure 6.10a.

Subsequently, the same as for RP-C_{18} chromatographic conditions were employed to demonstrate the separation of C_{60} and C_{70} fullerenes on the silica-bonded *C*-butylpyrogallol[4]arene HPLC stationary phase **8**. The chromatogram has resulted in the prominent base-line retention of C_{60}-fullerene at 1.08 min while C_{70}-fullerene was retained at 4.85 min under 10 min of run time, as shown in Figure 6.10b. The chromatographic data confirms the superior chromatographic separation and resolution of C_{60} and C_{70} fullerenes on the silica-bound *C*-butylpyrogallol[4]arene stationary phase **8** compared to utilizing a traditional RP-C_{18} HPLC column under the same chromatographic conditions.[34]

In general, the host-guest interactions of calix[4]arenes and fullerenes are due to self-assembly and van der Waals, π–π interactions, as the fullerenes are rich in π-electrons while the cavity of calix[4]arene consists of aromatic rings. Calix[n]arenes have unique structural features of well-ordered macrocyclic aromatic rings and flexible cavitnads to allow the guest molecules, such as fullerenes. Atwood and Shinkai used these structural features of calix[n]arenes to demonstrate the separation of C_{60} fullerene from the mixture of C_{60} and C_{70} fullerenes using *p*-tert-butyl calix[8]arene *via* complexation and recrystallization. The molecular complexation of fullerenes with calix[n]arene host molecules allows the successful separation *via* selective size exclusion and host-guest interactions.[30] Atwood also reported that calix[5]arene forms a host-guest complex with C_{70} fullerene in *p*-xylene solvent *via* van der Waals,[62] as shown in Figure 6.11. The host-guest complexation significantly occurs due to the size of the calixarene cavity (n) and functional groups at the upper rim of the cavitand.

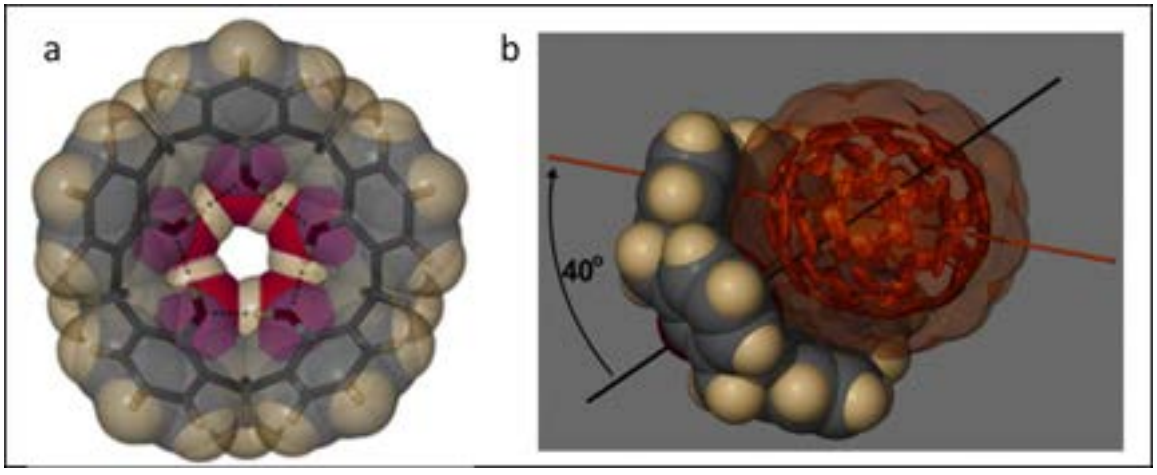

Figure 6.11 Calix[5]arene with intermolecular hydrogen bonding with phenolic hydroxy groups (a), and asymmetric representation of calix[5]arene with C_{70}. Orange represents fullerene, transparent layer shows the van der Waals surface, and grey color shows the calix[5]arene.[62]

The separation of C_{60} and C_{70} fullerenes using *C*-butylpyrogallol[4]arene silica-bound stationary phase **8** is due to the host-guest size exclusion, as the size of fullerene increases, the *C*-butylpyrogallol[4]arene allows the guest molecule to dock into the cavity,

like ball and socket type of host-guest interactions. The interaction of the fullerenes with the macrocyclic cavity increases with the size of the fullerene structure, from which we can develop the subsequent interaction strengths between the fullerene and the macrocyclic cavity: C80 > C70 > C60 > C50. Therefore, the C-butylpyrogallol[4]arene **5** cavity appears to be an efficient chromatographic stationary phase for purification of the mixture of fullerenes, as shown in Figure 6.12 and should be trialed for other size-selective chromatographic separation studies.[34]

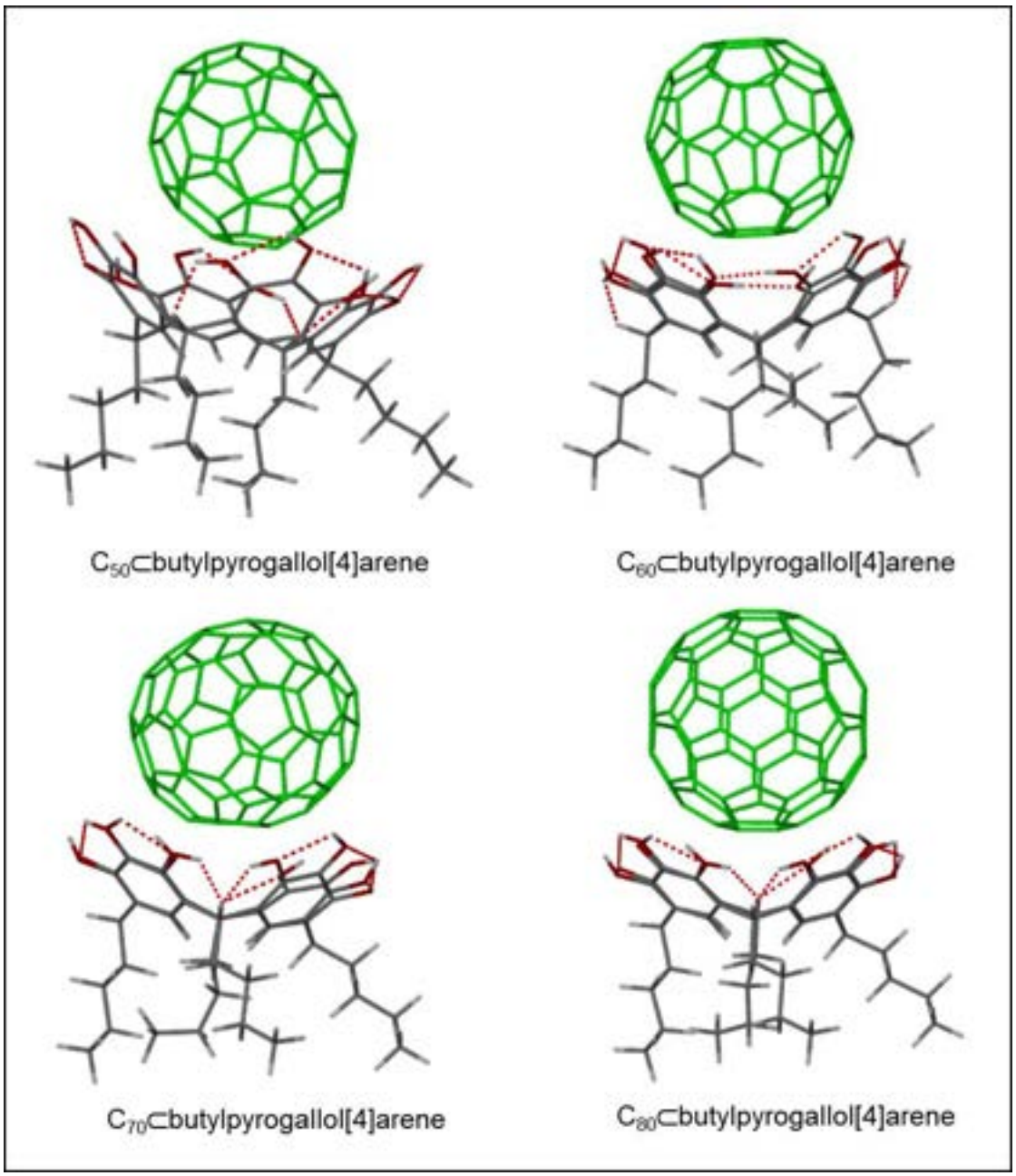

Figure 6.12 Illustration of C_{50}, C_{60}, C_{70}, and C_{80}⊂butylpyrogallol[4]arene. The green spheres represent fullerenes, and grey, white and red represent Carbon, Hydrogen, and Oxygen

6.2.4.2. Flash column separation of C_{60} and C_{70} fullerenes

Though HPLC is the most incredible successful and dominant chromatographic separation technique to purify the fullerenes and modified fullerenes at the analytical scale, it is unfeasible for the bulk purification of fullerenes from fullerene soot using HPLC. This is due to their high cost, solvent incompatibilities with the reversed phase stationary phases, less output amount, limited column loading amounts, and injection volumes of 1 mL.[34]

Technical and instrumental developments in flash column chromatography and HPLC has permitted the execution of a single compact system consisting of a flash column chromatography environment and preparative HPLC pumps. These advancements provide a quaternary gradient and a dedicated purge line. It is likely to attain large-scale purification of fullerenes and utilize a broadly implemented LuerLock series of flash columns. The columns efficiently withstand pressure up to 22 bar and flow rates ranging between 4 to 300 mL min^{-1}, stainless steel HPLC columns for scouter sample analysis, and preparative stainless-steel columns for high-pressure applications.[54]

The automated flash column chromatography is restricted to the efficient and fast preparative separation of fullerenes using molecular recognition selectors that offers multiple strong interaction sites with fullerenes and modified fullerenes. Conventional normal phase silica particles interact with fullerenes *via* van der Waals interactions leading to unresolved fullerenes with rapid elution even with the utilization of a weak nonpolar organic solvent such as hexane. Similar solvent incompatibility problems occur with RP-C_{18} silica particles.[34]

To create a flash column chromatographic stationary phase consisting of novel selectors to provide multiple interactions, Schipper *et al.,* for the first time, described a stationary silica phase consisting of functionalized bent aromatic molecules called iptycenes. The stationary phase was applicable for preparative scale purification of fullerenes *via* flash chromatography and UV detection technology. In their work, a mixture of fullerenes C_{60} and C_{70} (25 mg) was loaded on the silica functionalized with bent-aromatic iptycenes (12 gm), while eluting the column with hexane as a mobile phase. This subsequently resulted in the retention of C_{60} at 45 min and C_{70} at 90 min. This is because the bent aromatic molecules offer a larger surface area for enhanced π–π interactions leading to high resolution and increased retention times. However, when the mobile phase was switched to hexane: toluene (3:1), there was a decrease in retention times of C_{60} and C_{70} to 33 and 59 min compared to earlier retention times. Even though there is substantial separation

and resolution of fullerenes on silica-functionalized iptycenes stationary phase at milligram levels, the fullerenes are retained for longer times. In addition some loss of functionalized cavitand from the silica-bound stationary phases has been observed.[55]

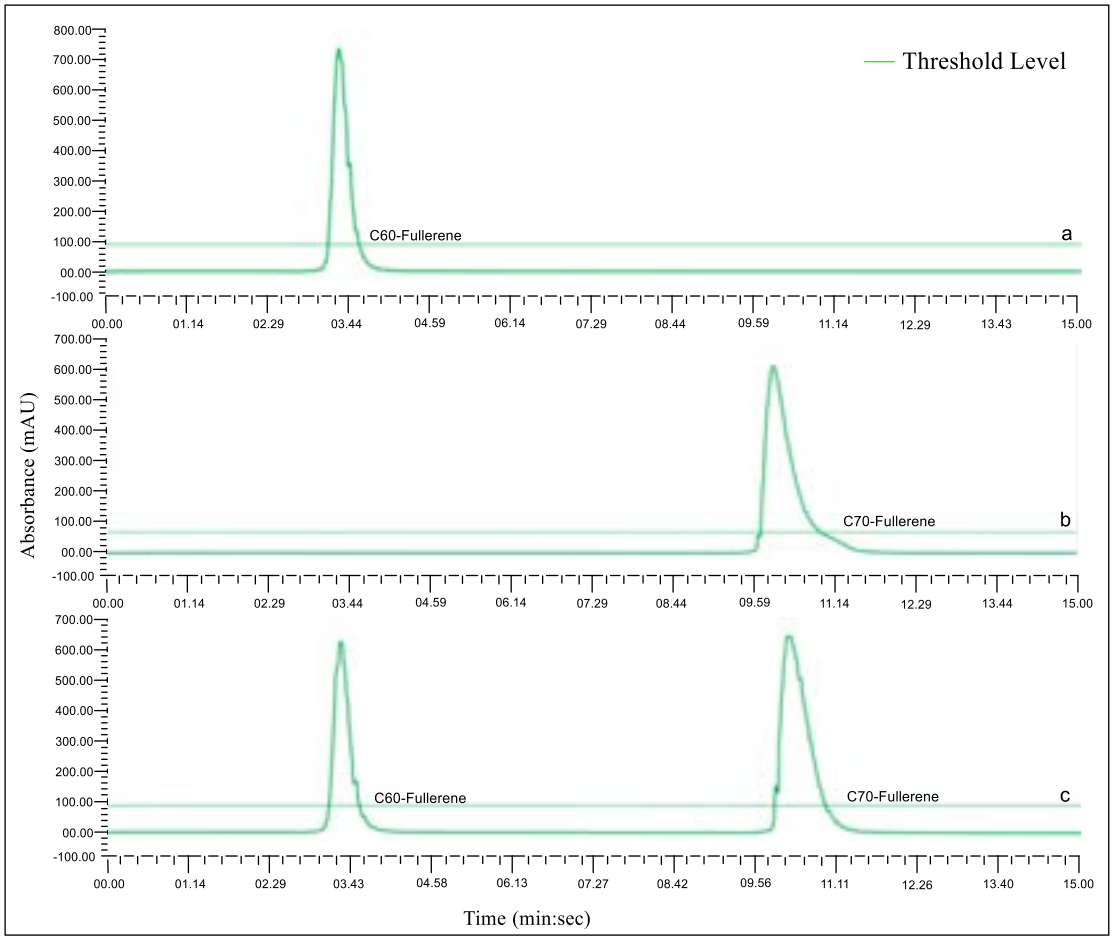

*Figure 6.13.Flash column chromatographic separation of fullerene standards: (a) C_{60}-fullerene, (b) C_{70}-fullerene and (c) an equimolar mixture of C_{60} and C_{70}-fullerenes (c) on silica-bound C-butylpyrogallol[4]arene stationary phases **9**.*

The separation of a mixture of fullerene C_{60} and C_{70} was studied on the silica-bound *C*-butylpyrogallol[4]arene stationary phase **9** using flash column chromatography, as shown in Figure 6.13. As the chromatographic separation of fullerenes is directly dependent on the solubility of fullerenes in a suitable solvent system, 25 mg mL^{-1} of individual C_{60} and C_{70} fullerene standards were dissolved in toluene. The flash column separation of fullerenes mixture on silica-bound *C*-butylpyrogallol[4]arene stationary phase **9** was carried out *via* ethyl acetate:toluene (35:65) as a mobile phase under isocratic conditions. As fullerenes are readily soluble in nonpolar solvents such as toluene, a mobile phase of ethyl acetate:toluene permits the fullerenes to move quickly through the pores of silica-bound *C*-butylpyrogallol[4]arene stationary phase **9**. Subsequently, this leads to a ball and socket reversible host–guest size-selective molecular recognition between the upper aromatic

rings of the pyrogallol[4]arene **5** cavity and fullerenes. This stationary phase **9** demonstrated rapid separation of fullerenes C_{60} in 3.20 min and C_{70} in 10.30 min, as shown in Figures 6.13 a and b, compared to the traditional reverse phase stationary phase and previously reported iptycene functionalized silica flash column phase.[34]

To validate the chromatographic separation efficiency of the silica-bound *C*-butylpyrogallol[4]arene stationary phase **9**, the separation of mixtures of C_{60} and C_{70}-fullerenes *via* the same optimised chromatographic conditions was explored. As a result, as shown in Figure 6.13, the silica-bound C-butylpyrogallol[4]arene stationary phase **9** resolved the mixture into two discrete peaks at the exact retention times as that of individual fullerene retention times 6.13c.[34]

Under these chromatographic separation conditions, the separation mechanism can be classified as a traditional normal phase chromatography, where the stationary phase is polar and the mobile phase consists nonpolar solvent system. For example, the silica-bound *C*-butylpyrogallol[4]arene flash column chromatographic stationary phase **9** separated a similar amount of fullerenes C_{60} and C_{70} (25 mg) in 3-11 minutes compared to the iptycenes bound silica phase of Schipper *et al*. which took 30-90 minutes. This illustrates the rapid separation of a C_{60} and C_{70} mixture by this new silica-bound C-butylpyrogallol[4]arene stationary phase **9** with minimum use of nonpolar solvents.[34]

In calix[n]arene and fullerene host-guest complexations, the role of the solvent system is an important parameter as the degree of host-guest fullerene and calix[n]arene complexations depends on the solubility fullerenes in the solvent system. The solubility of fullerenes increases in aromatic solvents, such as benzene, toluene, p-xylene, and chlorobenzene. The development of a host-guest complex is preferred in the solvent in which both host and guest systems can be poorly solvated or when the solvation-free energy of the host-guest complex goes beyond individual host and guest components.[63]

6.2.5. Quantum chemistry calculations

The *in-silico* host–guest interaction was studied to extend understanding of the unique molecular recognition that subsequently resulted in the favorable chromatographic separation of C_{60} and C_{70} using the silica-bound *C*-butylpyrogallol[4]arene stationary phases **8** and **9**. The Gibbs free binding energies of the gas and solvent phases for the most strongly binding motifs are represented in Table 6.2, along with their chromatographic retention times. Accompanying structures are presented in Figure 6.14. All computational calculations were undertaken using the DFTB engine in AMS and employed the mio-1-1 parameter set and UFF dispersion.[56-61]

Table 6.2. Gas and solvent phase DFTB/mio-1-1 Gibbs free binding energies of C_{60}⊂butylpyrogallol[4]arene and C_{70}⊂butylpyrogallol [4] arene alongside HPLC and flash column chromatographic retention times.

Guests	ΔGBE (kcal mol−1)		Experimental Chromatography	
	Gas Phase	Solvent Phase (Toluene)	HPLC (min:sec)	Flash Column (min:sec)
C_{60}-fullerene	−133.385	−123.862	1:08	03:26
C_{70}-fullerene	−135.569	−125.355	4:85	10:38

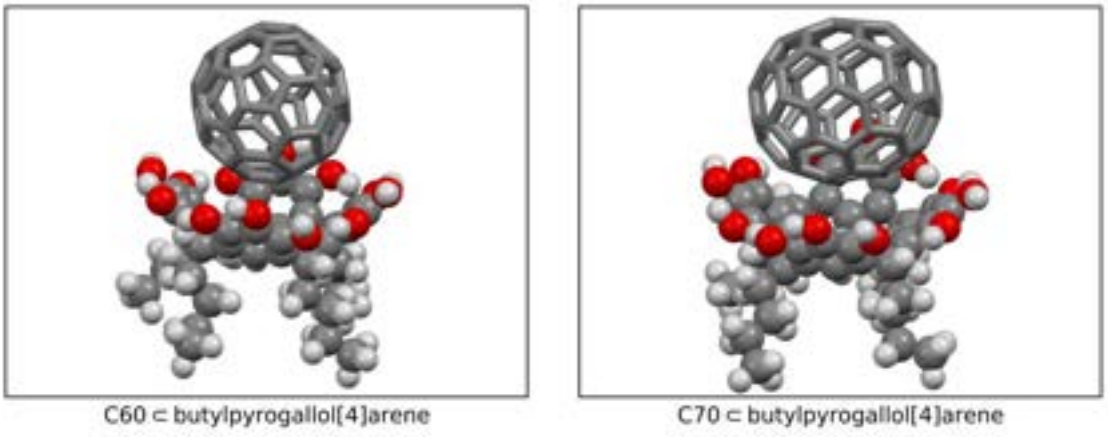

Figure 6.14. Illustration of the calculated binding modes of C_{60}⊂butylpyrogallol[4]arene and C_{70}⊂butylpyrogallol[4]arene. The red, light grey, and dark grey spheres represent oxygen, hydrogen, and carbon atoms.

The Gibbs free binding energies show stronger interactions of C_{70} with the macrocyclic cavity compared to C_{60}. It is essential to notice that these binding motifs are the actual local minima of the potential energy surface, with zero imaginary frequencies. The more vital interaction of the cavity with C_{70} is in line with experimental chromatographic separation, wherein C_{70} demonstrates a significantly superior retention time both in HPLC and flash column chromatography. The interaction of the fullerenes with the macrocyclic cavity is due to a series of strong non-covalent interactions; however, these interactions are identical for all fullerenes and therefore can not be utilized as a proxy for describing this favorable chromatographic separation. Instead, we hypothesize that this favored interaction of the cavity with C_{70} compared to C_{60} can most possibly be ascribed to size-selective molecular recognition. To assess this hypothesis, we computed further interaction energies and binding motifs for C_{50}⊂butylpyrogallol[4]arene and C_{80}⊂butylpyrogallol[4]arene, for which their solvated Gibbs free binding energies were −123.791 kcal mol^{-1} and −125.566 kcal mol^{-1}, respectively. This outcome demonstrates that the interaction of the fullerenes with the macrocyclic cavity increases with the size of

the fullerene structure, from which we can develop the subsequent interaction strengths between the fullerene and the macrocyclic cavity: $C_{80} > C_{70} > C_{60} > C_{50}$. Therefore, the *C*-butylpyrogallol[4]arene **5** cavity appears to be an efficient chromatographic stationary phase for purification of the mixture of fullerenes and should be trialed for other sie-selective chromatographic separation studies.[34]

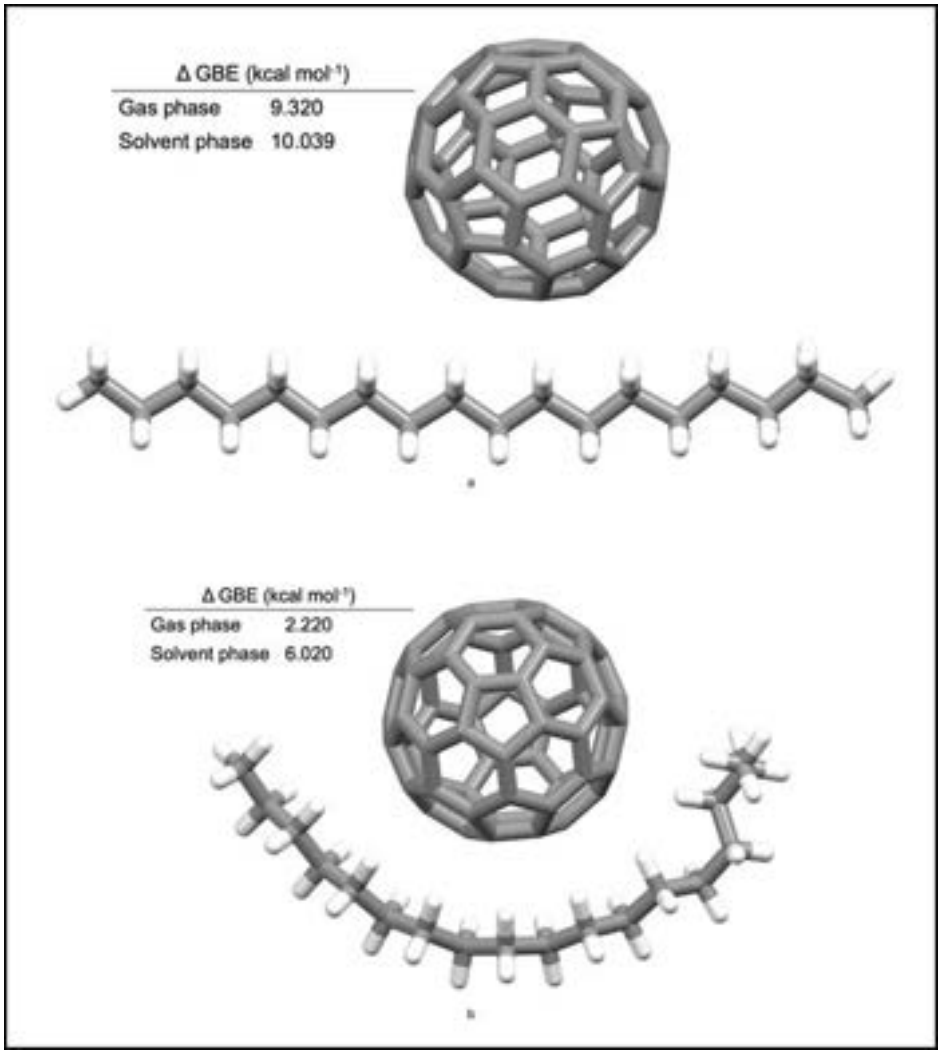

Figure 6.15. Illustration of the calculated gas and solvent phase binding energies and modes of C_{60}⊂RP-C_{18} interaction: a) represents the binding mode between the straight chain conformer of RP-C_{18} and C_{60}, and b) represents the binding mode between the curved conformer of RP-C_{18} and C_{60}.

Additionally, as shown in Figures 6.15 and 6.16, Gibb's free binding energies were also computed for C_{60}⊂RP-C_{18} and C_{70}⊂RP-C_{18} to compare the *C*-butylpyrogallol[4]arene cavity **5** and RP- C_{18} as chromatographic stationary phases for the selective separation of fullerenes from a mixture of fullerenes. The details of all the computations can be found at the link http:doi.org/10.5281/zenodo.4147306.

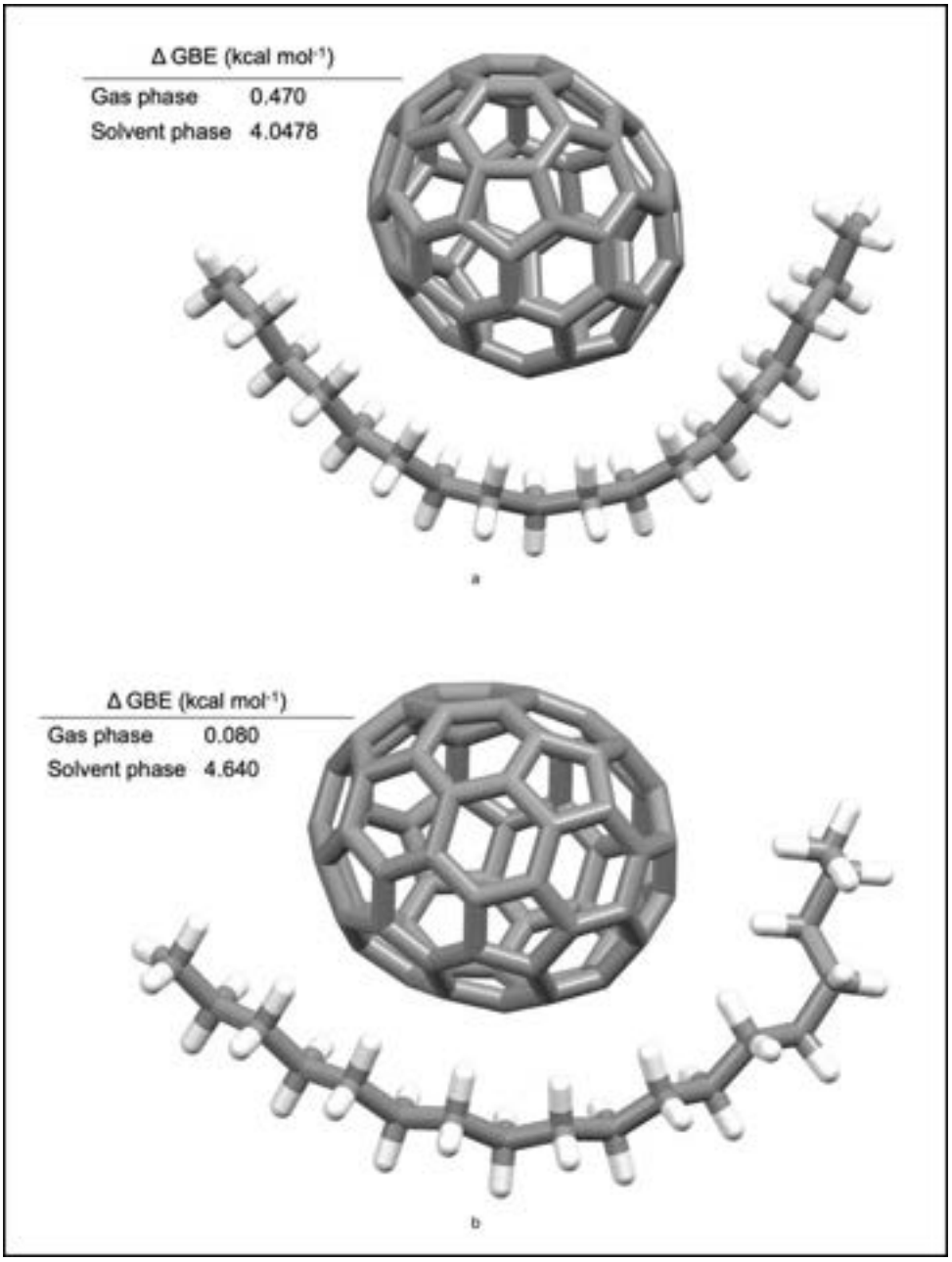

Figure 6.16. Illustration of the calculated gas and solvent phase binding energies and modes of C_{70}⊂RP-C_{18}. a and b represent the binding mode of two curved conformers of RP-C_{18} with C_{70}.

The change in Gibbs free binding energies, presented in Table 3, displays stronger interactions of C_{70} with RP-C_{18} compared to C_{60}. Unfortunately, though, the fullerene⊂RP-C_{18} interactions are significantly thermodynamically detrimental. Consequently, *C*-butylpyrogallol[4]arene **5**, which has a favourable thermodynamics interaction with fullerenes, is a more appropriate chromatographic stationary phase for the selective separation of fullerenes. The computed gas and solvent phase Gibbs free binding energies (ΔGBE) and electronic energies are presented in Table 6.3. The detailed energetic parameters are shown in Tables 6.4 and 6.5 for the gas and solvent phases, respectively.[34]

Table 6.3. Change in electronic energy and Gibbs free binding energy of fullerene⊂RP-C18 motifs. a and b represent the binding mode of two curved conformers of RP-C_{18} with C_{70}.

Systems	Gas phase (kcal mol^{-1})		Solvent phase (kcal mol^{-1})	
	ΔE	ΔGBE	ΔE	ΔGBE
C_{60}⊂RP-C_{18}-a	-0.0153	9.320	-9.478	10.039
C_{60}⊂RP-C_{18}-b	-0.028	2.220	-12.987	6.020
C_{70}⊂RP-C_{18}-a	-0.0311	0.470	-14.315	4.0478
C_{70}⊂RP-C_{18}-b	-0.0307	0.080	-14.301	4.640

E is the electronic change of the system; in practice is the final optimized energy of the system. *ΔE* is the change in electronic energy between the complex and the isolated systems.

$$\Delta E = E_{fullerene \subset RP-C_{18}} - \left(E_{fullerene} - E_{RP-C_{18}}\right)$$

$E_{fullerene \subset RP\text{-}C18}$ is the electronic energy of the fullerene⊂RP-C_{18} motif. $E_{fullerene}$ is the electronic energy of the isolated fullerene, and $E_{RP\text{-}C18}$ is the electronic energy of the isolated RP-C_{18}.

GBE is the Gibbs free energy of the system. This was computed as follows:

$$GBE = E + H - TS$$

H is the thermal correction to the enthalpy of the system. *S* is the thermal correction to entropy. *T* is the system's temperature, which is equal to 298.15 K.

$$\Delta GBE = GBE_{fullerene \subset RP-C_{18}} - \left(GBE_{fullerene} - GBE_{RP-C_{18}}\right)$$

$GBE_{fullerene \subset RP\text{-}C18}$ is the Gibbs free energy of the fullerene⊂RP-C_{18} motif. $GBE_{fullerene}$ is the Gibbs free energy of the isolated fullerene, and $G_{RP\text{-}C18}$ is the Gibbs free energy of the isolated RP-C_{18}.[34]

Table 6.4. Gas Phase UFF DFTB Mio-1-1 Contributions the Gibbs Free Energy (Hartree).

Systems	Electronic energies	RT	-TS	Internal energies	Enthalpies	Gibbs Free energies
C_{60}	-102.6746482	0.000944186	-0.064338271	-102.2522524	-102.2513083	-102.3156465
C_{70}	-119.8820304	0.000944186	-0.070701247	-119.387666	-119.3867218	-119.4574231
RP-C_{18}	-45.10614778	0.000944186	-0.079772362	-44.55891042	-44.55796623	-44.63773859
C_{60}⊂RP-C_{18}-a	-147.7961452	0.000944186	-0.111769899	-146.8277065	-146.8267623	-146.9385322
C_{60}⊂RP-C_{18}-b	-147.8088012	0.000944186	-0.111966711	-146.8388275	-146.8378833	-146.9498501
C_{70}⊂RP-C_{18}-a	-165.0192592	0.000944186	-0.117773367	-163.9775864	-163.9766423	-164.0944156
C_{70}⊂RP-C_{18}-b	-165.0188829	0.000944186	-0.118983495	-163.976999	-163.9760548	-164.0950383

Table 6.5. Solvent Phase UFF DFTB Mio-1-1 Contributions the Gibbs Free Energy (Hartree)

Systems	Electronic energies	RT	-TS	Internal energies	Enthalpies	SASA Free Energy	Gibbs Free energies
C_{60}	-102.7139323	0.000944186	-0.064366	-102.291834	-102.2908898	-0.0392905	-102.3552558
C_{70}	-119.9269967	0.000944186	-0.0707288	-119.4329698	-119.4320256	-0.0449730	-119.5027544
RP-C_{18}	-45.13065122	0.000944186	-0.0793391	-44.58411324	-44.58316905	-0.0245364	-44.66250824
C_{60}⊂RP-C_{18}-a	-147.8596879	0.000944186	-0.1095597	-146.8931503	-146.8922061	-0.0637294	-147.0017658
C_{60}⊂RP-C_{18}-b	-147.8652793	0.000944186	-0.1130198	-146.8960955	-146.8951513	-0.0578524	-147.0081712

C_{70}⊂RP-C_{18}-a	-165.0804601	0.000944186	-0.12000952	-164.0397467	-164.0388025	-0.06170926	-164.158812
C_{70}⊂RP-C_{18}-b	-165.080438	0.000944186	-0.1194558	-164.0393571	-164.038413	-0.06209017	-164.1578688

In conclusion, silica-bound *C*-butylpyrogallol[4]arene **8** and **9** have been efficiently synthesised and have demonstrated superior separation resolution and selectivity to C_{70}-fullerene compared to C_{60}-fullerene *via* size-selective molecular recognition using flash column chromatography and HPLC techniques. The flash column pyrogallol[4]arene stationary phase **9** demonstrated a substantial increase of isolated amounts of fullerenes to milligrams within 15 min in comparison to analytical separation from the HPLC supramolecular stationary phase **8**. The flash column **9** and HPLC **8** variants of silica-bound C-butylpyrogallol[4]arene phase proved superior separation selectivity *via* size-selective molecular recognition than an RP-C_{18} column separation selectivity for the mixture of C_{60} and C_{70}-fullerenes.

6.4 References

1. H. W. Kroto, J. R. Heath, S. C. O'Brien, R. F. Curl and R. E. Smalley, *Nature*, 1985, **318**, 162-163.
2. A. L. Balch and M. M. Olmstead, *Chem. Rev.*, 1998, **98**, 2123-2166.
3. S. Cai, W. Zhang, R. N. Zuckermann, Z. Li, X. Zhao and Y. Liu, *Adv. Mater*, 2015, **27**, 5762-5770.
4. C. Zhang, J. He, Y. Zhang, J. Chen, Y. Zhao, Y. Niu and C. Yu, Biosens. Bioelectron., 2018, 102, 94-100.
5. V. Krishna, S. Anand, E. Maytin and S. Grobmyer, Polyhydroxy fullerene sunscreen active agents and compositions, U.S. Patent US20190053991A1, 21 February 2021.
6. M. Martins, N. G. Azoia, M. Melle-Franco, A. Ribeiro and A. Cavaco-Paulo, *Eng. Life Sci.*, 2017, **17**, 732-738.
7. E. Castro, M. R. Cerón, A. H. Garcia, Q. Kim, A. Etcheverry-Berríos, M. J. Morel, R. Díaz-Torres, W. Qian, Z. Martinez and L. Mendez, *RSC Adv.*, 2018, **8**, 41692-41698.
8. V. Krishnan, Y. Kasuya, Q. Ji, M. Sathish, L. K. Shrestha, S. Ishihara, K. Minami, H. Morita, T. Yamazaki and N. Hanagata, *ACS Appl. Mater. Interfaces*, 2015, **7**, 15667-15673.

9. I. S. Neretin, K. A. Lyssenko, M. Y. Antipin, Y. L. Slovokhotov, O. V. Boltalina, P. A. Troshin, A. Y. Lukonin, L. N. Sidorov and R. Taylor, *Angewandte Chemie*, 2000, **112**, 3411-3414.
10. K. Y. Amsharov, J. Holzwarth, K. Roshchyna, D. I. Sharapa, F. Hampel and A. Hirsch, *Chem. Eur. J.*, 2017, **23**, 9014-9017.
11. N. Coustel, P. Bernier, R. Aznar, A. Zahab, J. Lambert and P. Lyard, *J. Chem. Soc. Chem. Commun.*, 1992, 1402-1403.
12. K. Nagata, E. Dejima, Y. Kikuchi and M. Hashiguchi, *Org. Process Res. Dev.*, 2005, **9**, 660-662.
13. N. Manolova, I. Rashkov, D. Legras and F. Beguin, *Carbon*, 1995, **33**, 209-213.
14. C. Yang, Y. Chen, H. Wang and X. Yan, *Chem. Eur. J.*, 2011, **17**, 11734-11737.
15. Y. C. Guillaume and E. Peyrin, *Anal. Chem.*, 1999, **71**, 1326-1331.
16. N. Casadei, M. Thomassin, Y. Guillaume and C. André, *Anal. Chim. Acta*, 2007, **588**, 268-273.
17. J. Xiao and M. E. Meyerhoff, *J. Chromatogr. A.*, 1995, **715**, 19-29.
18. H. Yi, G. Zeng, C. Lai, D. Huang, L. Tang, J. Gong, M. Chen, P. Xu, H. Wang and M. Cheng, *Chem. Eng. J.*, 2017, **330**, 134-145.
19. P. D. Boyd and C. A. Reed, *Acc. Chem. Res.*, 2005, **38**, 235-242.
20. S. Süß, V. Michaud, K. Amsharov, V. Akhmetov, M. Kaspereit, C. Damm and W. Peukert, *J. Phys. Chem. C*, 2019, **123**, 16747-16756.
21. S. Mekapothula, M. A. Addicoat, D. J. Boocock, J. D. Wallis, P. J. Cragg and G. W. Cave, *Chem. Commun.*, 2020, **56**, 1792-1794.
22. S. Mekapothula, A. D. Wonanke, M. A. Addicoat, J. D. Wallis, D. J. Boocock and G. W. Cave, *New J. Chem.*, 2021, **45**, 141-146.
23. C. D. Gutsche, *Calixarenes: an introduction*, Royal Society of Chemistry, Cambridge, UK, 2008.
24. K. Kimata, K. Hosoya, T. Araki and N. Tanaka, *J. Org. Chem.*, 1993, **58**, 282-283.
25. L. Li, M. Liu, S. Da and Y. Feng, *Talanta*, 2004, 62, 643-648.
26. M. Śliwka-Kaszyńska, K. Jaszczołt, A. Kołodziejczyk and J. Rachoń, *Talanta*, 2006, 68, 1560-1566.
27. R. Ludwig and N. T. K. Dzung, *Sensors*, 2002, 2, 397-416.
28. K. Cabrera, G. Wieland and M. Schäfer, *J. Chromatogr. A*, 1993, **644**, 396-399.
29. T. Andersson, K. Nilsson, M. Sundahl, G. Westman and O. Wennerström, *J. Chem. Soc. Chem. Commun.*, 1992, 604-606.
30. J. L. Atwood, G. A. Koutsantonis and C. L. Raston, *Nature*, 1994, **368**, 229-231.
31. J. Song, N. Aratani, H. Shinokubo and A. Osuka, *J. Am. Chem. Soc.*, 2010, **132**, 16356-16357.

32. N. Komatsu, *Org. Biomol. Chem*, 2003, **1**, 204-209.
33. M. Funck, D. P. Guest and G. W. Cave, *Tetrahedron Lett.*, 2010, **51**, 6399-6402.
34. S. Mekapothula, A. Wonanke, M. A. Addicoat, D. J. Boocock, J. D. Wallis and G. W. Cave, *Int. J. Mol. Sci.*, 2021, **22**, 5726.
35. G. W. Cave, J. Antesberger, L. J. Barbour, R. M. McKinlay and J. L. Atwood, *Angew. Chem. Int. Ed*, 2004, **43**, 5263-5266.
36. M. W. Heaven, G. W. Cave, R. M. McKinlay, J. Antesberger, S. J. Dalgarno, P. K. Thallapally and J. L. Atwood, *Angew. Chem. Int. Ed*, 2006, **45**, 6221-6224.
37. G. W. Cave, S. J. Dalgarno, J. Antesberger, M. C. Ferrarelli, R. M. McKinlay and J. L. Atwood, *Supramol. Che.*, 2008, **20**, 157-159.
38. D. B. Bassil, S. J. Dalgarno, G. W. Cave, J. L. Atwood and S. A. Tucker, *J. Phys. Chem. B*, 2007, **111**, 9088-9092.
39. J. DeStefano, T. Langlois and J. Kirkland, *J. Chromatogr. Sci.*, 2008, **46**, 254-260.
40. T. Hara, H. Kobayashi, T. Ikegami, K. Nakanishi and N. Tanaka, *Anal. Chem.*, 2006, **78**, 7632-7642.
41. R. E. Majors, *Anal. Chem.*, 1972, **44**, 1722-1726.
42. J. Kirkland, *Anal. Chem.*, 1992, **64**, 1239-1245.
43. K. Flídrová, A. Liška, J. Ludvík, V. Eigner and P. Lhoták, *Tetrahedron Lett.*, 2015, **56**, 1535-1538.
44. A. M. González-Delgado, J. J. Giner-Casares, G. Brezesinski, J. Regnouf-de-Vains and L. Camacho, *Langmuir*, 2012, **28**, 12114-12121.
45. Q. Yu, Y. Feng, Z. Shi and J. Yang, *Anal. Chim. Acta*, 2005, **536**, 39-48.
46. H. Ohta, Y. Saito, N. Nagae, J. J. Pesek, M. T. Matyska and K. Jinno, *J. Chromatogr A*, 2000, **883**, 55-66.
47. Q. Yu, Z. Shi, B. Lin, Y. Wu and Y. Feng, *J. Sep. Sci.*, 2006, **29**, 837-843.
48. A. Carboni, R. Helmus, J. R. Parsons, K. Kalbitz and P. de Voogt, *J. Chromatogr. A*, 2016, **1433**, 123-130.
49. D. E. Coutant, S. A. Clarke, A. H. Francis and M. E. Meyerhoff, *J. Chromatogr. A*, 1998, **824**, 147-157.
50. Q. Yu, B. Lin, H. He, Z. Shi and Y. Feng, *J. Chromatogr. A*, 2005, **1083**, 23-31.
51. K. Kimata, T. Hirose, K. Moriuchi, K. Hosoya, T. Araki and N. Tanaka, *Anal. Chem.*, 1995, **67**, 2556-2561.
52. NACALAI TESQUE, INC. [Cosmosil]. 2020. Available online: https://www.nacalai.co.jp/global/cosmosil/index/Buckyprep-D.html (accessed on 10 May 2021).
53. K. Jinno, T. Uemura, H. Ohta, H. Nagashima and K. Itoh, *Anal. Chem.*, 1993, **65**, 2650-2654.

54. A. Kasprowiak, F. Cazier-Dennin and P. Danjou, *J. Chem. Educ.*, 2020, **97**, 1145-1150.
55. S. Selmani, M. Y. Shen and D. J. Schipper, *RSC Adv*, 2017, **7**, 19026-19029.
56. M. A. Addicoat and G. F. Metha, *J. Comput. Chem*, 2009, **30**, 57-64.
57. R. Dennington, T. Keith, J. Millam, *GaussView*, Version 61; Semichem Inc.: Shawnee Mission, KS, USA, 2016.
58. M. Elstner, D. Porezag, G. Jungnickel, J. Elsner, M. Haugk, T. Frauenheim, S. Suhai and G. Seifert, *Phys. Rev. B*, 1998, **58**, 7260.
59. A. K. Rappé, C. J. Casewit, K. Colwell, W. A. Goddard III and W. M. Skiff, *J. Am. Chem. Soc.*, 1992, **114**, 10024-10035.
60. G. t. Te Velde, F. M. Bickelhaupt, E. J. Baerends, C. Fonseca Guerra, S. J. van Gisbergen, J. G. Snijders and T. Ziegler, *J. Comput. Chem*, 2001, **22**, 931-967.
61. A. V. Onufriev and D. A. Case, *Ann. Rev. Biophys*, 2019, **48**, 275-296.
62. J. L. Atwood, L. J. Barbour, M. W. Heaven and C. L. Raston, *Chem.commun.*, 2003 , 2270-2271.
63. A. Hosseini, S. Taylor, G. Accorsi, N. Armaroli, C. A. Reed and P. D. Boyd, *J. Am. Chem. Soc.*, 2006, **128**, 15903-15913.

7 Chapter 7: General discussion, Conclusion and Future work

7.1 Conclusion

Reverse phase liquid chromatography, RPLC, is the most frequently used high pressure liquid chromatography (HPLC) mode for separating nonpolar, weakly polar, and polar compounds. However, the separation of highly polar compounds on RPLC columns is far from easy; this can be overcome by employing hydrophilic interaction LC (HILIC) columns. RPLC/HILIC mixed-mode columns are typically used to separate nonpolar, weakly, moderately, and highly polar compounds on a single column. When compared with the conventional single-mode interaction stationary phases, multiple-mode interaction stationary phases hold the merits of high separation selectivity and high separation efficiency. The development of novel mixed-mode bonded chromatographic stationary phases, including the utilization of macrocyclic functionalized stationary phases, is rapidly emerging as a new generation of separation tools. The ability to tune these new stationary phases goes beyond polarity to also include host-guest supramolecular interactions.

Supramolecular cavitands, such as cyclodextrins, crownethers, calix[n]arene and pillar[5]arene macrocycles have been widely studied for host-guest chemistry of various analytes over the last 25 years. Their phenolic cores of calix[n]arenes and pillar[5]arenes have enabled chemists to functionalise them towards bespoke receptors readily.

In this work, co-pillar[4+1]arene and *C*-butyl pyrogallol[4]arene were proposed as a potential macrocyclic cavitand to covalently functionalize the surface of the chromatographic silica to improve the specificity for guest molecule interactions and subsequently enhanced flash column and HPLC chromatographic separation of positional isomers, calibration peptide mix and C_{60}- and C_{70}-fullerenes which are difficult to separate on traditional normal phase and reverse phase conditions.

Employment of new greener techniques for the preparation of calix[n]arenes such as pyrogallol[n]arenes and resorcinol[n]arenes *via* microwave irradiation has improved efficiency while reducing the reaction time considerably and increasing yields with minimal waste of organic solvent systems. Several reaction conditions have been explored to optimize the reaction conditions to synthesize the co-pillar[4+1]arene using microwave irradiation, such as temperature, the ratio of monomeric units, and the concentration of paraformaldehyde, and reaction time. As a result, a co-pillar[4+1]arene **3** containing two bromo-octyl substituents was successfully synthesized for the first time in high yields of 88% in under 4 minutes. Furthermore, the yield of co-pillar[4+1]arene by microwave

synthesis was compared with the conventional condensation method, resulting in a 26% yield in under 4 hours. Henceforth, the microwave synthesis of co-pillar[4+1]arene in under 4 minutes is an efficient method than that of the previously reported methods for pillar[n]arenes by T. Ogoshi and co-pillar[n+1]arenes by Huang. The major challenge of the synthesis of co-pillar[4+1]arene was the isolation of pure co-pillar[4+1]arene from the reaction crude mixture. Flash column chromatography and recrystallization techniques have been employed to separate pure components from the crude reaction mixture. However, there was no success with these separation techniques. Therefore, co-pillar [4+1]arene was isolated as a pure component after trituration of the crude product with acetone. The trituration process has played a significant role in speeding up the synthesis of the co-pillar[4+1]arene in higher yields. Similarly, The *C*-bromobutylpyrogaloll[4]arene was successfully synthesized in high yield in 64% yield from *C*-hydroxybutylpyrogallol[4]arene, which was synthesized *via p*reviously reported microwave irradiation.

The co-pillar[4+1]arene was successfully bound covalently on the flash column grade chromatographic silica surface. Thermogravimetric analysis was carried out to characterize the resulting new silica-bound co-pillar[4+1]arene flash column stationary phase to determine the mass loading of co-pillar[4+1]arene at 16% w/w. In addition, the silica-bound co-pillar[4+1]arene flash column was conditioned, and leaching studies were performed to determine the leaching of co-pillar[4+1]arene from the new silica-bound co-pillar[4+1]arene flash column. The mass spectrometric analysis of the eluents at the various column volumes (CV) confirms that there is no leaching of the co-pillar[4+1]arene from the silica-bound co-pillar[4+1]arene flash column. This confirms that the covalent bonding of the co-pillar[4+1]arene to silica is stable.

It has been proven that the efficient host-guest inclusion properties of pillar[5]arenes have been studied with various guest molecules, including hydrocarbons and alkyl chains. For example, host-guest chemistry between alkyl chains and pillar[5]arenes due to CH/π interactions and toluene and *m*-xylene with biphenyl-extended pillar[n]arene. With these unique features of non-covalent host-guest interactions of pillar[5]arenes with guest molecules, xylene isomers and their impurities such as toluene and ethylbenzene as selected as a linear threads fit into the cavity of pillar[5]arene to study host-guest interactions on the surface of the new silica-bound co-pillar[4+1]arene flash column. Moreover, the separation of xylene isomers and their impurities is challenging on traditional chromatographic normal phase and reverse phase columns that hold a single interaction mechanism. In contrast, the silica-bound co-pillar[4+1]arene flash column provides multiple host-guest non-covalent interactions.

Subsequently, a successful flash column chromatographic method was optimized using methanol: ethylacetate (10:90) under isocratic conditions. As a result, the individual xylene isomers and toluene resolved as separate components in less than 15 minutes on the silica-bound co-pillar[4+1]arene flash column stationary phase under the optimized mobile phase conditions. The xylene isomers and their impurities separation was very rapid compared to previously reported LC stationary phases, such as MIL-53(Fe), MIL-53(Al), and MIL-53(Cr). Furthermore, the silica-bound co-pillar[4+1]arene flash column stationary phase was validated by the separation of a mixture of xylenes, ethylbenzene, and toluene on both the normal phase and silica-bound co-pillar[4+1]arene flash column, where the normal phase resulted in a sharp peak which eluted all five eluents together while the co-pillar[4+1]arene bound-silica flash column separated out the mixture into five discreet bands in elution order of *m*-xylene, toluene, *o*-xylene, *p*-xylene, and ethylbenzene.

To further understand the chromatographic separation results from the host-guest interactions, the binding energies of three xylene isomers, toluene, and ethylbenzene in the pillar[5]arene host were studied. Binding energies of toluene, ethylbenzene, and the three xylene isomers in the pore of the pillar[5]arene molecule were calculated using the Density Functional Tight Binding (DFTB) method implemented in DFTB+ version 1.3. Ethylbenzene with calculated binding energy (−26.74 kcal mol^{-1}) showed a higher retention time towards the chromatographic separation through host-guest interactions, while m-xylene with the lowest binding energy (−22.19 kcal mol^{-1}) eluted most quickly from the chromatographic flash column. This excellent example of supramolecular chemistry at work will improve the efficiency of the separation and refining of aromatic hydrocarbons and may find industrial application, given the large volume of these compounds used as starting materials in the chemical industry.

To demonstrate the versatility of the silica-bound co-pillar[4+1]arene stationary phase, we further extended to explore their potential within the field of proteomics. A molecular binding model study compares the host-guest interactions of a library of peptides with the dimethoxy-pillar[5]arene macrocycle. Initially, A semi-stochastic approach was employed to determine the five peptides' likely binding motifs and energies. First, an ensemble of each peptide's low-energy (< 50 kcal mol^{-1}) conformers were generated using Open Babel. Each end of each peptide conformer was then docked into the pillar[5]arene cavity using a semi-stochastically approach wherein a minimum of 50 peptide⊂dimethoxy-pillar[5]arene complexes were generated for each peptide. Next, geometries of each peptide⊂dimethoxy-pillar[5]arene complex were optimized in the gas phase. Finally, the 20 energy minima complexes were selected for each conformer and reoptimized in implicit solvent (acetonitrile). However, this study did not try to provide answers to the

thermodynamic question corresponding to the balance between the various intramolecular forces that dictate the structures of the peptides, nor to the kinetic question of the different folding routes in each peptide. The computational modelling studies were able to predict how specific amino acid from the conformer of peptides interacts with the pillararene cavity through non-covalent interactions. For example, three conformers of peptide VFTPLEVDVAK interact effectively with the cavity with either the glutamic acid or valine units; the conformers of peptide SAEGLDASASLR show the strongest interactions with the cavity are *via* either the leucine adjacent to the terminal arginine; In peptide AVGANPEQLTR, the strongest binding interactions were observed with either the central proline or the threonine residues; Peptide VGNEIQYVALR, predominantly interacts with the cavity via its terminal valine and the adjacent glycine residues. The host-guest interactions is due to the several non-covalent interactions, such as hydrogen bonding between the amino acids of peptides with the pillar[5]arene cavity.

Subsequently, These *in-silico* studies were complimented experimentally by synthesizing a co-pillar[4+1]arene HPLC grade stationary phase and subsequent LC-MS/MS separation and characterization of a standard calibration mix peptides. The elution order of the peptides is in line with the *in-silico* computational binding energy predictions. For example, all conformers calculated of VFTPLEVDVAK, bind strongly to the cavity with binding energies between -20 and -50 kcal mol^{-1}. This prediction of consistently strong interaction between the peptide and cavity was supported experimentally as this peptide was observed to possess the highest retention time of 7.93 minutes. The retention times of AVGANPEQLTR and VGNEIQYVALR also correlate well with the range of binding energies for these peptides. The significant parameter to understand is that the interactions of peptide with pillar[5]arene cavity is not a static due to the conformational changes in the peptide structures. It is very hard to confirm the separation of particular peptide on the co-pillar[4+1]arene stationary phase is due to the particular peptide conformer. However, it is possible to predict the interactions of peptides with the pillar[5]arene cavity to predict the possible host-guest interactions leading to separation of peptides on silica-bound co-pillar[4+1]arene stationary phase

The computational supramolecular host-guest binding energies have been successfully used to design and predict a new class of chromatographic stationary phases for the efficient and effective separation of peptides that are highly significant in proteomic studies. This work will facilitate sample preparation before mass spectrometric analysis and lead to bespoke chromatographic systems that can be designed in silico to optimize the separation of physiological salts and peptides directly from trypsin digested proteins. In addition, these

assessments serve as proof of principle for further exploration of silica-bound co-pillar[4+1]arene stationary phase in the separation of biomolecules.

Chromatographic methods are currently satisfactory for small-scale purification of C_{60} and higher fullerenes from fullerene soot and for the purification of modified fullerene derivatives. Liquid chromatography (LC) is the major chromatographic technique available for the separation of fullerenes due to advances in modern LC chromatographic techniques and instrumental developments, which are readily available to separate fullerenes at the analytical scale. Since the discovery of fullerenes, to enable these new developments, several *p*-butyl pyrogallol[4]arenes have been extensively investigated for the isolation of fullerenes *via* host-guest complexation. However, this calixarene cavitand-bound stationary phases and other modified LC stationary phases have limited use in routine isolation and purification of fullerene mixture due to the requirements of a column with rapid analysis and increased sample loading capacity.

Henceforth, the other variant of supramolecular cavitand *C*-bromobutyl pyrogallol[4]arene was synthesized from *C*-hydroxybutylpyrogallol[4]arene using phosphorus tribromide. The abundance of potential hydrogen bonding sites led to the synthesis of this new class pyrogallol[4]arene derivative to study chromatographic applications. Subsequently, *C*-bromobutyl pyrogallol[4]arene was functionalized on the surface of chromatographic silica to study the host-guest interactions of fullerenes and pyrogallol[4]arene cavity. The synthesized stationary phase was characterized using NMR, Mass Spectrometry, TGA, and SEM. Silica-bound *C*-butylpyrogallol[4]arene has demonstrated superior separation resolution of C_{70}-fullerene than C_{60}-fullerene *via* size-selective molecular recognition using flash column chromatography and HPLC. The flash column pyrogallol[4]arene stationary phase showed a significant increase of isolated quantities of fullerenes to milligrams under 15 min compared to micrograms separation from the HPLC supramolecular stationary phase. The flash column and HPLC grade silica-bound C-butylpyrogallol[4]arene phase showed superior separation selectivity *via* size-selective molecular recognition than an RP-C_{18} column separation selectivity for the mixture of C_{60} and C_{70}-fullerenes.

Subsequently, an *in-silico* host–guest interaction study was performed to further our understanding of the molecular recognition that leads to the favourable chromatographic separation of C_{60} and C_{70} using the C-butylpyrogallol[4]arene stationary phase. In addition, C_{70} showed stronger π-π interaction with the cavity having the highest Gibbs free energy than C_{60}. The stronger interaction of the cavity with C_{70} is in line with experimental chromatographic separation, wherein C_{70} shows a remarkably higher retention time both in HPLC and flash column chromatography. Moreover, Gibbs's free binding energies were

also computed for C_{60}⊂RP-C_{18} and C_{70}⊂RP-C_{18} to compare the C-butylpyrogallol[4]arene cavity and RP-C_{18} as stationary phases for the selective separation of fullerenes. The change in Gibbs free binding energies shows stronger interactions of C_{70} with RP- C_{18} than C_{60}. However, the fullerene⊂RP-C_{18} interactions are significantly thermodynamically unfavourable. Consequently, C-butylpyrogallol[4]arene, which has a favourable thermodynamics interaction with fullerenes, is a more suitable stationary phase for the selective separation of fullerenes.

In conclusion, the synthesized macrocycles have been employed successfully to study the host-guest interactions of various guest analytes on the surface of silica-bonded macrocyclic host stationary phases. The host-guest non-covalent interactions played a significant role in the separation of positional isomers, peptides, and fullerenes. Computational *in-silico* binding energies played an important role to understand the possible non-covalent interactions between the host macrocyclic cavity and guest positional isomers, peptides, and fullerenes.

7.2 Future work

- Synthesis of the hydroxylated pillar[5]arene to functionalise with the active interacting sites, which will be predicted with *in-silico* computational modelling studies. Subsequently, these supramolecular cavitands will be functionalized on the surface of chromatographic silica to isolate preimplantation factor peptides from horse saliva. Furthermore, these modified supramolecular cavitands can also be used to determine the early-stage pregnancy of the horse by detecting preimplantation factor peptide for saliva.

- Development of synthetic protocols to synthesis pillar[5]arene fabricated with amino acids and their subsequent utilization in the chromatography as stationary phases. For example, Biomarker discovery *via* proteomics has enabled the identification of immunogenic MHC class I and II peptides to treat and prevent some cancer tumours. Identification of these peptides routinely involves LCMS; however, sample preparation requires the removal of biological background interference and is often problematic and time-consuming. Therefore, a column system that separates physiological salts and is designed specifically to detect immunogenic peptides directly from a trypsin digested sample will be of significant interest.

- To study *in-silico* the interactions of pillar[5]arene and pyrogallol[4]arene macrocycles and their modified derivatives with cannabis plant cannabinoids,

towards identifying and isolating new bioactive constituents. The cannabis plant contains at least 113 different cannabinoids and over 200 terpenes. However, despite the recent legalization of cannabis in many countries worldwide, including 32 states of the USA and in Canada, only THC (tetrahydrocannabinol) and CBD (cannabidiol) have been widely used and studied as isolates. Currently, the Mass Spectrometric analysis of cannabinoids requires high end mass spectrometers with specialized operational support while FTIR consists low sensitivity to identify the cannabinoids. Henceforth, the cannabis industry is in urge to develop a bespoke chromatographic column material that can separate all cannabinoids very rapidly with replicate nature.

8 Appendix

^{1}H NMR (400 MHz, $CDCl_3$) of 1,4-bis((8'-bromooctyl)oxy)benzene **2**

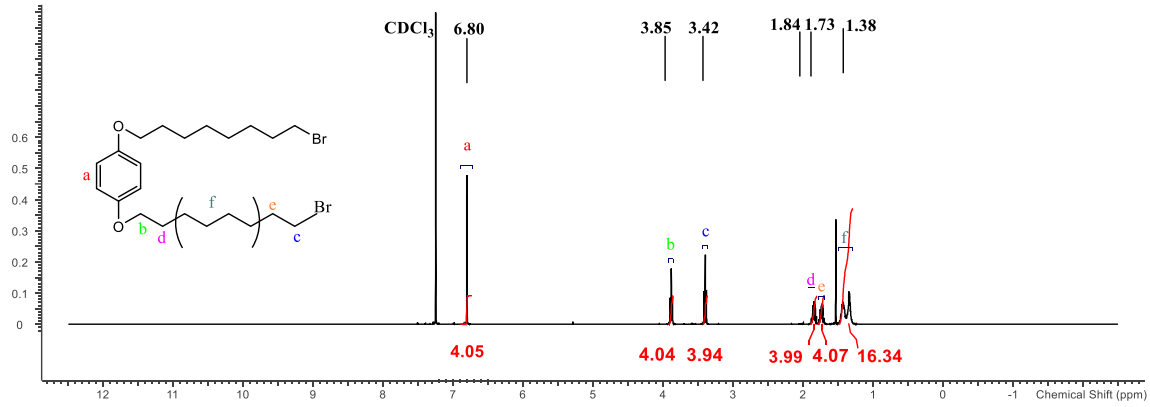

^{1}H NMR (400 MHz, $CDCl_3$) of co-pillar[4+1]arene **3** by microwave

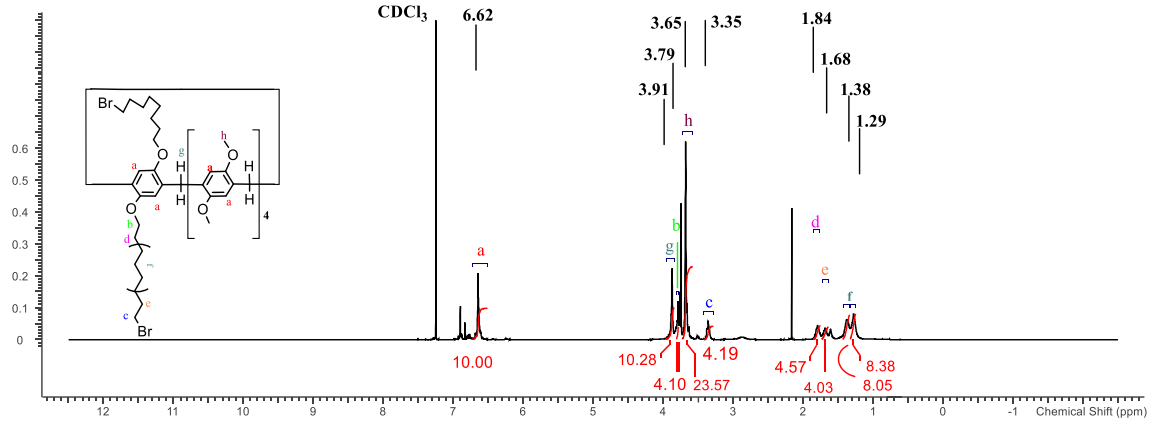

^{13}C NMR (100 MHz, $CDCl_3$, 25 °C) of co-pillar[4+1]arene **3** by microwave

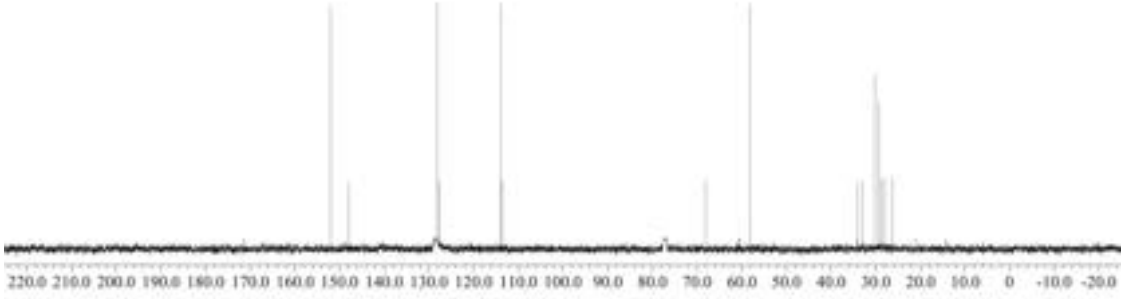

Direct Infusion Electrospray ionization mass spectrum of co-pillar[4+1]arene **3** by microwave

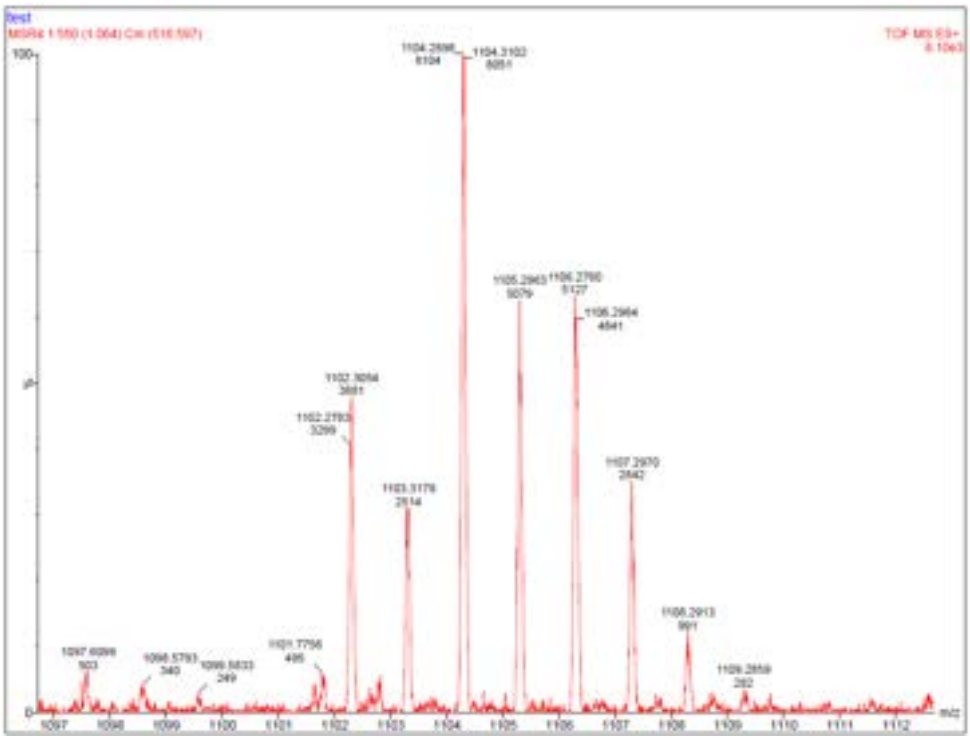

^{1}H NMR (400 MHz, $CDCl_3$) of co-pillar[4+1]arene **3** by condensation

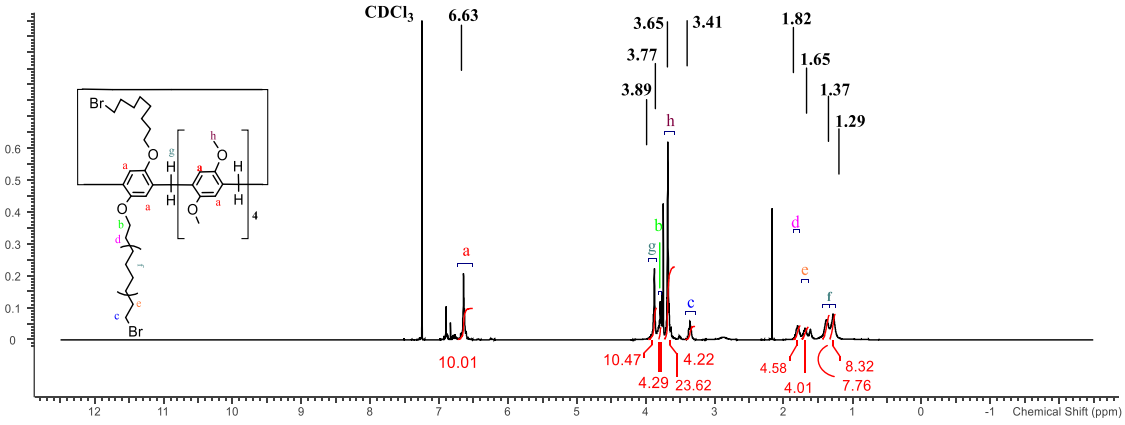

^{13}C NMR (100 MHz, $CDCl_3$, 25 °C) of co-pillar[4+1]arene **3** by condensation

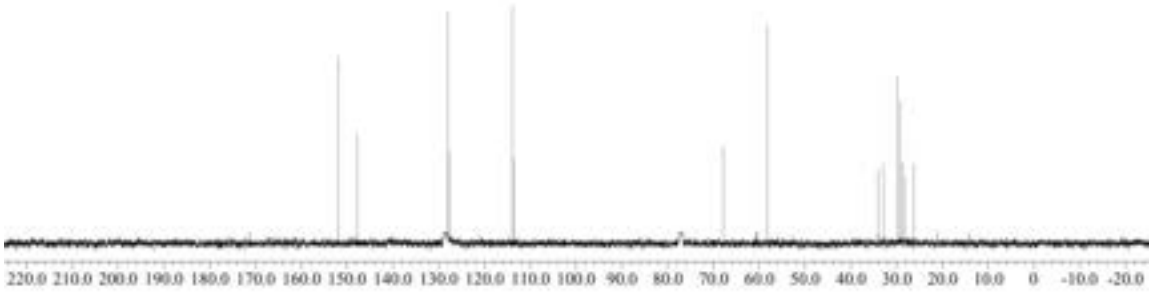

Direct Infusion Electrospray ionization mass spectrum of co-pillar[4+1]arene **3** by condensation

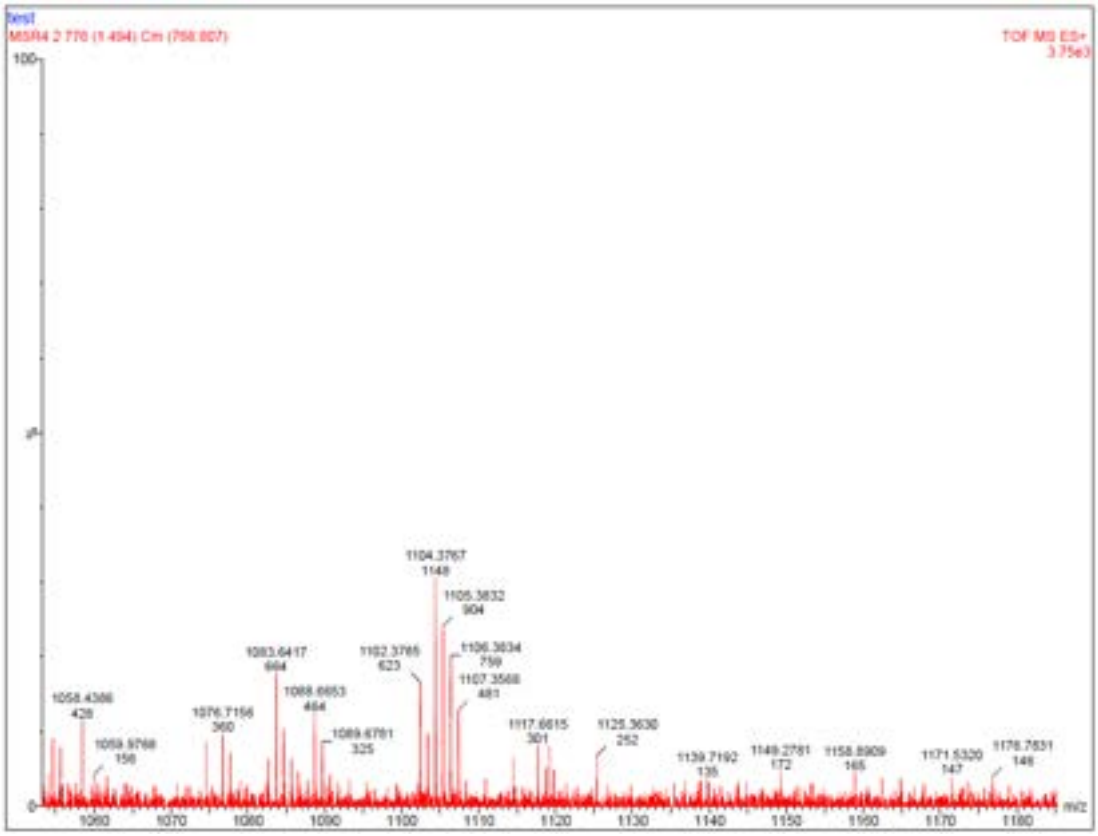

^{1}H NMR (400 MHz, d_6-Acetone) of *C*-Bromo butylpyrogallol[4]arene **5**

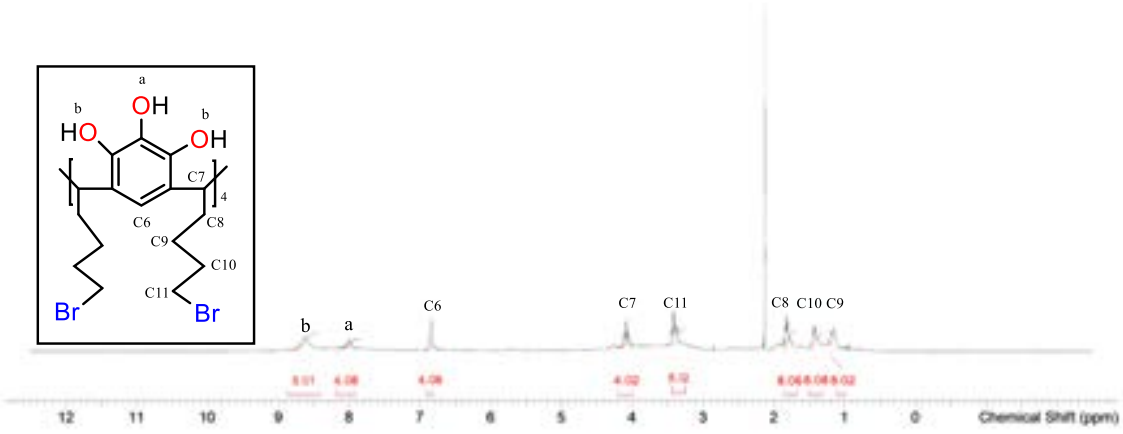

^{13}C NMR (100 MHz, $CDCl_3$, 25 °C) of *C*-Bromo butylpyrogallol[4]arene **5**

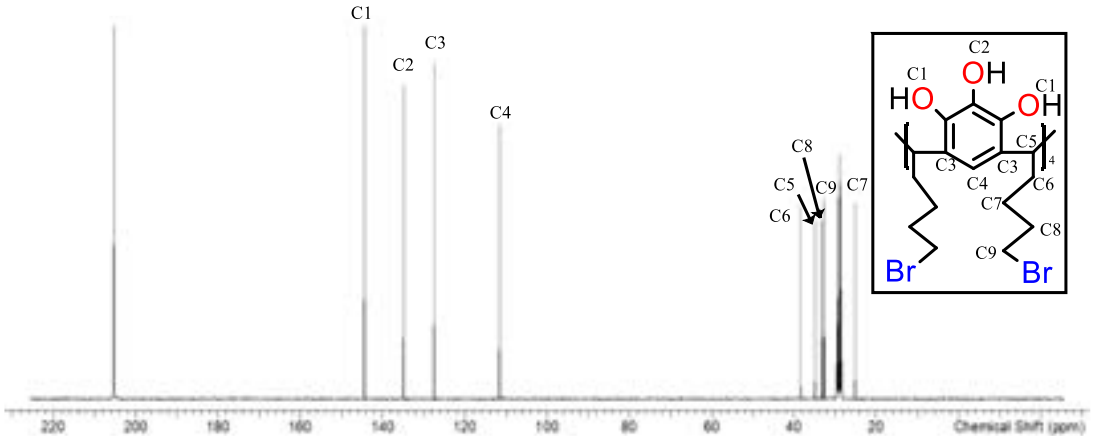

Direct Infusion Electrospray ionization mass spectrum of *C*-Bromo butylpyrogallol[4]arene **5**